Design of circuits to enhance the performance of high frequency planar Gunn diodes

Mohamed Ismaeel Maricar

(B.E, MSc)

A THESIS SUBMITTED TO

DE MONTFORT UNIVERSITY

IN THE FULFILMENT OF THE REQUIREMENTS

FOR THE DEGREE OF

DOCTOR OF PHILOSOPHY

June 2014

Supervised by: Dr. Chris Oxley

To my beloved parents (Jahabar Sathick Maricar and Asiya Mariyam, siblings (Yusoof Maricar, Rahmath Habeeb Nachiyar and Fathima Kathija)wife, (Wajida), Teachers (Dr.Subramaniyam, Mrs. Varalakshmi Balraj, Mr. Vinoth Kumar and Dr.T.Jayanthy)and friends (James Glover, Rubinaz Sheikh, Jamal Mohamed and so on)

DECLARATION OF ORIGINALITY

I confirm that the PhD thesis I am submitting is entirely my own work and that any material used from other sources has been clearly identified and properly acknowledged and referenced. In submitting this final version of my report to the JISC anti-plagiarism software resource, I confirm that my work does not contravene the university regulations on plagiarism as described in the Student Handbook. In so doing I also acknowledge that I may be held to account for any particular instances of uncited work detected by the JISC anti-plagiarism software, or as may be found by the project examiner or project organiser. I also understand that if an allegation of plagiarism is upheld via an Academic Misconduct Hearing, then I may forfeit any credit for this module or a more severe penalty may be agreed.

Design of circuits to enhance the performance of high frequency planar Gunn diodes

Mohamed Ismaeel Maricar

Author Signature Date: 24/11/2014

Supervisor's name: Dr. Chris Oxley

ABSTRACT

The project contains adventurous research, with an aim to understand and design a planar Gunn diode with a novel integrated circuit configuration to extract the 2nd harmonic. This will potentially enhance the Gunn diode as a high frequency source towards frequencies in excess of 600 GHz. The RF performance from the above integrated circuit was achieved by design and simulation of radial and diamond stub resonators, which were used to short the fundamental oscillation frequency while allowing the second harmonic frequency to pass through to the load. The diamond stub resonator is a new configuration offering a number of advantages which include a higher loaded quality factor and occupies 55% less chip area than a comparable radial stub resonator.

The designed novel circuits with integrated planar Gunn diode were fabricated using microwave monolithic integrated circuits (MMIC) technology at the James Watt Nanofabrication centre in Glasgow University. Full DC and microwave characterisation of the diodes and integrated circuits with diodes was carried out using a semiconductor analyser, network analyser (10 MHz to 110GHz) and spectrum analyser (10 MHz to 125GHz). The microwave measurements were carried out at the high frequency RF laboratories in Glasgow University.

Both GaAs and InP based Gunn diodes were characterised and RF characterisation work showed that higher fundamental frequencies could be obtained from Gunn diodes fabricated on InGaAs on a lattice matched InP substrate. Planar Gunn diodes with an anode to cathode spacing of 4 microns giving a fundamental frequency of oscillation of 60 GHz were fabricated as an integrated circuit with coplanar waveguide (CPW) circuit elements to extract the second harmonic. A second harmonic frequency of 120 GHz with an RF output power of -14.11 dBm was extracted with very good fundamental frequency suppression. To the authors knowledge this was the first time second harmonic frequencies have been extracted from a planar Gunn diode technology.

Aluminium gallium arsenide (AlGaAs) planar Gunn diodes were also designed with an integrated series inductor to match the diode at the fundamental frequency to obtain higher RF output powers. Devices with a 1 micron anode to cathode separation gave the highest

fundamental oscillation frequency of 121 GHz the highest reported for a GaAs based Gunn diode and with an RF output power of -9 dBm. These circuits will have potential applications in secure communications, terahertz imaging etc. The research programme was in collaboration with the University of Glasgow

Index term: InP, GaAs, Planar Gunn diode, Harmonics, MMIC, High Frequency, Power.

PUBLICATIONS

INTERNATIONAL JOURNALS

1. ***Mohamed Ismaeel Maricar***, A Khalid, D Cumming and C H Oxley,' Improving the Quality factor of the coplanar waveguide resonator', in Microwave optical technology letter 2014 ***(Submitted)***

2. ***Mohamed Ismaeel Maricar,*** A Khalid, D Cumming and C H Oxley,' Design, characterization and fabrication of an $In_{0.53}Ga_{0.47}As$ planar Gunn diode operating at milli-metric waves', in Terahertz Science and Electronics Information Technology-2014***(Submitted)***

3. ***Mohamed Ismaeel Maricar,*** A Khalid, D R S Cumming and C H Oxley,' Extraction of second harmonic from an InP based planar Gunn diode using diamond resonator for milli-metric wave frequencies' in Solid state Communication 2014 ***(Submitted)***

4. ***Mohamed Ismaeel Maricar,*** A Khalid, G Dunn, D Cumming and C H Oxley,' Experimentally estimated dead space for GaAs and InP based planar Gun diodes', in IOP Science Semiconductor Science and Technology 2014 ***(Accepted)***

5. ***Mohamed Ismaeel Maricar,***Mathunesan' Design of double layered circularly polarized self-diplexing antenna 'International Journal for advanced research engineering and technology, pp 127-129

6. ***Mohamed Ismaeel Maricar,*** J Glover, G A Evans. Ata Khalid, D R S Cumming and C H Oxley, 'Characterisation of Planar Gunn diodes and radial resonators for matching elements' International Journal on Intelligent Electronics Systems vol.8, Issue.1, pp.23-27.

7. ***Mohamed Ismaeel Maricar,*** A Khalid, D R S Cumming and C H Oxley,' An AlGaAs/GaAs based planar Gunn diode oscillator with a fundamental frequency operation of 120 GHz ' Microwave and Optical Technology Letters**,** vol.56.Issue 10. pp.2449-2451

8. ***Mohamed Ismaeel Maricar,*** Ata Khalid, D R S Cumming and C H Oxley, 'Design and Characterisation of a Novel Diamond Resonators' in Microwave and Optical Technology Letters, vol.56, Issue 7, pp. 1691-1693

9. ***Mohamed Ismaeel Maricar,*** A Khalid, D R S Cumming and C H Oxley,' Extraction of second harmonics from the InGaAs planar Gunn diode using radial stub resonators', in Solid state electronics, vol.99, pp. 38-40.

INTERNATIONAL CONFERENCE

1. ***Mohamed Ismaeel Maricar,*** Ata Khalid, D R S Cumming and C H Oxley, 'Second harmonic extraction of planar Gunn diode by using resonators for mill metric wave applications', ARMMS Conference on November 2014, Bedfordshire, UK.

2. ***Mohamed Ismaeel Maricar***, Yamini Raju, AhamedBahar, James Glover, Krishna Nama, Richard Cross,' DSP control the Smart Antennas' 4th IEEE International Conference on Advances in Engineering and Technology (ICAET-2014) on 2nd May 2014, Nagapattinam, India

3. ***Mohamed Ismaeel Maricar,*** James Glover, G A Evans, Ata Khalid,V Papageorgiou, Li Chong, G Dunn, D R S Cumming and C H Oxley, 'Improved Coplanar Waveguide resonators design for mill-metric application' 8th Annual Conference on Innovative electronics Manufacturing research Centre (IeMRC) on 25th September 2013, Loughborough, UK

4. ***Mohamed Ismaeel Maricar,*** James Glover, Chris Oxley, Li Chong,V Papageorgiou, Li Chong, G Dunn, A. Stephen, M Montes Bajo, M Kuball, D R S Cumming and C H Oxley 'Planar Gunn diode characterisation and resonators elements to realise oscillator circuits' in International conference on Advanced Nanomaterial and Emerging Engineering Technologies (ICAMEET-2013) on 24-26th July 2013, Chennai, India

5. ***Mohamed Ismaeel Maricar,*** James Glover, Chris Oxley, Li Chong,V Papageorgiou, Li Chong, G Dunn, A. Stephen, M Montes Bajo, M Kuball, D R S Cumming and C H Oxley 'Planar Gunn diode characterisation and Resonators' 4th Annual Seminar on Passive and RF Microwave components, on 18th March 2013, Birmingham, UK

6. James Glover, Richard Hopper, ***Mohamed Ismaeel Maricar***, Ata Khalid, David Cumming,M Montes, M Kuball, Geoff Dunn, Alex Stephen and C H Oxley 'Novel infra-red thermal measurements on GaAs Micro cooler', ARMMS Conference on 19th -20th November 2012, Bedfordshire, UK.

Awards

1. ***'Young Engineering Scholarship'*** in ARRMS conference, Bedfordshire, UK, Nov-2014

2. ***'Best Team Work Award'*** in YES Engineering competition, Birmingham, UK, May-2011

ACKNOWLEDGEMENTS

Over the past three years I have received help and support from a number of people around me. Without their assistance it would have been impossible for me to complete this work over this short time.

I must start thanking my principal supervisor **Dr. Chris H Oxley**, for trusting and offering me the opportunity to carry out my PhD study on this project. He has been constantly encouraging and guiding me through the last three years. His expertise in millimetre-wave engineering has helped me with the circuit development and characterisation throughout this project. Furthermore his critical and advisory reviews on my thesis were extremely helpful in building the final and solid body of work.

Dr. Ata Khalid from Glasgow University, for helping and assisting me to develop and improve my expertise in semiconductor devices as well as his top-class electron beam lithography and fabrication skills that made the project so fruitful.

Dr.Chong Li from Glasgow University, for helping me to understand the working principle of the planar Gunn device without his support and constant guidance it would have been impossible to complete this work.

Mr. James Glover from De Montfort University, for helping me to take thermal measurements on the Gunn device. His constant encouragement and support has helped me to complete my PhD on time.

Prof.Gwynne Evans from De Montfort University, for assisting me to develop a mathematical model for CPW and also for proof-reading this thesis.

Professor David R.S. Cumming from university of Glasgow, for allowing me to use their lab facilities

Dr.Geoff Dunn from University of Aberdeen, for his expertise on Monte-Carlo simulation.

I have received a lot of additional support and assistance from ***Mr Vasilleous Papageorge,Ms Yamini Raju, Mr Paul Taylor, Mr ErKrishan Nama, Dr Richard Cross, Dr NareGarbrielyan, Dr.T.Jayanthy, Ms Rallou de Sousa*** and many more.

I wish to express my sincere appreciation to my financial sponsors De Montfort University.

Last but not least I deeply thank my beautiful ***family*** for their support. They have been constantly supporting and encouraging me from every aspects of my life through my Masters and PhD studies over the past three years. Importantly, ***My parents (Jahabar Sathick Maricar and Asiya Mariyam), Grandparents (Mayimoon Sharifa Nachiyar) brother (Yusoof Maricar), sisters (Rahmath Habeeb Nachicyar and Fathima Kathija Nachiyar),wife (Wajida), sister-in-laws (Thahira), brother-in-law (Azeez Ahamed and Mohamed Firoze Ali)*** have also been supporting me to achieve the final completion of the PhD.

KEY ACRONYMS

AlGaAs	Aluminium Gallium Arsenide
CPW	Coplanar Waveguide
EBL	Electron Beam Lithography
FET	Field Effect Transistor
GaAs	Gallium Arsenide
GaN	Gallium Nitride
HEMT	High Electron Mobility Transistor
InP	Indium Phosphide
InGaAs	Indium Gallium Arsenide
IMPATT	Impact Ionization Avalanche Transit time
IR	InfraRed
LSA	Limited Space charge Accumulation
MBE	Molecular Beam Epitaxy
MMIC	Monolithic Microwave Integrated Circuits
MESFET	Metal Semiconductor Field Effect Transistor
NDR	Negative Differential Resistance
RF	Radio Frequency
SEM	Scanning Electron Microscopy
TRAPATT	Trapped Plasma Avalanche Triggered Transit Time
TEDs	Transfer Electron Devices
TLM	Transmission Line Model
VNA	Vector Network Analyser
QFI	Quantum Focus Instruments

TABLE OF CONTENTS

3. DESCRIPTION OF MEASUREMENT TECHNIQUES USED TO CHARACTERIZE PLANAR GUNN DIODE AND OSCILLATOR

4. DESIGN AND FABRICATION OF A PLANAR GUNN DIODE

LIST OF FIGURES

LIST OF TABLES

Chapter: 1

Introduction to the Gunn diode

1.1. BACKGROUND

Transfer electron devices (TEDs) are generally called Gunn diodes. The Gunn diode was first demonstrated by J.B. Gunn in 1963[1] and is an excellent microwave and lower millimetre (30 GHz to 100 GHz) wave signal source. The Gunn diodes are solid state and have lower power consumption than other solid state devices. Almost after 50 to 60 years of development Gunn devices are still widely used microwave signal sources [2] in industry, scientific, medical and military applications such as solid-state microwave diode sources which include the Impact Ionization Avalanche Transit Time (IMPATT), Trapped Plasma Avalanche Triggered Transit Time (TRAPATT) and resonant tunnelling diodes (RTD). The TRAPATT was used for high pulsed power from 0.9 to 16 GHz [3]–[5], pulsed output powers of around 1KW have been reported at 1 GHz [6] ,with very low mean power. The IMPATT diodes and resonant tunnelling diodes were used for a high frequency solid state microwave power source [7], [8];a pulsed output power of 1.2 mW has been achieved at 301 GHz from an IMPATT diode and 0.3 μW was achieved at 712 GHz for resonant tunnelling diode with very low input current [9], [10]. For very high power generation above 10 kW magnetrons, klystrons and travelling wave tube amplifiers (TWTA) are currently used [11]–[13]. **Figure.1.1.** shows the performance of different solid state microwave sources by plotting RF continuous and maximum pulsed power against frequency [2]. In recent years conventional vertical Gunn diodes are being investigated as possible solid state signal sources for operating in the upper millimetre-wave (between 100 GHz to 300 GHz) and into the terahertz (between 0.3 THz to 30 THz) frequency bands [14]–[16]. These frequency bands are used for applications including communication, radar, imaging, spectroscopy and security screening [17]–[19].

The recent renewed interest in the Gunn diode has spurred a number of technological advances on the Gunn diode, which include planar structures [20]–[23], heterostructure material growth [22], [24], [25] and harmonic power extraction [16], [26] to improve the upper frequency of operation and RF output power performance. In 2007 Ata Khalid et al published a paper demonstrating the operation of a AlGaAs/GaAs planar Gunn diode operating above 100 GHz [2], [21].

Figure 1.2 (a) shows a scanning electron microscope (SEM) image of a vertical Gunn diode. In the vertical Gunn diode the frequency of oscillation is controlled by the material growth of the active region, whereas in the planar Gunn diode the frequency of oscillation is controlled by the planar distance between the anode and cathode electrodes see schematic Figure 1.2 (b). The anode to cathode separation can be realised by lithographic techniques leading to the possibility of having multiple Gunn oscillators working at different frequencies on a single monolithic microwave integrated circuit (MMIC). In addition by realising sub-micron cathode and anode separation it is feasible to realise planar Gunn diodes working in the sub terahertz or even to the terahertz frequency bands [27]. Moreover, simple two terminals planar devices do not need the complicated process steps of transistors to realise complicated (T and MULTI-COMB) gate structures[28], [29].

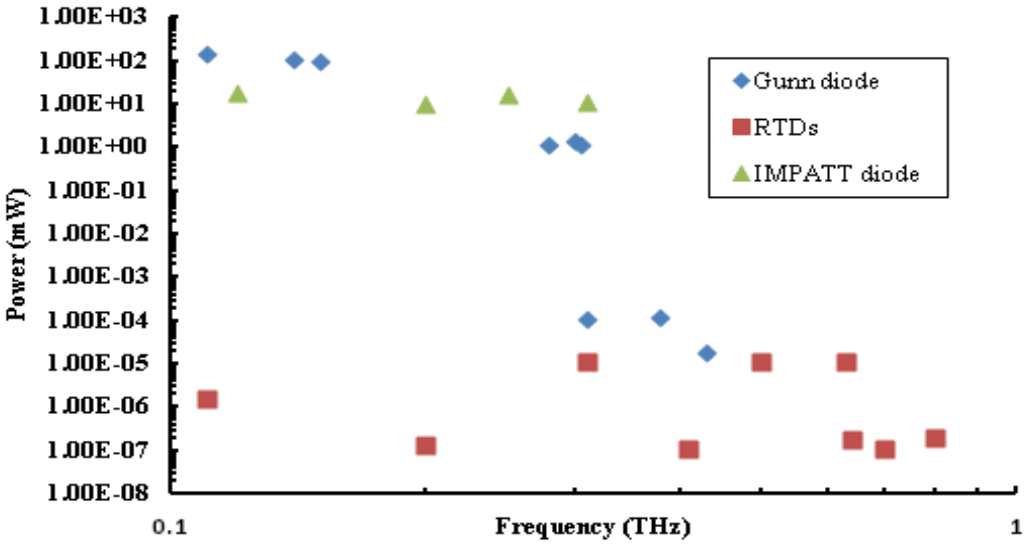

Figure.1.1. Performance of selected solid state electronic and millimetre-wave terahertz signal sources including the Gunn diode [14]–[17], [30]–[32]**, resonant tunnelling diode** [10], [33]–[39] **and Impact ionisation avalanche transit time (IMPATT) diodes** [17], [30], [40]**,** [9]**.**

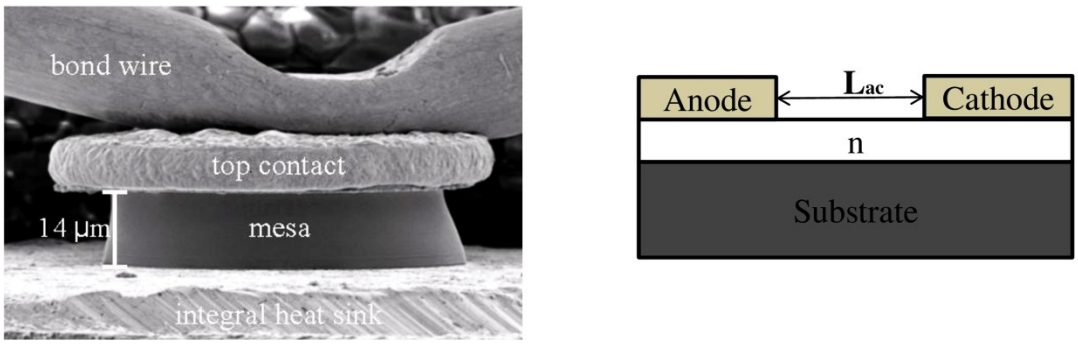

(a) **(b)**

Figure.1.2. Gunn diode (a) SEM image of a Vertical Gunn diode (b) Schematic view of the planar Gunn diode

To date the full potential of the planar Gunn diode has not been realised [2] for example the RF output power of the planar Gunn diode has not been fully extracted from the diode. Planar Gunn diodes to-date have been fabricated on GaAs and InP materials in MMIC format and a fundamental frequency of 298 GHz has been realised on InP material, however the output power was low (-26dBm) [24]. Although techniques have been used to increase the output power from the diode such as introducing an additional hetero-structures layer [21] and higher doping [2] to enhance the electron density the RF output powers have remained relatively low. In this thesis a coplanar waveguide (CPW) oscillator circuit using a hetero-structure InP based planar Gunn diode was developed to extract the second harmonic frequency, showing the potential of obtaining very high frequency oscillator performance in microwave monolithic integrated circuit (MMIC) format. For example, the recent published work of Ata et al [24] has shown the potential of a fundamental frequency of 298 GHz which will give a second harmonic frequency of 596 GHz.

In the presented work the Gunn diode used a cathode to anode separation of 4 microns giving a fundamental frequency of oscillation at 60 GHz and second harmonic extraction of 120 GHz[41]. Although this work shows a novel way of extracting the second harmonic, further work is still required to increase the RF output power.

In this thesis, the design and characterisation of planar Gunn diodes and the design of passive circuit components to extract the second harmonic in millimetre-wave frequencies are described. These components include a novel diamond resonator

[42] which was shown to out-perform the radial resonator and to the authors knowledge was the first time a CPW resonator with this geometrical outline had been designed, fabricated and tested, As mentioned, the planar Gunn diode still falls short in providing useful RF output power (>1mW) and it is thought an improved electrical equivalent circuit model of the planar Gunn diode will enable the design of matching circuits to realise higher RF output power. This research work has introduced the concept of a novel method of extracting the DC parasitics of the diode using a two port network, preliminary work is reported in [43]. Further work will be required to improve the method of parameter extraction and develop an improved electrical equivalent circuit model of the diode, and has been cited in the section of future work.

1.2. OBJECTIVES

The aim of this project is to understand and optimisethe electrode structure of the planar Gunn diode and integrate with a circuit to extract the 2nd harmonic, enhancing its potential as a milli-metric and low terahertz frequency source.It was important that theintegrated diode with circuit elements were compatible with microwave monolithic integrated circuit (MMIC) fabrication technologies. The proposed method of research is shown as a flow diagram in **Figure.1.3.**

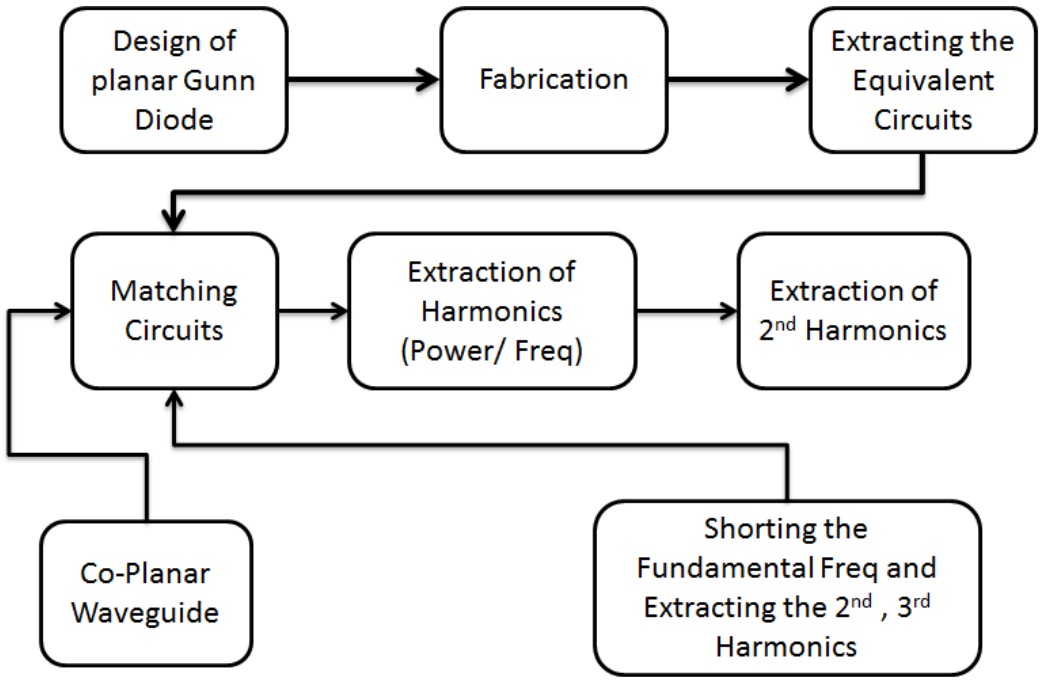

Figure.1.3 Proposed method of research

1.3. SCOPE OF THE PROJECT

The project required an understanding of the design and fabrication of the planar Gunn diode. This was carried out in close collaboration with the University of Glasgow. The planar Gunn diode was DC and microwave characterized using novel electrode structures to simplify de-embedding to the active region of the diode. When designing the integrated oscillator structure, a number of matching circuit techniques were pursued including series inductors and open circuit stub transmission lines. To extract the second harmonic, novel circuits will be presented including a novel diamond shaped resonator which has been shown to outperform the standard radial stub resonator. The technologies adopted for the diode and circuit elements were compatible with microwave monolithic integrated circuit (MMIC) technologies. Many of the high frequency measurements were carried out at Glasgow University in their nanotechnology facilities.

1.4. THESIS OUTLINE

The thesis has been divided into nine chapters and a summary of each chapter follows:

Chapter1: The first chapter describes the background to the Gunn diode, objective and scope of the research. This chapter outlines the important research activities for developing planar Gunn diode circuits for the extraction of the second harmonic frequency.

Chapter 2: Literature review of the Gunn diode including the hetero-structure vertical and the planar Gunn diode are described. The chapter also includes a description of different types of oscillation modes which can be obtained from the Gunn diode. The fabrication of the vertical Gunn diode is discussed in this chapter.

Chapter 3: Describes the different measurement techniques which were used to characterize the planar Gunn diode and include DC, RF, Infrared (IR) thermal and scanning electron microscopy (SEM) measurements. The DC measurements were described in more detail including pulsed IV using the semiconductor network ana-

lyzer and transmission line method (TLM) to obtain an estimate of the contact resistance for each wafer process. The RF measurements include a detailed description of the vector network analyzer (VNA), spectrum analyzer and Quantum Focus Instruments (QFI) infra-red (IR) microscope for preliminary thermal measurements of the diode under DC bias conditions.

Chapter 4: This chapter describes the electrode layout design of the planar Gunn diode and computer modeling using Agilent Advanced Design Software (ADS) to ascertain if the electrode geometries influence the transit frequency of operation of the Gunn diode. The chapter also includes material specification and fabrication technologies used in the realization of the diode and coplanar wave-guide circuit elements.

Chapter 5: This chapter describes the experimental results of the hetero-structure AlGaAs/GaAs planar Gunn diode fabricated on semi-insulating GaAs wafers. The experimental results consisted of DC, network analyzer, spectrum analyzer and thermal measurements. A GaAs planar Gunn diode with a 1 micron cathode to anode separation and on chip series inductor matching wasRF characterized and gave the highest experimentally measured fundamental frequency of 121 GHz obtained to date from a GaAs Gunn diode. This chapter also describes experimental measurements to estimate the dead space of a GaAs planar Gunn diode on GaAs substrate, and the results were similar to the published work by Ata and Li[2], [21].

Chapter6: This chapter describes the experimental results of the $In_{0.53}Ga_{0.47}As$ hetero-structure planar Gunn diode fabricated on semi-insulating InP substrate which provides an excellent lattice match. The InP material provides a higher transit mode oscillation frequency and higher mobility because of the relaxation time of the InP material [2]. The experimental results described include DC, network analyzer, spectrum analyzer and thermal measurements results on planar Gunn diode. The planar Gunn diodes were characterized and show that the operation frequenciescan be tuned by adding a series inductor closer to the device. This chapter also describes the dead space of the$In_{0.53}Ga_{0.47}As$ planar Gunn diode fabricated on an InP substrate.

Chapter 7: Covers the basic principles and design equations for coplanar waveguides (CPW) transmission lines. The design and simulation using method of moments to describe CPW radial resonators will be described and results compared with published data. This led to the realization of a novel diamond shaped resonator. The design equation for the diamond resonator was also developed. A comparison between the radial and diamond resonators was made showing performance improvements of the diamond resonator, for example occupying 55% less chip area when compared with a comparable radial resonator. Both CPW radial and diamond resonators were fabricated and experimentally characterized and compared with the respective simulation results.

Chapter 8: This chapter reports in detail, for the first time the circuit design, fabrication, and measurement of novel integrated CPW structures to extract the second harmonic oscillation frequency and suppress the fundamental frequency from the $In_{0.53}Ga_{0.47}As$ planar Gunn diode. The measurement results were directly compared with simulation results of the integrated planar Gunn diode oscillator circuit using ADS non-linear modeling techniques.

Chapter 9: Concludes the main body of the thesis. It contains the summary of the findings and description of suggested future work.

1.5. NOVELTY OF THERESEARCH

Novelties of the work are listed below:

- The design of a novel diamond shaped CPW resonator which out performs the published radial CPW resonator[42]

- Highest operational fundamental frequency 121 GHz achieved to datefrom a GaAs Gunn diode [44]. The planar Gunn diode had a 1 micron electrode separation and an on chip series inductor to match the diode and gave -9 dBm of RF power at the fundamental frequency.

- For the first time to the author's knowledge a novel on chip circuit to extract the second harmonic frequency from the planar Gunn diode has been developed.The circuit consisted of InGaAs planar Gunn diode and integrated circuit elements to extract the second harmonic frequency and to suppress the fundamental frequency[41]. The circuit design used an InGaAs heterostructure diode with an electrode separation of 4 microns which was fabricated on both InP and GaAs materials. For the circuit on InP material a second harmonic oscillation frequency of 120 GHz with an output RF power of -14.11 dBm was measured.

1.6. REFERENCE

[1] J. B. Gunn, "Microwave oscillations of current in III–V semiconductors," *Solid State Commun.*, vol. 1, no. 4, pp. 88–91, Sep. 1963.

[2] C. Li, "Design and Characterisation of millimeter-wave planar Gunn diode and integrated circuits," University of Glasgow, 2011.

[3] J. M. Borrego, R. J. Gutmann, H. J. Geipel, and S. K. Ghandhi, "Operation of Trapatt Oscillators under Transient Ionizing Radiation Conditions," *IEEE Trans. Nucl. Sci.*, vol. 20, no. 6, pp. 144–148, 1973.

[4] W. Tantraporn, "Device physics of a new TRAPATT oscillator," *IEEE Trans. Electron Devices*, vol. 22, no. 3, pp. 140–145, Mar. 1975.

[5] J. R. East, N. A. Masnari, and G. I. Haddad, "Experimental investigation of TRAPATT diode trigger conditions," *IEEE J. Solid-State Circuits*, vol. 12, no. 1, pp. 14–20, Feb. 1977.

[6] W. E. Wilson, "1 kW microstripline TRAPATT oscillator," *Electron. Lett.*, vol. 8, no. 7, p. 174, 1972.

[7] T. P. Lee and R. D. Standley, "Frequency Modulation of a Millimeter-wave IMPATT Diode Oscillator and Related Harmonic Generation Effects," *Bell Syst. Tech. J.*, vol. 48, no. 1, pp. 143–161, Jan. 1969.

[8] H. Gummel and D. Scharfetter, "Avalanche region of IMPATT diodes," *Bell Syst. Tech. J.*, vol. 45, no. 2, pp. 1797–1826, 1966.

[9] M. Ino, T. Ishibashi, and M. Ohmori, "C.W. oscillation with ppn silicon IMPATT diodes in 200 GHz and 300 GHz bands," *Electron. Lett.*, vol. 12, no. 6, p. 148, 1976.

[10] E. R. Brown, C. D. Parker, L. J. Mahoney, and K. M. Molvar, "Oscillations up to 712 GHz in InAs / AISb diodes," *Appl. Phys. Lett.*, vol. 58, no. May, pp. 2291–2293, 1991.

[11] G. Caryotakis, *High power klystrons: theory and practice at the Stanford Linear Accelerator center*, no. August 2004. 2004, pp. 0–138.

[12] J. Böhlmark, "Fundamentals of high power impulse magnetron sputtering," Linkoping University, 2006.

[13] D. Shiffler, J. Nation, and G. Kerslick, "A high-power, traveling wave tube amplifier," *Plasma Sci. IEEE …*, vol. IX, no. 3, 1990.

[14] H. Eisele, "InP Gunn devices for 400–425 GHz," *Electron. Lett.*, vol. 42, no. 6, p. 358, 2006.

[15] H. Eisele and R. Kamoua, "Submillimeter-Wave InP Gunn Devices," *IEEE Trans. Microw. Theory Tech.*, vol. 52, no. 10, pp. 2371–2378, Oct. 2004.

[16] H. Eisele, "480 GHz oscillator with an InP Gunn device," *Electron. Lett.*, vol. 46, no. 6, p. 422, 2010.

[17] P. H. Siegel, "Terahertz technology," *IEEE Trans. Microw. Theory Tech.*, vol. 50, no. 3, pp. 910–928, Mar. 2002.

[18] M. C. Kemp, "A review of millimetre-wave and terahertz technology for detection of concealed threats," *2008 33rd Int. Conf. Infrared, Millim. Terahertz Waves*, pp. 1–2, Sep. 2008.

[19] Naoya Kukutsu and Yuichi Kado, "Overview of Millimeter and Terahertz Wave Application Research," 2009.

[20] M. I. Maricar, J. Glover, G. A. Evans, A. Khalid, V. Papageorgiou, L. Chong, G. Dunn, and C. H. Oxley, "Planar Gunn diode characterisation and resonator elements to realise oscillator circuits," in *International Conference on Advanced Nanomaterials & Emerging Engineering Technologies ICANMEET-2013*, 2013, pp. 674–678.

[21] A. Khalid, N. J. Pilgrim, G. M. Dunn, M. C. Holland, C. R. Stanley, I. G. Thayne, and D. R. S. Cumming, "A Planar Gunn Diode Operating Above 100 GHz," *IEEE Electron Device Lett.*, vol. 28, no. 10, pp. 849–851, Oct. 2007.

[22] N. J. Pilgrim, A. Khalid, G. M. Dunn, and D. R. S. Cumming, "Gunn oscillations in planar heterostructure diodes," *Semicond. Sci. Technol.*, vol. 23, no. 7, p. 075013, Jul. 2008.

[23] W. H.Haydl, "Planar Gunn Diodes with Ideal Contact Geometry," *IEEE Electron Device Lett.*, vol. 61, no. 4, p. 1972, 1972.

[24] M. Montes Bajo, G. Dunn, A. Stephen, A. Khalid, D. R. S. Cumming, C. H. Oxley, J. Glover, and M. Kuball, "Impact ionisation electroluminescence in planar GaAs-based heterostructure Gunn diodes: Spatial distribution and impact of doping non-uniformities," *J. Appl. Phys.*, vol. 113, no. 12, p. 124505, 2013.

[25] I.-H. Kim, S. H. Park, T.-W. Lee, and M.-P. Park, "A study on Au/Ni/Au/Ge/Pd ohmic contact and its application to AlGaAs/GaAs heterojunction bipolar transistors," *Appl. Phys. Lett.*, vol. 71, no. 13, p. 1854, 1997.

[26] S. J. J. Teng and R. E. Goldwasser, "High-performance second-harmonic operation W-band GaAs Gunn diodes," *IEEE Electron Device Lett.*, vol. 10, no. 9, pp. 412–414, Sep. 1989.

[27] A. Khalid, G. M. Dunn, R. F. Macpherson, S. Thoms, D. Macintyre, C. Li, M. J. Steer, V. Papageorgiou, I. G. Thayne, M. Kuball, C. H. Oxley, M. Montes Bajo, A. Stephen, J. Glover, and D. R. S. Cumming, "Terahertz oscillations in an

In0.53Ga0.47As submicron planar Gunn diode," *J. Appl. Phys.*, vol. 115, no. 11, p. 114502, Mar. 2014.

[28] W. R. Deal, "Solid-state amplifiers for terahertz electronics," in *2010 IEEE MTT-S International Microwave Symposium*, 2010, pp. 1–1.

[29] J. A. del Alamo, "30-nm InAs PHEMTs With ft=644GHz and fmax =681 GHz," *IEEE Electron Device Lett.*, vol. 31, no. 8, pp. 806–808, Aug. 2010.

[30] H. Eisele, "State of the art and future of electronic sources at terahertz frequencies," *Electron. Lett.*, vol. 46, no. 26, p. S8, 2010.

[31] H. Eisele and G. I. Haddad, "Efficient power combining with D-band (110-170 GHz) InP Gunn devices in fundamental-mode operation," *IEEE Microw. Guid. Wave Lett.*, vol. 8, no. 1, pp. 24–26, 1998.

[32] T. W. Crowe, D. W. Porterfield, J. L. Hesler, W. L. Bishop, D. S. Kurtz, and K. Hui, "Terahertz sources and detectors," in *Proceedings of the SPIE*, 2005, pp. 271–280.

[33] E. R. Brown, W. D. Goodhue, and T. C. L. G. Sollner, "Fundamental oscillations up to 200 GHz in resonant tunneling diodes and new estimates of their maximum oscillation frequency from stationary-state tunneling theory," *J. Appl. Phys.*, vol. 64, no. 3, p. 1519, 1988.

[34] E. R. Brown, T. C. L. G. Sollner, C. D. Parker, W. D. Goodhue, and C. L. Chen, "Oscillations up to 420 GHz in GaAs/AlAs resonant tunneling diodes," *Appl. Phys. Lett.*, vol. 55, no. 17, p. 1777, 1989.

[35] M. N. Feiginov and D. Roy Chowdhury, "Operation of resonant-tunneling diodes beyond resonant-state-lifetime limit," *Appl. Phys. Lett.*, vol. 91, no. 20, p. 203501, 2007.

[36] M. N. Feiginov and D. R. Chowdhury, "Experimental demonstration of resonant-tunneling-diode operation beyond quasibound-state-lifetime limit," *J. Phys. Conf. Ser.*, vol. 193, p. 012016, Nov. 2009.

[37] S. Suzuki, A. Teranishi, K. Hinata, M. Asada, H. Sugiyama, and H. Yokoyama, "Fundamental oscillation up TO 831 GHz in GaInAs/AlAs resonant tunneling diode," in *2009 IEEE International Conference on Indium Phosphide & Related Materials*, 2009, pp. 192–195.

[38] N. Orihashi, S. Suzuki, and M. Asada, "One THz harmonic oscillation of resonant tunneling diodes," *Appl. Phys. Lett.*, vol. 87, no. 23, p. 233501, 2005.

[39] S. Suzuki, A. Teranishi, K. Hinata, M. Asada, H. Sugiyama, and H. Yokoyama, "Fundamental oscillation up to 831 GHz in GaInAs/AlAs resonant tunneling diode," in *2009 IEEE International Conference on Indium Phosphide & Related Materials*, 2009, pp. 192–195.

[40] F. Thrower and G. M. Hayashibara, “Millimeter-Wave Silicon IMPATT Sources and Combiners for the 110-260 GHz Range,” in *MTT-S International Microwave Symposium Digest*, 1981, vol. 81, pp. 344–346.

[41] M. I. Maricar, A. Khalid, J. Glover, G. A. Evans, P. Vasileious, C. Li, D. Cumming, and C. H. Oxley, “Extraction of second harmonic from the In0.53Ga0.47As planar Gunn diode using radial stub resonators,” *Solid. State. Electron.*, vol. 99, pp. 38–40, Sep. 2014.

[42] M. I. Maricar, J. Glover, G. Evans, D. Cumming, and C. Oxley, “Design and characterization of a novel diamond resonator,” *Microw. Opt. Technol. Lett.*, vol. 56, no. 7, pp. 1691–1693, Jul. 2014.

[43] T. Xueping, “Equivalent circuits of a planar Gunn diode,” De Montfort University, 2013.

[44] D. S. R. C. and C. H. O. Mohamed Ismaeel Maricar, James Glover, Ata Khalid, Chong Li, G Evans, “An AlGaAs/GaAs based planar Gunn diode oscillator with a fundamental frequency operation of 120GHz,” *Microw. Opt. Technol. Lett.*, 2014.

Chapter: 2

Overview of theplanar Gunn diode

2.1. OVERVIEW OF GUNN DEVICES

J.B. Gunn made an observation related to the effect of high electric fields on bulk semiconductor materials. He noticed current instability at microwave frequency ranges on a thin slab of n-type gallium arsenide (GaAs) when the electric field exceeded a certain critical threshold value of 35kV/cm[1,2,3]. Kroemer later was able to successfully explain Gunn's discovery using the transferred electron effect[4]. This discovery led to the possibility of replacinghigh voltage and bulky vacuum microwave sources by a simpler low voltage solid state source.

2.2. THEORIES BEHIND GUNN'S DISCOVERY

J.B. Gunn was studying the noise properties of gallium arsenide (GaAs) under the condition of a high electric field when he observed that coherent oscillation occurred in some of the GaAs devices when the field exceeded a critical voltage. Subsequently, he observed a similar effect in indium phosphide (InP). This empirical discovery founded the development of an active semiconductor device known as theGunn diode. It was Ridely and Watkins[5]who gave a proposal in 1961 that contained the essential details of the explanation of Gunn's observation in the so-called transferred electron effect. The transferred electron effect utilizes the relationship between the electron drift velocity and the electric field which is shown in**Figure 2.1. Figure 2.1**shows the drift velocity increasing with the electric field and passing through a maximum (the peak velocity v_p) at a threshold or critical electric field E_t.Beyond E_t there is a region of negative-differential mobility and the drift velocity falls asymptotically towards the valley velocity v_v. This behaviour is a consequence of particular properties of the conduction band structure and electron transport properties in some III-V materials for exampleGaAs and InP.

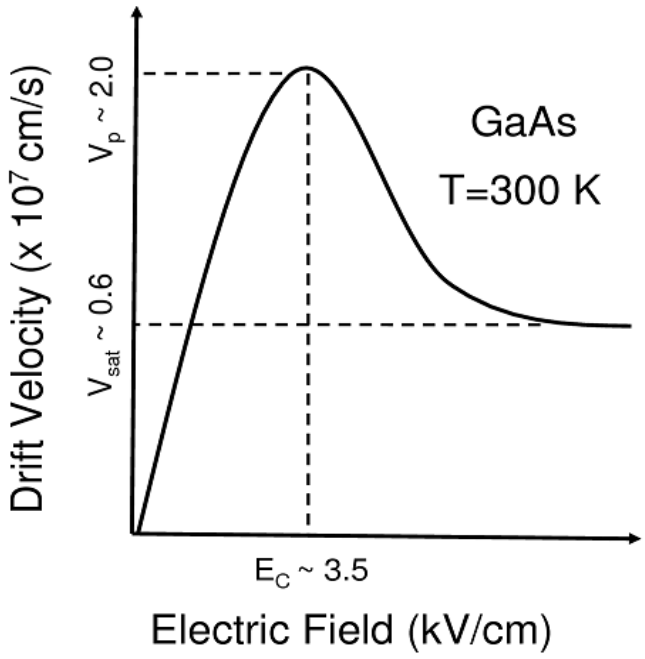

Figure.2.1 Velocity-field characteristics of electron in GaAs (Solid line)[6]

In 1963 Gunn observed that on the application of a high voltage (8-16 V) across a piece of n-type bulk semiconductor, oscillations in the current occur[6]. **Figure 2.2** shows the current waveform generated across an n-type gallium arsenide (GaAs) slab of thickness 25μm, when it was biased by a 16V voltage pulse. The observed frequency of the oscillation was 4.5 GHz,which was approximately the transit time of the electrons travellingacross the thickness of the slab.

However, Gunn was unable to give an explanation as to the cause of the oscillations. It was Kroemer who provided the explanationthat the current oscillations and negative differential resistance (NDR) were the result of a transferred electron effect. [4]

Gunn initially disagreed with the concept of thetransferred electron effect theory, as the physical mechanism of the observed oscillations in current[1].Kroemer maintained his belief of the concept of the transferred electron effect and he also suggested that charge domains should be observed with the transit time period,which would explain the observed Gunn effect[7]. Later, Heek's[8] experiments on electric field domains substantiated Kroemer's explanation[4]. The theory of the Gunn Negative Differential Resistance (NDR's) and current oscillation has been widely accepted after Heek's experiment and Kroemer's explanation.

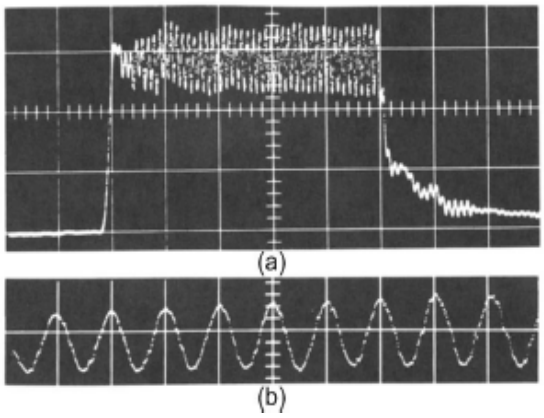

Figure.2.2. Current waveform reported in Gunn papers[6]**.**

After the explanation of the Gunn effect there was increased research interest in this area and further modes of operation were suggested other than the transit time mode oscillation. For example, Carroll[9] observed an oscillation named as the quenched domain mode where the frequencies and DC-RF conversion efficiency is significantly higher than the transit time mode of oscillation. Other modes of oscillation were also reported in 1968 by Copeland[10],thesewere known as the limited space-charge accumulation (LSA) and hybrid mode. In the LSA mode only the NDR characteristic is used and the current oscillation frequency is controlled by the circuit [10], [11] whereas in the hybrid mode the oscillation is due to a combination of transit time and the LSA mode[12].Simple comparison of the oscillation modesaregiven in ***Table 2.4*** and also an explanation of different modes is given in section 2.6.

2.3. BASIC PROPERTIES OF GaAs

In late 1960s to early1970s researchers were interested in the development of Gunn diodes. Many areas of the Gunn diode have been studied and investigated, which include alternate material properties, numerical and analytical investigation of the transferred theory to enable further potential applications of devices utilising the Gunn effects. In addition to the GaAs and InP materials which were reported by Gunn, other materials also have been studied which include germanium (Ge) [13], Indium antimonide (InSb)[14], cadmium telluride (CdTe)[14], and gallium arsenide phosphide (GaAsP) [15]. GaAs and InP were studied because of the high RF performance, device stability, easy of fabrication and low cost when compared to the other semiconductor materials.Recently, in 2008 Oktay Yilmazoglu et all [16]have

simulated a Gunn diode and observed bias oscillation in gallium nitride (GaN) Gunn diodes, the threshold field was 150 kW/cm and estimated drift velocity was 1.9×10^7 cm/sgiving possibilities of high frequency and high power Gunn diodes [16], [17].

The compound structure of GaAs and InP is shown in **Figure 2.3.**Gallium arsenide consists of gallium and arsenic atoms whereas indium phosphide consists of indium and phosphide atoms. Some of the basic material properties of GaAs, InP and GaN are shown in ***Table 2.1.***As far as this is work is concerned, GaAs and InP were chosen to design and fabricate Gunn diodesbut in a novel planar configuration.

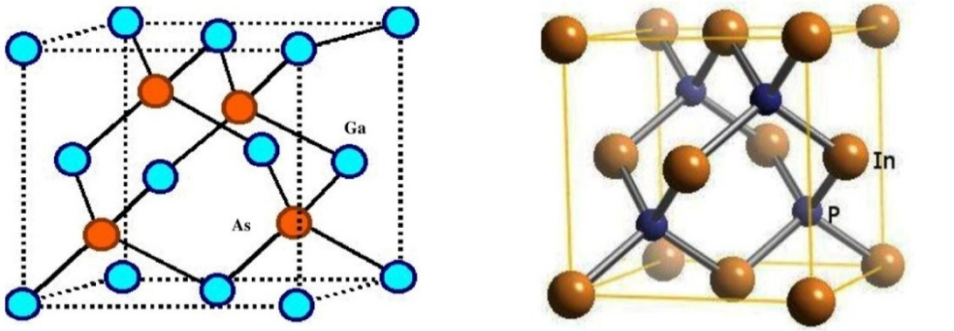

(a) GaAs consists of gallium and arsenic **(b) InP consists of indium and phosphide**

Figure.2.3. Bonding arrangement of GaAs and InP [17]

Parameter	**GaAs**	**InP**	**GaN**	
Crystal Structure	*Zinc blende*	*Zinc blende*	*Wurtzite*	*Zinc blende*
Lattice constant	*5.6532*	*5.8687*	*3.16-3.19(x) 5.12-5.19(z)*	*4.52(x)*
Thermal Conductivity (W/cm*C)	*0.55*	*0.68*	*1.3*	*1.3*
Breakdown field (V/cm)	4×10^5	5×10^5	3.3×10^6	5×10^6
Low field mobility (cm^2/V*s)	*8500*	*5400*	*440*	*1000*
Band Gap at 300 K(ev)	*1.424*	*1.344*	*3.39*	*3.2*
Energy separation between L and Γ valleys	*0.29*	*0.53*	*4.5-5.3*	*1.6-1.9*
Dielectric constant (Static)	*12.9*	*12.5*	*8.9*	*9.7*
Dielectric constant (high frequency)	*10.89*	*9.61*	*5.35*	*5.3*
Effective electron mass in the central valley	$0.63m_0$	$0.08m_0$	$0.2m_0$	$0.13m_0$
Electron affinity (eV)	*4.07*	*4.38*	*4.1*	*4.1*

Table.2.1. Showing a comparisons ofthe parameters of GaAs, InP and GaN

There are three important characteristics of semiconductors which are required to enable the generation ofGunn oscillations and these are listed below along with **Figure 2.4**showing the required energy band structure.

- In the semiconductor, the band gap must be greater than the inter valley band discontinuity to avoid avalanche breakdown before the onset of NDR[5].
- The inter valley discontinuity must be several times higher than the lattice temperature kT (approximately 0.027 eV) so that electron inter valley transfer is not due to a temperature effect [18].
- The effective mass of the electron in the satellite valley must be heavier than in the central valley, therefore the mobility of the electron in the satellite is lower than the central valley

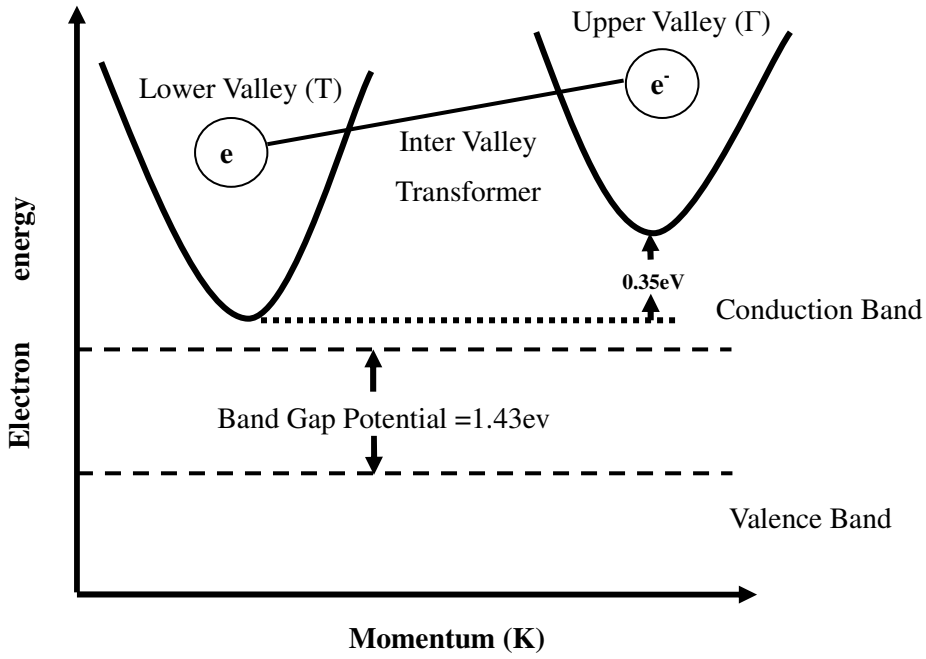

Figure 2.4 Band structure required for the Gunn effect

2.4. ELECTRON TRANSPORT IN SEMICONDUCTORS

There are many factors which occur during the transport of carriers (electrons and holes) from valence band to conduction band, and some of these factors will be briefly discussed.

2.4.1. DRIFT

In a semiconductor the magnitude of the drift velocity (v_{drift}) is dependent on the electric field (E)and it is small when compared to the magnitude of the thermal velocity ($v_{thermal}$). In GaAs most of the electrons remain in the Γ-valley at room temperature (300 K). The thermal velocity ($v_{thermal}$) can be calculated by using equation 2.1 [19]

$$v_{thermal} = \left(\frac{3kT}{m_{eff}}\right)^{\frac{1}{2}} \tag{2.1}$$

where k is the Boltzmann constant, T is the lattice temperature and m_{eff} is the effective mass.

Electron movement is randomat thermal equilibrium therefore the net drift velocity of the electrons is zero and no net current flows through the crystal. When a small electric field is applied across the semiconductor, the randomly scattered electrons will align to the direction of the electric field and they will travel at a combined thermal velocity and induced drift velocity in the direction of positive potential until theycollide with other atoms of the lattice. The drift velocity (V_{drift}) is given by[19] as

$$v_{drift} = \left(\frac{q\tau_c}{m_{eff}}\right) E \tag{2.2}$$

where τ_c represents the free time between the collision, m_{eff} the effective mass of the electrons and n the number of electrons respectively.Also, it can be seen that the drift velocity is directly proportional to the applied electric field (E) by a constant of μ which is known as the electron mobility and can be written as

$$\mu = \frac{q\tau_c}{m_{eff}} \tag{2.3}$$

2.4.2. DIFFUSION

In a semiconductor, the diffusion current only occurs when there is a flow of electrons or holes from a region ofhigher to lower carrier concentrationresulting in the diffusion current (J_n). This diffusion current will occur until there is equilibrium of carrier concentration in the two regions. A diagram representing the diffusion cur-

rent is shown in **Figure**. **2.5**. The diffusion current can be represented as a flux $F_n$and it is directly proportional to the gradient concentration[20].

$$J_n = -qF_n \tag{2.4}$$

$$F_n = -D_n \nabla n \tag{2.5}$$

In the above equation D_n represents the diffusion coefficient and $\nabla\eta$ represents the gradient concentration. The above equation can be rewritten to represent the diffusion current density for n-GaAs substrate.

$$J_n = q\, D_n \nabla n \tag{2.6}$$

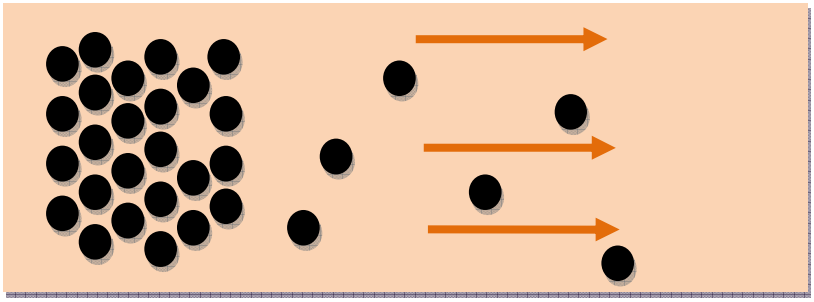

Figure2.5 Diffusion in a semiconductor substrate

2.4.3. IMPACT IONISATION

In the Gunn diode, an increase in the applied voltage will increase the current flowing in the diode, however when the threshold voltage (Vt) is reached the current will start to decrease and the negative resistance region is entered.**Figure 2.6**alsoshows that the current will continue to decrease until at a given applied voltage it starts to rise again. At the breakdown (V_B) it rises more steeply; this process is due to a high electric field phenomenon giving rise to impact ionisation. This process is also known as an avalanche process. The impact ionisation occurswhen electrons have sufficiently high kinetic energy to cross the band gap. The electrons attain a sufficiently high kinetic energy that when they collide with the lattice, a bond is broken and an electron-hole pair generated. This process will continue giving rise to a multiplication of electron hole pairs.A schematic of the avalanche processes is shown in the **Figure 2.7.** The number of electron-hole pairs (G_a) can be calculated using equation 2.7[21].

$$G_a = \frac{1}{q}\left(\alpha_n |J_n| + \alpha_p |J_p|\right) \tag{2.7}$$

where α_n and $\alpha_p$represent the electron and hole ionisation rates,and J_n and $J_p$are the electron and hole current densities.

Theavalanche breakdown process is directly utilised in impact ionization avalanche transit time (IMPATT) diodes, which are used in high frequency and high power oscillators [22], and are not part of this work.

With reference tothe Gunn diode, the impact ionization will occur only if the electron gains sufficient energy from the high electric field tocross the energy band gap between the valence band and conduction band. This process can give rise to Gunn oscillations becoming incoherent [21]. This impact ionisation effect can be minimised by placing the Schottky contact on the anode contact of the diode, the electron density will be reduced due to extension of the Schottky contact thereby reducing the impact ionisation effects [23].

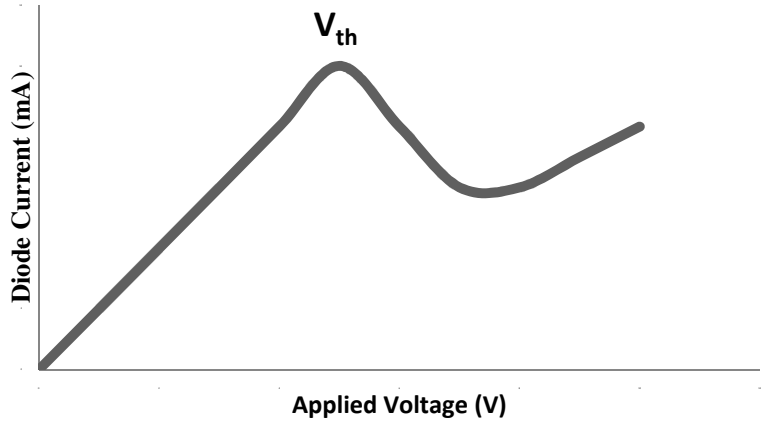

Figure.2.6. Current versus voltage of GaAs

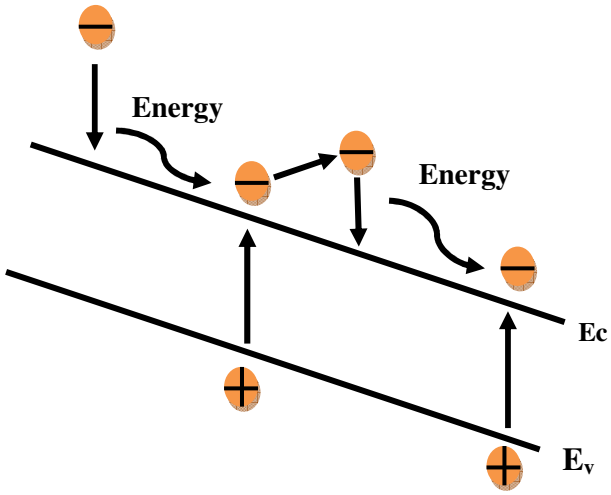

Figure.2.7 Schematic view of impact ionisation

2.4.4. RELAXATION TIME

The energy relaxation time for electrons in the lower valley has been measured directly by (Glover in 1973)[24] using an applied field varying at 140 GHz. At this frequency it was found that the ac current produced differed from that expected from knowledge of the low frequency differential conductivity. This enabled a value of relaxation time for the lower valley to be obtained τ_t = 1.0 X 10^{-12} sec. The corresponding value for the upper valley has also been calculated by Conwell and Vassell in 1966[25] using a deformation potential. Their result was $\tau_t = 10^{-14}$ sec. They also calculated the values of Γ – X transitions using a deformation potential. It appears to be a higher value when compared to the previous work reported by Tarnay and Begovich [26], [27]. More accurate results were given by Ruch in 1970s[28], their results are $\tau_{(\Gamma - X)}$ = 2.0x 10^{-14} secandare $\tau_{(X-\Gamma)}$ = 5.0 x 10^{-13} sec respectively.

The X-Γ transition is slower on account of the much lower density of electron states in the Γ minimum. The computed relaxation time suggests that the maximum frequency of operation of a gallium arsenide Gunn diode is approximately

$$f_{\max} = \frac{1}{2\pi\tau_t} \approx 150 \text{ GHz} \tag{2.8}$$

The highest frequency so far reported experimentally in a GaAs planar Gunn diode[29]is 108 GHzwhereas for a hetero junction AlGaAs planar Gunn diode the maximum experimental frequencyreported todate is218 GHz[30].

2.5. DIFFERENT TYPES OF OSCILLATION MODES IN GUNN DIODES

2.5.1. GUNN DOMAIN FORMATION AND TRANSIT TIME MODE OF OSCILLATION

Section 2.3. and 2.4. briefly describes the mechanism of the transfer electron theory. The physical mechanism of transfer electron theory isoften called the Gunn effect. The Gunn diode utilises the Gunn effect. A Gunn diode is a two terminal device and it is normally fabricated from GaAs and has a nonlinear IV characteristic,

which exhibits a negative resistance. The IV curve is shown in **Figure 2.1**which depicts a negative resistance region, which is seen as a current drop with a voltage increase. The coherent oscillations are produced in the NDR region. The oscillation is due to the formation and disappearance of the travelling space charge domains [4]. Later Gunn conducted a test experiment on a large GaAs substrate and found that high electric field domains are formed near the cathode contact with current reduction[7]. These domains then travel towards the anode, where the domains will nucleateand the current will return to a normal level. These high electric field domains are called Gunn domains. Once a domain disappears in the anode another domain is formed near the cathode contact. This successive formation of Gunn domains will give rise to the RF oscillations.The frequency of oscillation therefore depends on the distance the domain needs to travel from the cathode to the anode. The formation and disappearance of Gunn domainsis shown in the **Figure 2.8.**

These NDR oscillations can also be explainedusing the energy band structure of GaAs.The shape of the conduction band is a curve containing several distinct valleys as shown in the **Figure 2.9.** The figure also shows the energy band structures of GaN and InPare similar [31]. The band structure of the GaAs is quite complex but for realistic electron energies (E ≈ 2eV) only the lowest conduction band needs to be considered [32]. The effective mass of an electron, m_{eff} is given by

$$m_{eff} = \left(\frac{d^2 E_e}{dp_e^2}\right)^{-1} \tag{2.9}$$

where: E_e is the electron energy, and $p_e$is momentum

In GaAs, theslope of the central valley aremuch sharper than the satellite valley; this represents the effective mass of an electron in the satellite valley being greater than in the central valley. Due to the larger effective mass of an electron in the satellite valley, the mobility of the electron will be much less when compared to the central valley. Electrons will stay in the central valley (Γ-valley) only whenno bias voltage is applied as they will not have sufficient energy to reach the higher satellite valley which is called the L-valley. When a bias is applied tothe device, some of the electrons in the central valley gain sufficient energy and will transfer into the satellite valley. Lower average drift velocity only occurs if the transferred electrons have high effective mass and therefore lower electron mobility.Negative differen-

tial resistance (NDR) will be created where the current decreases as the voltage increases. In the NDR region, Gunn domains will be formed which are clearly shown in **Figure 2.8**. These arise due to a small disruption in the net charge of a domain. This is caused bythe electric field distribution giving rise to the lower drift velocity at different points in the sample. Because of this effect, electrons at some point will travel faster when compared to electrons at another point giving rise to building up of electrons forming the Gunn domain[10,11,12].

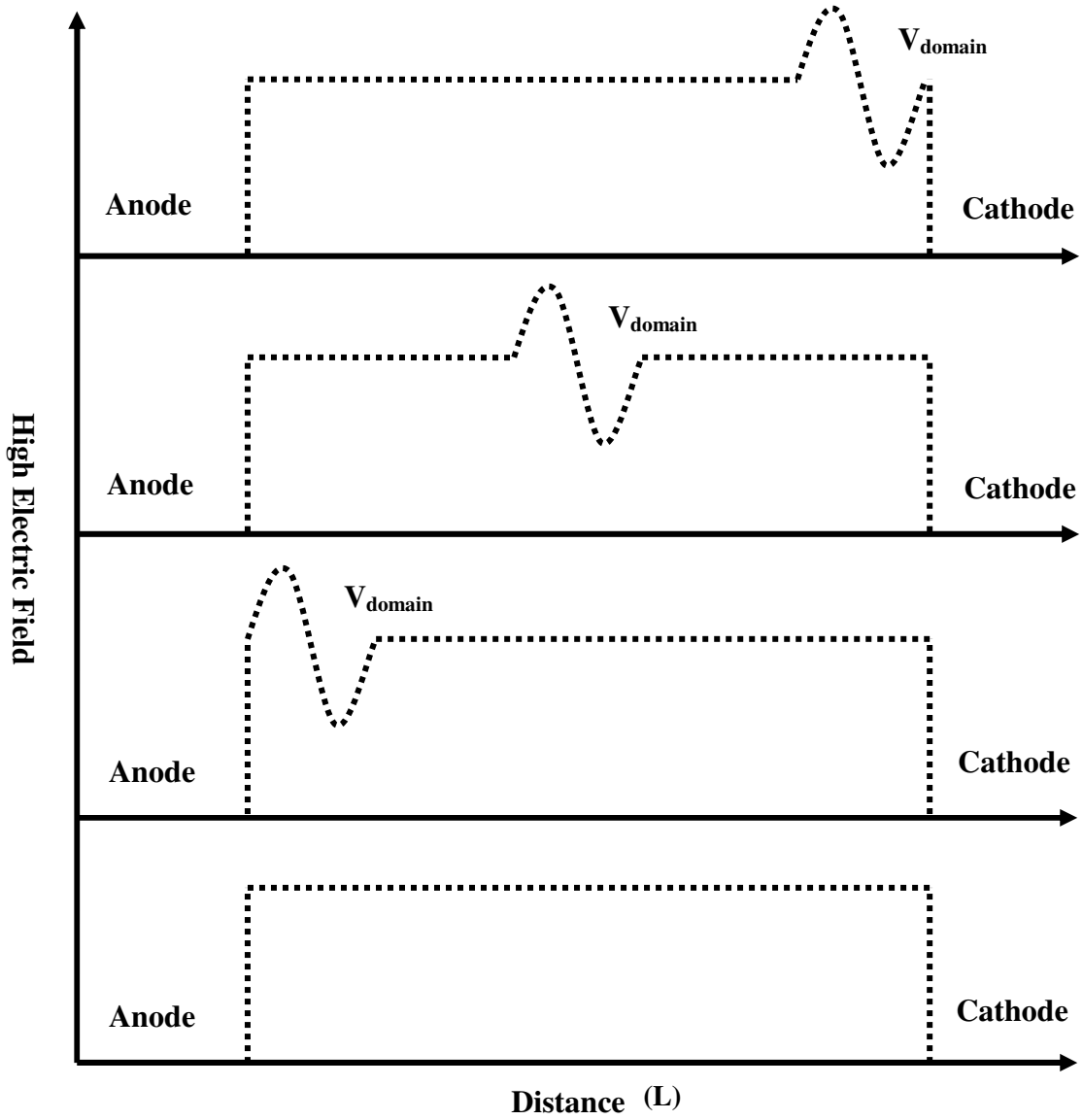

Figure.2.8. Domain formation in Gunn diode

The frequency of oscillation is determined by the distance travelled by the Gunn domain or the ratio of domain velocity ($V_{domains}$) to the distance*L*, given in equation

2.10. The DC bias will affect the drift velocity of the domain and so will also have an effect on the oscillation frequency.

$$f = \frac{V_{domain}}{L} \tag{2.10}$$

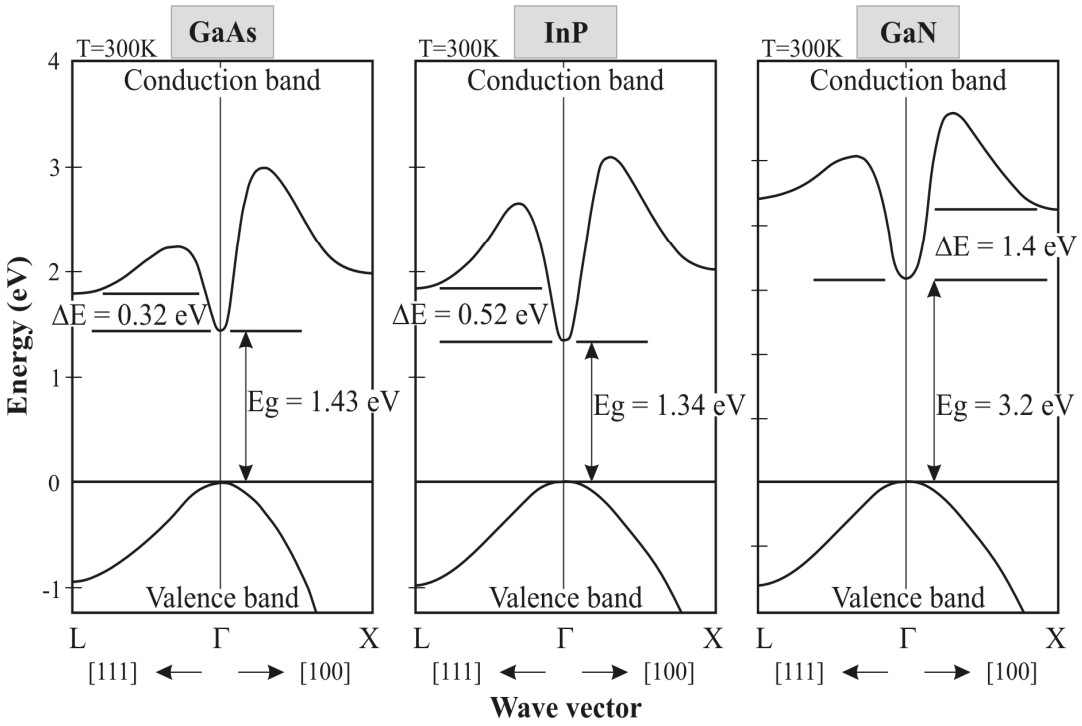

Figure.2.9. The band structures of GaAs, InP and GaN[31]

2.5.2. LIMITED SPACE CHARGE ACCUMULATION MODE OF OSCILLATION

Copland[11] investigated the modes of oscillation in a Gunn diode by using a bulk negative resistance operated in series with two parallel tuned circuits and a load resistance which is shown in **Figure 2.10**. Later in the 1960s, Copland found oscillation in the limited space charge accumulation (LSA) mode [35]. There are three important characteristics of LSA mode which are described below [36]

- The frequency of operation is mainly determined by the frequency of the circuit.
- The frequency of operation is reciprocal to the carrier transit time
- Power and efficiency of the device are equal or higher than the same device which is operated in the transit time mode oscillations.

The main principle of the LSA mode is to restrict the Gunn domain formation in the

channel where the Gunn diode is biased in the NDR region. If the period of oscillation is equal or greater than the dielectricrelaxation time, additional space charge distribution will not build up until the field across the diode decreases into the positive region. This is described by [36]

$$\frac{1}{f} \leq 3\varepsilon \frac{1}{n} |\mu_n| e \tag{2.11}$$

where ε is the permittivity of the substrate, *f* is the frequency, e is the electron, n is the doping level and μ_n is the average negative resistance

In order to make the Gunn diode work in the LSA mode, the ratio of operating frequency and the doping level should be within acertain range and the tuned circuits must be loaded so that the voltage across the diode drops below the threshold voltage for each cycle. For GaAs Gunn diodes, the LSA mode can be observed only if the voltage is twice or higher than the threshold voltage and the ratio of operating frequency to the doping level should be $2 \times 10^4 \geq \frac{n}{f} \gg 1.4 \times 10^3$ $(\mathrm{sec/cm^3})$[8,30].

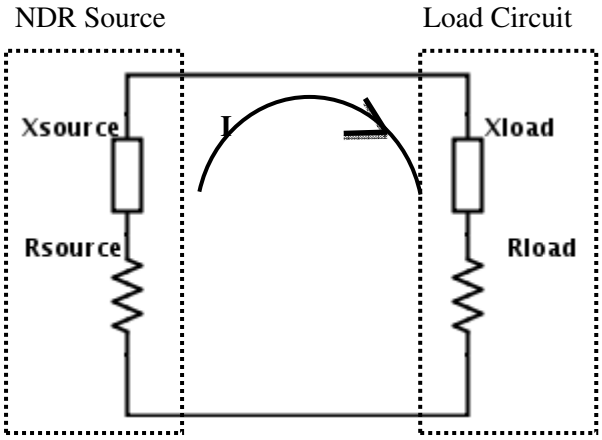

Figure.2.10. Schematic view of the parallel circuit for LSA mode

2.5.3. QUENCHED DOMAIN MODE OF OSCILLATION

Carroll reported in [9], the quenched domain mode oscillation which is completely determined by the electrical resonant circuits. Like the transit time mode of oscillation, in the quenched domain mode the Gunn domain is also formedand will travel towards the anode but before reaching the anode the domains will be quenched. The travel distance of these domains will be shorter than the transit time mode. When compared to the transit time mode, the oscillation frequency of the Gunn di-

ode will be higher. Carroll also reported that the oscillation frequency from a single Gunn diode can be produced from 2 GHz to 31 GHz when placed in different resonant circuits as summarised in***Table 2.2***.[9]

Frequency (GHz)	2	3.9	8	9.4	22	31
Power (mW)	NG	150	50	12	1	0.1

Table.2.2. Oscillation frequency and power level for a Gunn diode[7]

In 1969, Thim and Kurokawa[37] analysed the efficiency of the Gunn diode by varying the doping level in the GaAs active layer which is shown in the ***Table 2.3***[37]**.**The active layer of the Gunn diode is shown in **Figure 2.11.**In this experiment, the sample length (L) was chosen to be large enough to form the domains (approximately L =70 μ) and the donor density (n_o) is varied from $6*10^{14}$ $cm^{-3}$to $1*10^{7}$ cm.Later they found that, if the Gunn diode is to work in the quenched domain mode the doping level multiplied by its active length L should be greater then 10^{12} cm^{-2}($n_oL < 10^{12}cm^{-2}$).

Doping level (n_o)	Bias Voltage (V)	Load resistance (R_o)	Efficiency of the Gunn diode
10 %	3	30	10%
50%	3	30	5.5%
80%	3	30	None
10%	3	20	13%

Table.2.3. Oscillator efficiency with doping gradient

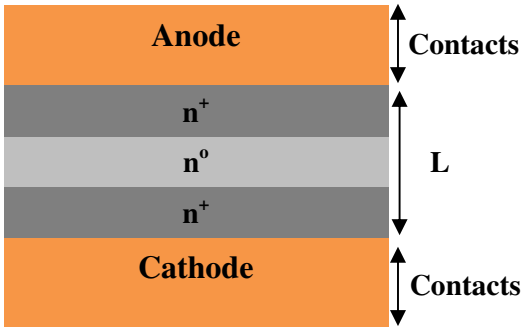

Figure.2.11. Active layer of the Gunn diode

2.5.4. DELAYED MODE

This mode has a shorter transit time than the time domain transit time. So the domain will reach the transit time well in advance and the next domain will be formed

only when that domain reaches the threshold voltage. The efficiency of this mode is greater than the transit time mode and is about 20% higher [38]–[40]. This mode is otherwise called the inhibited mode.

2.5.5. COMPARISON OF OSCILLATION MODES

In this section a comparison of oscillation modesin GaAsmaterial is presented as***Table 2.4***.

	Transit Time Mode	**LSA**	**Delayed Mode**	**Quenched Domain Mode**
fL(cm/s)	10^7	$fL > 2*10^7$	$10^6 < fL < 10^7$	10^7
Efficiency	10 %	20 %	20 %	13 %
Domain Formation	Domain reaches the anode	Prevent the formation of domain	Domain reaches the anode after the transit time	Domain collapses before it reaches the anode
Power	Low Power	High power	-	-
Resonant frequency	No external circuits	Circuit	No external circuits	Circuit
Time	$T = T_t$	$T > T_t\ 3T_d$	$T > T_t$	$T < T_t$
Waveform	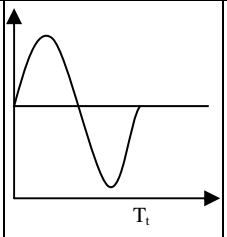	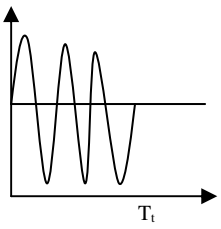	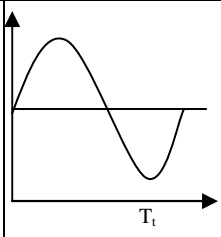	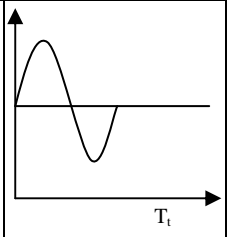

T= Oscillation Period; T_t = transit time and T_d = dielectric relaxation time

Table.2.4. Comparison of Gunn Modes[8,10,27,34]

2.6. FABRICATION OF A GUNN DIODE

BasicGunn diodes are fabricated from GaAs and consist of three layers, two highly doped contact regions which are separated by a relatively low doped transit layer. This forms an n^+nn^+ structure as shown in the **Figure 2.12 (a)**. Normally to fabricate a Gunn diode, vapour phase epitaxial (VPE) growth techniques are used. For a planar Gunn diode, the molecular beam epitaxy process (MBE) is used. The individual Gunn diodes and contacts can then be defined by standard photolithographic and etching procedures whereas for the planar Gunn diode, electron beam lithography (EBL) is used.

As already mentioned in the previous section, the frequency of the oscillation mainly depends on the Gunn domains travelling across the transit layer. Therefore the frequency of oscillation depends on the length of the transit region of the diode. When the electrons are initially injected into the cathode they remain in the Γ-valley(**Figure 2.4)**and do not instantly gain enough energy to transfer to the low mobility satellite valley (L-valley), so there will be a delay in formation of the domain. Hence when a bias is applied to the diode there will be a formation of a dead zone by the cathode region, which will reduce the output power [37] and efficiency of the diode. It will also reduce the transit length, thereby slightly increasing the operating frequency of the Gunn diode.Equation 2.13 shows how the frequency of the Gunn diode is changed when a dead space (L_{dead}) is present [17].

$$f = \frac{v}{L_{ac} - L_{dead}} \tag{2.13}$$

where L_{ac} represents the length of the anode and cathode and
L_{dead} represents the dead zone of a Gunn diode.

One of the methodsto reduce the dead spaceis to use a doping notch which is shown in **Figure 2.12 (b).**The notch will produce a high electric field in the cathode contact of the Gunn diode. Thehigh electric field will accelerate the carriers to a higher velocity in a shorter distance thereby gaining more energy to transfer to the satellite valley more quickly. Another method is to inject high energy electrons(hot electrons) directly to the transit region, which can be done using a graded-gap Gunn diode as shown**Figure 2.12(c)** 'Hot electrons' are injected withenough energy to jump from the Γ-valley directly into the L-valley. Thisresults in domain formation very near to the cathode allowing it to growalmost instantly.

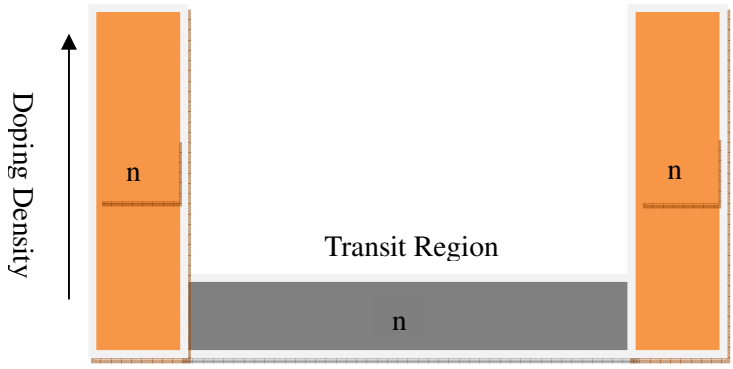

Figure.2.12 (a) Structure of a conventional vertical Gunn diode

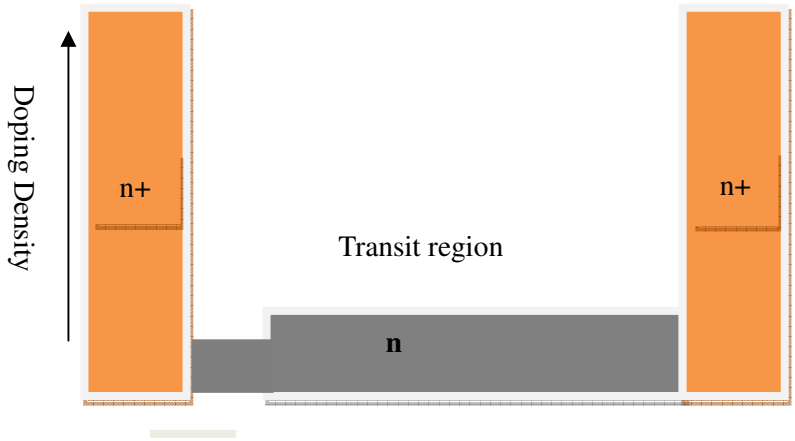

Figure.2.12 (b) Structure of a conventional vertical Gunn diode with a doping notch

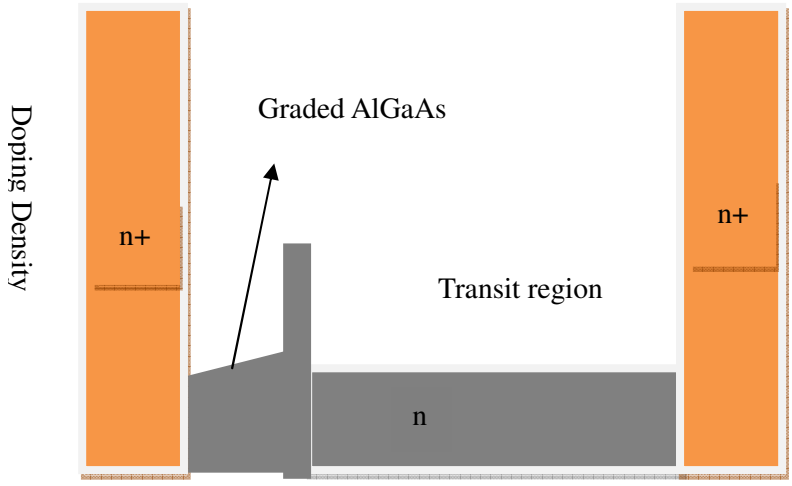

Figure.2.12 (c) Structure of graded gapvertical Gunn diode

2.7. DEVELOPMENT OF THE PLANAR GUNN DIODE

In this section the planar Gunn diode will be described. The classification of vertical and planar Gunn diode is made regarding the direction of current flow through the epitaxial layers of the devices. **Figure 2.13 (a)** shows that the operation of the vertical Gunn diode; it can be clearly seen that the current flow is perpendicular to the epitaxial layers. For the planar Gunn diode it is parallel to the epitaxial layer which is shown in **Figure 2.13 (b)**. The planar Gunn diode geometry was first proposed by Haydl [41]. However, the development of metal semiconductors field effect transistor (MESFET) overtook the development of the Gunn diode. In 1970s the research on the MESFET rapidlygrew because it could be easily integrated into

planar technologies unlike the vertical Gunn diode. Also, multi-stage wide-band amplification was more easily obtained using MESFETswhen compared to using Gunn diodes in a reflection amplifier configuration.

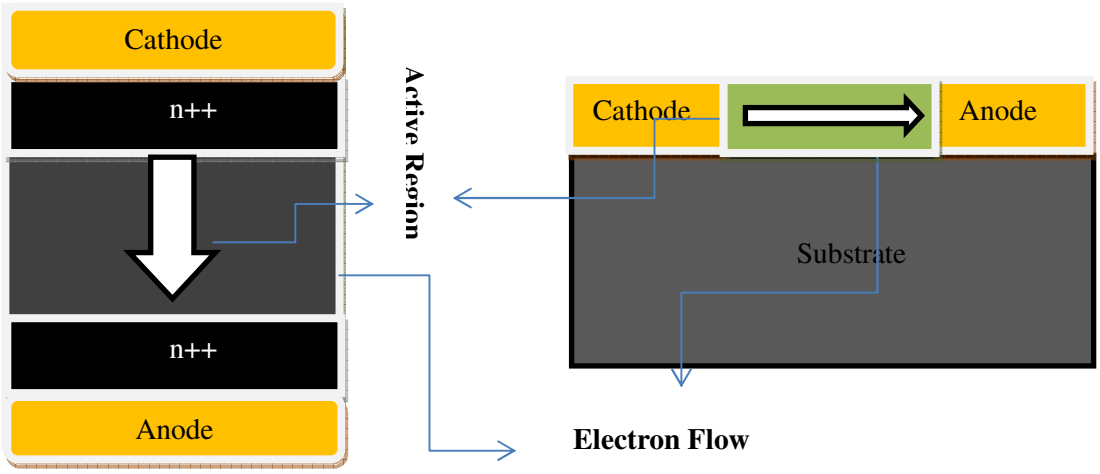

Figure.2.13. Schematic view of Gunn diode (a) vertical Gunn diode (b) planar Gunn diode [31]

Therefore the development of the Gunn diode slowed up and was only used in specialised applications for example the 77GHz microwave source for automotive cruise control [42].In 2005, Geoffrey Dunn proposed a Monte Carlo simulation for the Gunn diode [43], [44] and in 2007 Khalid and Dunn[45]produced a working model of a planar Gunn diode, which operated above 100 GHz [45]. The planar Gunn diode geometryenables fabrication and integration as an active element in microwave monolithic integrated circuit (MMIC) technologies. The planar Gunn device has lot of advantages when compared to the conventional vertical Gunn device. For example, the distance between the anode and cathode, will determine the frequency of operation of the device, this distance can be controlled during the fabrication process.Hence Gunn diodes with different frequenciescan be fabricated on the same chip.

Planar technology enables greater flexibility in adjusting the anode and cathode distance and therefore the oscillation frequency. However, more important devices with different operating frequencies can be fabricated on the same process wafer.The distance between the cathode and anode can be reduced to sub-micron

lengths using electron beam lithography, thereby giving the potential of planar Gunn diodes working to tera-hertz frequencies. The planar Gunn diode is also compatible withplanar coplanar waveguide technology. A schematic view of a coplanar waveguide is shown in **Figure 2.14.** Therefore it can be fabricated as the signal source and integrated to form a monolithic microwave integrated circuit (MMIC). A planar Gunn diode allows on wafer integration which will increase the number of applications of the Gunn diode,whereas a vertical Gunn diode has to be integrated with separate discrete components.. The on wafer integration will also enable the planar Gunn diode to be moresuitable for very high frequencies.

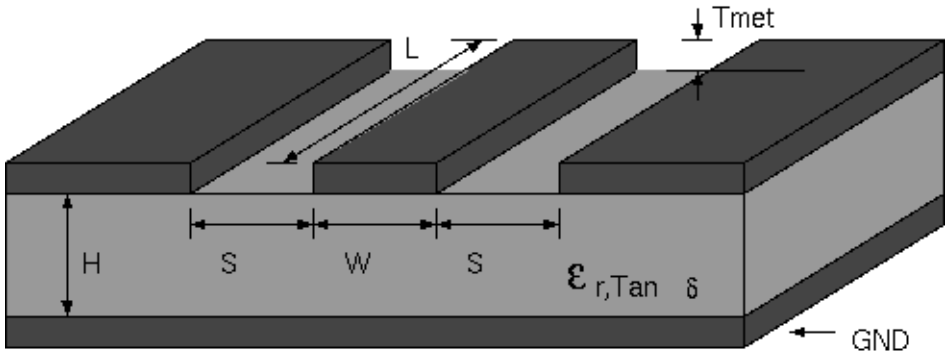

Figure.2.14. Schematic view of the coplanar waveguide[31]

The planar Gunn diode will enable sources operating at different frequencies to be fabricated on a single MMIC circuit. Whereas in conventional vertical Gunn diodes once the wafer is grown, the anode and cathode separation (L_{ac}) is fixed thereby fixing the transit time which is shown in **Figure 2.15**. The planar Gunn diodes also have some disadvantages including lowerRF power and higher phase noise[31]. However, theplanar structure will allow combining large numbers of devices to improve the power performance of the device[46].

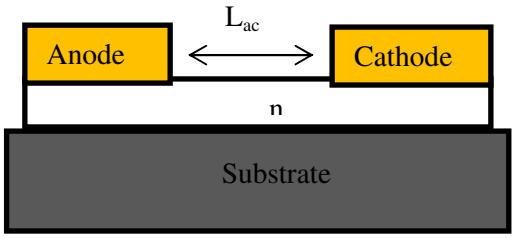

Cross sectional view of Planar Gunn diode with ideal contacts

Figure.2.15. Gunn diode with metal alloyed Ohmic contacts

Some of the properties of planar Gunn diodes compared to vertical Gunn diodes are summarisedin the ***Table 2.5***[47]

Vertical Gunn Diode	Planar Gunn Diode
Frequency is determined by the active layer	Frequency is determined by the electrode geometry
Difficult to integrate into a planar technology	Device can be integrated easily with planar technology
Current flow is perpendicular to the epitaxial layers.	Current flow is parallel to the epitaxial layer
Device operating at only one frequency can be fabricated on a process wafer	Device operating at different frequencies can be fabricated on a process wafer
Anode and cathode gap cannot be changed	Anode and cathode gap can be changed
High RF power	Low RF power
Difficult in fabrication and high cost	Easy in fabrication and low cost
Difficult in combining the device	In theory large number device can be combined to increase the power performance

Table.2.5 Comparison of Planar Gunn diode and vertical Gunn diode

2.8. NEW DEMANDS AND CHALLENGES FOR PLANAR GUNN DEVICES

Conventional vertical Gunn diodes are restricted to oscillation frequencies of approximately 100 GHz for GaAs, and 150 GHz for InP due to the energy relaxation time and inter valley relaxation time [48]. Conventional vertical Gunn diodes are further limited in frequency by their geometry, fabrication processes, doping levels and heating problems [48]. These limitations may be overcome in a planar Gunn diode [43]. The oscillation frequency can be controlled by varying the distance between the anode and cathode contacts. If the output power at the fundamental frequency of oscillation is sufficiently high, the extraction of higher harmonic oscillations for sub-millimetre-wave and terahertz operation is possible[29], [49]. To generate high power and high frequency Gunn oscillations, the other option is to use materials that have lower relaxation times, higher mobility and higher energy bandgaps, such as indium gallium arsenide InGaAs and gallium nitride (GaN) [16],

[50].

Research carried out on well-established materials, like (aluminium gallium arsenide)AlGaAs and (indium gallium arsenide) $In_xGa_1As_x$ for higher frequency operation. Experimentally,it has been observed thatby varying the anode and cathode distance in planar Gunn devices, oscillation frequencies can be varied from 100 GHz to 150 GHz for the fundamental oscillation and therefore 200 GHz to 300 GHz for second harmonic and 400 GHz to 600 GHz for third harmonic modeare possible [18,19,20]. To date for the GaAs based material, fundamental oscillation for the planar Gunn diode is 121GHz reported in this work[52], whereas for InGaAs material the fundamental oscillation frequency is 164 GHz [53]. Research on Gunn-like oscillations in selfswitching diodes [54] and nanowire diodes using InGaAs/ indium aluminium arsenide (InAlAs) hetero junction have shown oscillations up to the terahertz frequency range [55] although the major challenges with these devices is to produce sufficient RF power output. So far the highest RF power produced ina GaAs and a InGaAs planar Gunn diodewas around -4 dBm and -10 dBm respectively and for the second harmonics the maximum RF power produced was -26.6 dBm [48,51]. In the end the main challenge will be generating sufficient useful RF power in a planar Gunn diode.

2.9. COMMERCIALISATION AND OTHER DEVELOPMENTS OF GUNN DEVICES

To date the planar Gunn diode is not commercially available and it is anticipated it will provide a low cost frequency source for future applications particularly in integration and high frequency systems. The vertical Gunn is commercially available and is used in a wide range of applications in instrumentation for example, medical imaging, aerospace science, and defence. Primarily because they exhibit good microwave performance, low DC power consumption, moderate RF power, wide frequency tuning range, low phase noise, high temperature stability, and compact size.Self-mixing is also one prominent characteristic of Gunn devices and has been utilised in low cost Doppler modules (traffic control, door openers etc). The self-mixing effect is due to a Gunn diode having nonlinear IV characteristics that allows

an incident RF signal to mix with its own oscillation and produce a frequency difference and a sum.Thus, in a transceiver frontend circuit of a conventional RF system, a Gunn device can replace separate oscillators and mixers as it can provide both local oscillator and mixing function in a single device.

2.10. REFERENCES

[1] J. B. Gunn, "Microwave oscillations of current in III-V semiconductors," *Solid State Commun.*, vol. 88, no. 11–12, pp. 883–886, Dec. 1993.

[2] J. B. Gunn, "Recent work on the direct generation of microwaves in bulk semiconductors," in *1963 International Electron Devices Meeting*, 1963, vol. 9, pp. 24–24.

[3] J. B. Gunn, "Instabilities of Current in III–V Semiconductors," *IBM J. Res. Dev.*, vol. 8, no. 2, pp. 141–159, Apr. 1964.

[4] H. Kroemer, "Theory of the Gunn effect," *Proc. IEEE*, vol. 52, no. 12, pp. 1736–1736, 1964.

[5] B. K. Ridley and T. B. Watkins, "The Possibility of Negative Resistance Effects in Semiconductors," *Proc. Phys. Soc.*, vol. 78, no. 2, pp. 293–304, Aug. 1961.

[6] J. B. Gunn, "Microwave oscillations of current in III–V semiconductors," *Solid State Commun.*, vol. 1, no. 4, pp. 88–91, Sep. 1963.

[7] J.B.Gunn, "Progress in Semicondcutor," in *7th International Conference the physics of semiconductors,Paris,France*, 1964.

[8] J. S. Heeks, "Some properties of the moving high-field domain in Gunn effect devices," *IEEE Trans. Electron Devices*, vol. 13, no. 1, pp. 68–79, Jan. 1966.

[9] J. E. Carroll, "Oscillations covering 4 Gc/s to 31 Gc/s from a single Gunn diode," *Electron. Lett.*, vol. 2, no. 4, p. 141, 1966.

[10] Copeland Lii John, "Self-starting lsa mode oscillator circuit arrangement," US3414841 A, 1968.

[11] J. A. Copeland, "LSA Oscillator-Diode Theory," *J. Appl. Phys.*, vol. 38, no. 8, p. 3096, 1967.

[12] L. A. MacKenzie, "A Gunn diode operated in the hybrid mode," *Proc. IEEE*, vol. 56, no. 7, pp. 1232–1233, 1968.

[13] B. J. Elliott, "Bulk negative differential conductivity and travelling domains in n-type germanium," *Appl. Phys. Lett.*, vol. 11, no. 8, p. 253, 1967.

[14] D. Woode, J. Froom, and G. King, "The Gunn Effect in Polar Semiconductors," no. 1, 1966.

[15] Y. Y. Zhao, C. J. Wei, and H. Beneking, "Transferred-electron oscillations in In0.53Ga0.47As," *Electron. Lett.*, vol. 18, no. 19, p. 835, 1982.

[16] O. Yilmazoglu, K. Mutamba, D. Pavlidis, and T. Karaduman, "First Observation of Bias Oscillations in GaN Gunn Diodes on GaN Substrate," *IEEE Trans. Electron Devices*, vol. 55, no. 6, pp. 1563–1567, Jun. 2008.

[17] E. Alekseev and D. Pavlidis, "GaN Gunn diodes for THz signal generation," in *2000 IEEE MTT-S International Microwave Symposium Digest (Cat. No.00CH37017)*, 2000, vol. 3, pp. 1905–1908.

[18] C. Li, A. Khalid, L. B. Lok, N. J. Pilgrim, M. H. Holland, G. M. Dunn, and D. R. S. Cumming, "Millimeter-Wave Planar Gunn Diodes," in *(Unknown Conference in Sheffield)*, 2010.

[19] M Shur, *GaAs devices and circuits*, Microdevic. New York Plenum Press, 1987.

[20] Alan Doolittle, "Drift and Diffusion Currents," Atlanta, 2000.

[21] S.M.Sze, *Semiconductor Devices; Physics and Technology 2 Edition*. John Wiley & Sons, Inc., 2002, p. 564.

[22] M. Montes Bajo, G. Dunn, A. Stephen, A. Khalid, D. R. S. Cumming, C. H. Oxley, J. Glover, and M. Kuball, "Impact ionisation electroluminescence in planar GaAs-based heterostructure Gunn diodes: Spatial distribution and impact of doping non-uniformities," *J. Appl. Phys.*, vol. 113, no. 12, p. 124505, 2013.

[23] M. Montes, G. Dunn, a. Stephen, a. Khalid, C. Li, D. Cumming, C. H. Oxley, R. H. Hopper, and M. Kuball, "Reduction of Impact Ionization in GaAs-Based Planar Gunn Diodes by Anode Contact Design," *IEEE Trans. Electron Devices*, vol. 59, no. 3, pp. 654–660, Mar. 2012.

[24] G. H. Glover, "Study of electron energy relaxation times in GaAs and InP," *J. Appl. Phys.*, vol. 44, no. 3, p. 1295, 1973.

[25] E. Conwell and M. Vassell, "High-Field Transport in n- Type GaAs," *Phys. Rev.*, vol. 166, no. 3, pp. 797–821, Feb. 1968.

[26] K. Tarnay, "The domain transit time in Gunn-diodes," *Proc. IEEE*, vol. 54, no. 12, pp. 2001–2002, 1966.

[27] N. A. Begovich, "Extension of the Planar Diode Transit-Time Solution," *Proc. IRE*, vol. 37, no. 11, pp. 1340–1344, Nov. 1949.

[28] J. G. Ruch, "Electron dynamics in short channel field-effect transistors," *IEEE Trans. Electron Devices*, vol. 19, no. 5, pp. 652–654, May 1972.

[29] C. Li, A. Khalid, N. Pilgrim, M. C. Holland, G. Dunn, and D. S. R. Cumming, "Novel planar Gunn diode operating in fundamental mode up to 158 GHz," *J. Phys. Conf. Ser.*, vol. 193, p. 012029, Nov. 2009.

[30] A. Khalid, C. Li, V. Papageorgiou, N. J. Pilgrim, G. M. Dunn, and D. R. S. Cumming, "A 218-GHz second-harmonic multiquantum well GaAs-based planar Gunn diodes," *Microw. Opt. Technol. Lett.*, vol. 55, no. 3, pp. 686–688, Mar. 2013.

[31] C. Li, "Design and Characterisation of millimeter-wave planar Gunn diode and integrated circuits," University of Glasgow, 2011.

[32] K. W. Kobayashi, a. K. Oki, L. T. Tran, J. C. Cowles, a. Gutierrez-Aitken, F. Yamada, T. R. Block, and D. C. Streit, "A 108-GHz InP-HBT monolithic push-push VCO with low phase noise and wide tuning bandwidth," *IEEE J. Solid-State Circuits*, vol. 34, no. 9, pp. 1225–1232, 1999.

[33] A. Khalid, C. Li, G. Dunn, N. Pilgrim, and D. S. R. Cumming, "Observation of Multiple Domains in a Planar Gunn Diode," in *Microwave Integrated Circuits Conference, 2009. EuMIC 2009. European*, 2009, no. September, pp. 298–300.

[34] M. Masuda, T. Ogura, J. Koyama, H. Fujioka, T. Hosokawa, and K. Ura, "Analysis of the high-field domain dynamics in a planar Gunn diode by using a stroboscopic SEM," *J. Appl. Phys.*, vol. 50, no. 1, p. 530, 1979.

[35] J. A. Copeland, "Electrostatic domains in two-valley semiconductors," *IEEE Trans. Electron Devices*, vol. 13, no. 1, pp. 189–192, Jan. 1966.

[36] J. A. Copeland, "A new mode of operation for bulk negative resistance oscillators," *Proc. IEEE*, vol. 54, no. 10, pp. 1479–1480, 1966.

[37] H. W. Thim, "Quenched Bulk GaAs Oscillators with Doping Gradients," *J. Appl. Phys.*, vol. 40, no. 2, p. 904, 1969.

[38] S. K. R. Monojit Mitra, *Microwave Semiconductor Devices*. PHI Learning, 2004, pp. 187–190.

[39] Dilip K Roy, *Physics of Semiconductor*. Orient Blackswan, 2004.

[40] Annapurna Das, *Microwave Engineering*. Tata McGraw Hill, 2000.

[41] W. H.Haydl, "Planar Gunn Diodes with Ideal Contact Geometry," *IEEE Electron Device Lett.*, vol. 61, no. 4, p. 1972, 1972.

[42] B. P. Nigel Priestley, "A Compact 77GHz Transceiver Module Using G3D Diode Technology for Automotive Applications," *Springer Adv. Microsystems Automot. Appl.*, no. VDI-Buch 2003, pp. 175–187, 2003.

[43] N. J. Pilgrim, A. Khalid, G. M. Dunn, and D. R. S. Cumming, "Gunn oscillations in planar heterostructure diodes," *Semicond. Sci. Technol.*, vol. 23, no. 7, pp. 1–10, Jul. 2008.

[44] Y. P. Teoh, G. M. Dunn, N. Priestley, and M. Carr, "Monte Carlo simulations of asymmetry multiple transit region Gunn diodes," *Semicond. Sci. Technol.*, vol. 20, no. 5, pp. 418–422, May 2005.

[45] A. Khalid, N. J. Pilgrim, G. M. Dunn, M. C. Holland, C. R. Stanley, I. G. Thayne, and D. R. S. Cumming, "A Planar Gunn Diode Operating Above 100 GHz," *IEEE Electron Device Lett.*, vol. 28, no. 10, pp. 849–851, Oct. 2007.

[46] A. Khalid and D. R. S. Cumming, "A broadband circular combiner/divider for planar Gunn oscillators," in *2nd Annual Passive RF and Microwave Components Seminar*, 2011, pp. 15–20.

[47] T. W. Tucker, "Planar GaAs Gunn and field effect devices," University of British Columbia, 1972.

[48] M.-R. Friscourt, P. -a. Rolland, a. Cappy, E. Constant, and G. Salmer, "Theoretical contribution to the design of millimeter-wave TEO's," *IEEE Trans. Electron Devices*, vol. 30, no. 3, pp. 223–229, Mar. 1983.

[49] H. Eisele, "480 GHz oscillator with an InP Gunn device," *Electron. Lett.*, vol. 46, no. 6, p. 422, 2010.

[50] V. Papageorgiou, A. Khalid, C. Li, and D. R. S. Cumming, "Simulation and fabrication of InGaAs planar Gunn diode on InP substrate," in *2013 International Conference on Indium Phosphide and Related Materials (IPRM)*, 2013, vol. 28, pp. 1–2.

[51] C. Li, A. Khalid, L. B. Lok, N. J. Pilgrim, M. C. Holland, G. M. Dunn, and D. R. S. Cumming, "An In0.23Ga0.77As-based pHEMT-like planar Gunn diode operating at 116 GHz," in *35th International Conference on Infrared, Millimeter, and Terahertz Waves*, 2010, pp. 1–2.

[52] D. S. R. C. and C. H. O. Mohamed Ismaeel Maricar, James Glover, Ata Khalid, Chong Li, G Evans, "An AlGaAs/GaAs based planar Gunn diode oscillator with a fundamental frequency operation of 120 GHz," *Microw. Opt. Technol. Lett.*, 2014.

[53] A. Khalid, C. Li, V. Papageogiou, G. M. Dunn, M. J. Steer, I. G. Thayne, M. Kuball, C. H. Oxley, M. Montes Bajo, A. Stephen, J. Glover, and D. R. S. Cumming, "In0.53Ga0.47As Planar Gunn Diodes Operating at a Fundamental Frequency of 164 GHz," *Electron Device Lett. IEEE*, vol. 34, no. 1, pp. 39–41, Jan. 2013.

[54] K. Y. Xu, G. Wang, and A. M. Song, "Gunn oscillations in a self-switching nanodiode," *Appl. Phys. Lett.*, vol. 93, no. 23, p. 233506, 2008.

[55] S. Pérez, T. González, D. Pardo, and J. Mateos, “Terahertz Gunn-like oscillations in InGaAs/InAlAs planar diodes,” *J. Appl. Phys.*, vol. 103, no. 9, p. 094516, 2008.

[56] A. Khalid, C. Li, G. M. Dunn, and D. R. S. Cumming, “Multi-Channel GaAs-based Planar Gunn Diodes,” in *40th International Symposium on Compound Semiconductors*, 2013, no. August.

Chapter: 3

Description of measurement techniques used to characteriseplanar Gunn diode and oscillators

3.1. INTRODUCTION

This chapter describes the different measurement techniques, which were used to characterise the planar Gunn diode. The techniques included DC, RF, thermal and scanning electron microscopy (SEM) measurements; SEM was used to determine the spacing between the anode and cathode electrodes. These measurement techniques were required to more fully understand the planar Gunn diode and develop its electrical equivalent circuit model, which was used for designing the matching circuits to extract the fundamental and second harmonic oscillations.

3.2. DC MEASURMENT

One of the important DC measurements to be carried out on the planar Gunn diode was the measurement of the IV characteristic of the diode. The IV characteristic was used to give a first indication of the turn-on resistance and the negative resistance of the diode and therefore the diodes suitability for further testing. The IV characteristic of a planar Gunn diode is shown in **Figure 2.1.** From the figure it can be seen that when the applied DC voltage across the diode was increased, the current increased until the threshold voltage (V_t) was reached. At voltages greater than the threshold voltage the current decreased, giving rise to the negative differential resistance region (NDR). This effect is due to the formation of a Gunn domain in the planar Gunn diode, which was discussed in chapter 2.6.

A simple block diagram of the I-V measurement setup is shown in **Figure 3.1,** and in its simplest form consists of a power supply and voltmeter connected to the diode. The voltage across the device was measured by the voltmeter and the current supplied to the diode was measured directly from the current meter on the power supply.

The DC measurements were made using two techniques (i) two probe for the IV characteristics and (ii) four probe systems for the diode contact resistance measurements; which will be fully discussed in this section.

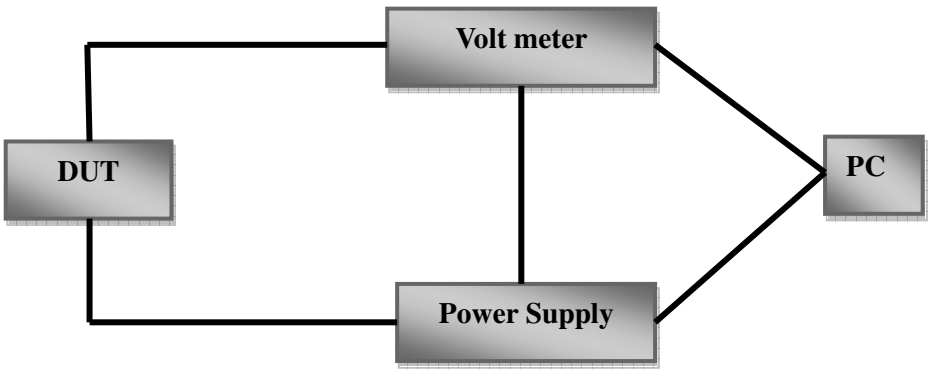

Figure.3.1.Block diagram of IV measurements setup

3.2.1. TWO PROBE IV-MEASUREMENT

Two probe IV measurements were carried out at Glasgow University by using a multipurpose Cascade MicroTech M150 probe station. This system was mainly used to characterise the semiconductor device when making RF measurements from DC to 110GHz.**Figure 3.2** shows the Cascade MicroTech M150 probe station. This probe station is computer automated, and consists of a device under test (DUT) holder, a probe station with a fine lift mechanism and a high magnification microscope

To make IV measurements using the computer automated probe station a Cascade MicroTech air coplanar probe (ACP 110-100) was used to make electrical contact with the chip device, which was normally presented as a chip on a wafer. The Cascade MicroTech (ACP 110-100) series probe is

shown in**Figure 3.3**, and consisted of a coplanar waveguide configuration with GSG (Ground-Source-Ground) spacing of 40-60-40μm which was the same spacing fabricated on the device to enable contact to the device structure. The probe was connected to an Agilent semiconductor parameter analyser (B1500A), which displayed the IV characteristics of the diode. The same ACP 110-100 probe was used when measuring the S-parameters of the diode; the S-parameter measurements will be described later in this chapter. The Agilent semiconductor parameter analyser test set-up was also used to measure the C-V (Capacitance-Voltage) and pulse IV characteristics of the diode. The change in diode capacitance with voltage was used in conjunction with S-parameters when developing simple diode electrical equivalent circuit models. Pulsed IV can be used to measure the IV characteristics to minimise internal self-heating of RF and microwave devices and the results used to develop more accurate electrical device models. The pulsed IV was used to characterise the planar Gunn diode in order to obtain an improved picture of the NDR region. A photograph of the Agilent semiconductor analyser is shown in **Figure 3.4**. This analyser is embedded with Windows 7 and powerful Easy Expert software which will support an efficient means of selecting device parameters to be measured. The automated probe station was programmed to place the GSG probe on the device and make the required measurement for example DC, and/or pulsed IV. The plots were stored along with the xy coordinates of the diode on the wafer using the Easy Expert software. The test conditions applied to the diode, output data and the xy coordinates of the diode on the wafer can be interrogated later, giving valuable information regarding the variation of the diode DC performance across the wafer. Diodes with poor or no NDR regions were identified and RF characterisation was not carried out on these diodes.

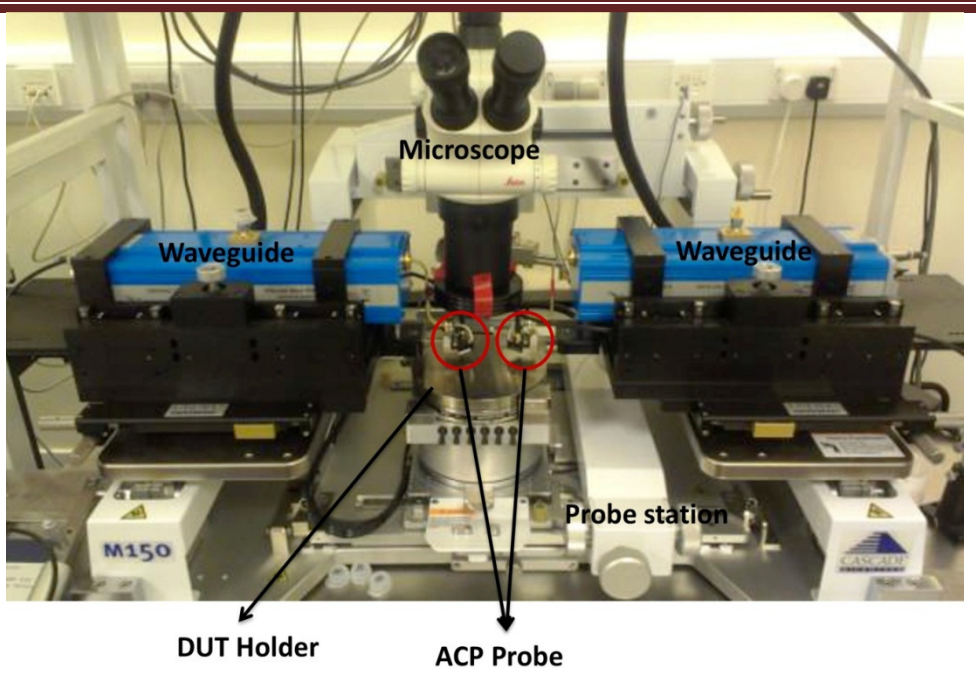

Figure.3.2 Cascade Microtech M150 probe station

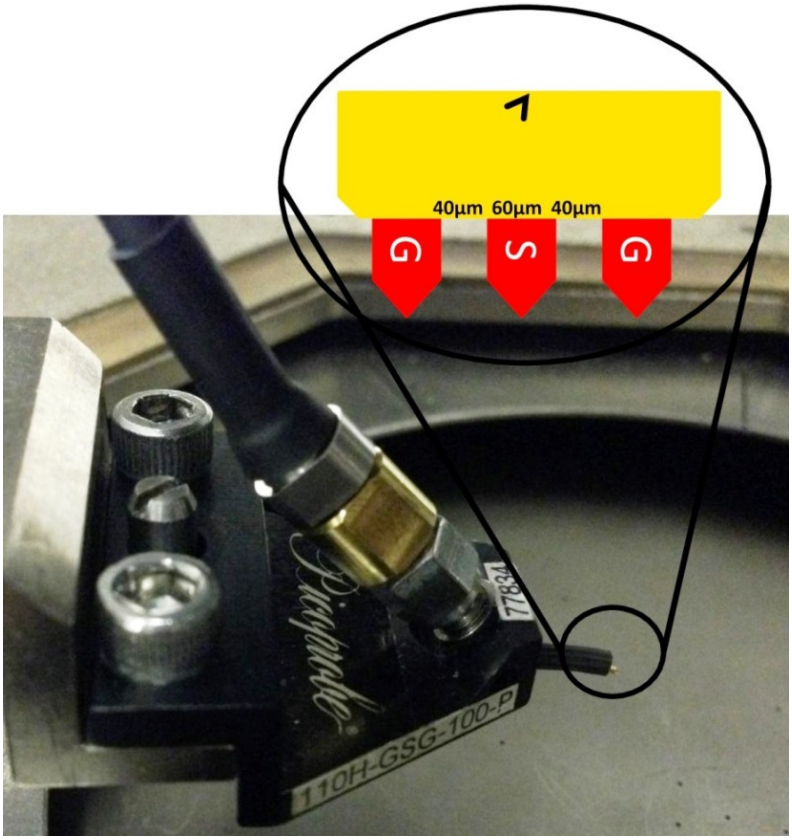

Figure.3.3. Cascade MicroTech Probe

Figure.3.4. Agilent semiconductor parameter analyser B1500A

3.2.2. FOUR PROBE IV-MEASUREMENT

The four probe measurements were used to obtain more accurate measurement of the ohmic contact resistance of the planar Gunn diode. The four probe measuremnt was setup at De Montfort University using Wentworth probe manipulators fitted with DC probe tips. The probe tips had a diameter of 0.5μm which was needed to place the probes centrally on the small area planar ohmic contacts. The four probe station was part of the Quantum Focus Instruments (QFI) infra-red microscope, which was used for thermal characterisation of electronic devices and in particular the planar Gunn diode, which will be described in more detail later in this chapter. **Figure 3.5** shows the four probe measurements set-up and the QFI infra-red microscope. In this measurement the QFI infra-red microscope was used to locate and place the probes on the device to be measured. The four probe DC measurement was semi-automated [1], using a programmable volt meter (Agilent 34450A), and power supply (PL 303 QMD), a QFI infra-red microscope probe station and four Wentworth probe manipulators. The complete system was controlled by the Agilent V programme. A schematic view of the on-wafer IV measurement probe system is shown in the **Figure 3.6.** In the set-up the upper voltage and current limits could be specified.

The set bias voltage limit depended on the anode and cathode separation of the planar Gunn diode.The order of magnitude of this voltage was theoretically estimated using results from Monte Carlo simulation program developed by Li and Geoff Dunn [2], [3]. Their work indicated that the operating voltage of a planar Gunn diode was close to the threshold voltage of the diode. For example, a planar Gunn diode having a 4 micron gap between the anode and cathode had a threshold voltage of around 4 volts and the experimental operating voltage was around 5V. For a 1 micron gap between the anode and cathode the threshold voltage was around 2 volts and the experimental operating voltage was around 3.5V [4].

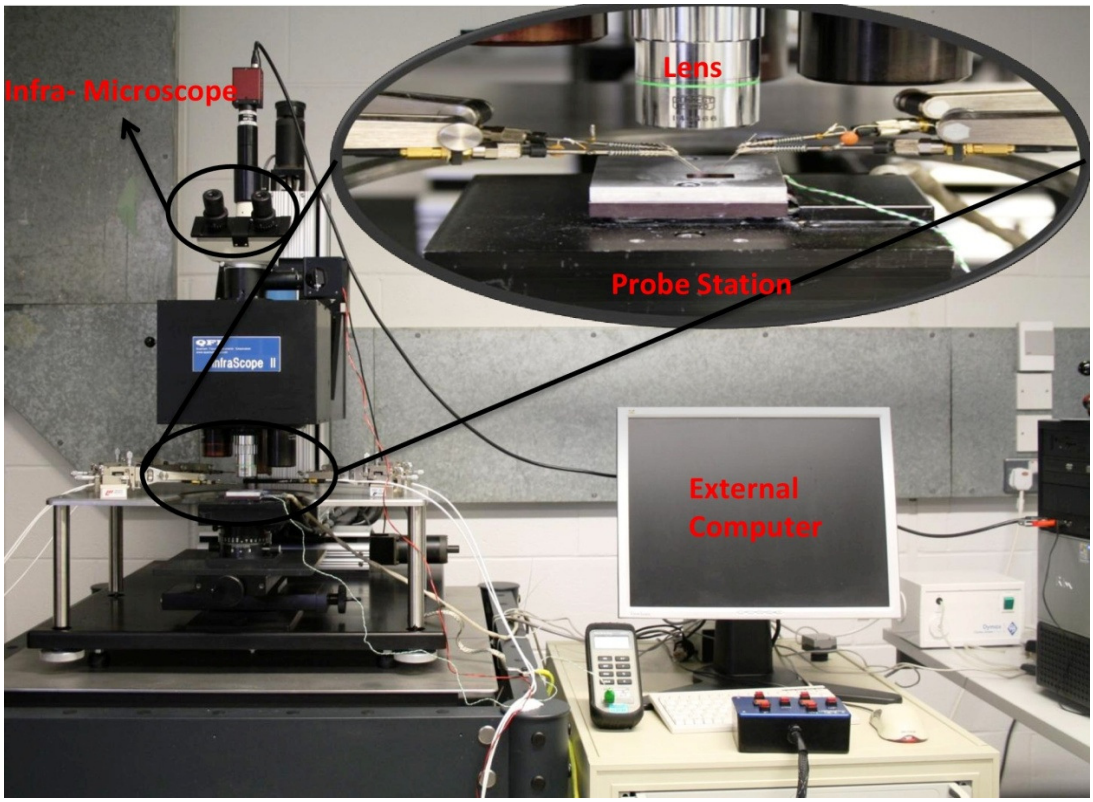

Figure.3.5. QFI Infra Microscope

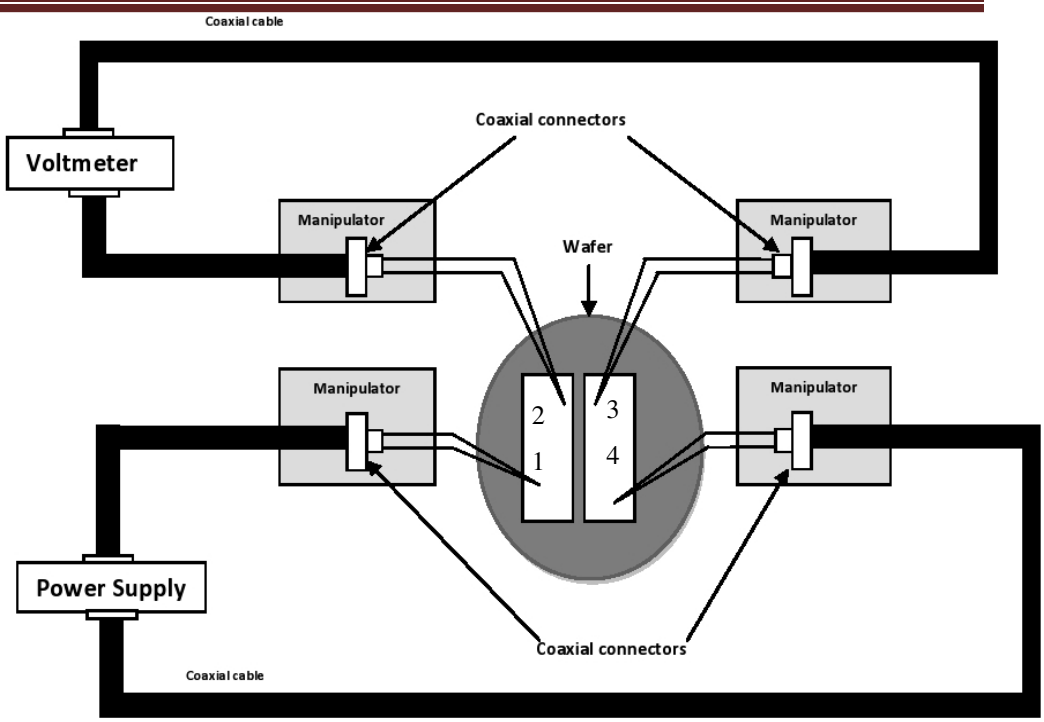

Figure.3.6. Probe system

3.3. TRANSMISSION LINE MEASURMENTS (TLM)

The anode and cathode ohmiccontact resistance of a Gunn diode has to be very small and is critical to its RF operation. Therefore, the measurements of the contact semiconductor/alloyed metal (R_s) interface and semiconductor sheet resistance (R_s) are very important. As the metal-semiconductor contact resistance can be very small it is necessary to take into account the probe resistance (R_p) and the contact resistance between the probe and device (R_{cp}), which can be achieved using a 4 probe measurement system. The block diagram representing the different defined resistances is shown in **Figure 3.7**.

The transmission line method (TLM) was used to measure the contact resistance (R_c) of the Gunn diodes by including TLM structures on the processed wafer with the Gunn diodes. Therefore, the metallised contact region of the TLM structure will have the same metallisation and process parameters as the contacts making up the Gunn diode. An electrical equivalent circuit for the measurement of the contact resistance using four probe systems is shown in **Figure 3.8.**

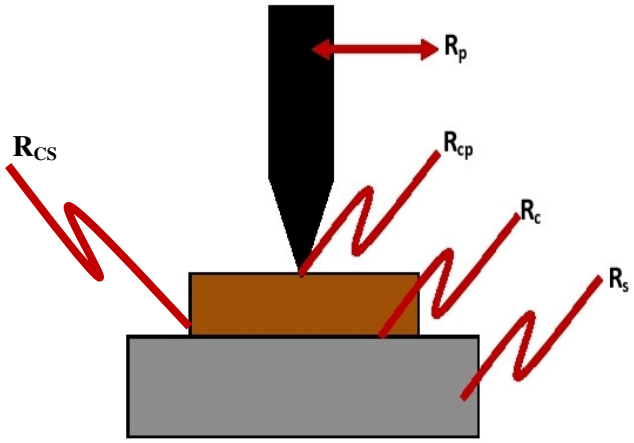

Figure.3.7. Different types of resistance in semiconductor metal

By using four probes the resistance across the structure can be measured by two of the probes, while the other two probes enable the current to be passed through the structure. This technique eliminates the probe resistance (R_p) and probe to metal resistance (R_{cp}) which will increase due to self-heating. The total resistance (R_T) can be calculated using Ohm's law shown in equation (3.1).

$$R_T = 2R_{cs} + R_s = \frac{V}{I} \tag{3.1}$$

where V is the measured voltage using probes 2 and 3 while I is the current supplied by the two current carrying probes 1 and 4

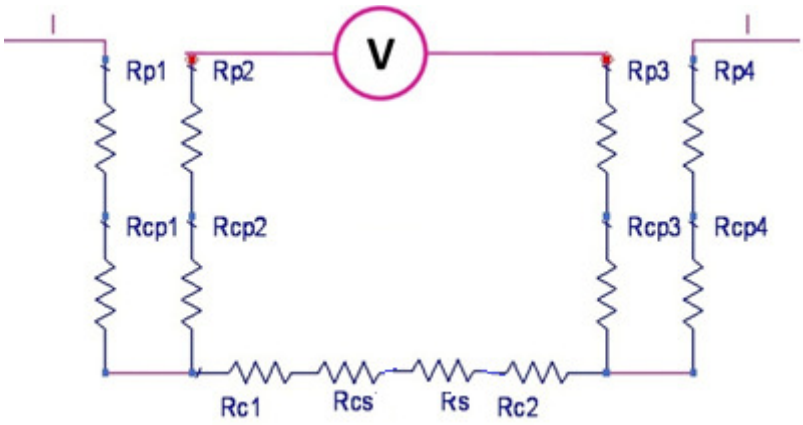

Figure.3.8. Four probe equivalent circuit model to measure the contact resistance

The measured contact resistance R_c of the TLM structure willrepresent the diode contact resistance. A schematic view of the TLM structure is shown in **Figure 3.9**, and consists of rectangular metallised ohmic contacts of length and width (W) 100μm respectively and each rectangular contact is separated from an adjacent contact by a gap which increases from 1μm to 6μm.

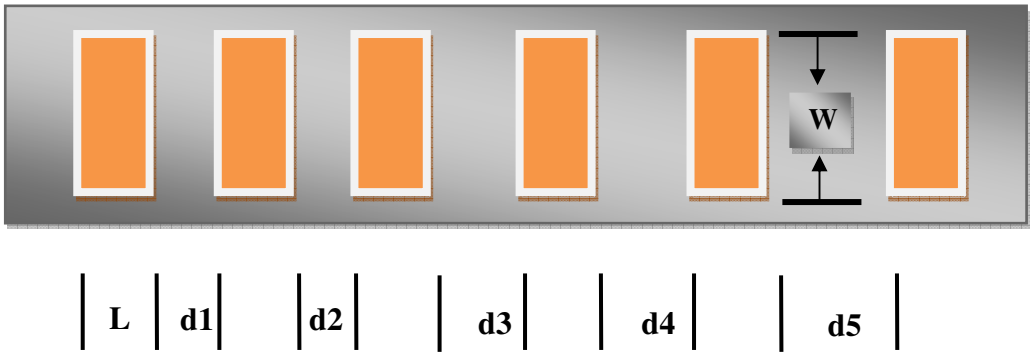

Figure.3.9 Simple geometry of the contact resistance

The contact resistance was measured by placing the probe 1 on the first metal contact and the second probe 2 on the adjacent metal contact and passing a current through the structure. The voltage between the pads was measured using probes 3 and 4 as shown in **Figure 3.10**, thereby eliminating the probe resistance (R_{cp}) and the resistance of the probe (R_p) in contact with metallised layer. The second probe and fourth probesarethen stepped to the next metal contact and the measurement repeated. Knowing the current and voltage the resistance can be calculated and plotted against the gap between the pads, see **Figure 3.11**. The contact resistance Rcxwas estimated by extrapolation of the line across the x-axes of the plot. The semiconductor sheet resistance R_s can be computed using equation (3.2). Note the method assumes that the contacts are totally symmetrical. ***Table 3.1*** show the measured contact resistance of the planar diodes fabricated on different wafers.

$$R_{sheet} = \frac{\rho}{d} \tag{3.2}$$

where ρ - resistivity of the material and

d - thickness of the semiconductor material.

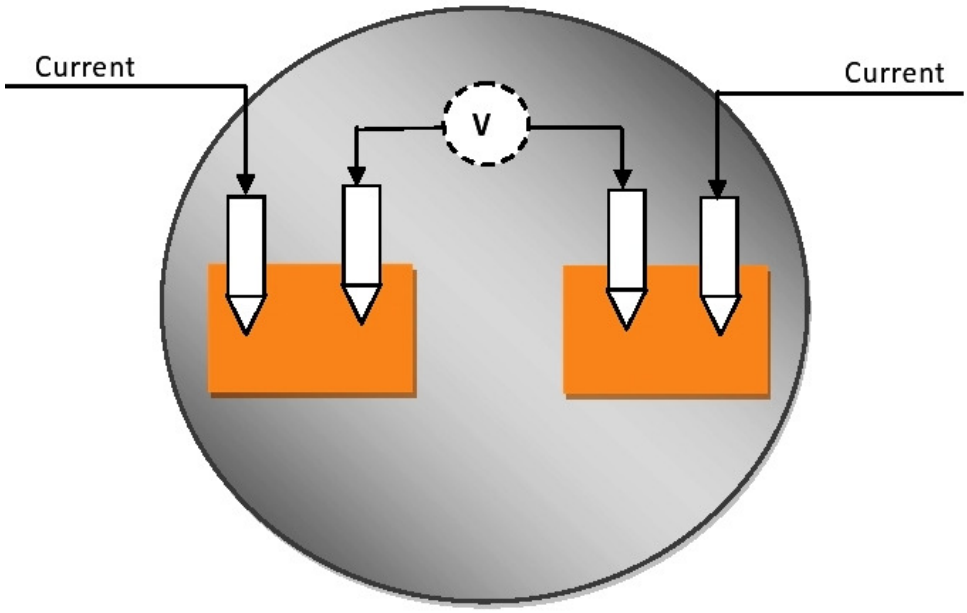

Figure.3.10 Contact pads and probe system

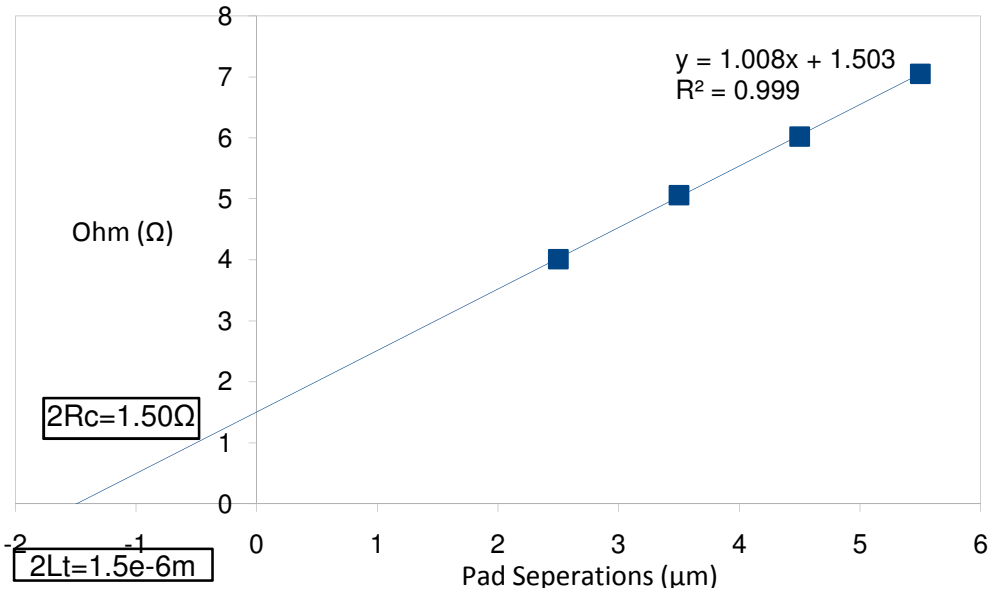

Figure.3.1l. Contact resistance of a TLM structure

Wafer No	Substrate	Contact Resistance (Ohm)
S18163/AKH3063	GaAs	0.75
S18132/AKH0953	GaAs	0.90
S18165/AKH4065	GaAs	0.76
S16860/AKH0866	GaAs	0.81
S18164/AKH1064	GaAs	0.83
S18159/AKH3159	InP	0.73
S18158/AKH1058	InP	0.76

Table.3.1. Contact resistance of different wafers

3.4. MICROWAVE CIRCUITS

Some of the fundamental principles of microwave wave circuit network analysis are summarised to help with the description of the measurement techniques.

A microwave device or component can be described as a circuit network. For example, a transistor, transmission line or amplifier can be described as a two port circuit network.

A two port network (**Figure3-12**) can be represented by Z-parameters, which can be written in matrix form.

$$\begin{pmatrix} V_1 \\ V_2 \end{pmatrix} = \begin{pmatrix} Z_{11} & Z_{12} \\ Z_{21} & Z_{22} \end{pmatrix} \begin{pmatrix} I_1 \\ I_2 \end{pmatrix} \tag{3.3}$$

As admittance Y =1/Z the two port network can also be described as an admittance matrix

$$\begin{pmatrix} I_1 \\ I_2 \end{pmatrix} = \begin{pmatrix} Y_{11} & Y_{12} \\ Y_{21} & Y_{22} \end{pmatrix} \begin{pmatrix} V_1 \\ V_2 \end{pmatrix} \tag{3.4}$$

At microwave frequencies it is difficult to measure impedance and admittance, due to the practical problems of measuring the voltage and current. This is because voltage and current vary with position along the transmission line.

The two port circuit network at microwave frequencies can be experimentally characterised by measuring the incident and reflected voltage, current or power at each port. Therefore, a two port microwave circuit network can be simply represented as in **Figure 3.12.**

Figure.3.12. Block diagram of a two port network

Consider port 1 with incident voltage (V_i) and current (I_i); at an instant of time the voltage and current at port 1 can be represented by equations 3.5 and 3.6 respectively.

$$V_i = V_o^+ + V_o^- \tag{3.5}$$

$$I_i = I_o^+ - I_o^- \tag{3.6}$$

The input impedance (Z_i) of the system can be calculated by using the above equations (3.5 and 3.6)

$$Z_{in} = \frac{V_i}{I_i} = \frac{V_o^+ + V_o^-}{I_o^+ - I_o^-} \tag{3.7}$$

The input voltage reflection co-efficient $\Gamma_v = \frac{Vr}{V_i}$, and substituting into(3.7)

$$\Gamma_v = \frac{Z_{in} - Z_0}{Z_{in} + Z_0} \tag{3.8}$$

where Z_0 is the characteristic impedance of the measurement system. Hence by measuring the voltage reflection coefficient Γ_v and knowing the characteristic impedance Z_0 of the signal generator the input impedance Z_{in} of the device under test can be found. The voltage reflection coefficient is also known as the reflection S-parameter.

Scattering parameters [S] are used to describe the two port network in terms of voltage reflection (S_{11}, S_{22} …) and transmission coefficients (S_{21}, S_{12}etc). the reflection and transmission coefficients can be easily measured at

microwave frequencies. The S-parameter relationship for a two port network is given by equation (3.9) and the importance of S-parameter in microwave circuit design and measurement will be fully discussed in section 3.4.1.

$$\begin{pmatrix} b_1 \\ b_2 \end{pmatrix} = \begin{pmatrix} S_{11} & S_{12} \\ S_{21} & S_{22} \end{pmatrix} \begin{pmatrix} a_1 \\ a_2 \end{pmatrix} \tag{3.9}$$

3.4.1. IMPORTANCE OF S-PARAMETER MEASURMENTS

As introduced in section 3.4, S-parameter measurements are important for characterising microwave active and passive components. At RF and microwave frequencies standing waves are set-up in the component due to incident and reflected waves interacting and it is easier to characterise the component using reflection and transmission coefficients than measuring discrete voltage and currents. A directional coupler is used to measure the reflection and transmission coefficients, which is the principle of the network analyser. **Figure 3.13,** shows a schematic diagram of a directional coupler.

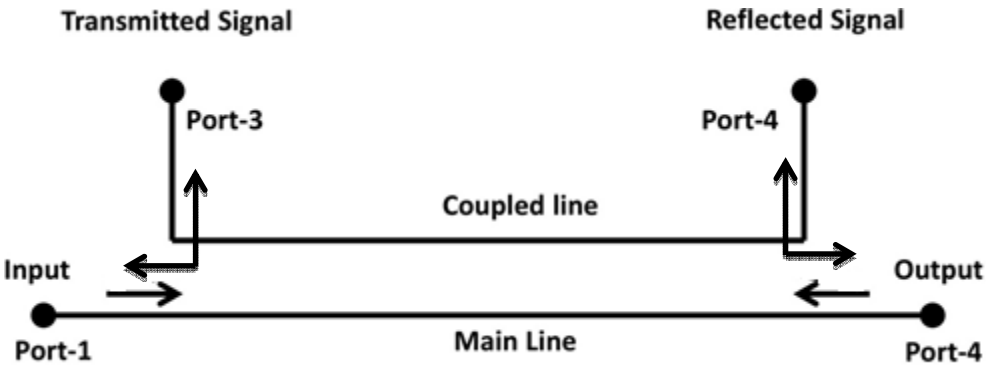

Figure.3.13. Operational diagram of directional coupler

The microwave measurements described in this thesis only considers one and two port circuit networks referenced to the measurement system with characteristic impedance of Z_0. In most measurement systems Z_0 is 50 Ohms to enable parity of measurements in different laboratories.

A block diagram of a one port network is shown in **Figure 3.14.** In the diagram the a_1 wave is the incident wave and the b_1 wave is the reflected wave.

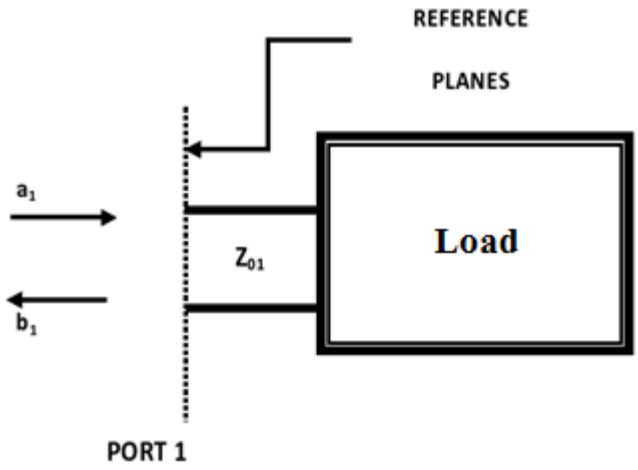

Figure.3.14. Block diagram of one port network

$$b_1 = S_{11}a_1 \tag{3.10}$$

S parameters are expressed in magnitude and phase angle therefore can be described as having real and imaginary components. When the transmission line is matched with Z_0, S_{11} will be 0, as there is no reflected b wave, if the transmission line is short circuited S_{11} magnitude is 1 with a phase angle of 180 degree with respect to the input port and for an open circuited load S_{11} magnitude will be 1 and the phase angle 0 degrees with respect to the input reference port.

A two port network where port 1 is connected to a signal generator of impedance Z_0 and to port 2 a load Z_0 is show in **Figure 3.15.**

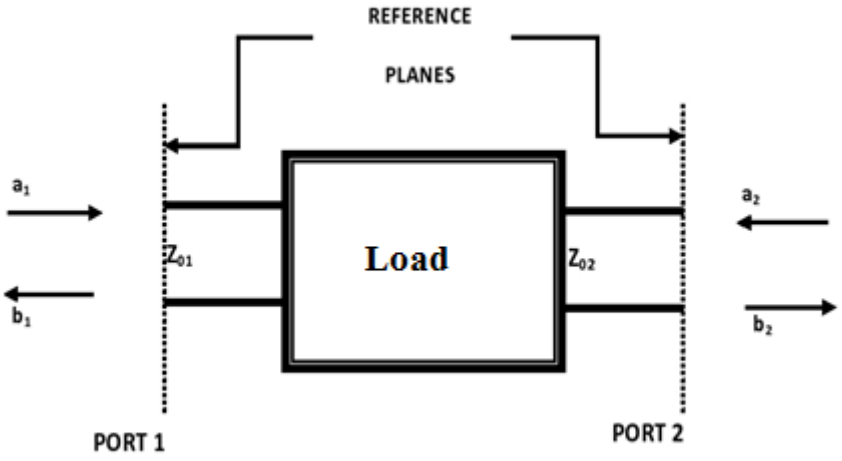

Figure.3.15. Block Diagram of S-Parameters

The a and b waves at port 1 and 2 can be defined as a set of S-parameters, where S_{11} is the reflected wave at port 1, S_{21} is the transmitted wave from port 1 to port 2, S_{22} is the reflected wave at port 2 and S_{12} is the transmitted wave from port 2 to port1. The reflected wave b_1 at port 1 can be written as (3.11(a))

$$b_1 = S_{11}a_1 + S_{12}a_2 \qquad (3.11\ (a))$$

Similarly, the reflected wave from port-2 can be described below

$$b_2 = S_{21}a_1 + S_{22}a_2 \qquad (3.11\ (b))$$

The same approach can be applied to nports.In the case of n=2the above equations can be expressed as a 2x2 matrix.

$$\begin{pmatrix} b_1 \\ b_2 \end{pmatrix} = \begin{pmatrix} S_{11} & S_{12} \\ S_{21} & S_{22} \end{pmatrix} \begin{pmatrix} a_1 \\ a_2 \end{pmatrix} \qquad (3.12)$$

From the above matrix, S_{11} represents the forward reflection coefficient or input match. S_{22} represents the reverse reflection coefficient or output match. $S_{21}$the forward transmission coefficient, and sometimes referred to as the forward gain. S_{12} represents the reverse transmission coefficient from the output to the input port sometimes referred to as the isolation or reverse transmission coefficient. The individual S parameters are evaluated by using these relationships.

$$S_{11} = \left.\frac{b_1}{a_1}\right|_{a_2=0} \quad S_{12} = \left.\frac{b_1}{a_2}\right|_{a_1=0} \quad S_{21} = \left.\frac{b_2}{a_1}\right|_{a_2=0} \quad S_{22} = \left.\frac{b_2}{a_2}\right|_{a_1=0} \qquad (3.13)$$

The S-parameters matrices can be transformed into both Z (impedance) and Y (admittance) matrices.

3.5. VECTOR NETWORK ANALYSER

3.5.1. INTRODUCTION TO VECTOR NETWORK ANALYSERS

Most microwave networks are represented and characterised using S- parameters, and are measured using a Vector Network Analyser (VNA). **Figure 3.16** shows a schematic diagram of a two port VNA system. A VNA has two internal signal sources which sweep over the measurement frequency bands. A high precision directional coupler is used at each of the two test ports to separate the reflected waves enabling S_{11} and S_{22} to be computed.

To understand the VNA a two port network measurement is considered: when port-1 is being used for the measurement, the VNA terminates the port-2 with a broadband matched load. The input RF signal to port 1 is divided into two halves in terms of power. One part (3dB) travels to the mixer and is mixed down by the local oscillator (LO) to an (intermediate frequency) IF as a reference signal, and the other part (3dB) goes into the DUT via the port 1 directional coupler. The reflected port 1 signal returns via the directional coupler and is mixed down by the LO to generate a test IF. The DUT measured reflection coefficient $S_{11,}$is derived from the measured magnitude and phase between the test and reference IF signals. The ratio of the power and phase of the measured signals gives the forward transmission coefficient S_{21} of the DUT. The reflection coefficient $S_{22,}$ and reverse transmission S_{12} are measured by a similar method, when port 1 is connected to an internal matched load, and port 2 to the signal generator. It is essential to calibrate the VNA to obtain accurate, reliable and repeatable measurements. One and two port VNA calibration methods will be described in section 3.5.2.

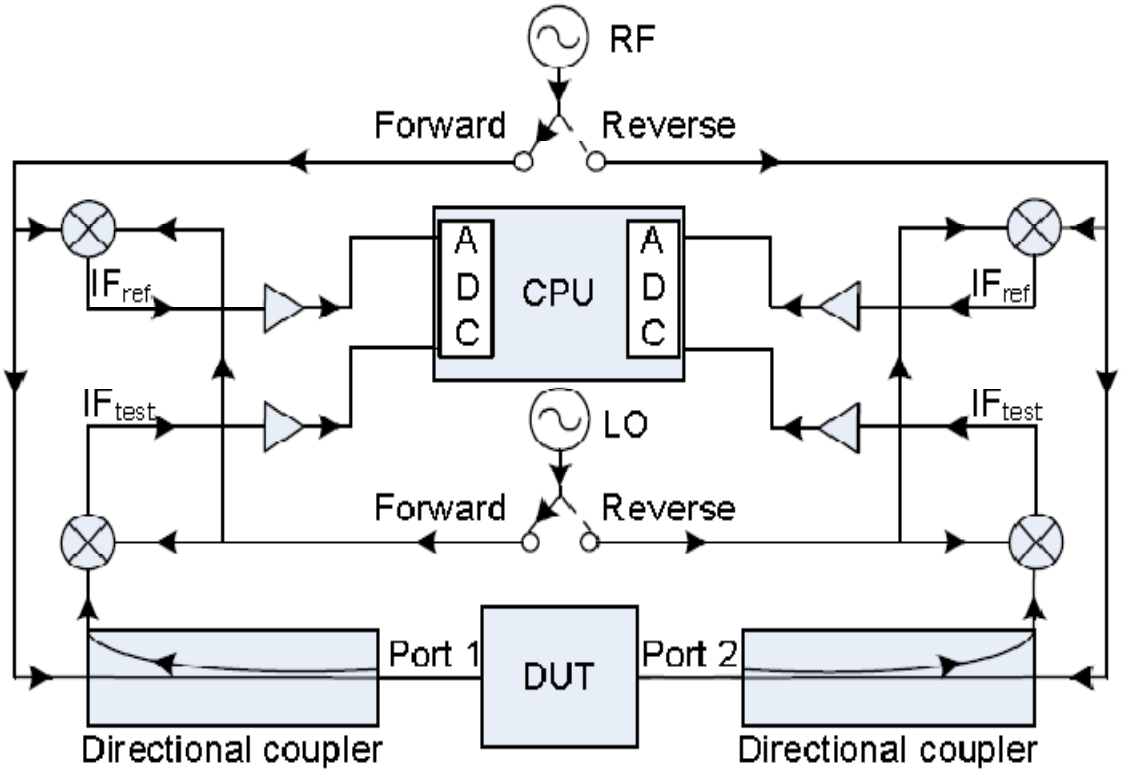

Figure.3.16. Two port vector network analyser

3.5.2. VECTOR NETWORK ANALYSER CALIBRATION

To make accurateS-parameter measurementsusing a VNA it is necessary to calibrate the instrument correctly.The frequency response of external circuit-components, for example cables, probes, waveguides externally connected to the VNA must be calibrated out to obtainmore accurate, and repeatableS-parameter measurements. Other systematic errors (for example mismatch between the connectors or imperfect components) are also removed during calibration.

There are many calibration options and a number of these are described in ***Table 3.2***. Generally the calibration is carried out by measuring a known standard for examplean open, a short, matched loads and different line lengths depending on the calibration method. Most of the calibration methods are presented in the literature and are implemented internally within the VNA.

Calibration Algorithm	Description	Advantage	Disadvantage
SOLT (short-open-load-thru)	Common coaxially	Simple, redundant standards; not band limited	Requires very well defined standards, poor on wafer, lower accuracy at high frequency
SSLT (short-short-load-thru) Short with different offset length	Common in waveguide	Same as SOLT	Same as SOLT and band limited
SSST (short-short-short-thru) All sorts with different offset lengths	Common in waveguide or high frequency coax	Same as SOLT but better accuracy at high frequency	Requires very well defined standards, poor on wafer, band-limited
SOLR/SSLR/SSSR Like as above but with reciprocal instead of thru	Like the above but when the good thru is not available	Does not require well defined thru	Some accuracy degradation, but slightly less definition, other disadvantage of parent calibration
LRL (Line-Reflect-Line) Also called TRL	High performance coax, waveguide on wafer	Highest accuracy, minimal standard definition	Requires very good transmission lines, less redundancy so more care is required, band limited
LRM (Line-Reflect-Match) Also called TRM	Relatively high performance	High accuracy, only one line length so easier to fixture/on-wafer, not band limited usually	Requires load definition. Reflect standard setup may require care depending on load model used

Table.3.2. Different types of calibration method *[5]–[10]*

3.5.2.1. ONE PORT CALIBRATION PROCEDURE

In this section a procedure to calibrate the one-port network is discussed. To calibrate the one port network for measuring input reflection S-parameters of the Gunn diode from DC to 110GHz,the Short-Open-Load (SOL) calibration method was used. Short-Open-Load (SOL) was first introduced by Eric-

Stridin 1986[8] and uses three known standards(i) Open (probe placed in air),(ii) Short (a line) and (iii) matched load (50 Ohm). These are shown in **Figure 3.17**. By using the SOL calibration method, the VNA system was calibrated up to the CPW probe tip as the reference plane (**Figure 3.18**) and therefore the diode input is connected to the CPW probe at the reference plane.After the calibration the results are verified and it is shown in **Figure 3.19. Figure 3.19** showsthe Smith chart results for a one port calibration for the frequency range of DC to 110 GHz using the SOL method. It can be seen from **Figure3.19**, the reflected voltage is equal and in phase with the incident voltage on the open circuit (Blue) end whereas the voltage of the reflected wave at a short circuit must cancel the voltage of the incident wave so that zero potential exists across the short circuit (Green). The reflection coefficient is equal to 1(Red).

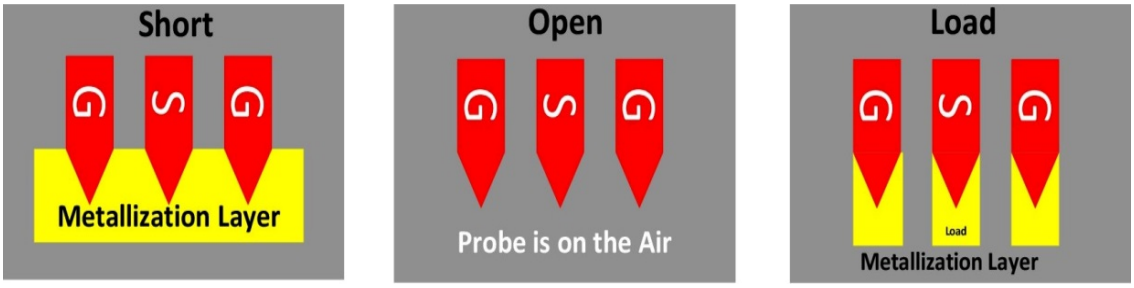

Figure.3.17. Schematic view of the SOL calibration substrate

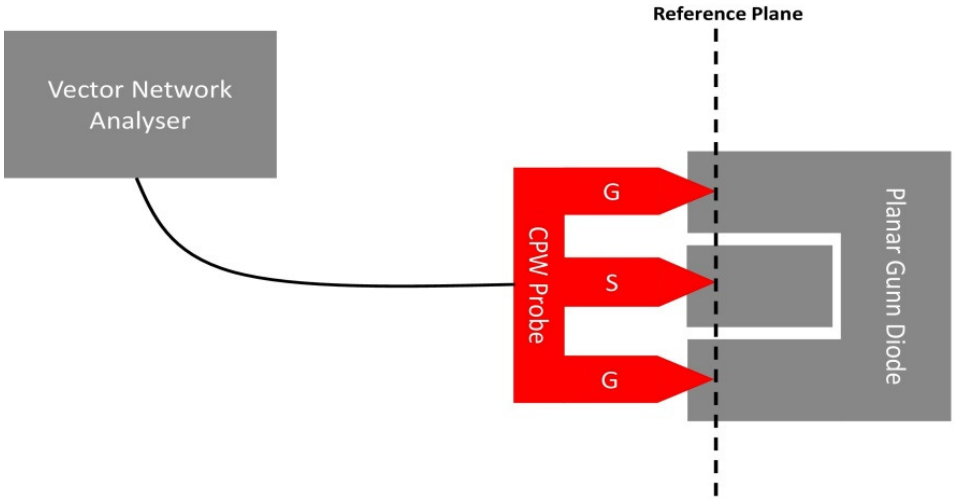

Figure.3.18 Setup of the VNA with the planar Gunn diode

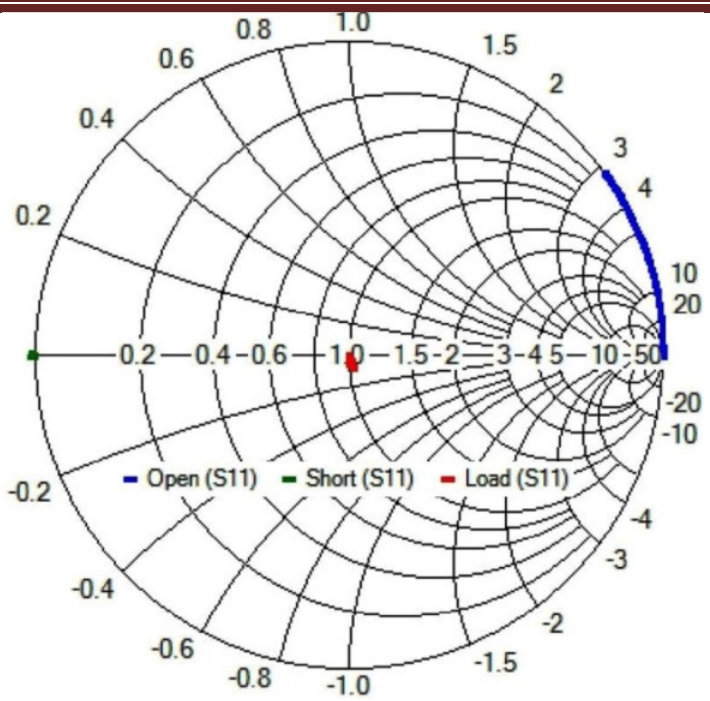

Figure.3.19. Smith chart representing one port calibration

3.5.2.2. TWO PORT CALIBRATION PROCEDURE

The SOLT method was used to calibrate the two port network because of its reliability and advantage which is described in the ***Table.3.2***. A further reason for choosing the SOLT calibration method is the lack of suitable calibration pieces in CPW format on a substrate for other calibration methods i.e. SOLR, SSST and TRL. A schematic view of the SOLT calibration substrate for a CPW probe system is shown in **Figure 3.20**. In the SOLT two port calibrations, the following measurement sequence is required and is represented as a block diagram in **Figure 3.21**.The reference plane of Port 1 of the network analyser is first connected to a calibrated short circuit, then an open circuit and a matched load (this will cover the full range of possible reflection coefficients). The reference planes of port 1 and port 2 of the VNA are connected to calibrate out the transmission losses. The sequence is then repeated at the reference plane of port 2 of the VNA.After the calibration the results are verified. **Figure 3.22** shows the measured results of the SLOT calibration method of a two port network and plotted on the Smith chart. It can be seen from the Smith chart results that the VNA was calibrated up to the CPW probe tip from DC to 110 GHz to measure the S-parameter of the device.

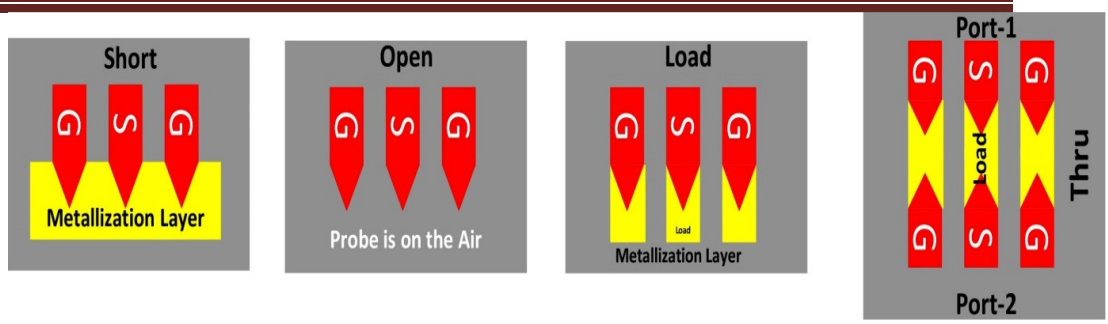

Figure.3.20. Schematic view of the SLOT calibration substrate

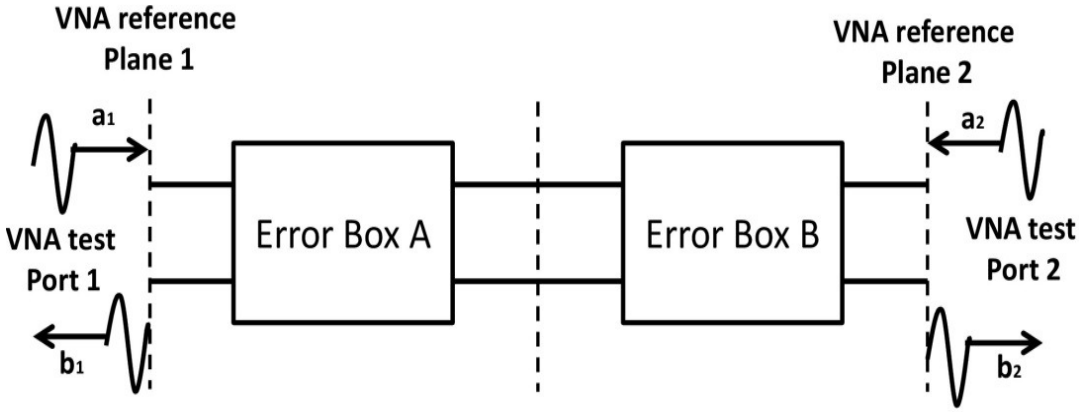

Figure.3.21. Block diagram of two port network calibration [3]

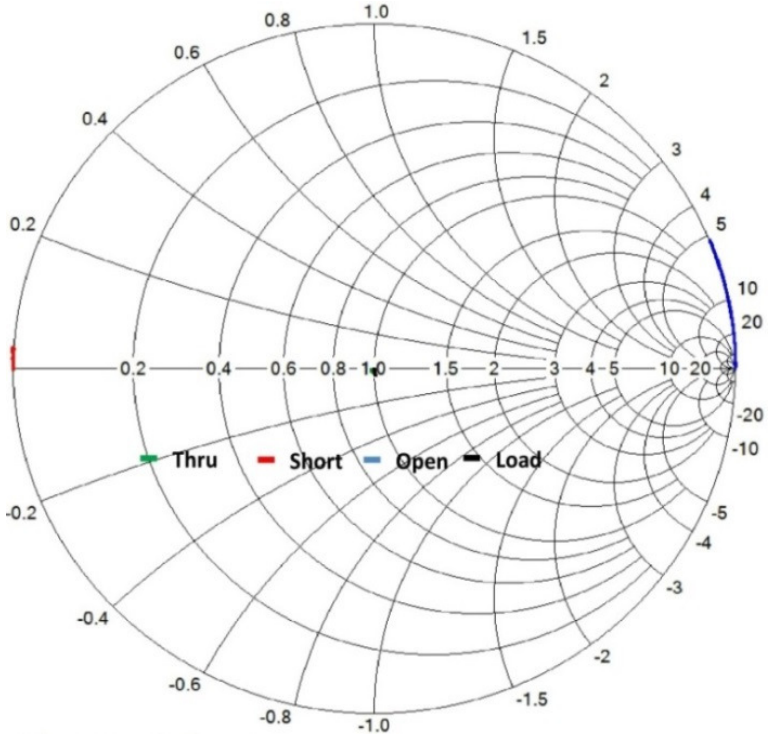

Figure.3.22. Smith chart representing two port SOLT calibration

3.5.2.3. *VNA TO MEASURE ACTIVE AND PASSIVE NETWORKS*

The basic 1 and 2 port calibration methods of VNAs, have been described and can be used to make microwave measurements of active and passive networks from DC to 325 GHz. The University of Glasgow has three VNA test set-ups to cover the frequency range from DC to 325GHz. **Figure 3.23** shows the S-parameter measurement setup using an Agilent E8364B VNA with a cascade probe station to measure active and passive components from DC to 110 GHz (Test Bench-1). **Figure 3.24**shows the S-parameter measurement setup with frequency extenders to measure the S-parameters from 140 GHz to 220 GHz and 220GHz to 325GHz (Test Bench-2 and 3).

Step 1: Choosing the right VNA for different applications.

It was important to choose the correct VNA setup to measure the S parameter of the active and passive test components. There are number factors to be considered, for example availability, frequency of operation, calibration substrate, and external source and CPW probe station.

Step 2: VNA Setup.

When setting the VNA to make experimental measurements, the following was considered: frequency span, number of experimental measurement points, IF bandwidth and input power level

Frequency Span & Number of Measurements Points*:* The start and stop frequency and number of frequency measurement points are specified.

IF Bandwidth*:* The IF bandwidth has to be as small as possible for the regular S-parameter measurement on passive components because a narrow IF bandwidth leads to more accurate measurements. However for the circuits identifying the oscillation frequencies like a planar Gunn diode, the IF bandwidth of the VNA is recommended to be larger so that it can detect the signal from the neighbouring sample points. Normally the IF bandwidth is set to 50 kHz for planar Gunn diode measurements. A further advantage of setting up a wider IF bandwidth is to speed up the measurements.

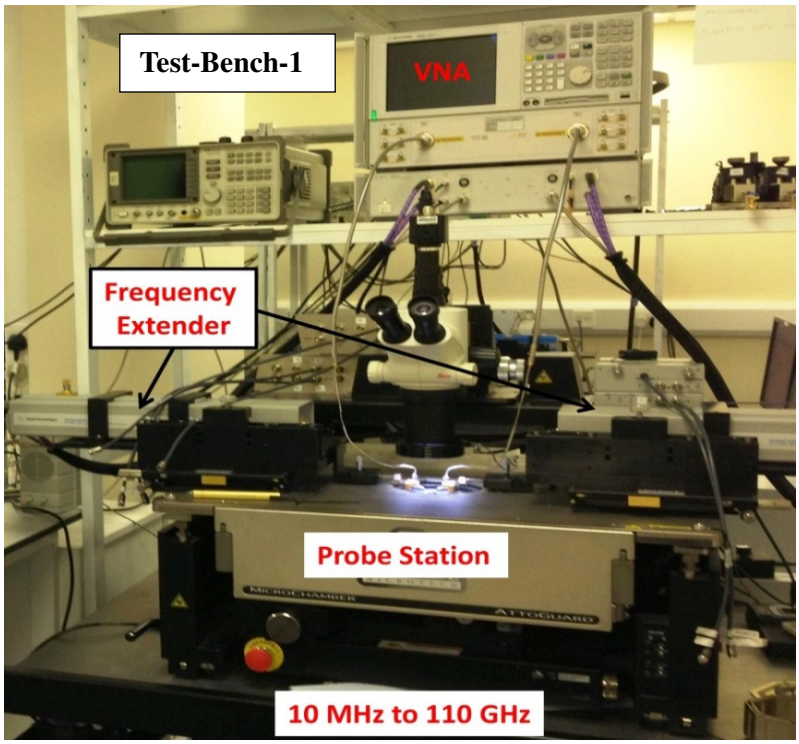

Figure.3.23 S-Parameter measurement setup using Agilent E8364B VNAup to 110GHz

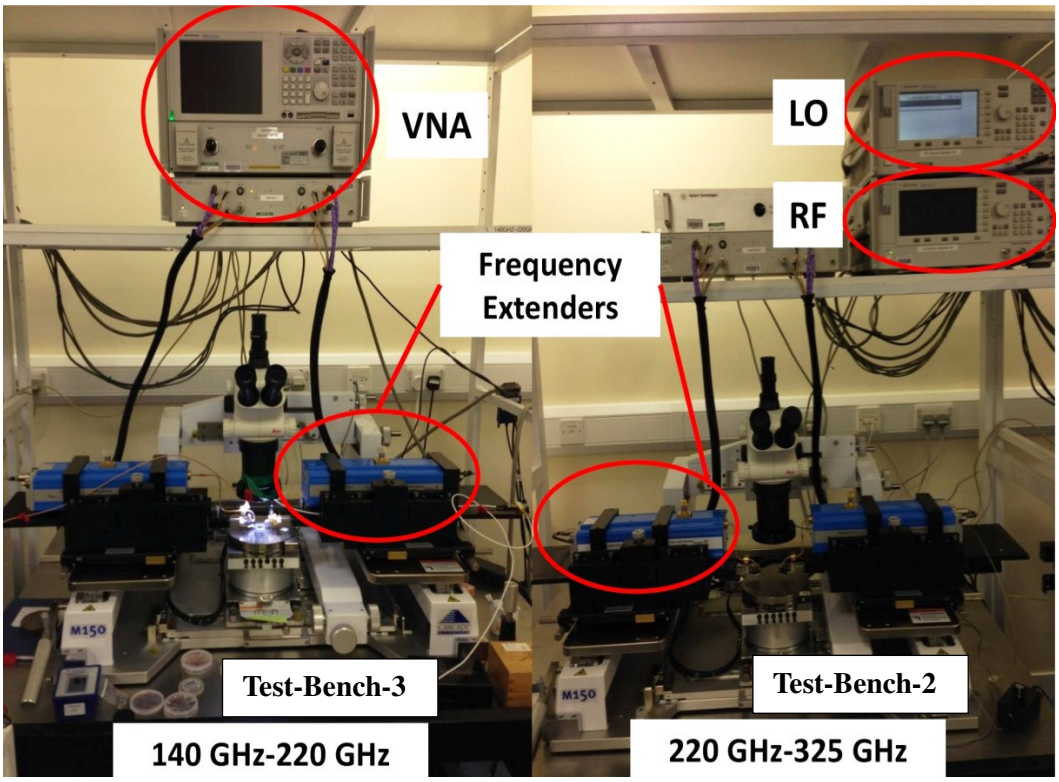

Figure.3.24.Two S-parameter measurement setup using Agilent VNA up to 325GHz

Power Level: the input RF power level has to be correctly set, too high and RF power will damage the CPW probe and possibly the DUT. Note the input power has to be set before calibrating the system as a change of the input signal level will require the RF attenuator to be re-set, changing the RF match and therefore the calibration conditions.

Step 3: Calibration of the System for S-parameter measurements.

As described in section 3.5.2, SOLR calibration was used for off wafer and SLOT calibration was used for on wafer.

Step 4: Verification/Validation.

After the VNA was calibrated, the calibration was verified, by taking a known standard (for example the 50 Ohm matched load on the calibration wafer) and measuring its S-parameters and comparing with the calibration measurement using the WINCAL software. This validation process was also used to verify that the measurement was well behaved for example no resonances or glitches.

Step 5: Measurements.

On completion of the VNA calibration and validation the probe station alignment with the test wafer needs to be set-up. To help with this process an alignment marker is fabricated on the device wafer and is used to align the wafer correctly so the probes will step automatically from device to device. **Figure 3.25** shows the alignment markers on the device.

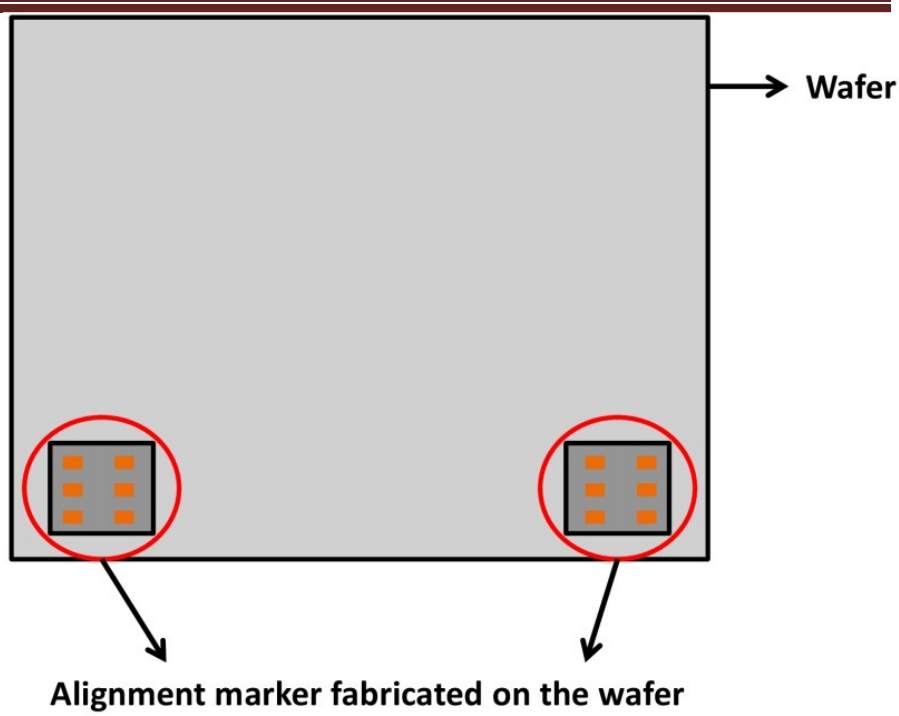

Figure.3.25. Alignment marker on the wafer

3.6. SPECTRUM ANALYSER MEASURMENT SETUP

A spectrum analyser measurement was used to characterise both frequency of operation and output power of the Gunn diodes integrated with on chip matching and resonant components. It was found on some Gunn diodes the device electrode configuration provided the right conditions for the sample to oscillate and therefore these could also be characterised using the spectrum analyser.

The spectrum analyser (Agilent E4448) used to measure the planar Gunn diode oscillators covered the frequency band from 3 KHz to 50 GHZ. To extend the frequency band to 125 GHz, external mixers and diplexers were used. For example to cover the V-band (50 to 75GHz) an external mixer was used, while to cover the W-band (75 to 125GHz) an external diplexer was used. The three bench set-ups covering DC to 125GHz will be described in further detail. All the measurement carried out were with two IF bandwidths of 300 KHz and 30 MHz respectively.

3.6.1. FIRST TEST BENCH MEASUREMENT SETUP FOR KA BAND

Figure 3.26 shows the measurement setup of the spectrum analyser covering the DC to Ka band. The setup consisted of an RF probe from GGB industries, a bias T from Anritsu, a DC power supply from Keithely, 2.5 mm low-loss coaxial cable and a spectrum analyser from Agilent (E4448). The RF probe (with G-S-G spacing of 40-60-40μm) is connected to the bias tee. One end of the bias tee is connected to the Keithely power supply and other end is connected to the 2.5 mm low loss coaxial cable. The coaxial cable is connected to the spectrum analyser for measurements up to 50 GHz.

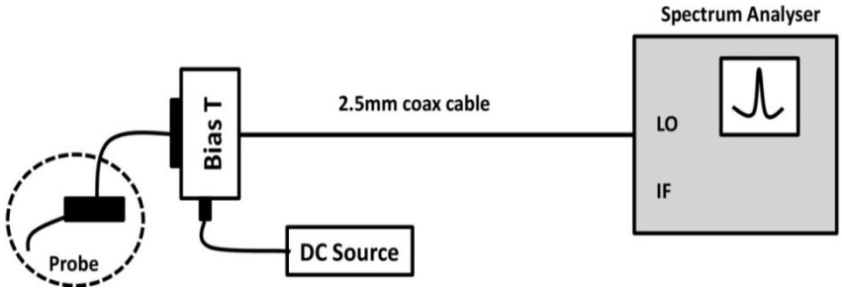

Figure 3.26Measurements setup up to 50 GHz

3.6.2. SECOND TEST BENCH MEASUREMENT SETUP FOR V-BAND

Figure 3.26 shows the V-band (50 to 75 GHz) measurment setup. The setup consisted of a V-band probe from GGB Industries, bias tee (Anritsu), diplexer and V-band mixer from Farran Technologies and an Agilent(E4448) spectrum analyser. The probe had aground-source-ground (GSG) separation of 40-60-40μm and was connected to the bias tee; one end of the bias teewas connected to the V-band mixer and the other end the diode while the third terminal was connected to the DC source to bias the diode. A low loss coaxial cable of 2.5mm diameter was used to connect the mixer and diplexer.

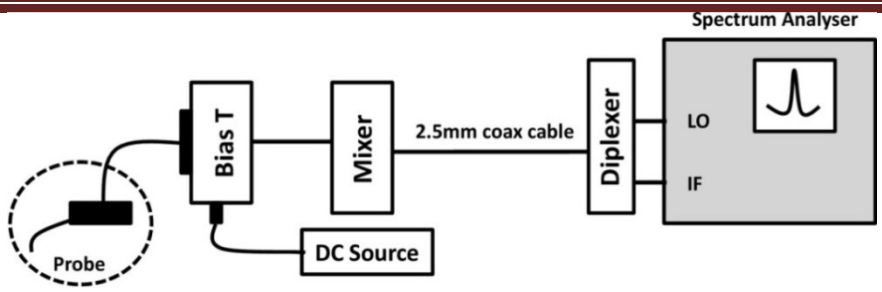

Figure 3.27 Measurements setup for V-Band

3.6.3. THIRD TEST BENCH MEASUREMENTS SETUP FOR W-BAND

Figure 3.28(a) shows a block diagram of the extended W-band (75 to 125GHz) measurement setup. **Figure 3.28(b)** shows a photograph of the actual measurement setup The extended W-band test bench consisted of a W band probe (GGB Industries), a W-band harmonics mixer and a diplexer from Agilent and a spectrum analyser (Agilent E4448). The RF probe had a ground-source-ground (G-S-G) separation of 40-60-40 microns and was attached to a W-band rectangular waveguide with a built in bias teeto DC bias the diode. The rectangular waveguide output was connected to the mixer and diplexer. The W-band waveguide has a cut-off frequency of 63 GHZ and therefore rejected signals below the cut-off frequency.Low loss coaxial cables with a 2.5mm diameter were used to connect the local oscillator (LO) and intermediate frequency (IF) from the mixer to the spectrum analyser.

The setupsenabledidentification of the oscillation frequency and an estimation of the RF output power (section 3.6.4).

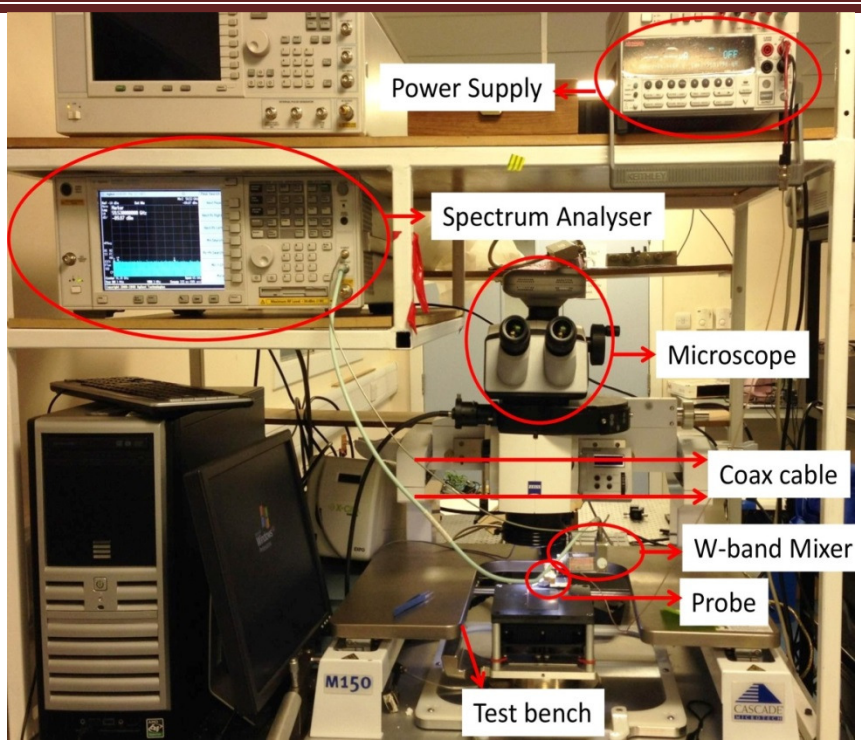

(b)

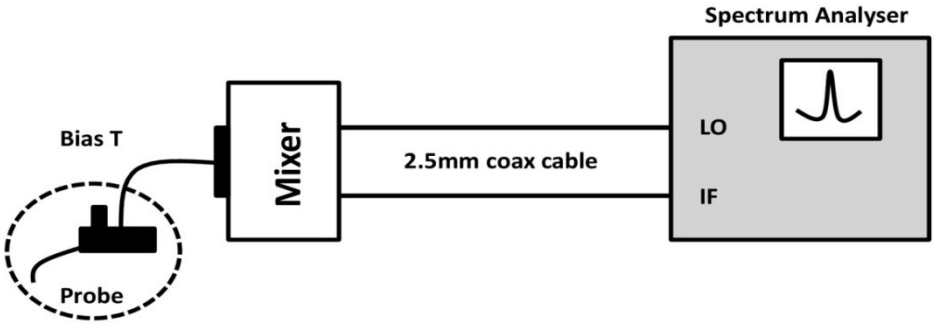

(a)

Figure 3.28. Spectrum analyser measurement setup (b) practical measurement setup of spectrum analyser (a) Block diagram of spectrum analyser setup with an external mixer

3.6.4. RF LOSSES IN THE SPECTRUM ANALYSER TEST BENCH

To measure the RF output power from the Gunn oscillator using the spectrum analyser set-up requires the total RF losses of the external components (mixer, diplexer, connectors, cable etc) to be known.

$$P_{loss} = P_{probe} + P_{cable} + P_{mixer} + P_{others} \tag{3.14}$$

The total RF loss of the measurement benches is given by P_{loss}, where P_{probe} is the insertion loss of the RF probe, P_{cable} is the transmission loss of the 2.5mm low loss coaxial cable, P_{mixer} is the conversion loss of the mixer and P_{others} represents the losses introduced by connectors. The RF losses of the V and extended W band benches were experimentally found to be approximately 50 dB between 60 and 125 GHz, where as for frequencies between 10Hz to 50GHz, the RF loss is taken into the account by the spectrum analyser (E4448).

3.7. SCANNING ELECTRON MICROSCOPE (SEM)

Different microscopy techniques were available and used in the characterisation of the Gunn diode devices. They included scanning electron microscopy (SEM),[11], and infra-red (IR) microscopy[12].

Scanning electron microscopy was used to measure the small dimensions of the planar Gunn, for example, the channel length between the anode and cathode electrodes. It was also used to perform energy dispersive X-ray(EDX) analysis of the planar Gunn diode surface. The SEM operates by imaging the surface using a collimated beam of electrons in a vacuum. The electron wavelength is 100,000 times smaller than the wavelength of visible light thereby substantially improving the resolution[13], [14]. The SEM can image any type of conductive material, however if the material is nonconductive a thin layer of conductive coating (gold or carbon) has to be applied to avoid electron charging and degrading the image [12]. **Figure 3.29**shows the internal construction of a SEM, an electron gun generates an electron beam which is focused on a sample by electromagnetic lenses. When electrons hit the sample they are scattered by either:-

1. Elastic scattering
2. Inelastic scattering

Elastic scattering occurs when the kinetic energy of the electron remains constant but the direction of its path changes and is used in the measurement of the dimensions of the sample. Whereas, in inelastic scattering, the

kinetic energy of the electron is changed producing X-ray radiation[15] and is used for analyzing the different materials making up the sample.**Figure-3.30** shows an image of two types of SEM used to verify the anode and cathode separation and device construction.

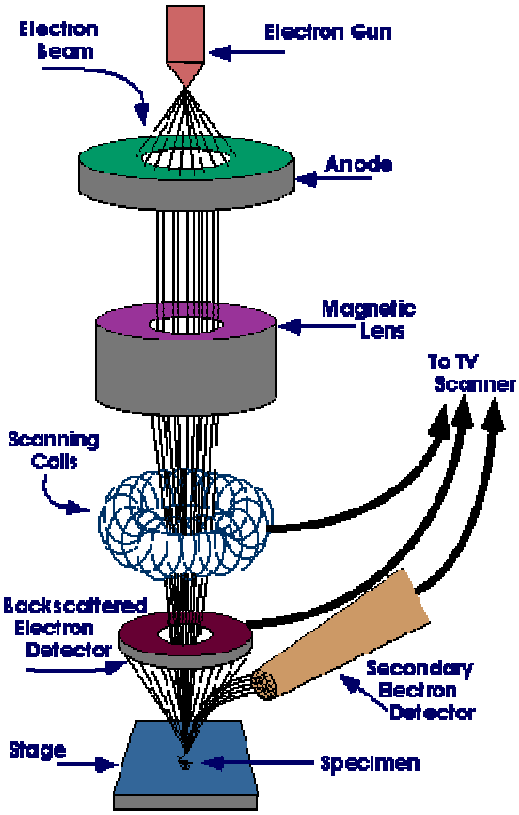

Figure.3.29. Schematic Diagram of the SEM operation

(a) (b)

Figure.3.30 (a) Leica S430 (b) Carl-ZesisEVoHD 15

3.8. THERMAL MEASURMENTS

Thermal measurement of the planar Gunn diode was carried out using a thermal infrared (IR) microscope. De Montfort University has a Quantum Focus Instrument (QFI) IR microscope, which enabled a profile of the surface operating temperature of the planar Gunn to be measured. The profile of the surface operating temperature of the planar Gunn diode was measured along the width and across the length of the Gunn diode channel respectively, using a novel IR micro-particle sensor in conjunction with the QFI microscope. The micro-particle sensor technique was developed at De Montfort University in 2010 [16].

The QFI infrared thermal microscope measurement system is shown in **Figure 3.31** and consists of an infra-red (IR) microscope with a range of objective lens (x1, x5 and x25 magnification), a digital optical camera, a temperature controlled stage, a micro-probe manipulator, and a probe table. A technology using a high emissivity micro-particle for more accurately mapping of the surface temperature on materials transparent to infra-red radiation, for example semiconductors, was developed at De Montfort University by Hopper etal.This technique was used to make thermal measurements in the active channel of the planar Gunn diode [16]–[18]. The thermal techniques have been further enhanced by J Glover [19] and will not be part of this work; however the technique was used to measure the surface channel temperature of a Gunn diode and some of the temperature profiles will be presented, along with an estimation of the diode thermal impedance.

The temperature measurements were made on a biased Gunn diode by manipulating the particle sensor from the anode across the channel to the cathode.**Figure 3.32** shows a typical planar Gunn diode having an anode to cathode separation 4µm and width of 120µm. The temperature of the planar Gunn diode was measured across the channel for the different Gunn bias voltages. **Figure 3.33** shows the mapped temperature profile of the planar Gunn diode at different bias levels. The measured thermal impedance was

75^0C/W, which suggested the Gunn diode junction temperatures were not excessively high.

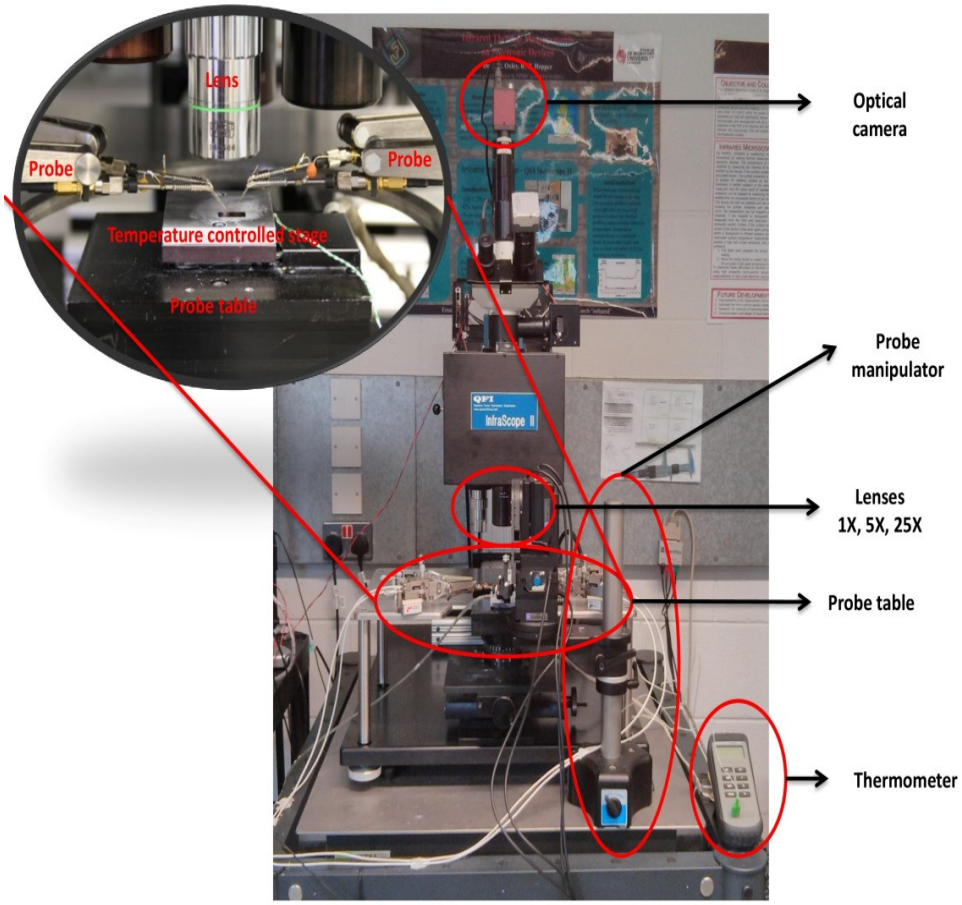

Figure.3.31 Thermal measurement setup from QFI

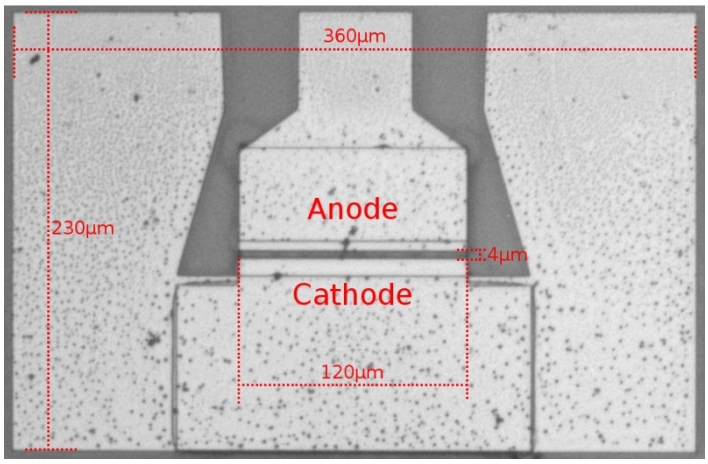

Figure.3.32. Typical Planar Gunn diode having an anode to cathode separation of 4µm and width 120µm

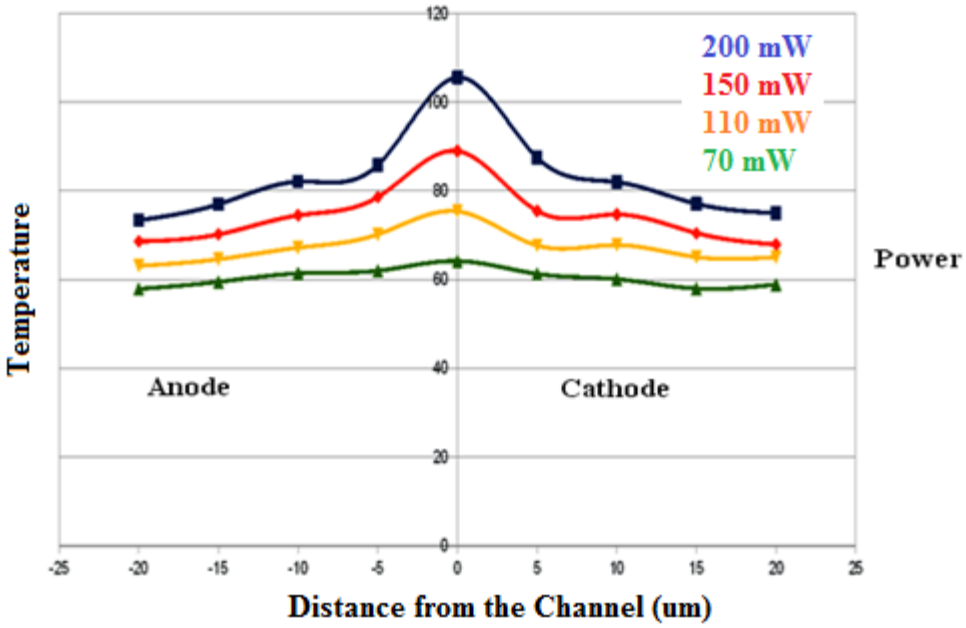

Figure.3.33. Temperature across the length of the channel of a planar Gunn diode

3.9. REFERENCES

[1] Sooraj Chandran, "IV Automation of Gunn Diode," De Montfort University, 2011.

[2] M. Montes Bajo, G. Dunn, A. Stephen, A. Khalid, D. R. S. Cumming, C. H. Oxley, J. Glover, and M. Kuball, "Impact ionisation electroluminescence in planar GaAs-based heterostructure Gunn diodes: Spatial distribution and impact of doping non-uniformities," *J. Appl. Phys.*, vol. 113, no. 12, p. 124505, 2013.

[3] C. Li, "Design and Characterisation of millimeter-wave planar Gunn diode and integrated circuits," University of Glasgow, 2011.

[4] M. Montes, G. Dunn, a. Stephen, a. Khalid, C. Li, D. Cumming, C. H. Oxley, R. H. Hopper, and M. Kuball, "Reduction of Impact Ionization in GaAs-Based Planar Gunn Diodes by Anode Contact Design," *IEEE Trans. Electron Devices*, vol. 59, no. 3, pp. 654–660, Mar. 2012.

[5] Anritsu, "Understanding VNA Calibration," 2012.

[6] A. Ferrero and U. Pisani, "Two-port network analyzer calibration using an unknown 'thru,'" *IEEE Microw. Guid. Wave Lett.*, vol. 2, no. 12, pp. 505–507, Dec. 1992.

[7] H.-J. Eul and B. Schiek, "Thru-Match-Reflect: One Result of a Rigorous Theory for De-Embedding and Network Analyzer Calibration," in *18th European Microwave Conference, 1988*, 1988, pp. 909–914.

[8] E. Strid, "Planar Impedance Standards and Accuracy Considerations in Vector Network Analysis," in *27th ARFTG Conference Digest*, 1986, pp. 159–166.

[9] K. Jones and E. Strid, "Where Are My On-Wafer Reference Planes?," in *30th ARFTG Conference Digest*, 1987, pp. 27–40.

[10] W. Deng and T. Chu, "A three-port vector network analyzer - measurement system, calibration and results," in *2001 IEEE MTT-S International Microwave Sympsoium Digest (Cat. No.01CH37157)*, 2001, vol. 3, pp. 1531–1534.

[11] S. Asahina, T. Togashi, O. Terasaki, S. Takami, T. Adschiri, M. Shibata, and N. Erdman, "High resolution and Low voltage scanning electron microscope study of nanostructured materials," *Nanotechnol. Suppl.*, no. November, pp. 12–14, 2012.

[12] N. Gabrielyan, "Low temperature fabrication of one dimensional nanostructures and their potential application in gas sensors and biosensensors (PhD Thesis)," De Montfort University, 2013.

[13] Michael J. Dykstra, *Microscopy, A manual of Applied techniques for Biological Electron*. Slenum Publishing Corporation, 1993.

[14] B. S. FINE, A. J. TOUSIMIS, and L. E. ZIMMERMAN, "Some General Principles of Electron Microscopy," *Arch. Ophthalmol.*, vol. 62, no. 6, pp. 931–934, Dec. 1959.

[15] Y.-P. Sun, Q. Miao, A. Pietzsch, F. Hennies, T. Schmitt, V. N. Strocov, J. Andersson, B. Kennedy, J. Schlappa, A. Föhlisch, F. Gel'mukhanov, and J.-E. Rubensson, "Interference between Resonant and Nonresonant Inelastic X-Ray Scattering," *Phys. Rev. Lett.*, vol. 110, no. 22, p. 223001, May 2013.

[16] R. H. Hopper, "Accurate Temperature Measurements on Semiconductor Devices (PhD Thesis)," De Montfort University, 2010.

[17] R. Hopper and C. Oxley, "Thermal measurement a requirement for monolithic microwave integrated circuit design," in *ARMMS Conference*, 2008.

[18] J Glover, R Hopper, M I Maricar, A Khalid, D Cumming, M Montes, M Kuball, G Dunn,A. Stephen. and C. H. Oxley. "Novel Infra-Red (IR) Thermal Measurements on GaAs Micro-coolers," in *ARMMS Conference*, 2012.

[19] James Glover, "Novel thermal managment of power electronic devices: high power high frequncy planar Gunn diode." (Yet to be submitted)

Chapter: 4

Design and fabrication of a planar Gunn diode

4.1. INTRODUCTION

The last chapter discussed the experimental methodologies to characterise the planar Gunn diode. In this chapter the design and fabrication of gallium arsenide (GaAs) and Indium phosphide (InP) based planar Gunn diodes will be discussed. The design changes to the planar Gunn diode include different electrode geometries to investigate the device electrode parasitics and the inclusion of matching elements (for example a series inductor) close to the active region of the device. The effect of varying the basic device geometry for example the anode to cathode separation (L_{ac}) and channel width (W) are also discussed. These circuit and geometry changes were made on two different semiconductor materials, GaAs and InP. The diodes were experimentally characterised using DC measurements; high frequency network analyser (VNA), a spectrum analyser (Agilent E4448) and thermal measurements (QFI), and the results will be fully described and discussed in chapters 5 and 6.

4.2. DESIGN OF A PLANAR GUNN DIODE

The planar Gunn diode design includes two important parts (i) the semiconductor layer structures and (ii) the metallized geometry: both of which will be discussed in this section

4.2.1. LAYER STRUCTURE OF A PLANAR GUNN DIODE FABRICAED ON AGaAs SUBSTRATE

The planar Gunn diode was first demonstrated by Ata Khalid in 2007 [1], [2] and the schematic view of the planar Gunn diode is shown in the **Figure 4.1.** A 50 nm thick un-doped GaAs layer is sandwiched between two δ doping AlGaAs layers with doping levels of$8 \times 10^{11}\text{cm}^{-2}$. A quantum well is formed due to the natural conduction band discontinuity between the GaAs and the AlGaAs. The undopedGaAs active layer has a high concentration of electrons with high electron mobility, which is not achievable in a conventional GaAsGunn diode. According to the basic criteria for the transit time mode of Gunn oscillations, the nl[3], [4] product (product of the active channel length l and the doping densityn) must be greater than 10^{12}cm^{-2}. Therefore, by raising the channel doping, the active length can be reduced leading to a higher frequency of operation of the Gunn diode.

The published paper[1] shows a GaAs based planar Gunn diode, with anode to cathode separation of 1.3 µm, which operated at a fundamental frequency of 108GHz. In 2010 Chong Li [5]confirmed the transit oscillation frequency of a planar Gunn diode by using Monte-Carlo simulation (material parameters used can be found in ***Table.4.1.***) and his results suggested the nl product of the device was greater than 10^{12}cm^{-2}.which is similar to the conventional Gunn diode.The experimental oscillation frequency was found by the ratio of domain velocity (v_{domain}) and the distance between the anode and cathode (L_{ac}).

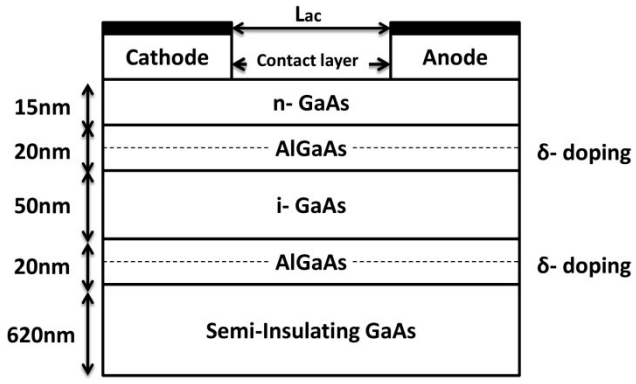

Figure.4.1. Schematic view of the planar Gunn diode demonstrated by Ata Khalid

Parameter (at 300K)	GaAs	$Al_{0.23}Ga_{0.77}As$
Permittivity	12.9	12.2
Bandgap (eV)	1.424	1.71
Affinity (eV)	4.07	3.82
Effective conduction band density of states (cm^{-3})	4.7×10^{17}	5.9×10^{17}
Low field mobility ($cm^2/(V.s)$)	8500	4000
Electron saturation velocity (cm/s)	1×10^7	0.8×10^7

Table.4.1. Semiconductor material used in the first experimental planar Gunn diode [1], [5]

4.2.1.1. FIRST PLANAR GUNN DIODE

First experimental GaAs based planar Gunn diode device produced an RF output power of -43.5 dBm [2] and more recently planar Gunn diodes have achieved RF output powers of -4.5 dBm at a fundamental frequency of 100 GHz [5]. Monte Carlo simulations suggest that planar Gunn diodes will provide higher RF output power when compared to conventional Gunn diodes [6], [7], however this has to be experimentally confirmed. Like the high electron mobility transistor (HEMT) [8]–[10], the RF output power can be increased by increasing the current density in the channel of the planar Gunn diode. A number of techniques have been researched to increase the current and therefore the RF output power. One of the techniques was to increase the number of δ-doping layers,which wasresearched by Chong Li [5]. **Figure 4.2 (a & b)** show the layer structures of the planar Gunn device with two and four δ-doping layers respectively in a single channel. The modified design hasfour AlGaAs δ-doping layers and each layera thickness of 10nm and doping level giving $8X10^{11}$ cm^{-2}. According to Chong Li [5], [11], the closer the AlGaAs δ-doping layers, the higherthe electron concentration in the GaAs channel and therefore a higher device current density. It should be noted that the higher the current density will result in higher device junction temperatures. His experimental results showed that increasing the δ-doping in the AlGaAslayers will increase the current density by 120% [5]. This effect was also modelled by Monte Carlo simulation by Geoff Dunn et al from the University of Aberdeen[12] and showed a similar current increase of 120%. In the research work reported here, four δ-

doping AlGaAs layers were used to increase the current density in the active layer of the planar Gunn diode.

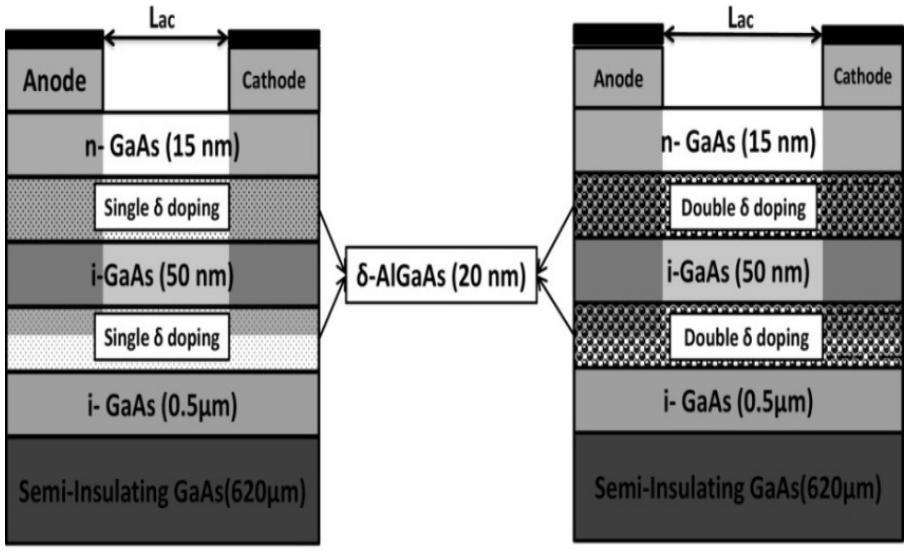

Figure-4.2. Schematic view of the planar Gunn diode
(a) Simple contact geometry of the Planar Gunn diode having single δ-doping layer
(b) Planar Gunn diode having two δ-doping layers on either side of the channel.

4.2.2. LOW RESISTANCE OHMIC CONTACTS

A schematic diagram of the Gunn diode with the planar Ohmic anode and cathode contacts are shown in **Figure 4.3.**There are two important design features of the Ohmic contacts for the planar Gunn diode. Firstly, to provide a low contact resistance with good thermal stability, and secondly, the contacts were required to be of a composite design to avoid premature breakdown, thereby reducing device failure. The Ohmic and composite contacts will be discussed in more detail in this section.

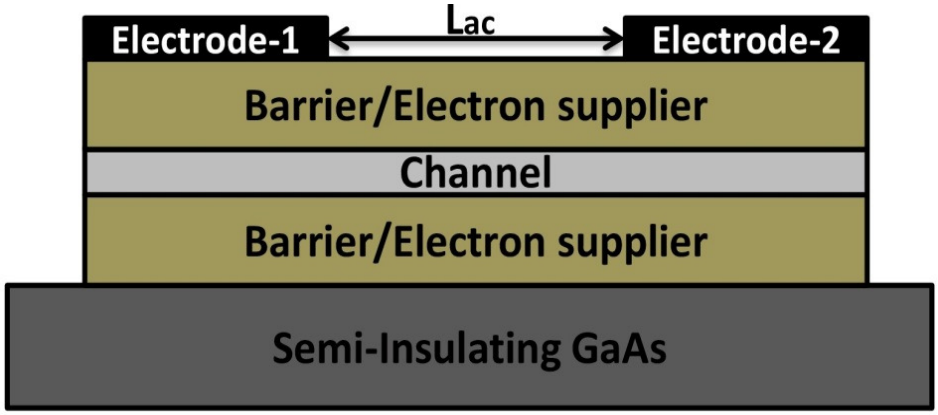

Figure.4.3. Electrodes structure of a planar Gunn diode

4.2.3. OHMIC CONTACTS FOR THE PLANAR GUNN DIODE

Ohmic contacts with low ohmic contact resistance are highly desirable for the planar Gunn diode as the resistance will dissipate both DC and RF power reducing the diode DC to RF efficiency. There are two methods of improving the design of the ohmic contacts:

- (i) Reducing the metal-semiconductor barrier and
- (ii) Increasing the doping level of the semiconductor layer

4.2.3.1. Metal to Semiconductor barrier

A literature review has shown that the metal-semiconductor barrier height is independent of the metal work function [6–8]. Therefore, using different contact metals on the n-type GaAs will have little effect on the metal-semiconductor barrier height. **Figure 4.4** shows the metal-semiconductors barrier heights for three different semiconductors: - n-GaAs, n-Ge and n-InAs.

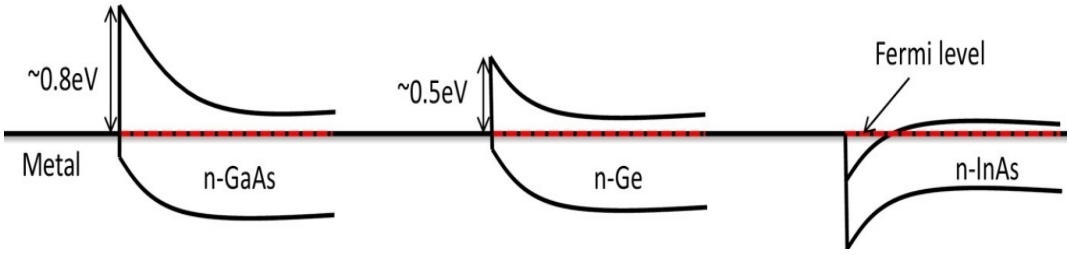

Figure.4.4. Schematic view of metal-semiconductor barrier for n-GaAs, n-Ge and n-InAs

4.2.3.2. INCREASING THE DOPING LEVEL

A method to achieve a good low resistance ohmic contact is to increase the doping level of the top semiconductor layer. Ata Khalid et al [16] designed an ohmic contact for the planar Gunn diode which consisted of annealed Pd/Ge/Au/Pd on top of a highly doped n region. This ohmic contact was well characterised by Ata Khalid and Chong Li [5], [16]. In this work, similar ohmic contact design was used on top of the planar Gunn diodes. **Figure.4.5.** shows a schematic view of the material composition of the ohmic contact, and TLM measurements have shown specific contact resistances of the order of 1.5×10^{-6} Ωcm^2 which are similar to the results obtained by other research groups [5] . ***Table 4.2*** summarizes a comparison of different ohmic contact technologies from the literature and shows that

the adopted (Red) contact technology gives a low contact resistance comparable to other technologies and research groups

Figure.4.5.Metal alloys for ohmic contacts of planar Gunn diode

Metallisation	**Anneal or inter-layer**	**Doping of n-GaAs (cm^{-3})**	**ρ_c ($\Omega.cm^2$)**	**R_c(Ω.mm)**	**Ref**
Ge/Ni	Anneal (450-650C)	$1.1x\ 10^{17}$	$3x10^{-5}$, $-5x10^{-4}$	N/A	[17]
Ge/Au/Ni	Anneal (400C)	$2.0x10^{18}$	N/A	0.2	[18]
Au(or Ag)/Ge/Pd	Anneal (150-175 C)	$1.0x10^{18}$	$1.0x10^{-6}$	N/A	[19]
Ge/Pd	Anneal (325 C)	$1.0x10^{18}$	$1x10^{6}$	N/A	[20]
Pd/Ge/Au/Pd/Au	Anneal (400 C)	$6x10^{17}$	$2x10^{-6}$	N/A	[21]
Au/Ni/Au/Ge/Pd n-InGaAs	Interlayer Anneal (400 C)	$3.0\ x\ 10^{19}$	$3.7x10^{-6}$	N/A	[22]
Ni/Ge/Au/Ti/Au InGaAs	Interlayer Anneal (475 C)	$1.0x10^{18}$	$2.56x10^{-7}$	0.019	[23]
Au/InGaAs	Interlayer	$2.4x10^{19}$	$5\text{-}8x10^{-7}$	N/A	[24]
Ni/AuGe/Ni/Au n-InGaAs	Interlayer	$4x10^{18}$	$1x10^{-7}$	N/A	[25]
Pd/Ge/Au/Pd/Au	**Interlayer/ Anneal (400 C)**	**$3.5x10^{18}$**	**$4x10^{-6}$**	**0.15**	[5]

Table.4.2.Summary of Ohmic contact resistance from the literature

4.2.4. COMPOSITE CONTACTS

One of the problems in designing a low contact resistance for the planar Gunn diode is thermal breakdown [26], [27]. Thermal breakdown in the planar Gunn diode is thought to be caused by excess heat generated near the device anode contact. This is due to the formation of the Gunn domain, when the Gunn domain reaches the anode, the high electric field will lead to electron hole injection. The electron-hole pair increases the current and therefore heat generated near the anode contact. To resolve the problem a number of techniques were considered including cooling the anode [26], [27], using concentric anode and cathode electrodes [28], enlarged anode mesa layer [29] and a Schottky layer on top of the anode contact.

Figure 4.6 shows the current distribution of a planar Gunn diode with the conventional ohmic and composite anode contacts. The Schottky contact was fabricated using Ti and Au overlay with thicknesses of 20nm and 200nm respectively. The extension of the Schottky contact was experimentally varied from 0.1 μm to 0.5 μm. Chong Li [5] reported that 0.3μm was the optimum length to achieve both low contact resistance and higher breakdown voltage for the planar Gunn diode. **Figure 4.6 (b)** shows the schematic view of the planar Gunn diode having a composite contact on the anode and also shows the spreading of the current when compared to the conventional ohmic contact in **Figure 4.6 (a).** The Schottky contact acts as a dissipation mechanism for the Gunn domain. When the domain approaches the edge of the Schottky region facing the cathode electrode, high energy carriers within the domain are able to exit via the Schottky barrier. When the high energy domain reaches the anode contact it is spread over a large distance thereby reducing the localized high electric field regions at the anode contact.

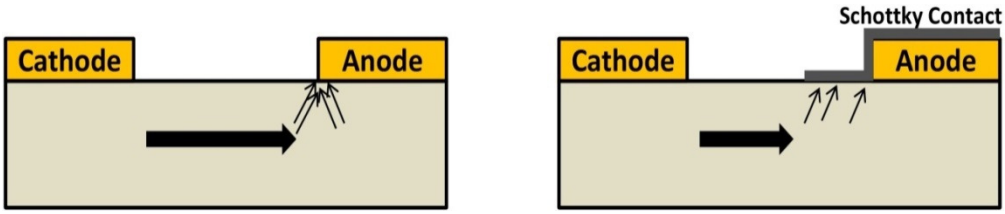

(a) **(b)**

Figure.4.6. Current crowding of planar Gunn diode (a) Conventional planar Gunn diode having Ohmic contact (b) Composite contacts for the planar Gunn diode having Schottky on anode

4.3. FABRICATION PROCESS OF THE PLANAR GUNN DIODE

The more important parts of the planar Gunn diode technology are discussed below:

4.3.1. CRITICAL FABRICATION PROCESSES

As discussed in section 4.2 the semiconductor layers making up the wafer are important to the performance of the Gunn diode, however to obtain a high frequency operations the physical definition of the channel length (L_{ac}) is critical, and will be described in this section 4.3.

4.3.1.1. LITHOGRAPHIC PROCESS TO REALIZE SUB-MICRON FEATURES.

For devices operating at frequencies in excess of 100GHz the channel length will be required to be <1 micron and over substantial channel widths, for example 120 microns. These small channel length dimensions need to be maintained over relatively large distances and therefore require high definition photolithographic processes. Two processes can be considered(i) photolithography usingultra-violet (UV) and (ii) electron beam lithography (EBL).For the very high resolution (sub-micron) required for the high frequency planar Gunn diode EBLwas used. This process uses an electron beam to bombard polymer photoresists e.gpolymethyl methacrylate (PMMA) which is sensitive to electron bombardment. PMMA is a positive tone resist and therefore the exposed part of the resist to electron bombardment can be developed and removed. Metal is then coated across the wafer and the areas

on which the metal lies on the resist can be removed by 'float-off' leaving the metal on the desired areas of the wafer. A further feature using EBL is that a mask is not required and different geometries can be easily written on to the same process wafer. **Figure 4.7** schematically shows the fabrication process of a single layer using EBL.

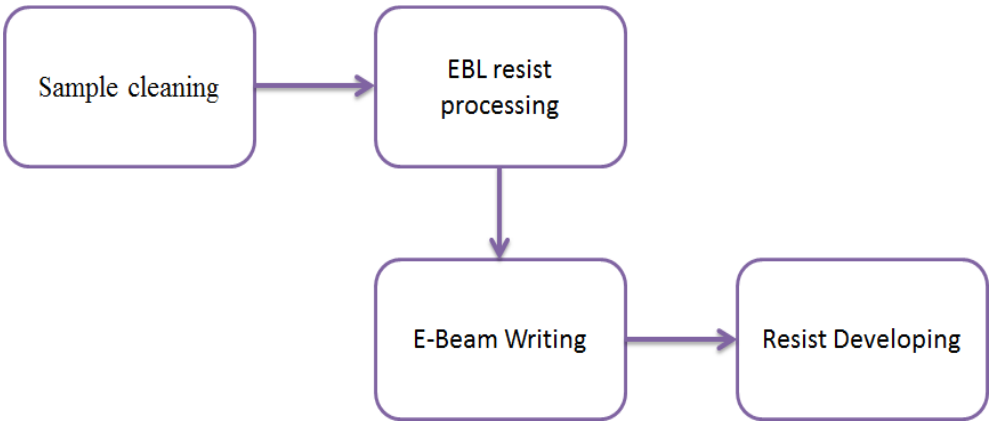

Figure 4.7. Block diagram of EBL process of single layer

4.3.2. DESCRIPTION OF THE FABRICATION PROCESS OF THE PLANAR GUNN DIODE

The processsteps for fabricating the planar Gunn diode are summarised in **Figures 4.8a to j**.The required semiconductor layer structure is grown by MBE technology on a 3-inch diameter wafer. The wafer can be scribed into smaller sections of 12mm by 12mm for different Gunn diodedevelopment process runs. **Figure 4.8a** shows a schematic view of the MBE grown layers on a semi-insulating GaAs substrate.

The first step **(Figure 4.8b)** is to define EBL alignment markers for the fabrication of subsequent layers**.** A 10/100nm layer of Ti/Au is deposited on the surface to create the EBL alignment markers. There are two types of markers: big crosses and small squares. The big crosses are used as reference points for the EBL operator while the small squares are fine alignment markers used by the EBL machine to trace the origin of pattern coordinates and guarantee accurate alignment between process steps.

The second step is the realization of the mesa which is shown in **Figure**.**4.8**

(c). The mesa layer contains the active and interlayer ohmic contacts for the Gunn diode. The height of the mesa layer depends on the device layer structure and can range between 200nm to 1000nm. A wet etching technique is used to realise the mesa as it minimises damage to the exposed active device layers. The etchant used was citric acid/hydrogen peroxide, which has a slow etch rate of 1000 Å/min at 20 ˚C.

The fourth and fifth **(Figures 4.8 d and e)** steps include the EBL device patterning as it includes the small dimensions L_{ac} between the anode and cathode electrodes, this is followed by the deposition of the adopted ohmic contact metallisation scheme (Pd/Ge/Au/Pd/Au)**.** E-beam evaporation was used for depositing the ohmic contact metal stack. A rapid thermal annealing (RTA) was used at a temperature of 400˚C for 60 seconds. This process gives the lowest contact resistance and also defines the channel length $L_{ac}$of the planar Gunn diode.

The sixth step is the fabrication of the Schottky contact. At the anode, a layer of 10/200 nm of Ti/Au respectively was evaporated on the anode contact to make a Schottky contact as shown in **Figure**.**4.8 (f),** Gold metallisation is then evaporated over the complete wafer to give low resistance (low RF loss) CPW lines.
The seventh step is the removal of the graded band gap layer to electrically isolate the individual Gunn diodes processed on the same wafer.

The final step **(Figure 4.8 (i))**of the fabrication process is to passivate the devices on wafer by using silicon nitride. Silicon nitride is used to supress trapping and to minimize surface oxidation

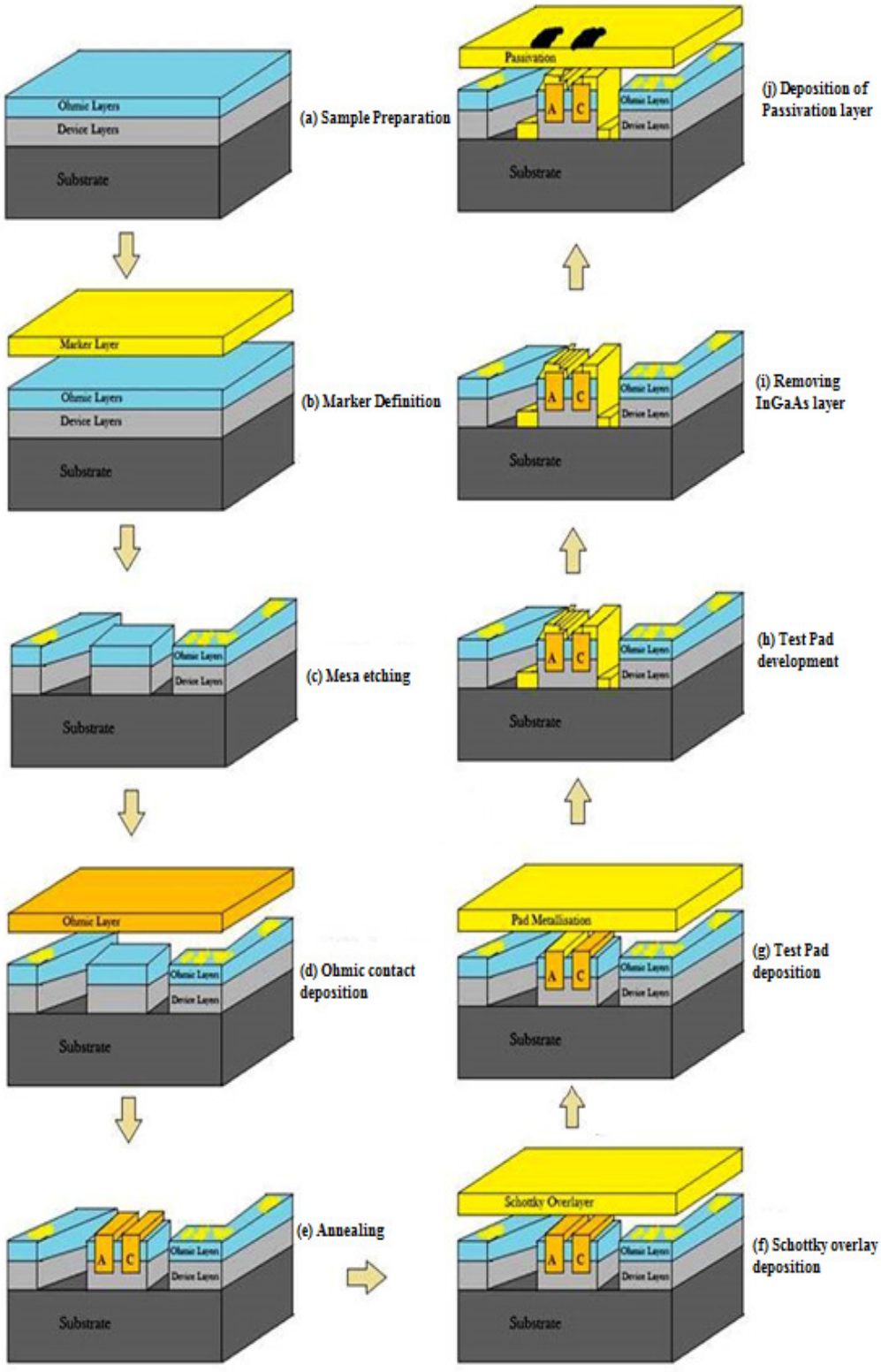

Figure.4.8. Fabrication process of planar Gunn diode (a) Sample cleaning/preparation (b) Marker definition (c) Mesa etching (d) ohmic contact deposition (e) annealing (f) Schottky over layer deposition (g) Test pad deposition (h) Test pad development (i) Deposition of passivation layer

4.4. DIFFERENT CHANNEL WIDTHS FOR A PLANAR GUNN DIODE

The effect of the geometry on the performance of the planar Gunn diode was studied by changing the active length (L_{ac}), width (W) of the channel and the shape of the CPW compatible electrodes (**Figure 4.9**).

Initially the DC characteristics of the planar Gunn diode wereexperimentally studied as a function of the active channel length (L_{ac}) which was varied from 1 to 4µm and then the channel width (W) from 30 to 120µm.

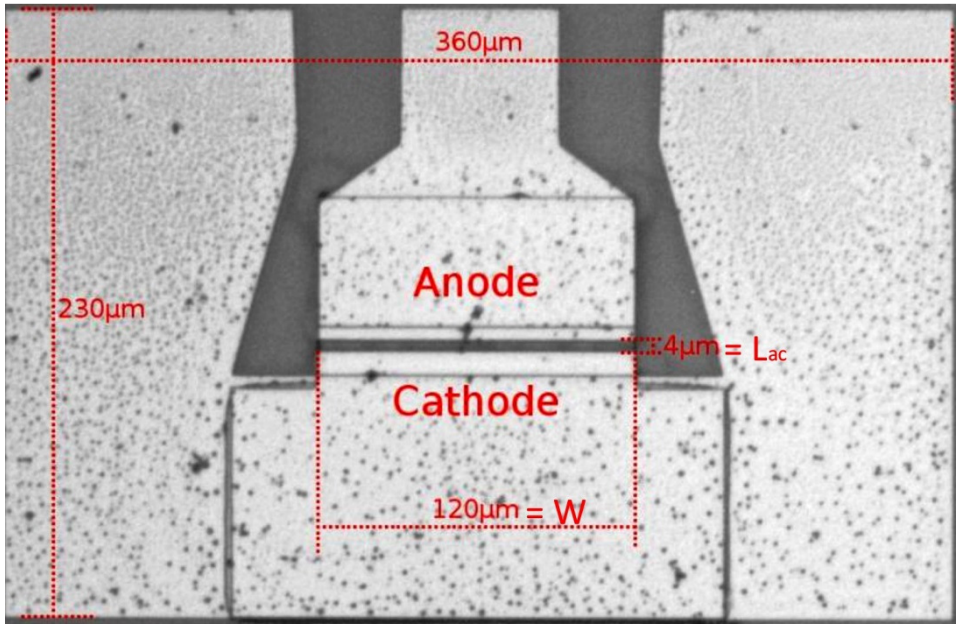

Figure.4.9. Typical planar Gunn diode

Figure 4.10, shows the DC characteristics of a typical planar Gunn diode which was measured using the semiconductor analyserB1500A from Agilent Technologies. The experimental results showas we expect a current increase of 400% when the channel widthwas increased from 30 to 120µm. The in-crease in current will result in an increase in RF output power provided the device DC to RF efficiency remains constant.

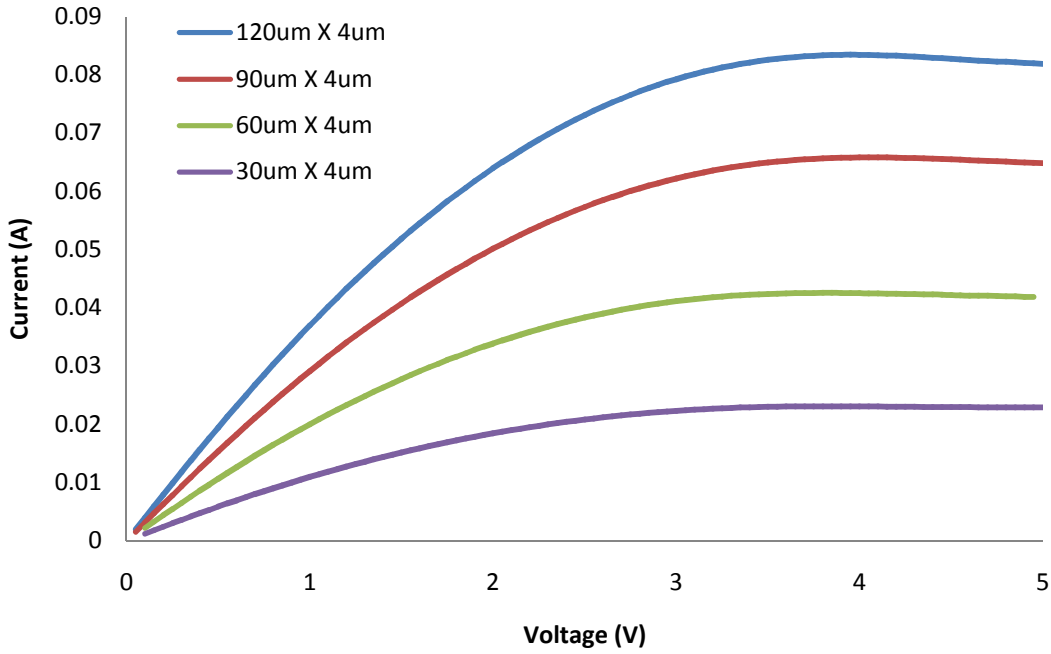

Figure.4.10. IV- characteristics of a typical Planar Gunn diode

The transit time mode of the device depends on the anode and cathode separation (L_{ac}). The transit oscillation frequency of the planar Gunn diode can be approximated by (4.1):

$$f = \frac{v_{domain}}{L_{ac}} \tag{4.1}$$

where v_{domain} is the domain velocity and L_{ac} is the anode to cathode separation. The oscillation in the planar Gunn diode is due to the periodic nucleation, transportation and collapse of the Gunn domain between anode and cathode gap (L_{ac}) leading to the RF current oscillation. The domain is not formed instantaneously but takes time to form in the active channel thereby creating a dead zone in the channel (see section 2.7). It was assumed the length of the dead zone is given by L_{dead}. According to Chong Li [5] the estimated value for the L_{dead} is 0.25μm and is similar length to that obtained for the vertical Gunn diode [30]. Therefore, the transient frequency oscillation mode for the Gunn diode is given by the modified equation (4.2). ***Table 4.3*** shows the estimated natural oscillation frequency of the planar Gunn diode as a function of the anode cathode separation including the dead space using equation 4.2.

$$f = \frac{v_{domain}}{L_{ac} - L_{dead}} \tag{4.2}$$

L_{ac} (Anode and cathode separation)	Operating Frequency(GHz)	Dead Space (µm)
1 µm	133.34	0.25
2 µm	57.14	0.25
3 µm	36.36	0.25
4 µm	26.67	0.25

Table.4.3 Transit time of the planar Gunn diode

The calculated Gunn transient mode oscillation frequency (Table 4.3) assumed the dead space was constant and gives a first order estimation; however in reality $L_{dead}$is bias voltage dependent. It can be argued that L_{dead}will decrease with increasing the bias voltage as the channel will heat more rapidly leading to an earlier onset of the domain formation, resulting in lowering the frequency of oscillation.

4.5. DIFFERENT ELECTRODE GEOMETRIES FOR A PLANAR GUNN DIODE

Planar Gunn diodes were designed with different CPW electrode geometries to investigate the effect of (i) parasitics associated with the shape of the electrodes, (ii) to improve the de-embedding of the active region of the device and (iii) provide on chip matching close to the active region of the diode.**Figure 4.11** shows the outline of four CPW geometries applied to the planar Gun diode.Type (a) was the same geometrical electrode layout as used by Glasgow University and was used as the reference diode.[31]–[33].Type (b) was a modification to the geometrical layout to investigate the effect of reducing the fringing parasitic capacitance with respect to type (a).Type (c) was designed to enable easier de-embedding of the active diode by extending the CPW 50 Ω feed line reducing the unknown impedance transformation to the active region of the Gunn diode and type (d) wherethe CPW line to the active region of the Gunn diode was made narrow to provide a series inductive element to match the active diode capacitance.

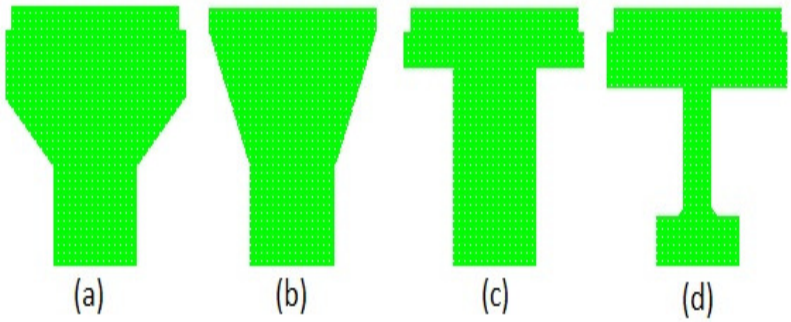

Figure.4.11. Types of coplanar waveguide structure: (a) standard CPW electrode structure. (b) CPW model to reduce fringing capacitance. (c) CPW model with 50 Ω feed line. (d) CPW model with series inductor

These structures were first analysed using the momentum (electromagnetic simulator which computes S-parameters for general planar circuits) package within the Advanced Design System (2009) to determine the self-resonant frequency of each of the structures on both a GaAs and InP semi-insulating substrate respectively. The substrate thickness was of the order of 600 microns mimicking the Gunn diode. The results are given in ***Table.4.4.***

Electrodes Type	Resonant Frequency (GHz) for GaAsmaterial	Resonant Frequency (GHz) for InPmaterial
Type-A	109.5	110.36
Type-B	108.1	109.38
Type-C	110.6	112.01
Type-D	116.0	117.36

Table.4.4. Resonant frequency of the electrodes on GaAs and InP substrate

The fundamental self-resonant frequencies of the four electrode structures were of the order of 110 GHz and the second harmonic self-resonant frequencies were of the order of 220 GHz. **Figure 4.12**, compares the simulated and measured resonant frequency of the electrode structure type A as an example at 0 bias voltage on GaAs and InP substrate material. The electrode structure resonated at a frequency of around 94 GHz with the return loss of -19 dB. The decrease in the measured resonant frequency when compared with simulated was thought to be due to the presence of other layers (mesa layer) leading to electrical parasitics which have not been included in the simulation..

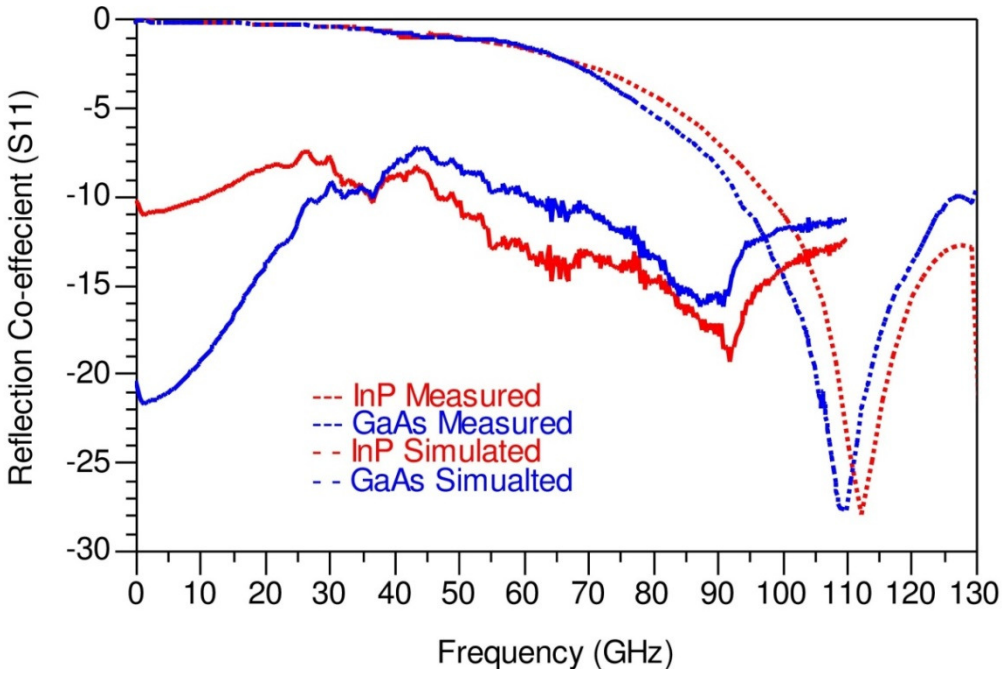

Figure.4.12. Resonant frequency of the Type-A electrode structures on GaAs and InP substrates

With reference to the electrode structure (d) the theoretical series inductance of CPW line was calculated as a function of the width of the CPW line at two frequencies 60 and 100GHz by using equation 4.3 and is shown in Figure**.4.13**. The quality factor (Q) of the inductor was found to decrease as the inductance value was increased as the parasitic resistance of the line increased.

$$L = \frac{Z_0\sqrt{\varepsilon_{reff}}}{c} \tag{4.3}$$

where c is the velocity of light ($c=3x10^8$), ε_{reff} effective dielectric constant which can be calculated by using the equation 7.4. andZ_o is the characteristics impedance of the CPW line and it will be discussed in Chapter-7,

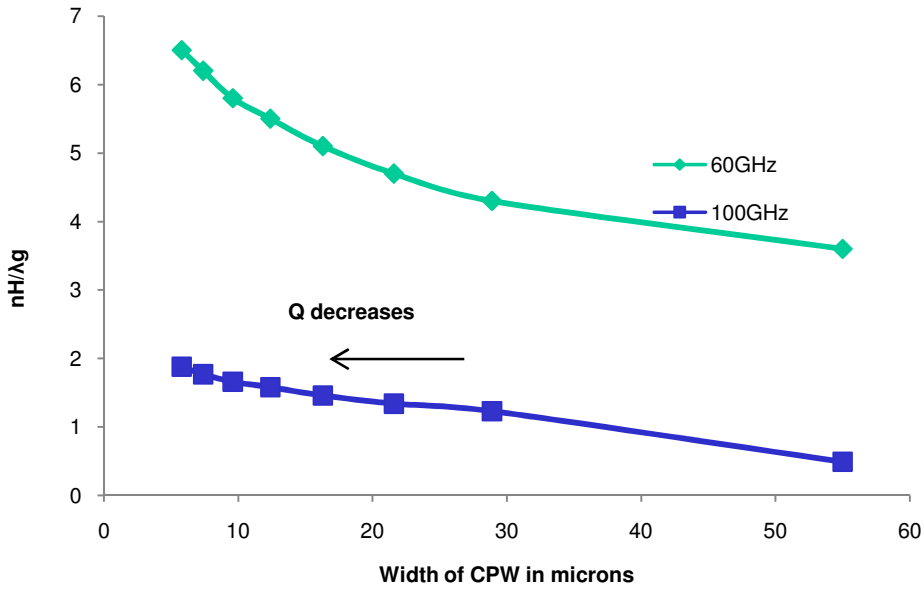

Figure-4.13. Inductance of CPW line as a function of width

All the described electrode geometries were applied to Gunn diodes which had a range of anode to cathode separations of 1, 2, 3 and 4 μm, and channel widthsfrom 30 to 120 microns.

4.6. REFERENCES

[1] A. Khalid, N. J. Pilgrim, G. M. Dunn, M. C. Holland, C. R. Stanley, I. G. Thayne, and D. R. S. Cumming, "A Planar Gunn Diode Operating Above 100 GHz," *IEEE Electron Device Lett.*, vol. 28, no. 10, pp. 849–851, Oct. 2007.

[2] A. Khalid, G. M. Dunn, N. Pilgrim, C. R. Stanley, I. G. Thayne, M. Holland, and D. R. S. Cumming, "Planar Gunn-type triode oscillator at 83 GHz," *Electron. Lett.*, vol. 43, no. 15, p. 837, 2007.

[3] W. Kowalsky, A. Schlachetzki, and H.-H. Wehmann, "Transferred-electron domains in In0.53Ga0.47As in dependence on the the nl product," *Solid. State. Electron.*, vol. 27, no. 2, pp. 187–189, Feb. 1984.

[4] A. Khalid, C. Li, V. Papageogiou, G. M. Dunn, M. J. Steer, I. G. Thayne, M. Kuball, C. H. Oxley, M. Montes Bajo, A. Stephen, J. Glover, and D. R. S. Cumming, "In0.53Ga0.47As Planar Gunn Diodes Operating at a Fundamental Frequency of 164 GHz," *Electron Device Lett. IEEE*, vol. 34, no. 1, pp. 39–41, Jan. 2013.

[5] C. Li, "Design and Characterisation of millimeter-wave planar Gunn diode and integrated circuits," University of Glasgow, 2011.

[6] K. Jones and E. Strid, "Where Are My On-Wafer Reference Planes?," in *30th ARFTG Conference Digest*, 1987, pp. 27–40.

[7] E. Strid, "Planar Impedance Standards and Accuracy Considerations in Vector Network Analysis," in *27th ARFTG Conference Digest*, 1986, pp. 159–166.

[8] C. Li, A. Khalid, L. B. Lok, N. J. Pilgrim, M. C. Holland, G. M. Dunn, and D. R. S. Cumming, "An In0.23Ga0.77As-based pHEMT-like planar Gunn diode operating at 116 GHz," in *35th International Conference on Infrared, Millimeter, and Terahertz Waves*, 2010, pp. 1–2.

[9] H. M. Shieh, W. C. Hsu, and C. L. Wu, "Very high two-dimensional electron gas concentrations with enhanced mobilities in selectively double-δ-doped GaAs/InGaAs pseudomorphic single quantum well heterostructures," *Appl. Phys. Lett.*, vol. 63, no. 4, p. 509, 1993.

[10] H.-M. Shieh, C.-L. Wu, W.-C. Hsu, Y.-H. Wu, and M.-J. Kao, "Enhanced Two-Dimensional Electron Gas Concentrations and Mobilities in Multiple δ- D o p e d G a A s / I n 0.25 G a 0.75 A s / G a A s Pseudomorphic Heterostructures," *Jpn. J. Appl. Phys.*, vol. 33, no. Part 1, No. 4A, pp. 1778–1780, Apr. 1994.

[11] A. Khalid, C. Li, V. Papageorgiou, N. J. Pilgrim, G. M. Dunn, and D. R. S. Cumming, "A 218-GHz second-harmonic multiquantum well GaAs-based

planar Gunn diodes," *Microw. Opt. Technol. Lett.*, vol. 55, no. 3, pp. 686–688, Mar. 2013.

[12] Y. P. Teoh, G. M. Dunn, N. Priestley, and M. Carr, "Monte Carlo simulations of asymmetry multiple transit region Gunn diodes," *Semicond. Sci. Technol.*, vol. 20, no. 5, pp. 418–422, May 2005.

[13] A. Baca and C. Ashby, *Fabrication of GaAs Devices*. The Institution of Engineering and Technology, Michael Faraday House, Six Hills Way, Stevenage SG1 2AY, UK: IET, 2005.

[14] C. Mead and W. Spitzer, "Fermi Level Position at Metal-Semiconductor Interfaces," *Phys. Rev.*, vol. 134, no. 3A, pp. A713–A716, May 1964.

[15] R. T. Tung, "Recent advances in Schottky barrier concepts," *Mater. Sci. Eng. R Reports*, vol. 35, no. 1–3, pp. 1–138, Nov. 2001.

[16] A. Khalid, C. Li, N. J. Pilgrim, M. C. Holland, G. M. Dunn, and D. R. S. Cumming, "Novel composite contact design and fabrication for planar Gunn devices for millimeter-wave and terahertz frequencies," *Phys. status solidi*, vol. 8, no. 2, pp. 316–318, Feb. 2011.

[17] W. T. Anderson, A. Christou, and J. E. Davey, "Development ot ohmic contacts for GaAs devices using epitaxial Ge films," *IEEE J. Solid-State Circuits*, vol. 13, no. 4, pp. 430–435, Aug. 1978.

[18] H. R. Kawata, T. Oku, A. Otsuki, and M. Murakami, "NiGe-based ohmic contacts to n-type GaAs. II. Effects of Au addition," *J. Appl. Phys.*, vol. 75, no. 5, p. 2530, 1994.

[19] E. D. Marshall, B. Zhang, L. C. Wang, P. F. Jiao, W. X. Chen, T. Sawada, S. S. Lau, K. L. Kavanagh, and T. F. Kuech, "Nonalloyed ohmic contacts to n-GaAs by solid-phase epitaxy of Ge," *J. Appl. Phys.*, vol. 62, no. 3, p. 942, 1987.

[20] L. C. Wang, P. H. Hao, and B. J. Wu, "Low-temperature-processed (150–175 °C) Ge/Pd-based Ohmic contacts (ρc□1×10−6 Ω cm2) to n-GaAs," *Appl. Phys. Lett.*, vol. 67, no. 4, p. 509, 1995.

[21] J. Lim, J. Mun, M. Kwak, and J. Lee, "Performance of Pd / Ge / Au / Pd / Au ohmic contacts and its application to GaAs metal-semiconductor field effect transistors," *Solid State Electron.*, vol. 43, pp. 1893–1900, 1999.

[22] I.-H. Kim, S. H. Park, T.-W. Lee, and M.-P. Park, "A study on Au/Ni/Au/Ge/Pd ohmic contact and its application to AlGaAs/GaAs heterojunction bipolar transistors," *Appl. Phys. Lett.*, vol. 71, no. 13, p. 1854, 1997.

[23] I. Mehdi, U. K. Reddy, J. Oh, J. R. East, and G. I. Haddad, "Nonalloyed and alloyed low-resistance ohmic contacts with good morphology for GaAs using a graded InGaAs cap layer," *J. Appl. Phys.*, vol. 65, no. 2, p. 867, 1989.

[24] A. Wakita, N. Moll, A. Fischer-Colbrie, and W. Stickle, "Design and surface chemistry of nonalloyed ohmic contacts to pseudomorphic InGaAs on n+GaAs," *J. Appl. Phys.*, vol. 68, no. 6, p. 2833, 1990.

[25] F. A. Amin, A. A. Rezazadeh, and S. W. Bland, "Non-alloyed ohmic contacts using MOCVD grown n+-InxGa1−xAs on n-GaAs," *Mater. Sci. Eng. B*, vol. 66, no. 1–3, pp. 194–198, Dec. 1999.

[26] B. Jeppsson and I. Marklund, "Failure mechanisms in Gunn diodes," *Electron. Lett.*, vol. 3, no. 5, p. 213, 1967.

[27] R. J. Tree, M. J. Josh, and C. T. Foxon, "On a failure mechanism in indium phosphide microwave oscillators," *Solid. State. Electron.*, vol. 14, no. 6, pp. 519–520, Jun. 1971.

[28] D. Ullrich, "Observation of recombination radiation in planar Gunn-effect devices," *Electron. Lett.*, vol. 7, no. 8, p. 193, 1971.

[29] W. F. Fallman and H. L. Hartnagel, "Metallic channels formed by high surface fields on GaAs planar devices," *Electron. Lett.*, vol. 7, no. 23, p. 692, 1971.

[30] A. Förster, J. Stock, S. Montanari, M. I. Lepsa, and H. Lüth, "Fabrication and Characterisation of GaAs Gunn Diode Chips for Applications at 77 GHz in Automotive Industry," *Sensors*, vol. 6, no. 4, pp. 350–360, Apr. 2006.

[31] C. Li, A. Khalid, L. B. Lok, N. J. Pilgrim, M. H. Holland, G. M. Dunn, and D. R. S. Cumming, "Millimeter-Wave Planar Gunn Diodes," in *(Unknown Conference in Sheffield)*, 2010.

[32] M. I. Maricar, J. Glover, G. Evans, V. Papageorgiou, D. Cumming, and C. Oxley, "Planar Gunn Diode and Resonators," in *4th Annual Seminar on Passive RF and Microwave Components*, 2013, pp. 2–5.

[33] M. I. Maricar, J. Glover, G. A. Evans, A. Khalid, V. Papageorgiou, L. Chong, G. Dunn, and C. H. Oxley, "Planar Gunn diode characterisation and resonator elements to realise oscillator circuits," in International Conference on Advanced Nanomaterials & Emerging Engineering Technologies ICANMEET-2013, 2013, pp. 674–678.

Chapter: 5

Measurement results of an AlGaAs/GaAs planar Gunn diode on a GaAs substrate

5.1. INTRODUCTION

A description of the design and fabrication of the planar Gunn diode was briefly discussed in chapter 4. In this chapter the AlGaAs/GaAs based hetero-structure planar Gunn diode with different electrode geometries and separations between the anode and cathode (L_{ac}) electrodes are characterised for DC and RF performance. This chapter will present the results, which include DC, S-parameter and spectrum analyser measurements.

5.2. FABRICATION PROCESS OF A PLANAR GUNN DIODE USING A GaAs SUBSTRATE.

The first planar Gunn diode of this type was developed by the Universities of Glasgow and of Aberdeen in 2007 [1]–[3]. A description of the fabrication process was discussed in section-4.2. The planar Gunn diodes were fabricated on GaAs wafers with material specification given in ***Table 4.1***. Each wafer was given a unique identification number. The first process run in which all four electrode structures (Section 4.3) were fabricated was on wafer S18132;this particular process run had no silicon nitride passivation. Initial studies on this wafer revealed that the device surfaces oxidised due to exposure of the top layer to the atmosphere. This oxidation layer was observed with a SEM, and will be discussed later in this chapter. It is well

known that silicon nitride deposited [4] on the surface will minimize the surface oxidation of electronic devices. All subsequent wafers containing planar Gunn diodes with different electrode geometries and external circuit elements were passivated using silicon nitride. The unique numbers of the wafer and the corresponding fabricated device and circuit configurationsare given in ***Table 5.1.***

Wafer No	Material	Circuit Configuration
S18132/AKH0862	GaAs	Planar Gunn diodes with different electrode geometries and no silicon nitride passivation
S18163/AKH3063	GaAs	Planar Gunn diode with different electrode geometries and passivated using silicon nitride
S18165/AKH4065	GaAs	Planar Gunn diode with different electrode geometries including fundamental and second harmonic extraction circuits were passivated using silicon nitride
S16860/AKH0866	GaAs	Planar Gunn diode with different electrode geometries including fundamental and second harmonic extraction circuits were passivated using silicon nitride
S18164/AKH1064	GaAs	Planar Gunn diode with different electrode geometries including fundamental and Second harmonic extraction circuits were passivated using silicon nitride

Table.5.1. Different wafer identification numbers.

5.3. DESIGN AND ANALYSIS OF ELECTRODE GEOMETRIES FOR A PLANAR GUNN DIODE

An outline of the different electrode geometry designs incorporated in the planar Gunn diode was discussed in the section 4.4. Preliminary DC measurement results on the planar Gunn diode indicate that the current can be increased by increasing the width (can be considered similar to a FET device) of the active channel of the planar Gunn diode, which was also discussed in the section 4.4. The increase in current will increase the device RF output power, provided the DC to RF conversion efficiency remains constant. To obtain the highest RF output power from the device, only those devices with a width of 120 microns were characterised, however the active

length of the device was varied between 1 to 4 microns, as this will influence the fundamental transit mode frequency of the planar Gunn diode.

5.3.1. DC MEASUREMENTS ON DIFFERENT TYPES OF PLANAR GUNN DIODE

Initially DC pulse measurements were made on all the planar Gunn diodes to give an indication if the diodes had a NDR region. The pulsed DC characteristic (Chapter 3) was measured using a semiconductor device analyser from Agilent technologies (B1500A) connected to the automated probe station manufactured by Cascade Microtech, enabling measurements to be made across the wafer. **Figure 5.1** shows the pulsed and continuous IV characteristics of a Type-A planar Gunn diode. The measurement of the diode pulsed IV characteristic willminimize diode self-heating allowing the NDR region to bemore easily detected.The measured pulsed IV characteristic can also be used to represent the voltage dependent current generator in the electrical equivalent circuit model of the planar Gunn diode, by fitting an n^{th} order polynomial equation to simulate the IV characteristic; this will be discussed in more detail in Chapter-8.

The pulsed IV characteristics of a number of Types-A devices with different anode to cathode separations (L_{ac}) were measured. **Figure.5.2**. shows the pulsed IV characteristics of the Type-A planar Gunn diode with different active channel lengths (from 1 to 4 microns). The device with a 1 micron active channel length (L_{ac}), the NDR was noticeable at a bias voltage of 2.85V with the peak current of 92mA, whereas for the device with 4μm active channel length (L_{ac}) the NDR was noticeable at 4.38V with a peak current of 85mA. For the latter type of device, the NDR region occurred at a similar threshold voltage reported by Glasgow University [5].The pulsed IV measurement results of the Type-A planar Gunn diode were directly compared with the experimental results of the Glasgow device with the same active width (120 microns) and length (4 microns) which was published by Chong Li and Geoff Dunn et al [5], [6] and the comparison is shown in ***Table.5.2.*** The results

show that Type-A planar Gunn diodes in this work gave a higher current when compared to Chong Li et al [5]. This may be due to an improved material or fabrication technology leading to a lower device contact resistance discussed in section 3.3.

Anode to Cathode separation (L_{ac})	**Literature[5] (Chong Li Work)**		**Measurements from this work**	
	Bias Voltage (V)	*Peak Current (mA)*	*Bias Voltage (V)*	*Peak Current (mA)*
1µm	2.5	58	2.85	92
2µm	-	-	3.42	88
3µm	-	-	3.85	86
4µm	5.33	52.5	4.35	85

Table 5.2 Peak current of Planar Gunn diodes

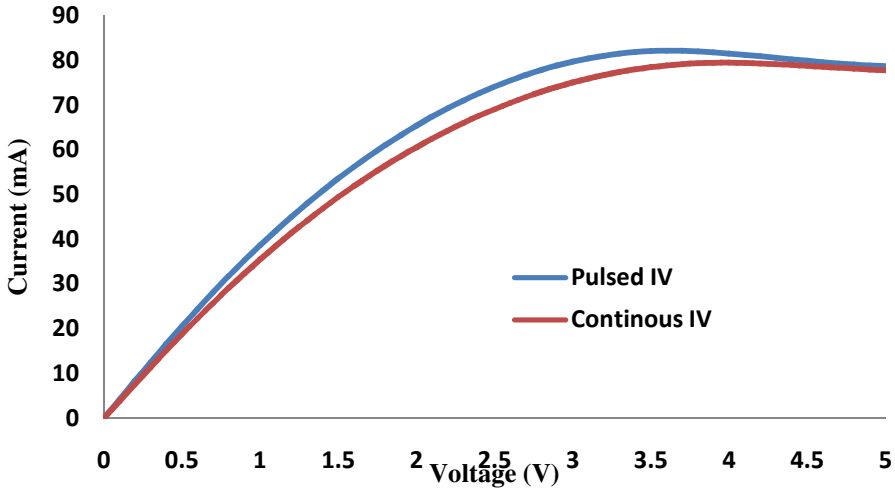

Figure.5.1 Continuous and pulsed IV measurements of a Type-A planar Gunn diode

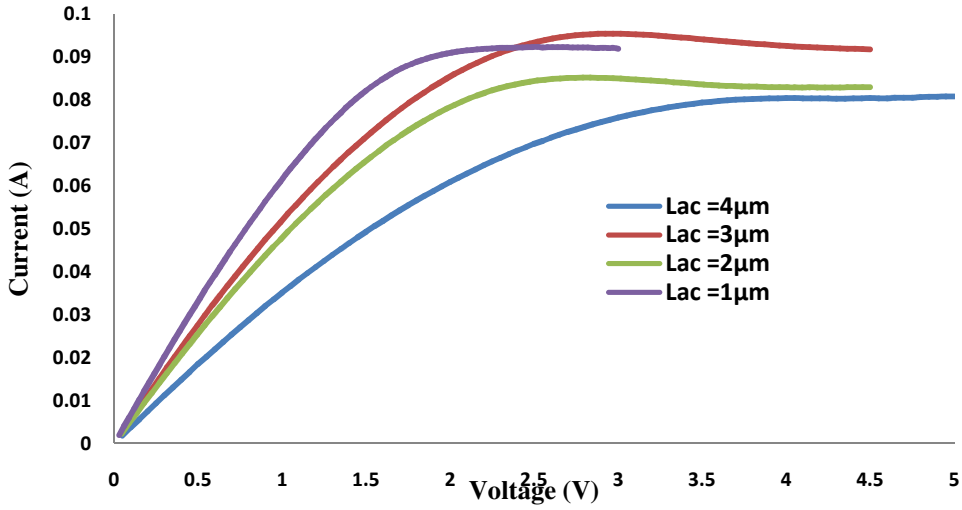

Figure.5.2.Pulsed IV Characteristics of a Type-A planar Gunn diode having different L_{ac}

Figure.5.3. shows the pulsed IV measurement results for the different electrode geometry (type A, B, C & D) planar Gunn diodes with an active channel length of 4 micron. The NDR region of these diodes was detected at a bias voltage of around 3.8V with a peak current of around 85 mA. The devices which exhibited a poor or no NDR region were identified and RFcharacterisation was not carried out on these devices.

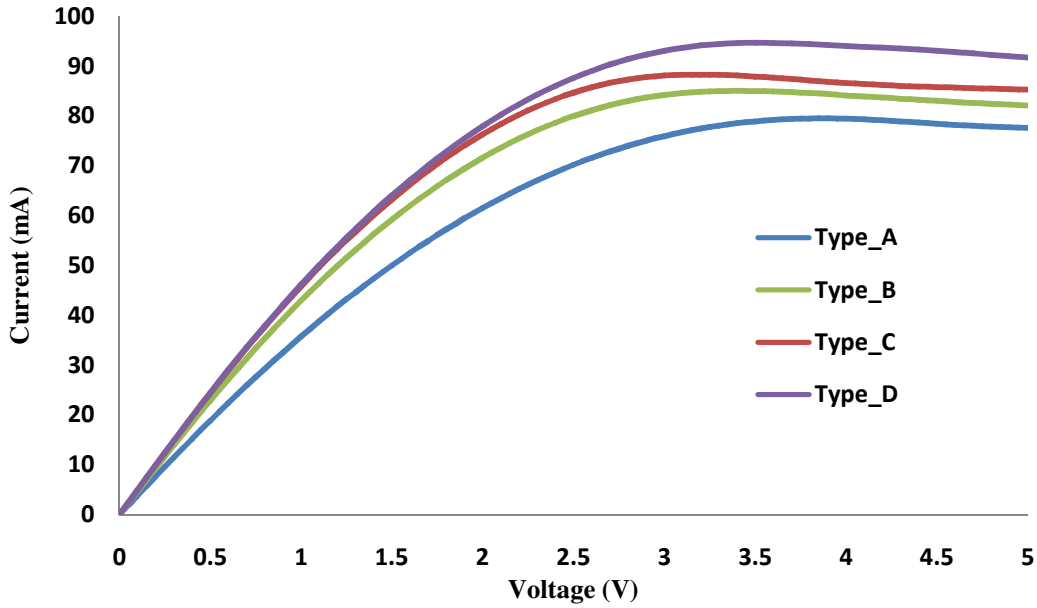

Figure.5.3. Pulsed IV measurementsresults on different types of planar Gunn diode with an active channel length of 4 micron (Lac=4µm)

5.3.2. RF MEASUREMENTS ON PLANAR GUNN DIODES WITH DIFFERENT ELECTRODES GEOMENTRIES

As discussed, the DC measurement results were used to identify the NDR region of the device. If the device gave no NDR region or showed a short or open circuited DC characteristic then these were marked and no further evaluation of them took place. Small-signal S-parameter measurements were made to determine the one port input impedance from DC to 110 GHz of the different electrode structure planar Gunn diodes, using the Agilent vector network analyser (VNA). The 40-60-40µm pitch 50 Ohm probes from GGB industries were connected to the VNA and the system was calibrated from

DC to 110 GHz using a calibration substrate (109-102B) from Cascade Microtech (which was described in chapter-3, section 3.5). The VNA measurements gave a first insight as to whether the diode had RF negative resistance; if the diode had a magnitude of S_{11} greater than 1 then the diode had negative resistance and if the diode had magnitude of S_{11} less than 1 then it had no negative resistance. If the diode with negative resistance is placed in a circuit which resonates out its reactance then the diode will oscillate at the resonate frequency of the circuit. **Figure 5.4** shows the magnitude S_{11}as a function of frequency for a Type-A planar Gunn diode (with an active channel length of 4 microns) and the bias voltage was increased from 0 to 6.2V. From the plot it can be seen that the magnitude of$S_{11}$was positive and greater than 1 for bias voltages between 5 to 6.2 V. This was in reasonable agreement with the pulsed DC IV measurement which indicated the start of the NDR region the bias voltage was greater than 4.4 V. Maximum S_{11} occurred at a frequency of 26.20 GHz, which is close to the expected transit mode frequency of the diode, ***Table 4.3***. This experiment also shows the importance of using VNA to detect the maximum RF negative resistance of the diode.

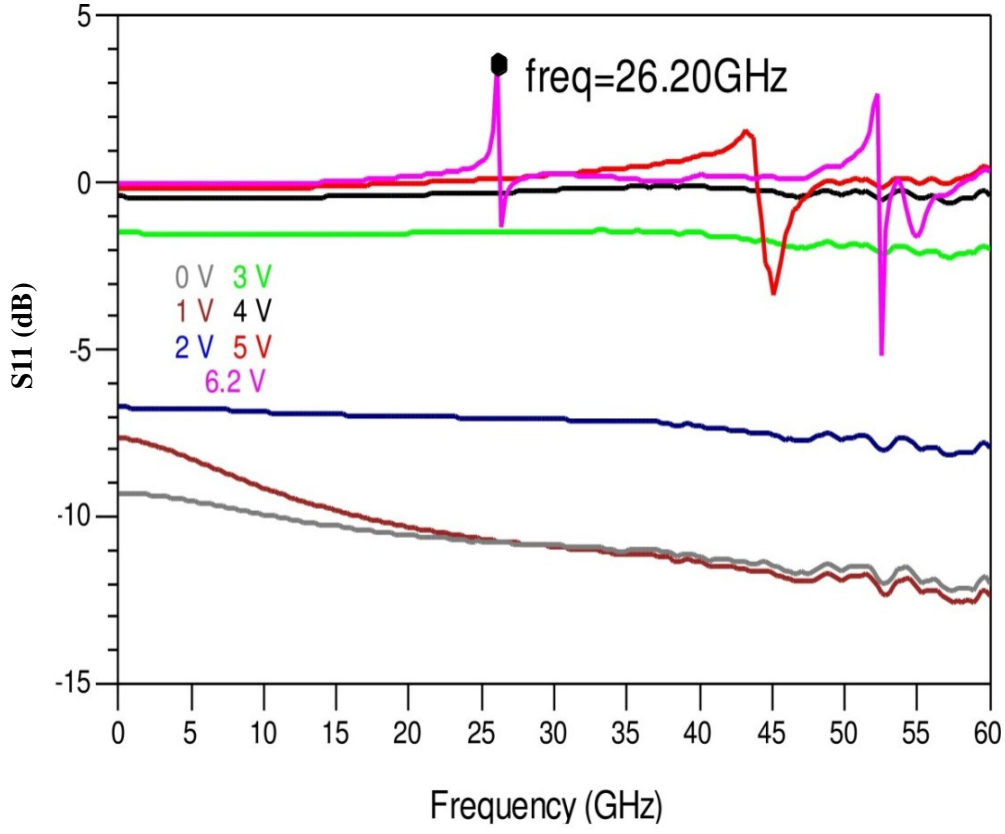

Figure.5.4. Magnitude of S_{11} of the Type-A planar Gunn diode with different bias level

Preliminary VNA measurements over the frequency range DC to 110GHz were also made on the remaining three device structures (type B, C and D) and at different bias voltages. The devices chosen were those which showed an NDR region during DC pulsed IV testing and had an active region length L_{ac} = 4 microns. **Figure 5.5** shows the measured magnitude of S_{11} of the four planar Gunn diode types, and all the structures gave an indication of negative resistance for bias levels between 4 to 6.2V. The VNA measurements of these devices showed the magnitude of S_{11} as having an almost smooth frequency response over the entire frequency band (DC to 110GHz), peaking at 26.01 GHz for the Type-B device at 5.31V, 28.12 GHz for the Type-C device at 4.86 V, and 24.28 GHz for the Type-D device at 5.26 V. The VNA measurements of the four planar Gunn diodes with different electrode geometries showed that the devices were oscillating at the fundamental frequencies of 26.20 for the Type-A device, 26.01 GHz for the Type-B device, 28.12 GHz for the Type-C device and 24.28 GHz for the Type-D device. The results also suggest that the oscillation frequency of these (L_{ac} = 4μm) planar Gunn diodes with different electrode geometries is similar to the theoretical results ***Table.4.3***, However, the Type-D device the oscillation frequency was a little lower than expected ***Table.5.3.***

The oscillation frequency of the planar Gunn diode is due to the formation and nucleation of a Gunn domain towards the anode with increasing bias voltage. This may occur sooner if the electrons in the channel heat rapidly leading to the earlier onset of the domain formation. The space in the active channel in which the domain forms is known as the dead space and can be calculated using equation (5.1) which was rearranged from equation 4.2.

$$L_{dead} = L_{ac} - \frac{v_{domain}}{f} \tag{5.1}$$

For the selected devices measured, the Type-D device gave a higher current

and this may lead to an increase in self-heating reducing the dead space and therefore decreasing the transient mode frequency of oscillation.

Electrodes structures	Peak Current (mA)	Theoretical oscillation frequency of planar Gunn diode (GHz)	Measured oscillation frequency of planar Gunn diode (GHz)	Bias Voltage (V)	Calculated dead space for the planar Gunn diode (microns)
Type-A	85	25	26.20	5.36	0.183
Type-B	83	25	26.01	5.41	0.155
Type-C	90	25	28.12	4.86	0.301
Type-D	94	25	24.28	5.26	≈0.001

Table.5.3. Comparison of theoretical and measurement results of the planar Gunn diode with an active channel length of 4 micron

From the measurements it was not surprising that the Type-B device showed very similar performance when compared to the Type-A device (as they are very similar in structure), so Type B devices have not been included for further experimental analyses. Only Type-A, Type-C and Type-D devices were fully studied including spectrum analyser measurements, which will be discussed later in this chapter. It was interesting to note that the Type-C device gave the highest positive magnitude of S_{11} ($S_{11} \approx +5.87$ dB) and Type- D device the second highest S_{11} positive magnitude ($S_{11} \approx +4.2$ dB) when compared to Type-A and Type-B devices.

Figure.5.6. shows the magnitude of the measured S_{11} for the type-C planar Gunn diode with different active channel lengths (L_{ac}). As expected the devices with smaller L_{ac} oscillated at a higher frequency. ***Table.5.4.*** shows the measured maximum negative resistance(frequency at which S_{11} was greatest) of the planar Gunn diodes with different electrode structures (Type A, C and D) with anode and cathode separations of L_{ac} =1 to 4 micron. The small differences in the fundamental oscillation frequency between the different device types (maximum negative resistance) was probably due to parasitic variations associated with the different electrode geometries and small differ-

ences in the dead space in the active region of the device due to fabrication variance Type-D planar Gunn diode consistently oscillated at a higher frequency; this might be due to the device working at the Quenched mode or the internal series inductance matching pulling the device to higher frequency.

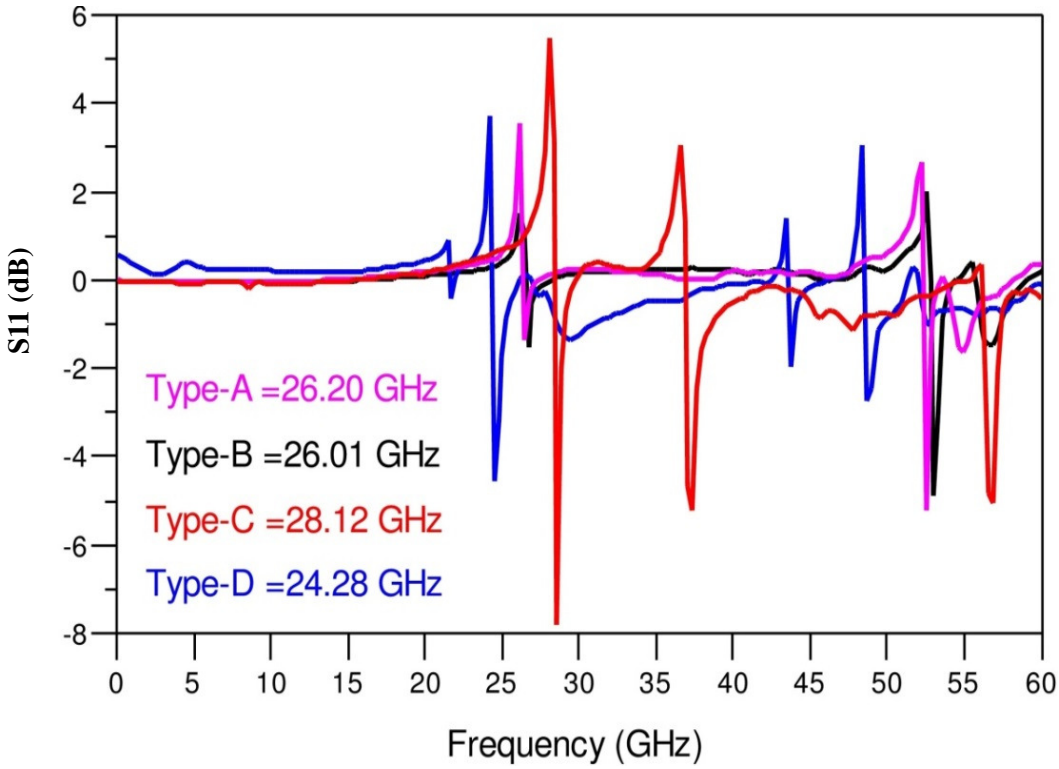

Figure.5.5. Magnitude of the planar Gunn diode with different electrodes geometries

Different types of Planar Gunn diode	Oscillation frequency (GHz) for 4µm device	Oscillation frequency (GHz) for 3µm device	Oscillation frequency (GHz) for 2µm device	Oscillation frequency (GHz) for 1µm device
Type-A	28.17	39.01	66.32	106.71
Type-B	27.79	38.73	65.67	103.36
Type-C	27.03	40.49	65.49	105.05
Type-D	30.18	36.43	51.76	<110

Table.5.4. The frequency at which S_{11} was greatest for each of the device Types A,B,C and D, and with active channel lengths stepping from 1 to 4 microns in 1 micron steps

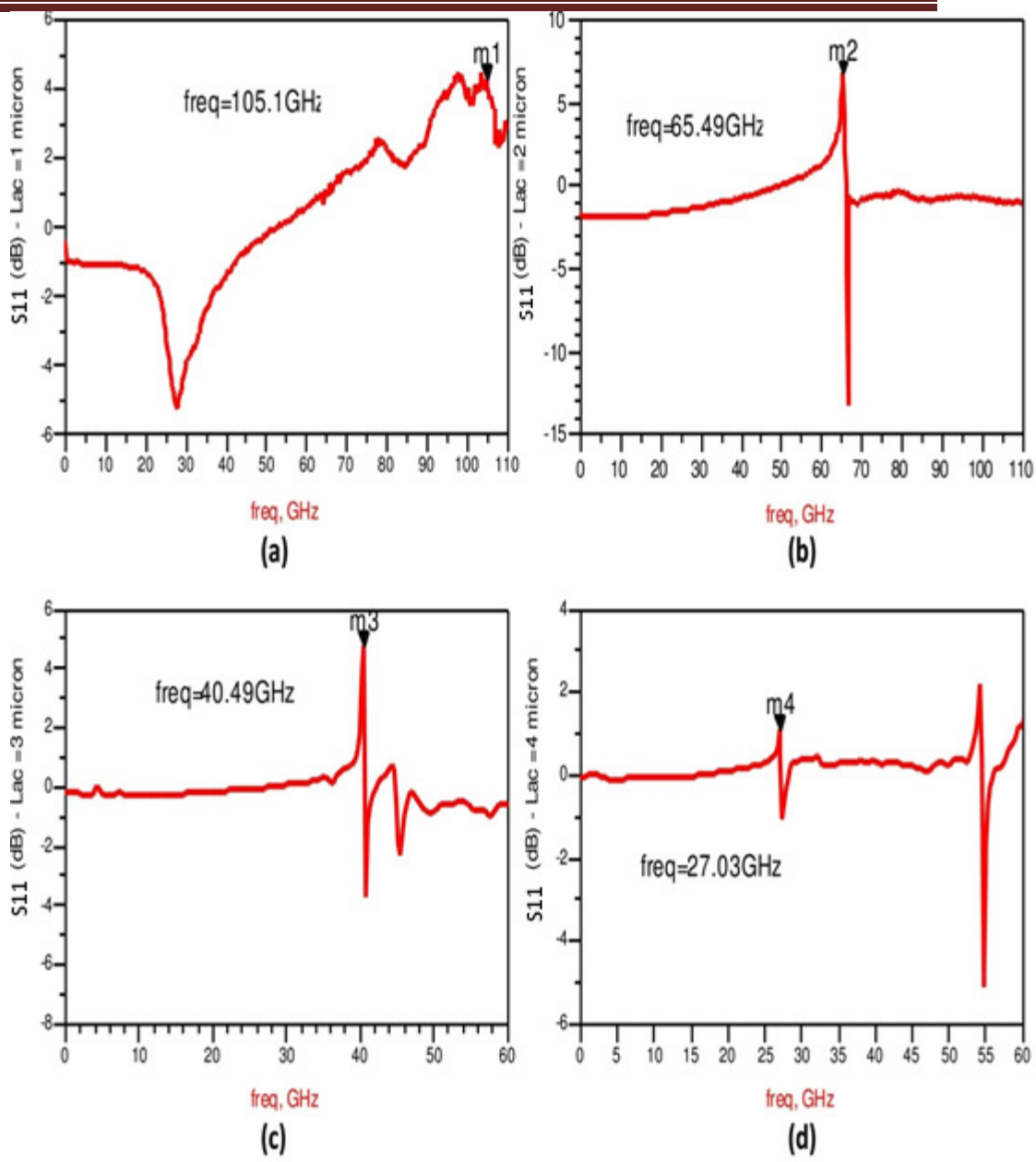

Figure.5.6. Magnitude of S_{11} expressed in dB's for the Type-C planar Gunn diode with different active channel lengths (a)Active channel length Lac =1 µm (b) Active channel length Lac =2 µm (c) Active channel length Lac =3 µm (d) Active channel length Lac =4 µm

5.3.3. SPECTRUM ANALYSER MEASUREMENTS ON DIFFERENT TYPES OF PLANAR GUNN DIODE

Apart from the IV and VNA measurement of the planar Gunn diodes (L_{ac}= 1 to 4 µm); spectrum analyser measurements were used to confirm the oscilla-

tion frequency and to give an indication of RF output power from the devices. The RF output spectrum was measured using the E4448 spectrum analyser from Agilent technologies, a GSG probe 50 Ohm (40-60-40μm pitch separation) manufactured byCascade Microtech and a mixer from Farran technology. An external harmonic mixer (V-band or W-band) was used to increase the frequency range of the spectrum analyser from 50 GHz to 125 GHz respectively. The detailed description of the measurement test bench was discussed in Chapter-3. TheType-A device was the base-line device for this work as it represented the electrode configuration adopted by Glasgow University (chapter 4). A number of type-A devices were measured to obtain a base-line for comparison with the Type-C and Type-D planar Gunn diodes. Spectrum analyser measurements made on a Type-A device with 4 microns of electrode separation were found to naturally oscillate at 41 GHz (with an RF output power of -29.36 dBm) which is higher than the theoretical calculation (***Table 5.3)*** and measurements made on comparable Type A devices using the VNA**.**It was thought theactual physical separation between the anode and cathode electrodes on this device may be <4 microns. The distance between the anode and cathode separation was measured using a scanning electron microscope (SEM) and found to be of the order of 3.6 μm, which partially accounted for the higher oscillation frequency of 41 GHz. Also, the estimated dead space by Li [5] was approximately 0.25 μm, which will reduce the channel width further, thereby increasing the theoretical transit frequency mode of operation to 29.8 GHz.As mentioned earlier in section 5.3.2. Type-C and Type-D devices were also studied using spectrum analyser measurements as both device types gave a higher positive magnitude of $S_{11}(|S_{11}| > 1)$ when compare to Type A and B devices from the same process wafer.

Type-C planar Gunn diode

Initially the Type-C planar Gunn diode was designed to simplify the de-embedding of the active region of the diode. This was arranged by extending the 50 Ohm CPW line as close as possible to the active region of the diode. The thought process was that models exist for 50 Ohm CPW which

can be used to de-embed the measured S-parameters, thereby obtaining an improved set of S-parameters for the active region of the diode. This device type was used to obtain the de-embedded diode reactance. The output RF spectrum of the Type-C planar Gunn diode was obtained by using the spectrum analyser measurement setup.It was found that the Type-C planar Gunn diode started to oscillate when the bias voltage was between 4.4 to 5.6 V. **Figure 5.7** shows the RF output spectrum of a Type-C planar Gunn diode. The result indicated that the Type-C planar Gunn diode oscillated at a fundamental frequency of 25.17 GHz with an RF output power of -19.69 dBm, at a bias voltage of 4.56 V. To obtain the maximum RF output power and the corresponding transit mode oscillation frequency from the device, the bias voltage applied to the planar Gunn diode was optimised; this process is known as bias voltage tuning. The Type- C planar Gunn diode was oscillating at 25.17 GHz with the highest power of -19.69 dBm ata bias voltage of4.46 V and the results are shown in **Figure 5.8.** The oscillation frequency of Type-C device was closer to the theoretical transit mode frequency. The output power from this device was relatively low and to obtain higher RF output power the device will need to be matched to the 50 Ohm CPW line, and will be more fully discussed in Chapter-8.A number of Type-C planar Gunn diodes with different anode to cathode separation were measured to identify the transit mode oscillation frequency and the corresponding RF output power from each of the devices. ***Table.5.***5 shows the transit mode oscillation frequency and RF output power of the above variants of the Type-C planar Gunn diode. The transit mode oscillation frequencies of these devices were in good agreement with the maximum S_{11} obtained from the VNA measurements, which was discussed in the section 5.3.2.

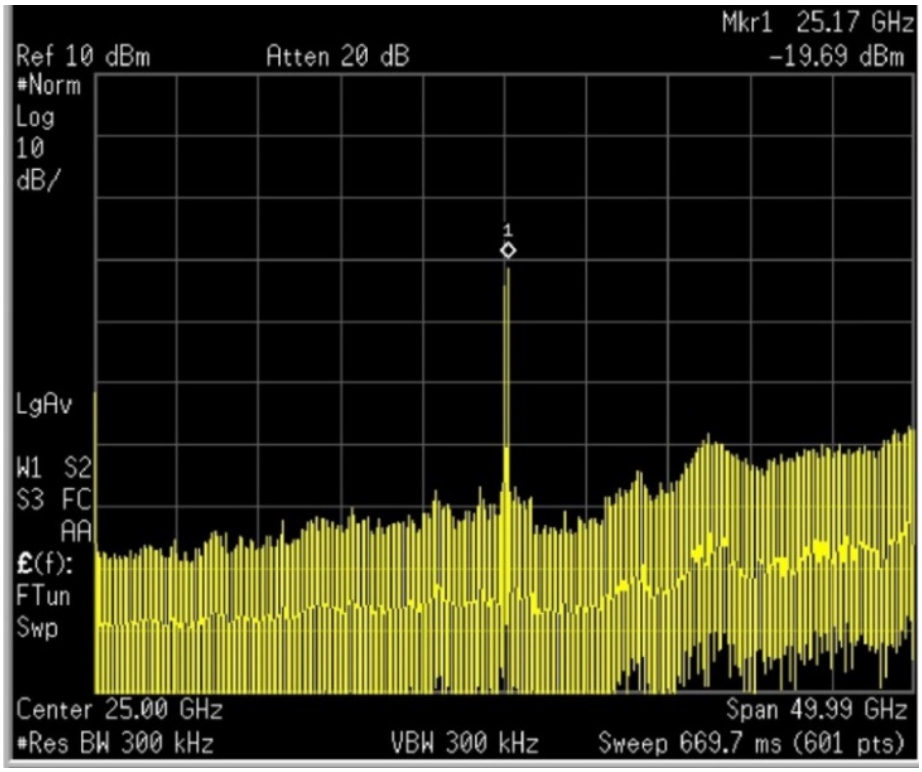

Figure.5.7.Spectrum analyser results of 4μmType-C planar Gunn diode

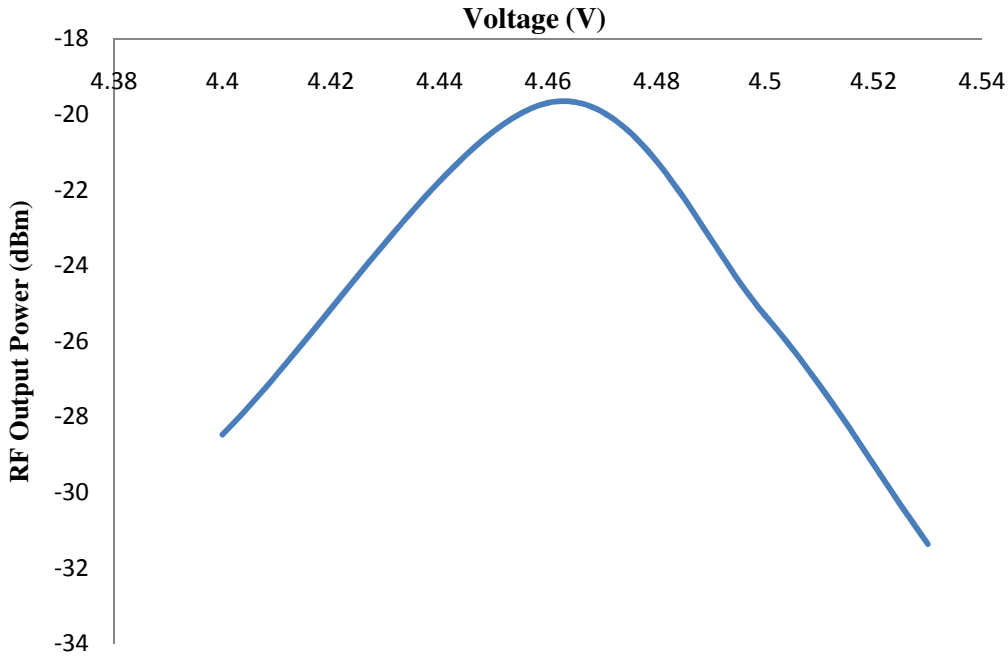

Figrue.5.8.The maximum frequency and output power obtained from a type C device by optimising the applied bias voltage

Anode to Cathode separation (L_{ac}) in µm	Oscillation frequency of the Type-C planar Gunn diode (GHz)		RF output Power (dBm)
	Network Analyser Results	Spectrum Analyser Results	
1	105.1	105.08	-21.36
2	65.49	64.32	-16.46
3	40.49	-	-
4	27.03	25.17	-19.69

Table.5.5. Oscillation frequency and RF output power of the Type-C planar Gunn diode

Type-D planar Gunn diode

The Type-D planar Gunn diode was designed to improve the matching to obtain higher RF power at the transit mode frequency from the planar Gunn diode. The anode to cathode separation of this device wasalso varied from 1 to 4 microns and keeping the channel width (W=120 micron) constant. The Type-D AlGaAs/GaAs based hetero-structures planar Gunn diode was RF characterised by measuring its fundamental oscillation frequency and RF output power. A Type D device with an anode and cathode separation of 1 micron and biased with 2.81 V, oscillated at a natural fundamental frequency of 120.47 GHz with an RF output power of -9.14 dBm. To-date this represents both the highest 'transit type' mode frequency of oscillation and RF output power ever recorded for an AlGaAs/GaAs based hetero-structures planar Gunn diode with an anode to cathode separation of 1 micron.**Figure-5.9** [7]**.**shows the measured output spectrum of the Type-D planar Gunn diode. The experimental results of this device suggested that it was oscillating at a higher fundamental frequency than predicted by simple theory (***Table.5.3***). SEM measurements were made on this device to verify the anode to cathode separation(L_{ac}) of the planar Gunn diode. **Figure-5.10** shows a scanning electron microscope (SEM) image of the Type-D device with verification that the anode to cathode separation was 1 micron.The CPW line to the active region of the planar Gunn diode was made narrow to

represent a series inductor as discussed in chapter 4 and the SEM images confirm that the line width was 100nm.***Table.5.6*** shows that the fundamental oscillation frequency of the Type-D planar Gunn diode was reduced as the active channel length of the device was increased suggesting that the device was functioning in the transit mode. The RF output power from the Type-D devices with anode to cathode separation of 3 and 4 microns respectively was lower when compared to other planar Gunn diode geometries, for example Type A and C. This may be due to the series inductor providing a poorer match at the lower frequencies, but a good match at the higher frequency, which may be a hybrid transit mode [7].

A simple calculation was carried out to confirm that the series inductor provided a good match at the high frequency. The total capacitance of the Type-D planar Gunn diode was found from the experimental S-parameters to be ≈ 26 fF and will be discussed in Chapter-8. The series inductance was calculated from the equations given in chapter-4. The oscillation frequency of the device was calculated using $f_0 = \frac{1}{2\pi\sqrt{LC}}$and was found to be of the order of 113 GHz which is close to the experimentally measured 120 GHz, given that parasitics were not taken into account this in reasonable agreement with the experimental result.

Anode to Cathode separation (L_{ac}) in µm	**Oscillation frequency of the Type-D planar Gunn diode (GHz)**		**RF output Power (dBm)**
	Network Analyser Results	**Spectrum Analyser Results**	
1	<110	120.47	-9.14
2	51.76	-	-
3	36.43	37.12	-41.65
4	30.18	28.31	-28.67

Table.5.6. A comparison of the oscillation frequency measured using VNA and spectrum analyser results and RF output power of the Type-D planar Gunn diode

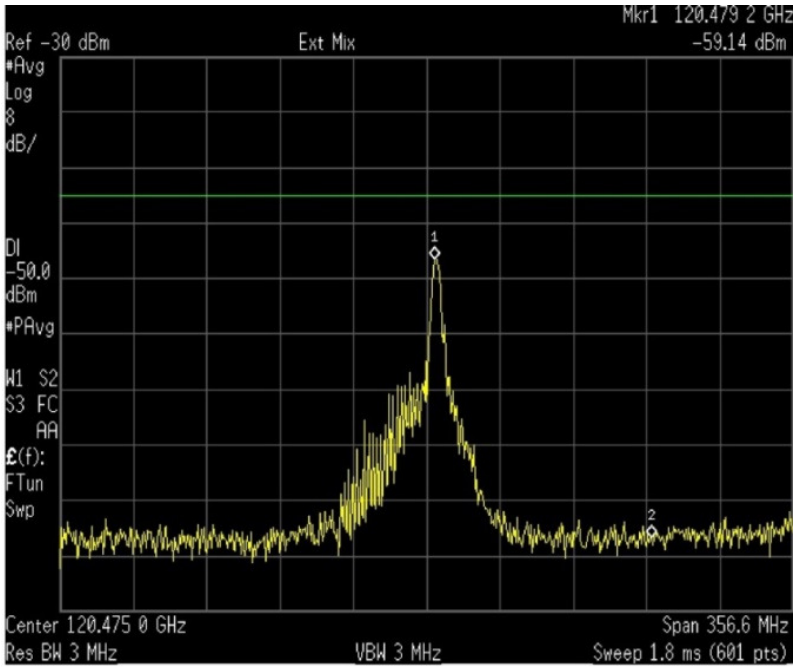

Figure.5.9. Spectrum analyser measurement for second harmonics frequency using W-band setup

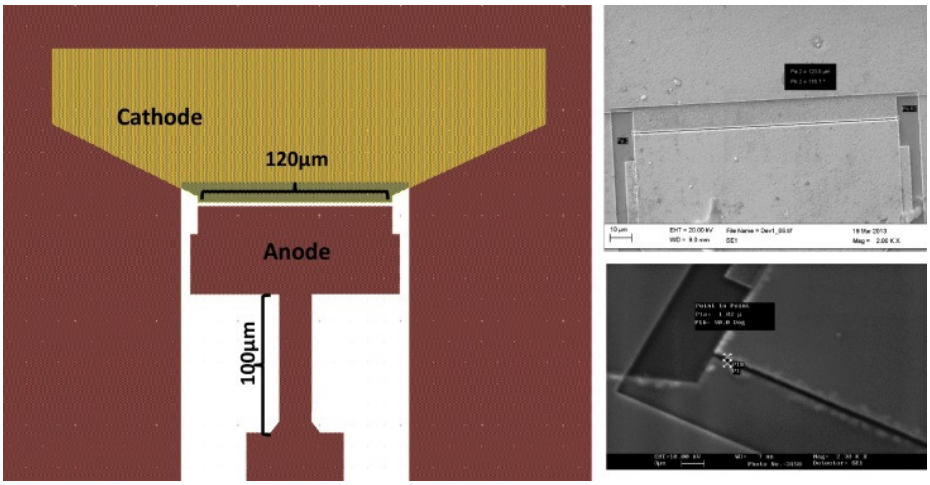

Figure.5.10. Scanning Electron Microscopy image ofthe Type-D planar Gunn diode

5.3.4. ANALYSIS OF THE PLANAR GUNN DIODE WITH DIFFER-ENT ELECTRODE GEOMETRIES

Figure 5.11shows the measured transit mode oscillation frequency of the Type-A, Type-C and Type-D planar Gunn diodes with different anode to

cathode separations. It can be seen that the planar Gunn diodeswith a 1µm anode to cathode separation oscillated in the frequency range of 96 GHz for Type- C device which is represented in red colour in **Figure.5.11.** and 121 GHz for Type D device which is represented in black colour in **Figure.5.11.** It is interesting to note that the maximum frequency of oscillation was observed to be greater than the simple analysis for the transit time mode, which was described in the chapter-4. A possible reason for the higher frequency of oscillation is the existence of the dead space which occurs in the active region of the planar Gunn diode.

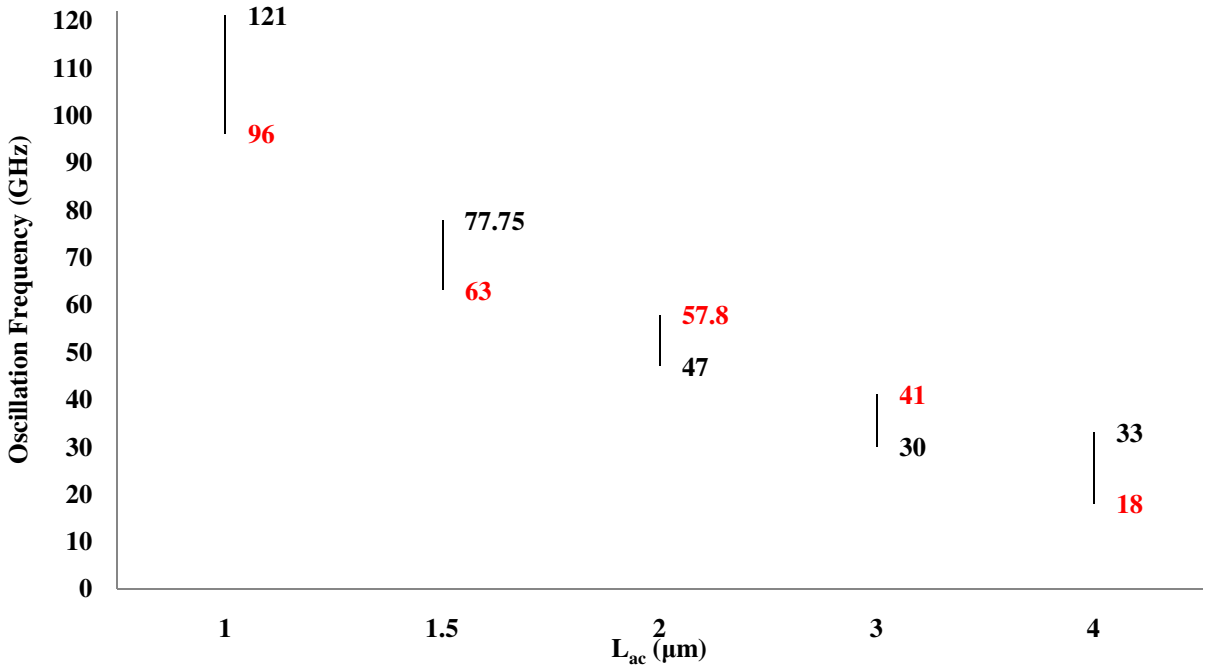

Figure.5.11.Measured frequency of oscillation for a L_{ac} from 1µm to 4µm of Type-C and Type-D planar Gunn diode

Table.5.11. shows the oscillation frequency for the respective active channel length (L_{ac}) of the Type-A and Type-D planar Gunn diode. It shows that the frequency can be changed by varying the active channel length of the device.

Figure 5.12 shows the estimated dead space which was obtained by plotting 1/*f* against active channel length for device Types A and C, where f was the measured transit mode frequency. The gradient of the resulting linear line will represent the domain velocity and where the line intersects the x-axis gives an

estimate of the dead space. The Type-D planar Gunn diode was not included as it was considered not to be representative as it included an on chip matching circuit element, and the experimental results suggest that it is not working in a pure transit mode, but rather a 'hybrid transit mode'. From **Figure 5.12,** the channel dead space of the devices appears to be constant with decreasing active channel length, however, there was evidence of departure from the linear nature as the active channel length approached 1 micron. The calculated dead space (0.23 microns) for the planar Gunn diode was in good agreement with previous work (0.25 microns) which was reported by Li Chong and Ata Khalid [2], [5]. Recently, Ata Kahlid[8] has reported on measurements on planar Gunn diodes with sub 1 micron active channel length and his work suggests at these channel lengths the dead space is very much smaller than the reported 0.23 microns which would be in agreement with the experimental observation in **Figure 5.12** departing from linearity as the active length of the device approaches 1 micron.

Types	Oscillation Frequency (GHz)	L_{ac} (μm)
Type-A	27.57	4
	35.68	3
	36.83	3
	55.45	2
	54.85	2
	104.32	1
Type-C	27.17	4
	27.32	4
	27.06	4
	26.98	4
	36.71	3
	36.43	3
	54.98	2
	105.09	1

Table.5.7. Oscillation frequency type-c and type-a planar Gunn diode

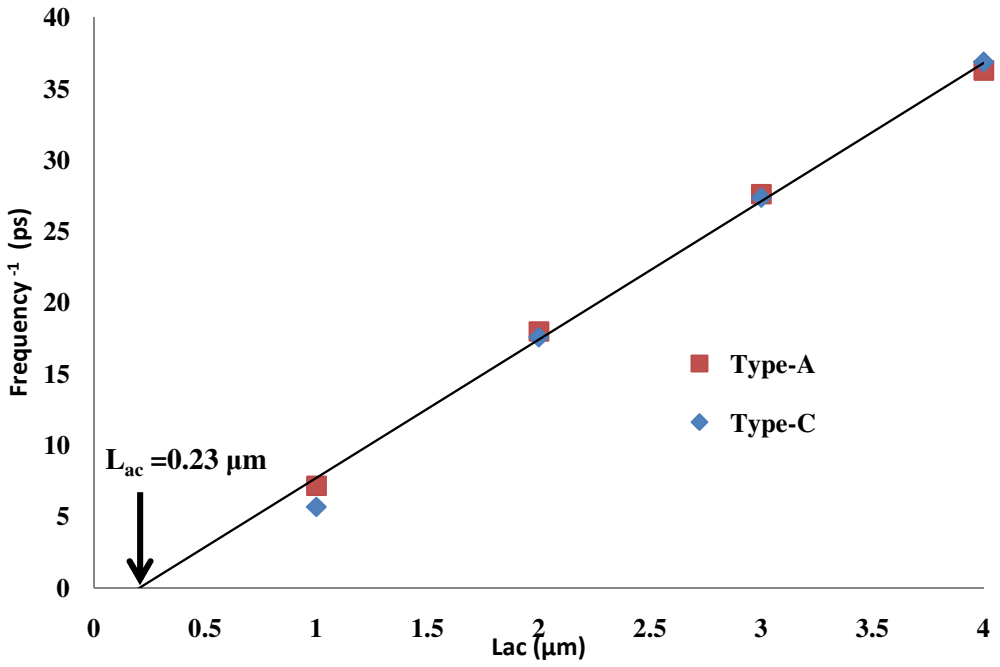

Figure.5.12.Estimater dead space for a L_{ac} from 1µm to 4µm of Type-A and Type-C planar Gunn diode

5.4. ANALYSIS OF MEASUREMENTS ON DIFFERENT WA-FERS

Work was carried out to investigate if there was a correlation between diode pulsed IV showing NDR, and subsequent RF measurements (VNA showing high positive S_{11} and transit mode oscillation frequency using the spectrum analyser measurement). The total number of devices fabricated and tested was to some degree dependent on the area of the wafer. ***Table 5.8*** shows the number of devices fabricated and tested on each of the wafers. The devices from wafers No.S18161, S16862, S181613, S181164 and S18142 which were measured using pulse IV and RF characterisationand giving both NDR and a measured transit mode oscillation frequency were plotted as percentage of the total number of devices actually measured in a histogram **Figure.5.13.** The resultsindicated very good correspondence between devic-

es with a measured NDR region, most of which showed transit mode oscillation; therefore pulsed IV characteristics can be used to identify devices with RF oscillation performance. The percentage of diodes with no or poor NDR were also plotted on the histogram. It is interesting to note that the diodes on wafer S18142 gave a high percentage of device failures (no NDR) and on this wafer the fabricated TLM structures had a high measured contact resistance. ***Table.5.9***. shows the percentage of device failures as a function of the contact resistance, and it was found that the wafers with the highest percentage of failures were those wafers with the highest measured TLM contact resistance.

Wafers	Number of device Fabricated	Number of device Measured
S18132	112	112
S18163	400	240
S18165	40	36
S16860	40	36
S18164	40	36

.5.8.Total number of device fabricated and measured

Wafers	Contact Resistance	Device failure
S18132	0.90	64.29
S18163	0.75	12.08
S18165	0.76	16.67
S16860	0.81	11.11
S18164	0.83	25.02

Table.5.9.Percentage of device failure as a function of contact resistance

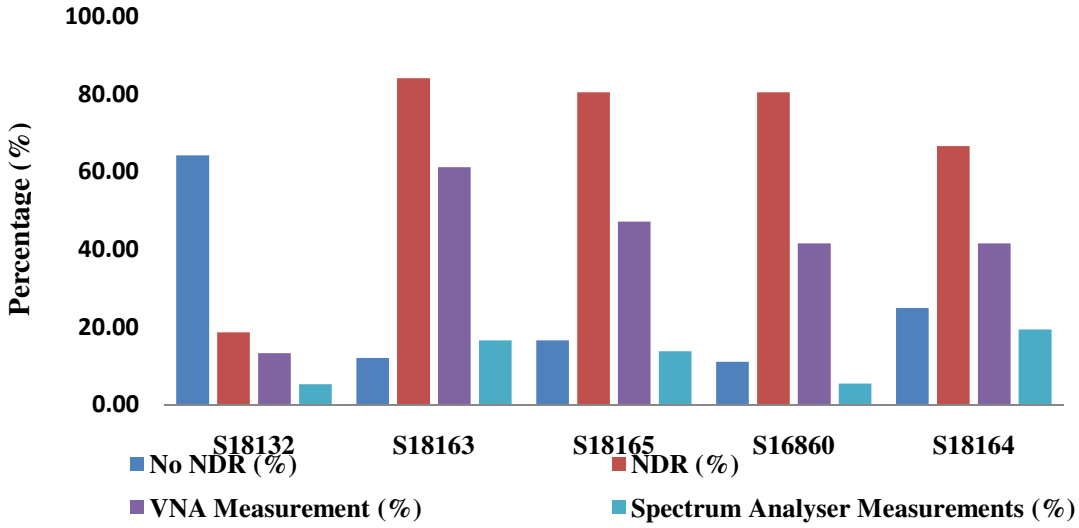

Figure.5.13. Comparison of measurement results on different wafers

5.5. REFERENCES

[1] A. Khalid, G. M. Dunn, N. Pilgrim, C. R. Stanley, I. G. Thayne, M. Holland, and D. R. S. Cumming, "Planar Gunn-type triode oscillator at 83 GHz," *Electron. Lett.*, vol. 43, no. 15, p. 837, 2007.

[2] A. Khalid, N. J. Pilgrim, G. M. Dunn, M. C. Holland, C. R. Stanley, I. G. Thayne, and D. R. S. Cumming, "A Planar Gunn Diode Operating Above 100 GHz," *IEEE Electron Device Lett.*, vol. 28, no. 10, pp. 849–851, Oct. 2007.

[3] N. J. Pilgrim, A. Khalid, G. M. Dunn, and D. R. S. Cumming, "Gunn oscillations in planar heterostructure diodes," *Semicond. Sci. Technol.*, vol. 23, no. 7, pp. 1–10, Jul. 2008.

[4] S. Helland, "Electrical Characterization of Amorphous Silicon Nitride Passivation Layers for Crystalline Silicon Solar Cells," Norwegian University of Science and Technology, 2011.

[5] C. Li, "Design and Characterisation of millimeter-wave planar Gunn diode and integrated circuits," University of Glasgow, 2011.

[6] M. Montes Bajo, G. Dunn, A. Stephen, A. Khalid, D. R. S. Cumming, C. H. Oxley, J. Glover, and M. Kuball, "Impact ionisation electroluminescence in planar GaAs-based heterostructure Gunn diodes: Spatial distribution and impact of doping non-uniformities," *J. Appl. Phys.*, vol. 113, no. 12, p. 124505, 2013.

[7] Mohamed Ismaeel Maricar, James Glover, Ata Khalid, Chong Li, G Evans, D. S. R. Cumming. and C. H. Oxley. "An AlGaAs/GaAs based planar Gunn diode oscillator with a fundamental frequency operation of 120GHz," *Microw. Opt. Technol. Lett.*, 2014.(Accepted)

[8] A. Khalid, G. M. Dunn, R. F. Macpherson, S. Thoms, D. Macintyre, C. Li, M. J. Steer, V. Papageorgiou, I. G. Thayne, M. Kuball, C. H. Oxley, M. Montes Bajo, A. Stephen, J. Glover, and D. R. S. Cumming, "Terahertz oscillations in an In0.53Ga0.47As submicron planar Gunn diode," *J. Appl. Phys.*, vol. 115, no. 11, p. 114502, Mar. 2014.

Chapter: 6

Measurement results of an $In_{0.53}Ga_{0.47}As$ planar Gunn diode on InP material

6.1. INTRODUCTION

A description of the design and fabrication of the planar Gunn diode was briefly discussed in chapter-4 and also a description of the measurement results on GaAs based planar Gunn diodes were described in chapter-5. In this chapter DC and RF characterisation of InP based planar Gunn diodes with same electrode geometries as described in Chapter-4 and 5, and separation (L_{ac}) between the anode to cathode electrodes will be described. The chapter will present the measurement results, which include DC, S-parameter and spectrum analyser.

6.2. FABRICATION PROCESSES OF THE PLANAR GUNN DIODE ON AN InP SUBSTRATE.

The InP hetero-structure planar Gunn diode was first proposed and developed by the Universities of Aberdeen and University of Glasgow in 2010 [1] . Later in 2013 Vasileious and Ata Khalid published simulation, fabrication and RF measurement results for an InP based planar Gunn diode with a 1.3 micron active channel length which operated at 164 GHz [2], [3]. Early in 2014 Ata Khalid published work on a planar Gunn diode with an active length (L_{ac}) of 600 nanometres which operated at 298 GHz the highest recorded fundamental frequency from an InP based planar Gunn diode [4]. The

hetero-structure $In_{0.53}Ga_{0.47}As$ planar Gunn diode was fabricated on a lattice matched InP substrate giving improved performance (higher frequency of oscillation and higher RF output power) figures when compared with GaAs based planar Gunn diodes. A comparison between the electrical properties of InP and $In_{0.53}Ga_{0.47}As$ are shown in ***Table 6.1***. For example, in $In_{0.53}Ga_{0.47}As$, the low-field electron mobility is much higher, enabling the carriers to reach the saturation velocity at a lower electric field [5]. The other advantage of hetero-structures devices is higher electron concentration in the active layer which is necessary for the high frequency Gunn oscillation [6].

Parameter	**InP**	**$In_{0.53}Ga_{0.47}As$**
Permittivity	12.4	13.9
Bandgap (eV)	1.336	0.857
Affinity (eV)	4.4	4.55
Low field mobility ($cm^2V^{-1}S^{-1}$)	4500	16000
Electron Saturation Velocity (cms^{-1})	$1x\ 10^{17}$	$0.92x10^{17}$
Reference field strength (Vcm^{-1})	4000	4000

Table.6.1. Properties of InP substrate

Similar design methodology was adopted for the $In_{0.53}Ga_{0.47}As$ planar Gunn diode as was used for the GaAs based planar Gunn diodes. **Figure 6.1** shows a schematic view of a cross section of the $In_{0.53}Ga_{0.47}As$ planar Gunn diode. A brief description of the fabrication process was discussed in section-4.2. The $In_{0.53}Ga_{0.47}As$ planar Gunn diodes were fabricated on semi-insulating InP wafers with the similar material specification as in ***Table 6.1***. [2], [3].

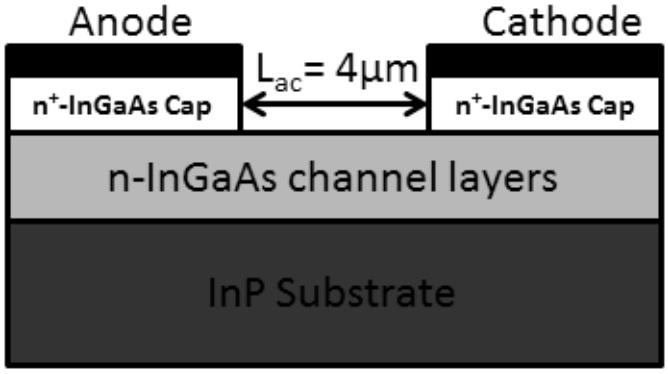

Figure.6.1. Schematic view of the hetero-structures $In_{0.53}Ga_{0.47}As$ planar Gunn diode

Similar to the GaAs devices the InP based planar Gunn diodes were passivated with silicon nitride over both semiconductor and metallised regions. The unique number of the wafer and the corresponding fabricated device and circuit geometrical configuration are given in ***Table 6.2.***

Wafer No	Material	Circuit Configuration
S18159\AKH3059	InP	Planar Gunn diode with different electrode geometries and were passivated using silicon nitride
S18158\AKH1058	InP	Planar Gunn diode with different electrode geometries including fundamental and second harmonic extraction circuits were passivated using silicon nitride

Table.6.2. Different wafer identification numbers.

6.3. DESIGN AND ANALYSIS OF ELECTRODE GEOMETRIES FOR InP BASED PLANAR GUNN DIODES

An outline of different electrode geometrical designs for the planar Gunn diode was discussed in the section 4.4. Initially GaAs based planar Gunn diodes with different electrode geometries were characterised from DC to RF frequencies by using the measurement setups, which were discussed in chapter-3 and chapter-5. The different electrode geometry designs were applied to the hetero-structure $In_{0.53}Ga_{0.47}As$ planar Gunn diodes which were then characterised from DC to RF using the measurement setups described in chapter-3. The pulsed IV measurement results made on the hetero-structures $In_{0.53}Ga_{0.47}As$ planar Gunn diode were similar to those described for the hetero-structure AlGaAs planar Gunn diode, refer to chapter 5.

6.3.1. DC MEASUREMENTS ON PLANAR GUNN DIODE WITH DIFFERENT ELECTRODE GEOMENTRIES

Initially, DC pulsed measurements were made on all the InP based planar Gunn diodes to give an indication of the existence of a NDR region. The pulsed DC characteristic (Chapter 3) was measured using a semiconductor

device analyser from Agilent technologies (B1500A) connected to the automated probe station manufactured by Cascade Microtech, enabling measurements to be made across the wafer. **Figure 6.2** shows a comparison between the pulsed and continuous IV characteristics of an InP based Type-A planar Gunn diode. The measurement is similar to the GaAs based planar Gunn diode and shows that the diode pulsed IV characteristic will minimize diode self-heating allowing the NDR region to be more easily detected. The measured pulsed IV characteristic can again be used to represent the voltage dependent current generator in the electrical equivalent circuit model of the InP planar Gunn diode, by fitting an n^{th} order polynomial equation to simulate the IV characteristic; it should be noted that the polynomial will have different coefficients to the one used to describe a GaAs based planar Gunn diode.

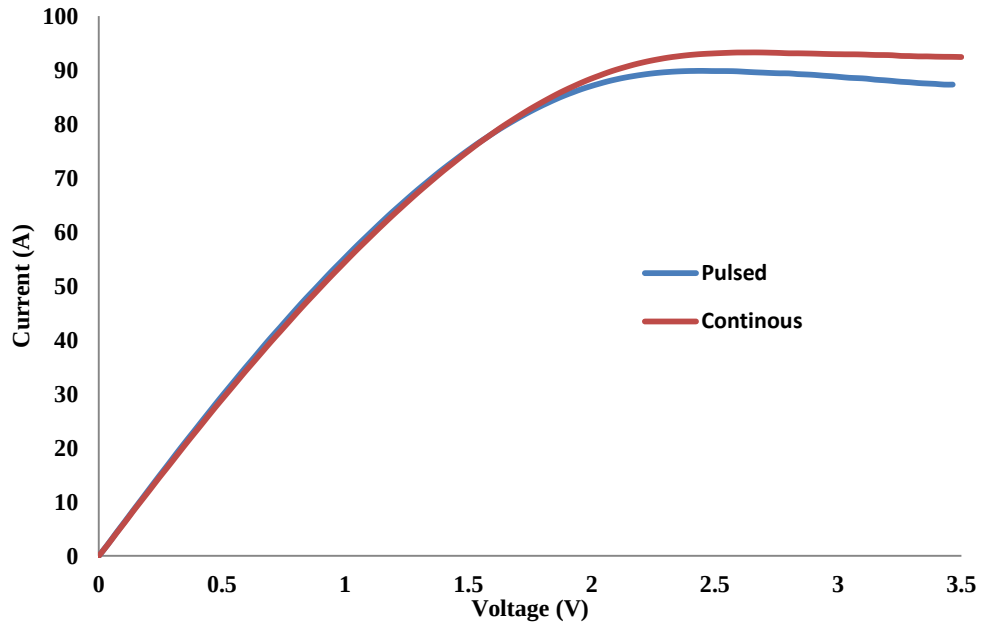

Figure.6.2 Continuous and pulsed IV measurements of an InP based Type-A planar Gunn diode

A number of InP based Type-A Gunn diodes with different anode to cathode separation (L_{ac}) were measured. **Figure.6.3**. shows the pulsed IV characteristics of the InP based Type-A planar Gunn diode with different active channel lengths (from 1 to 4 microns). The device with a 1 μm active channel length

(L_{ac}), the NDR was detected at 1.86 V with a peak current of 96.3 mA, whereas for the device with 4μm active channel length (L_{ac}) the NDR was detected at 2.61 V with a peak current of 89.8 mA. The NDR region of the device occurred close to the threshold voltage reported by Glasgow University and it is lower when compared to the threshold voltage applied to the AlGaAs planar Gunn diode [6]. The pulsed IV measurement results of the InP based Type-A planar Gunn diode were directly compared with the experimental results of the Glasgow Gunn diode with same active width (120 microns) and length (4 microns) published by Chong Li and Ata Khalid et all [2], [3], [6]. The comparison is shown in ***Table.6.3.*** The results show that $In_{0.53}Ga_{0.47}As$ planar Gunn diodes in this work gave a consistently higher current when compared to Chong Li [6] published work, this may be due to an improved contact technology leading to a lower device contact resistance and it's been discussed in chapter-3.

Anode to Cathode separation (L_{ac})	**Published Work by Li et al**		**Measurements from this work**	
	Bias Voltage (V)	*Peak Current (mA)*	*Bias Voltage (V)*	*Peak Current (mA)*
1μm	-	-	1.86	96.3
1.3 μm	2.5	70.4 [2]	-	-
2μm	-	-	2.25	99.8
3μm	-	-	2.52	91.5
4μm	4.2	24.5[6]	2.61	89.9

Table.6.3. Peak current of InP based hetero-structure Planar Gunn diodes

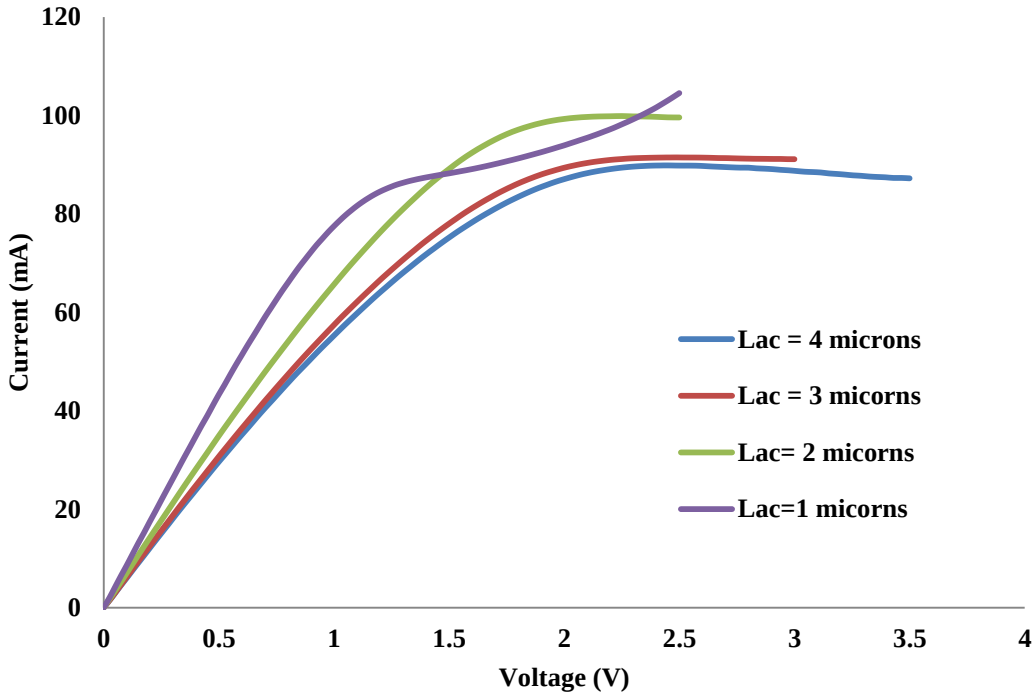

Figure.6.3 Pulsed IV Characteristics of an InP based Type-A planar Gunn diode having different L_{ac}

Figure.6.4 shows the pulsed IV measurements for the different electrode geometries (Type A, B, C & D) InP based planar Gunn diodes with an active channel length of 4 micron. The NDR region of these diodes was noticeable at a bias voltage of approximately 3 V with a peak current of around 92 mA. The saturated currents are higher than the GaAs based planar Gunn diodes. The InP diodes which exhibited a poor or no NDR region were identified and RF characterisation was not carried out on these diodes.

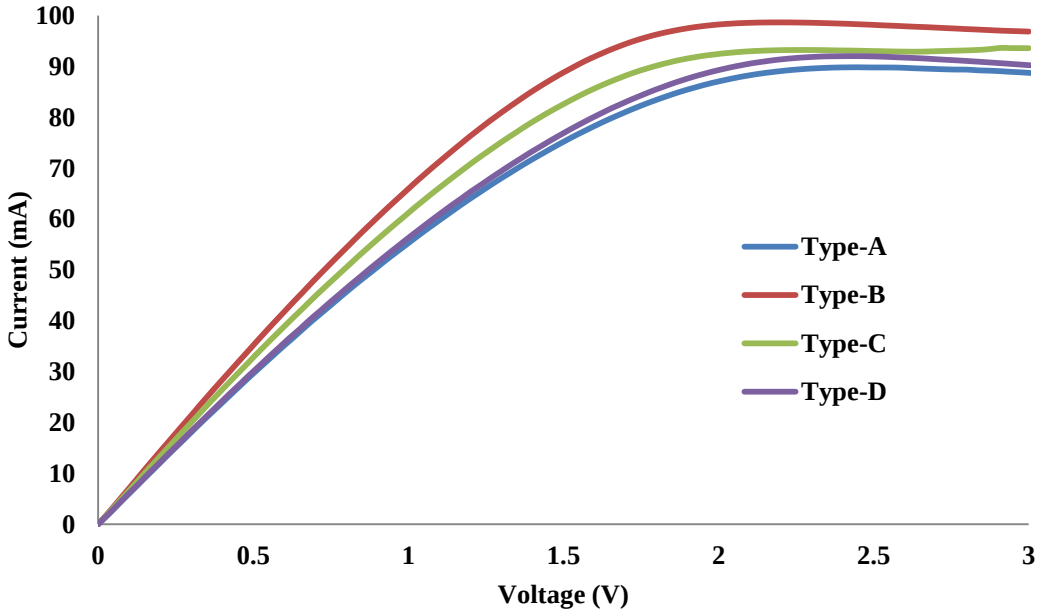

Figure.6.4. Pulsed IV measurements results on different types of InP based planar Gunn diode with an active channel length of 4 micron (Lac=4µm)

6.3.2. RF MEASUREMENTS ON PLANAR GUNN DIODES WITH DIFFERENT ELECTRODE GEOMETRIES

As discussed in Chapter-5, the DC measurement results were used to identify the NDR region of the device. If the diodes gave no NDR region or showed a short or open circuited DC characteristic then these diodes were marked and no further evaluation took place. RF measurements were made on diodes with different electrode geometries having an active channel length (L_{ac}) of 2,3 and 4 microns The diodes with an active channel length of 1 microns were not measured as the calculated transit mode frequency was 250 GHz making them difficult to RF characterise at these high frequencies. Small-signal one port S-parameter measurements were made on the diodes to determine the input impedance from DC to 110 GHz and at different bias voltages, using an Agilent vector network analyser (VNA). The 40-60-40µm pitch 50 Ohm probes from GGB industries were connected to the VNA and the system was calibrated from DC to 110 GHz using a calibration substrate (109-102B) from Cascade Microtech (which was described in chapter-3, section 3.5). The VNA measurement was used to give an indication whether the diode had RF nega-

tive resistance, for example, a diode with S_{11} greater than 1 presented a RF negative resistance, whereas a diode with magnitude of S_{11} less than 1 presented no RF negative resistance. **Figure 6.5** shows the magnitude $|S_{11}|$ as a function of frequency for a Type-A InP based planar Gunn diode (with an active channel length of 4 microns), and with a bias voltage which was increased from 0 to 3.7 V. From the plot it can be seen that the magnitude of S_{11} was positive and greater than 1 for bias voltages between 3.2 to 3.7V.

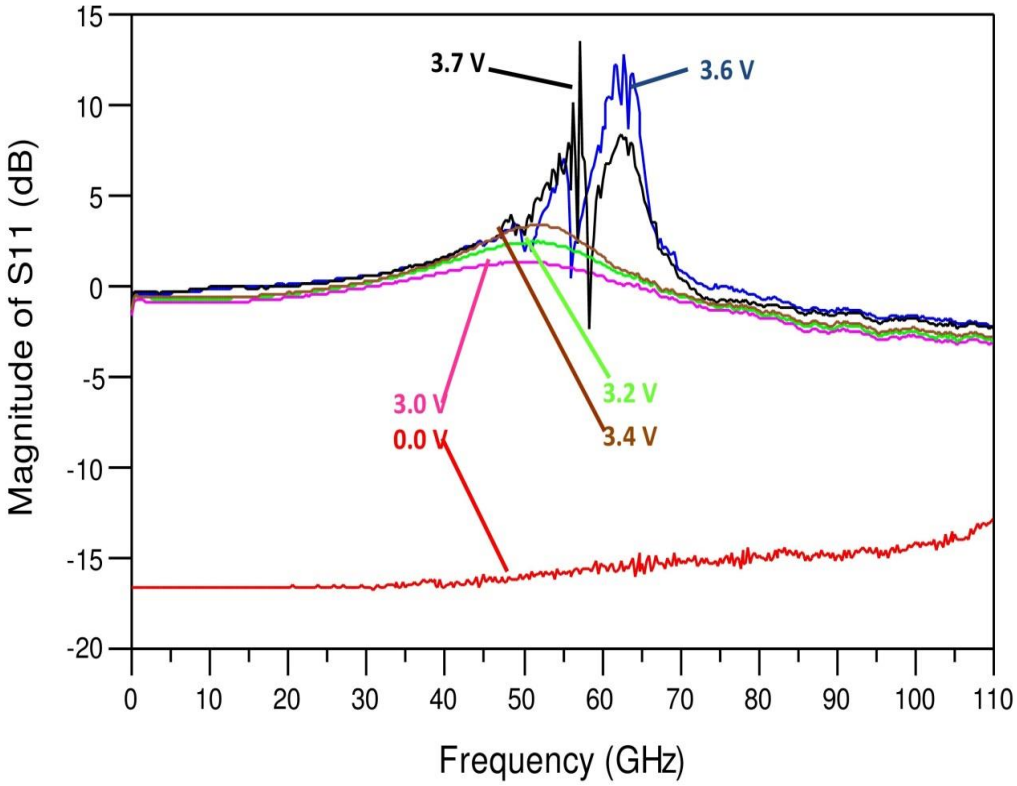

Figure.6.5 Magnitude of the Type-A InP based planar Gunn diode with different applied bias voltages

VNA measurements from DC to 110 GHz were also made on the remaining three device structures (Types B, C and D) with an active channel length of 4 microns and at different bias voltages. **Figure 6.6** shows the measured magnitude of S_{11} of the four planar Gunn diode types, and all the structures gave an indication of negative resistance for bias levels between 2.8 to 4 V. The VNA measurements of these devices showed that the magnitude of S_{11} was greater

than 1 (S_{11}>1) and had almost smooth frequency response over the entire frequency band (DC to 110GHz), peaking at 59.72 GHz for Type-B device at 3.6 V, 60.27 GHz for Type-C device at 3.66 V, and 63.02 GHz for Type-D device at 3.78 V. The frequency at which the negative resistance peaked was assumed to be natural transit frequency of the diodes. The VNA measurements indicated that the devices were oscillating at the transit mode as the experimental natural oscillating frequencies was in good agreement with Ata Khalid and Chong Li et all [1], [2], [4], [6], The higher transit mode frequency of these devices indicate that the saturation velocity of the domain was approximately 2.4×10^5m/sec. The higher saturation was in good agreement with the higher mobility as expected with GaInAs which is lattice matched to InP. The transit mode oscillating frequency of the device was almost double the transit mode oscillation frequency of AlGaAs/GaAs hetero-structure planar Gunn diode with identical anode to cathode spacing.. The hetero-structure InP based planar Gunn diode will also have a dead space [2] which will be the distance required to accelerate the electrons to saturation and will be discussed later in this chapter. ***Table.6.4*** shows the bias voltage and measured oscillation frequency of the InP based planar Gunn diode.

Electrodes structures	**Peak Current (mA)**	**Measured natural oscillation frequency of planar Gunn diode (GHz)**	**Bias Voltage (V)**
Type-A	89	59.56	3.70
Type-B	96	59.72	3.60
Type-C	94	60.27	3.66
Type-D	93	63.02	3.78

Table.6.4. Measurement results of the InP based planar Gunn diode with an active channel length of 4 micron

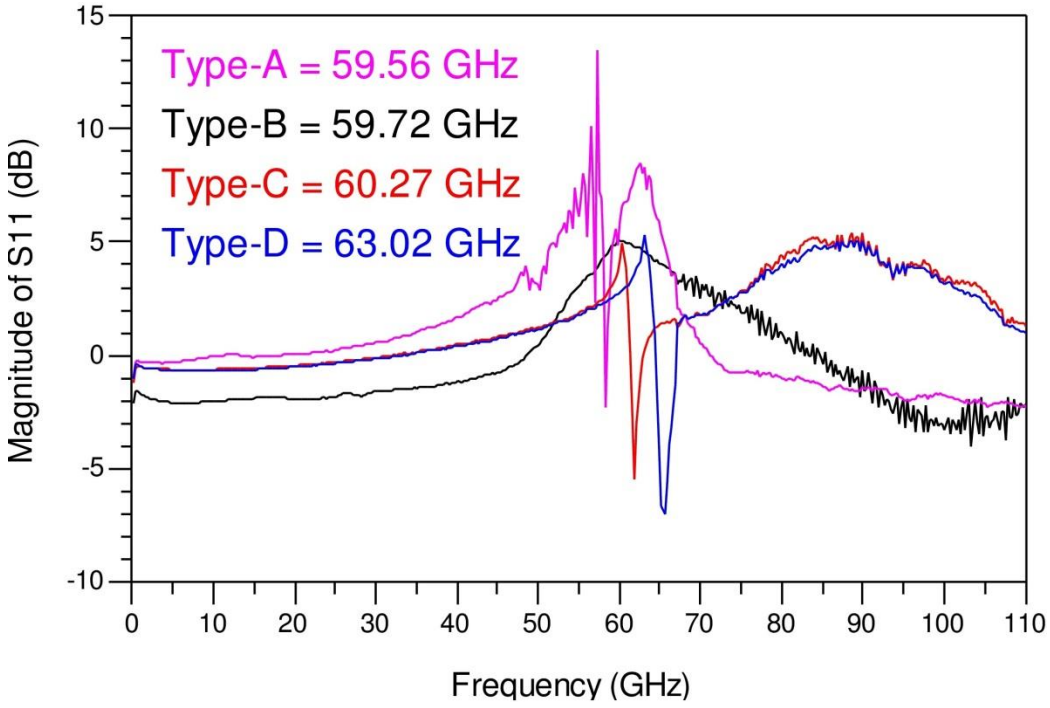

Figure.6.6. Magnitude of the planar Gunn diode with different electrodes geometries

As argued for the AlGaAs/GaAs planar Gunn diodes, it was assumed that the Type A and Type B diodes were similar and so the Type B diode was not pursued any further. Only Type-A, Type-C and Type-D diodes were fully RF characterised, which included the spectrum analyser measurements. It was interesting to note that the Type-C and Type-D device gave similar performance and also gave the highest oscillation frequency of 60.27 GHz for Type-C device and 63.02 GHz for Type-D device. The Type-C diode electrode structure was designed to simplify de-embedding the 50 Ohm CPW feed line to the active region of the diode and will be discussed in chapter-8. **Figure.6.7**. shows the magnitude of the measured S_{11} for the Type-C planar Gunn diode with different active channel lengths (L_{ac}). As expected the devices with smaller L_{ac} oscillated at a higher frequency. ***Table.6.5.*** shows the measured maximum negative resistance (frequency at which S_{11} was greatest) of the planar Gunn diodes with different electrode structures (Type A, C and D) with anode and cathode separations of L_{ac} = 2, 3 and 4 micron. The small difference in the oscillation frequency (maximum negative resistance) between diodes with

same electrode structure and electrode separation was probably due to variations in fabrication from diode to diode, assuming uniform material properties.

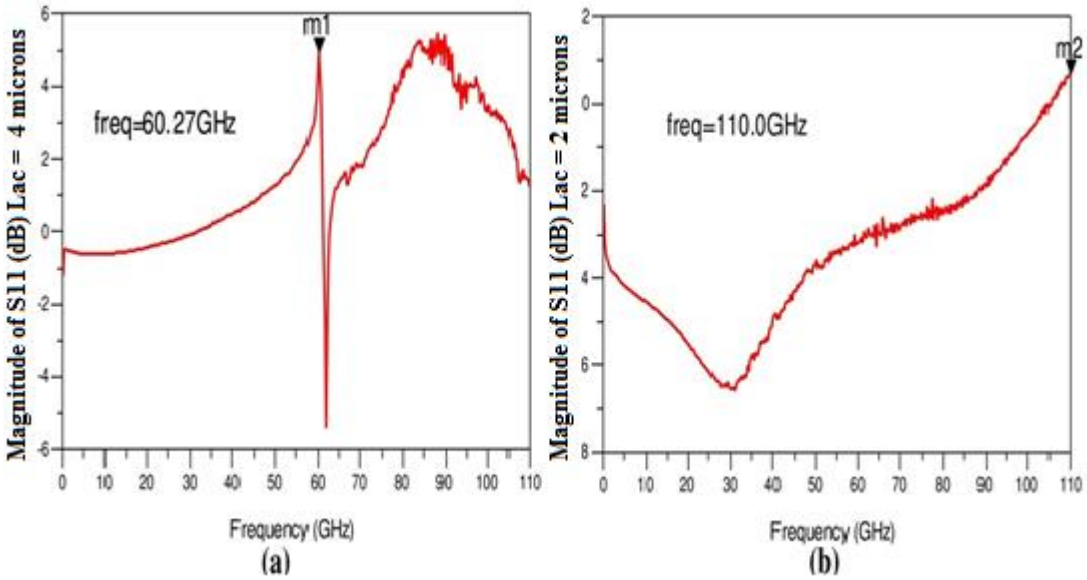

Figure.6.7. Magnitude of S_{11} expressed in dB's for the Type-C planar Gunn diode with different active channel lengths (a)Active channel length Lac =4 µm (b) Active channel length Lac =2 µm

Different types of Planar Gunn diode	Oscillation frequency (GHz) for 4µm device	Oscillation frequency (GHz) for 3µm device	Oscillation frequency (GHz) for 2µm device
Type-A	59.56	81.06	101.96
Type-C	60.27	83.39	104.93
Type-D	63.02	84.06	109.93

Table.6.5. The frequency at which S_{11} was greatest for each of the device Types A, C and D, and with active channel lengths of 2, 3 and 4 microns

6.3.3. SPECTRUM ANALYSER MEASUREMENTS ON PLANAR GUNN DIODES

Apart from the IV and VNA measurement of the planar Gunn diodes (L_{ac}= 2, 3 and 4 µm); spectrum analyser measurements were used to confirm the 'transit mode' oscillation frequency and to give an indication of RF output

power from the diode. A brief description of measurement setup was given in chapter-3. As already stated the Type-A device was used as a base-line device as it represented the same electrode configuration used by University of Glasgow. A number of Type-A diodes were measured to obtain the base line for comparison with the Type-C and Type-D diodes. As already stated the type B diode was not measured as it had a very similar electrode structure to the diode Type A. **Figure.6.8**) shows the spectrum analyser measurement made on the Type-A diode with a 4 microns active channel length, which was found to oscillate at 65.42 GHz (with an RF output power of -24.91 dBm). This is similar to the earlier results published by University of Glasgow and Aberdeen [2].

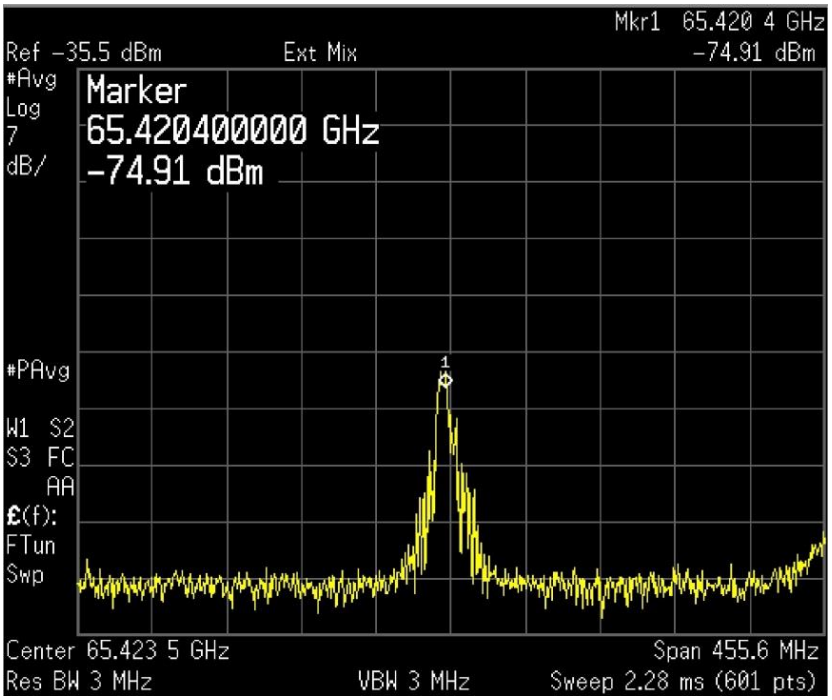

Figure.6.8. Spectrum analyser results of 4 microns InP planar Gunn diode

Type-C planar Gunn diode

It was found that Type-C planar Gunn diode started to oscillate when the bias voltage was between 3.1 to 3.9 V. **Figure 6.9** shows the RF output spectrum of an InP Type-C planar Gunn diode with an electrode spacing of 4 microns. The measurement indicated that the InP Type-C planar Gunn diode oscillated at a fundamental frequency of 63.5 GHz with an RF output

power of -5.64 dBm, at a bias voltage of 3.76 V. Bias voltage tuning process was used to obtain the maximum RF output power and the corresponding 'transit mode' oscillation frequency from the device and is shown in **Figure.6.10**. The highest power obtained from the Type-C planar Gunn was -5.64 dBm at 3.76 V which is the highest power ever recorded at this frequency (62 GHz) from an InP based planar Gunn diode. A number of Type-C planar Gunn diodes with different anode to cathode separations were measured to identify the transit mode oscillation frequency and the corresponding RF output power from each of the devices. ***Table.6.6*** shows the 'transit mode' oscillation frequency and RF output power of the above variants of the Type-C planar Gunn diode. The oscillation frequency measured using the spectrum analyser was in agreement (within expected experimental error) with VNA measured frequency at which the magnitude of S_{11} was the greatest. The experimental frequency of oscillation was similar to the calculated 'transit mode' frequency, assuming the carrier saturation velocity was $2.4x10^5$ m/sec.

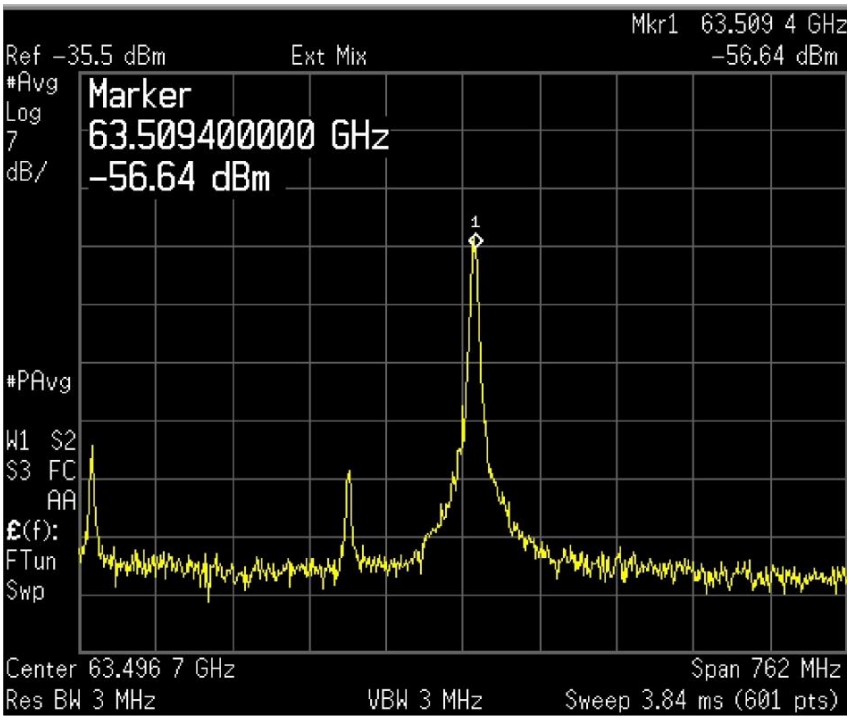

Figrue.6.9.Spectrum analyser results of 4µm InP Type-C planar Gunn diode

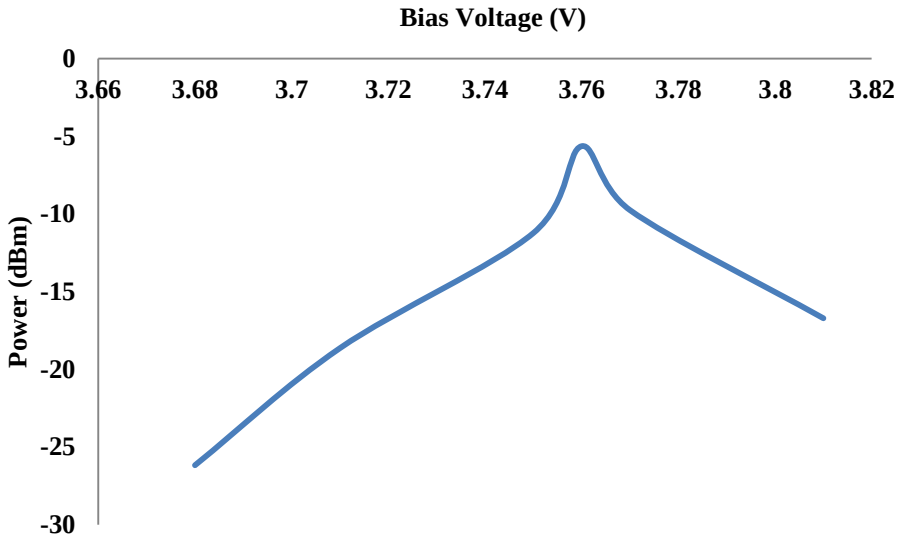

Figrue.6.10.The maximum frequency and output power was obtained from an InP type C device by optimising the applied bias voltage

Anode to Cathode separation (L_{ac}) in µm	Oscillation frequency of the Type-C planar Gunn diode (GHz)		RF output Power (dBm)
	Network Analyser Results	Spectrum Analyser Results	
1	-	-	-
2	88.61	92.21	-5.32
3	83.39	85.36	-17.32
4	60.27	63.50	-5.64

Table.6.6. Oscillation frequency and RF output power of the InP Type-C planar Gunn diode

Type-D planar Gunn diode

The CPW line to the active region of the planar Gunn diode was made narrow to represent a series inductor as discussed in Chapter 4. Initially the Type-D planar Gunn diode was designed with different in series inductor line lengths to improve diode matching to obtain higher RF power at the Gunn diode oscillation frequency. The anode to cathode separation for this device was also varied from 1 to 4 microns and the channel width (W=120 micron) was kept constant. The Type-D InP based planar Gunn diode was

RF characterised by measuring its fundamental oscillation frequency and RF output power. A Type D device with an anode and cathode separation of 2 micron with the inductor length of 120 microns was biased at 2.74 V and the diode oscillated with an oscillation frequency of 104.93 GHz and an RF output power of -16.83 dBm as shown in **Figure.6.11**. The inductor length of the device was varied from 100 to 150 microns in steps of 25 microns and it was found that the oscillation frequency of the diode can be tuned by changing the length of the inductor line. **Figure.6.12**. shows the RF output power and oscillation frequency of the Type-D device as a function of the length of the transmission line representing the series inductor.

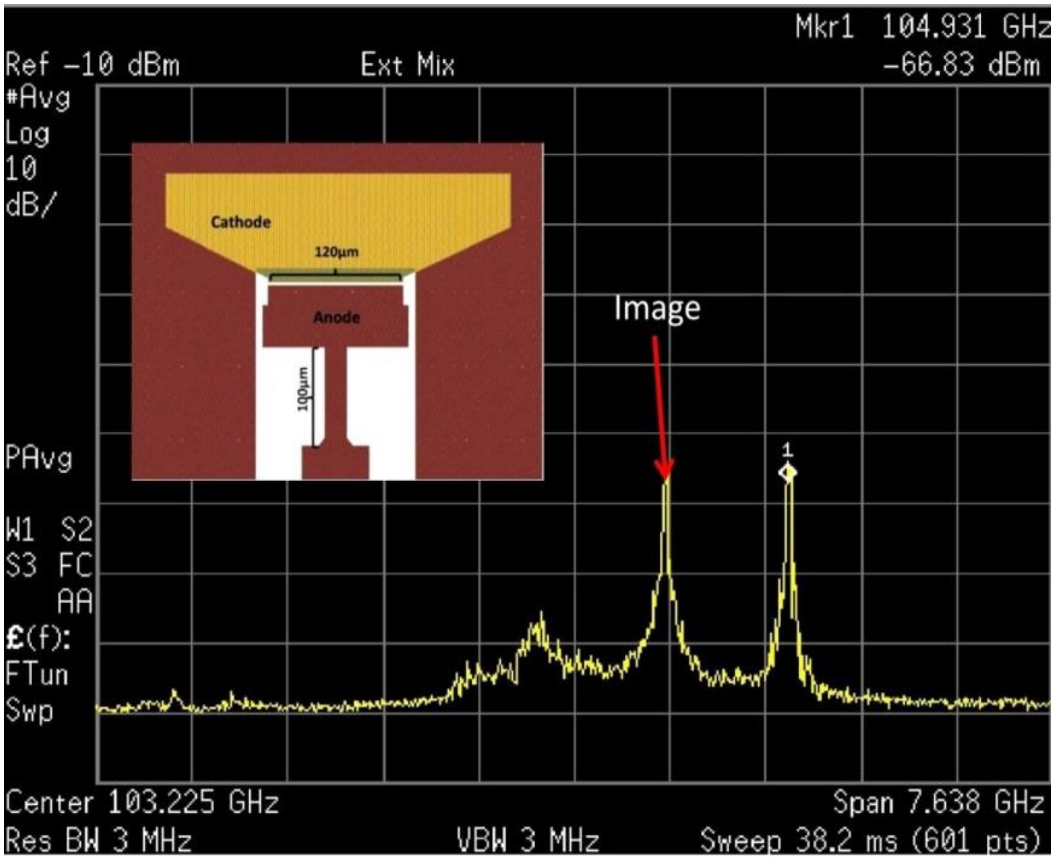

Figure.6.11. Spectrum analyser measurement results of the 2 microns InP Type-D planar Gunn diode with an length of 120 microns

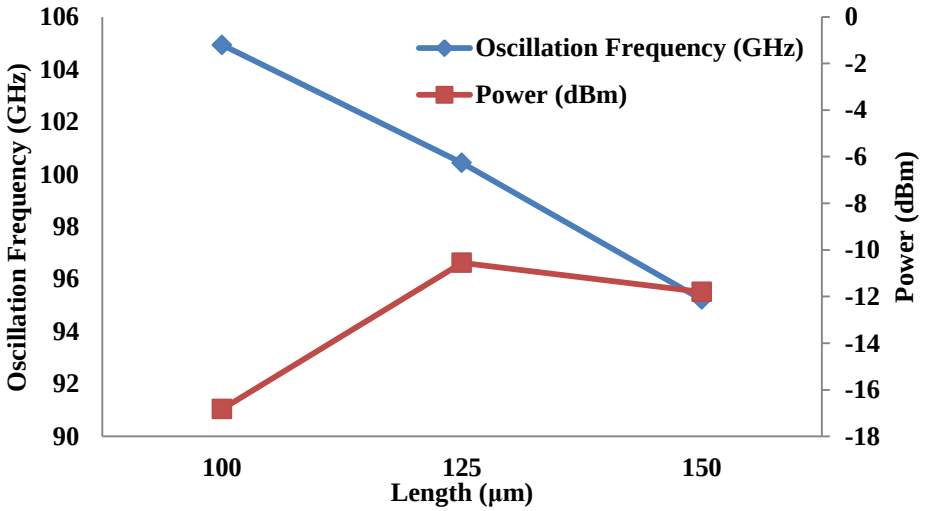

Figure.6.12. Power and oscillation frequency of the 2 microns hetero-structures $In_{0.53}Ga_{0.47}As$ Type-D planar Gunn diode with a varying inductor line length (series inductor) from 100 to 150 µm with a step of 25 µm

The experimental results from this device suggested that the oscillation frequency of the device can be tuned by changing the inductor length (a series inductor) to match the diode capacitance, which will be discussed later in the section. SEM measurements were made on this device to verify the anode to cathode separation (L_{ac}) of the planar Gunn diode. **Figure-6.13** shows a scanning electron microscope (SEM) image of the Type-D device verifying the anode to cathode separation was 2 micron.

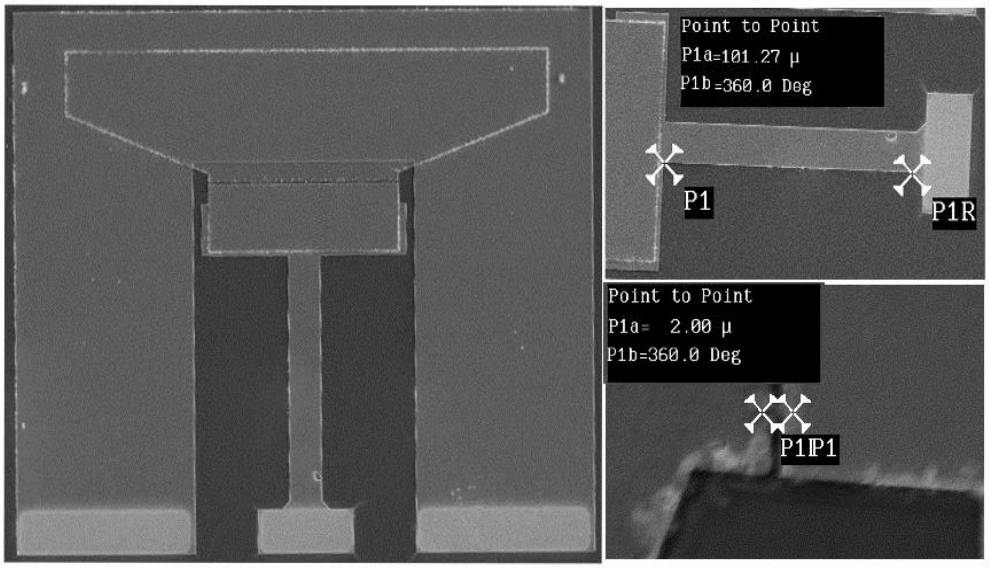

Figure.6.13 Scanning electron microscope (SEM) image of the Type-D planar Gunn diode with an active channel length of 2 microns

Table.6.7 shows the oscillation frequency and RF output power of the hetero-structure $In_{0.53}Ga_{0.47}As$ Type-D planar Gunn diode as a function of the active channel length of 2 to 4 microns in 1 micron steps and varying the inductor line length from 100 microns to 150 microns with a step of 25 microns (series inductor). It can be seen that the oscillation frequency of the planar Gunn diode from the spectrum analyser measurements was lower than the oscillation frequency measured using the network analyser, and may be partly explained by different bias voltages. For the VNA the bias voltage was 2.36 V and for the spectrum analyser measurement the bias voltage was 2.31 V. The different bias voltage occurred as it was found necessary to tune the bias voltage to obtain a good signal on the spectrum analyser. This suggests that the match to the VNA and spectrum analyser may have been slightly different.

As the inductor line length increased the oscillation frequency and output power from the device was decreased. The results indicate that the optimum match was for an inductor length of 125 microns where the output power was a maximum, at a frequency of around 100GHz. If the inductor length was further decreased the oscillation frequency increased but the output power significantly decreased. A first-order calculation was carried out to confirm that the series inductor provided a good match at the high frequency (104 GHz). The total capacitance of the 2 microns InP Type-D planar Gunn diode was found from the experimental S_{11} parameters to be ≈ 49 fF and was constant over the frequency range of 102.4 GHz to 106.7 GHz. The inductor line length was calculated from the equations given in chapter-4. The transit mode oscillation frequency of the device was calculated by using $f_0 = \frac{1}{2\pi\sqrt{LC}}$ and found to be 118 GHz which is close to the experimental frequency of 104 GHz, given that the parasitics were not taken into account. The results suggest that the device is working close to the transit mode. ***Table.6.8*** shows the calculated and measured oscillation frequency of the hetero-structures of $In_{0.53}Ga_{0.47}As$ Type-D planar Gunn diode. The calculat-

ed oscillation frequency of the device was higher than the measurement results and is thought to be due to parasitics in the real diode which were not taken into account in the calculation.

Anode to Cathode separation (L_{ac}) in µm	Inductor line length (µm)	Oscillation frequency of the Type-D planar Gunn diode (GHz)		RF output Power (dBm)
		Network Analyser Results	Spectrum Analyser Results	
2	100	109.91	104.931	-16.83
	125	102.67	100.46	-10.58
	150	98.97	95.215	-11.80
3	100	85.36	83.26	-29.36
	125	81.01	79.86	-31.68
	150	78.58	77.19	-24.41
4	100	63.02	61.36	-21.68
	125	62.58	60.89	-16.27
	150	60.06	59.68	-28.96

Table.6.7. Oscillation frequency of the 2 and 4 microns hetero-structures $In_{0.53}Ga_{0.47}As$ Type-D planar Gunn diode by varying the CPW line length (series inductor) of the device

Anode to Cathode separation (L_{ac}) in µm	Inductor		Total Capacitance from S_{11} (fF)	Oscillation frequency of the Type-D planar Gunn diode (GHz)	
	CPW line length (µm)	Calculated Inductor (pH)		Calculated Oscillation Frequency	Spectrum Analyser Results
2	100	36.58	49	118.93	104.931
	125	39.2	53	110.46	100.46
	150	47.59	52	101.21	95.215
3	100	80.11	38	91.26	83.26
	125	90.1	40	83.86	79.86
	150	93.81	41	81.19	77.19
4	100	83.40	69	66.36	61.36
	125	83.21	65	68.89	60.89
	150	89.13	68	64.68	59.68

. ***Table.6.8 Calculated and measured oscillation frequency of the hetero-structures $In_{0.53}Ga_{0.47}As$ planar Gunn diode***

6.3.4. ANALYSIS OF THE PLANAR GUNN DIODE WITH DIFFERENT ELECTRODE SEPARATIONS

A comparative study has been made on hetero-structures $In_{0.53}Ga_{0.47}As$ planar Gunn diodes to find the natural transit oscillation frequency of the device with different anode to cathode separation. **Figure 6.14** shows the measured transit mode oscillation frequency of Type-A, Type-C and Type-D planar Gunn diodes with different anode to cathode separations. It can be seen that the planar Gunn diodes with a 2µm anode to cathode separation oscillated in the frequency range of 91 GHz to 110 GHz. The Type D diode gave a slightly higher frequency and may be due to the inductive tuning of the series inductor discussed in section 6.3.3. It is interesting to note that the oscillation frequency of the all diodes were good agreement with the results which were published by Universities of Glasgow and Aberdeen [2], [6].

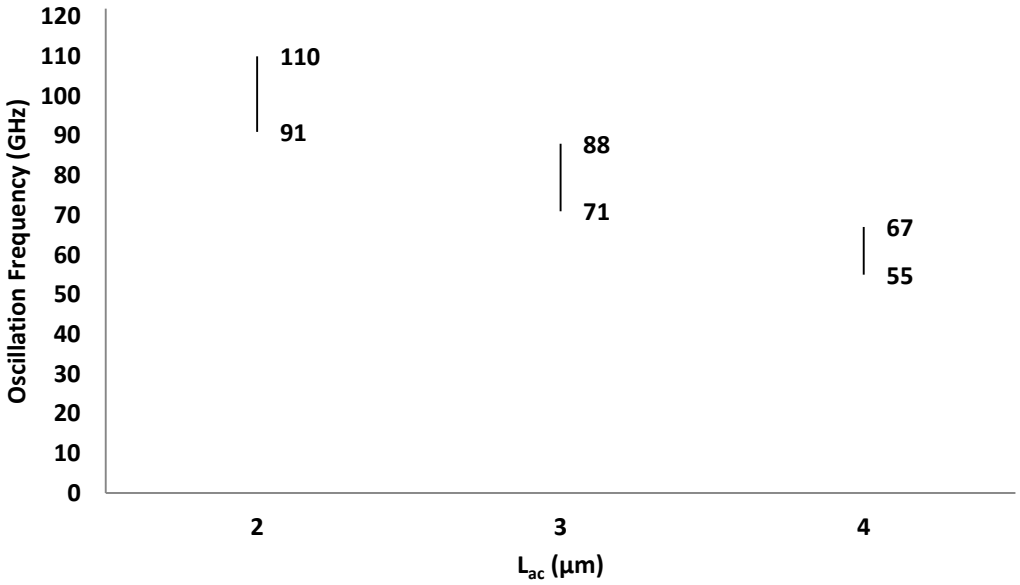

Figure.6.14.Measured frequency of oscillation for a L_{ac} from 2µm to 4µm of hetero-structures $In_{0.53}Ga_{0.47}As$ Type-A, Type-C and Type-D planar Gunn diodes

Figure 6.15 shows the estimated dead space obtained by plotting $1/f$ (f is the transit mode oscillation frequency) against active channel length for device

Types A and C. The gradient of the linear line will represent the domain velocity v_d, and where the line intersects the x-axis gives an estimate of the dead space (L_{dead}). The Type-D planar Gunn diode was not included as it was considered not to be representative as it included an on chip matching circuit element which would be a further factor influencing the oscillation frequency of the device, refer to Figure 6.12.. The dead space of the device (Type-A and Type-C) were calculated by using the experimental results and is shown in **Figure 6.15.** From **Figure 6.15,** the dead space appears to be constant with decreasing active channel length. The experimentally estimated dead space was 0.21 microns for the hetero-structure $In_{0.53}Ga_{0.47}As$ planar Gunn diode. The author believes this is first time an estimate of the dead space for an $In_{0.53}Ga_{0.47}As$ planar Gunn diode fabricated on an InP semi-insulating substrate has been estimated from experimental results. The estimated dead space was less than the dead space estimated (0.26 microns) for the AlGaAs planar Gunn diode, which is consistent with the material parameters.

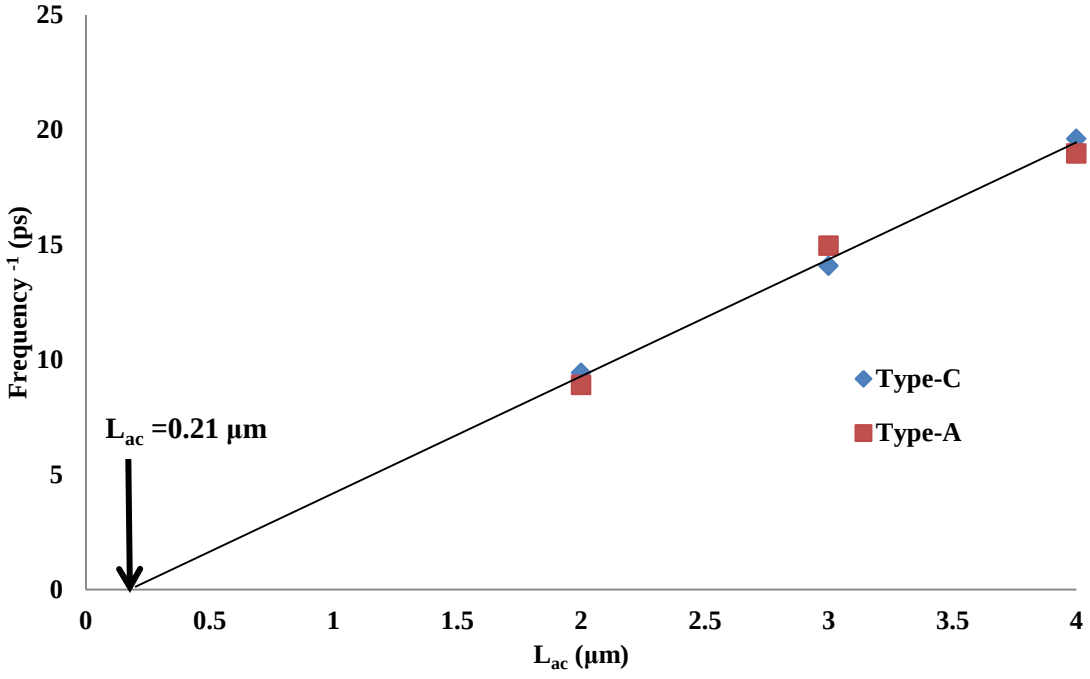

Figure.6.15.EstimateD dead space for diodes with L_{ac} from 2µm to 4µm; Type-A and Type-C InP planar Gunn diodes

6.4. ANALYSIS OF MEASUREMENTS ON DIFFERENT WAFERS

Similar analysis as applied to the GaAs based planar Gunn diodes was carried out on $In_{0.53}Ga_{0.47}As$/InP planar Gunn diodes and it was found that the number of high NDR devices was greater when compared to devices fabricated on the GaAs material. The total number of diodes fabricated and tested on InP wafer material is shown in ***Table 6.9.*** The diodes from wafers No.S18159 and S18158 measured using pulse IV and RF characterisation giving both NDR and a measured transit mode oscillation frequency respectively were plotted as percentage of the total number of devices actually DC probed from the wafer, in **Figure.6.16.** Like the GaAs diodes the results showed good correspondence between devices with a measured NDR region and giving RF measured oscillation frequency using the spectrum analyser. It is interesting to note that there were fewer $In_{0.53}Ga_{0.47}As$ diodes giving no NDR region when compared with similar geometry diodes fabricated on GaAs. The reason for this may be purely down to wafer to wafer device fabrication.

Wafers	Number of device Fabricated	Number of device Measured
S18159	400	120
S18158	40	20

Table.6.9.Total number of device fabricated and measured

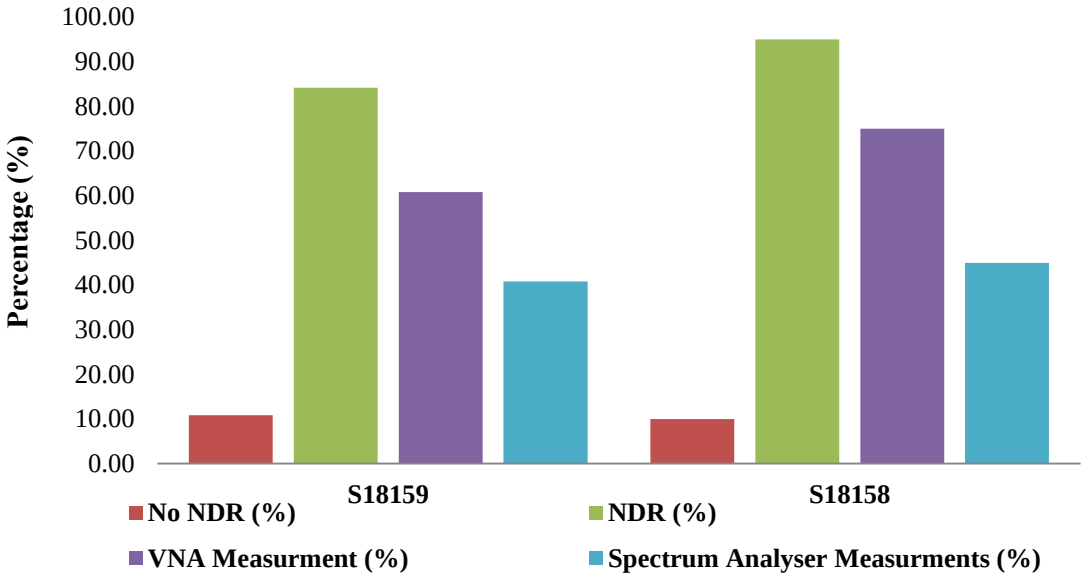

Figure.6.16. Comparison of measurements results on different InP wafers

6.5. REFERENCES

[1] C. Li, A. Khalid, L. B. Lok, N. J. Pilgrim, M. C. Holland, G. M. Dunn, and D. R. S. Cumming, "An In0.23Ga0.77As-based pHEMT-like planar Gunn diode operating at 116 GHz," in *35th International Conference on Infrared, Millimeter, and Terahertz Waves*, 2010, pp. 1–2.

[2] A. Khalid, C. Li, V. Papageogiou, G. M. Dunn, M. J. Steer, I. G. Thayne, M. Kuball, C. H. Oxley, M. Montes Bajo, A. Stephen, J. Glover, and D. R. S. Cumming, "In0.53Ga0.47As Planar Gunn Diodes Operating at a Fundamental Frequency of 164 GHz," *Electron Device Lett. IEEE*, vol. 34, no. 1, pp. 39–41, Jan. 2013.

[3] V. Papageorgiou, A. Khalid, C. Li, and D. R. S. Cumming, "Simulation and fabrication of InGaAs planar Gunn diode on InP substrate," in *2013 International Conference on Indium Phosphide and Related Materials (IPRM)*, 2013, vol. 28, pp. 1–2.

[4] A. Khalid, G. M. Dunn, R. F. Macpherson, S. Thoms, D. Macintyre, C. Li, M. J. Steer, V. Papageorgiou, I. G. Thayne, M. Kuball, C. H. Oxley, M. Montes Bajo, A. Stephen, J. Glover, and D. R. S. Cumming, "Terahertz oscillations in an In0.53Ga0.47As submicron planar Gunn diode," *J. Appl. Phys.*, vol. 115, no. 11, p. 114502, Mar. 2014.

[5] X. Wallart, B. Pinsard, and F. Mollot, "High-mobility InGaAs/InAlAs pseudomorphic heterostructures on InP (001)," *J. Appl. Phys.*, vol. 97, no. 5, p. 053706, 2005.

[6] C. Li, "Design and Characterisation of millimeter-wave planar Gunn diode and integrated circuits," University of Glasgow, 2011.

Chapter: 7

Passive components for integrated planar Gunn diode circuits

7.1. INTRODUCTION

In this chapter the design, modeling, fabrication and characterisation of passive components in coplanar waveguide (CPW) format are described, which have been used to form integrated planar Gunn diode oscillator circuits. The passive components will include CPW transmission lines and resonator structures. In this work open stub transmission line, radial stub and a novel diamond stub resonator were developed using the momentum package in Advanced Design Systems (ADS-2009) software. The novel diamond stub resonator has a number of advantages in comparison with the radial stub resonator, which include smaller surface area and a higher loaded Q factor. The author believes this is the first time this form of resonator geometry has been described using CPW format. Both radial and novel diamond resonators were fabricated on GaAs and InP semi-insulating substrate material and measured using a high frequency network analyser. The measurement results of the radial and diamond resonators were then directly compared with the simulation results.

7.2. PLANAR TRANSMISSION LINE

To realise a microwave integrated circuit (MIC), the transmission line structure is required to be planar and have low microwave transmission losses. The characteristic impedance (Z_0) of the planar transmission line can be

shown to be a function of the metallised width (W) of the transmission line, thickness (h) of the insulating substrate [1] and the permittivity (ε) of the substrate. A large W/h gives low characteristic impedance $Z_0$and small W/h gives high characteristic impedance $Z_0$of the transmission line. When the characteristic impedance is controlled by a single metallised dimension W, the circuit fabrication is straight forward and it can be realised by a photo-lithographic process [2] which was described in the chapter-4. These fabrication techniques are used for both microwave and millimetre wave circuits, leading to both hybrid and monolithic microwave integrated circuits (MMIC) [3], [4]. The most commonly used planar microwave transmission lines are summarised below and include: [5]

- ✓ Microstrip (MIC) – the conductor is fabricated on insulating substrate which is metallized on the back face providing the ground plane.
- ✓ Coplanar Waveguide (CPW) – is fabricated on the front face of the substrate and consists of three parallel conductors the outer two forming the ground planes
- ✓ Slotline – is the inverse of microstrip
- ✓ Coplanar Strips - is the inverse of the CPW

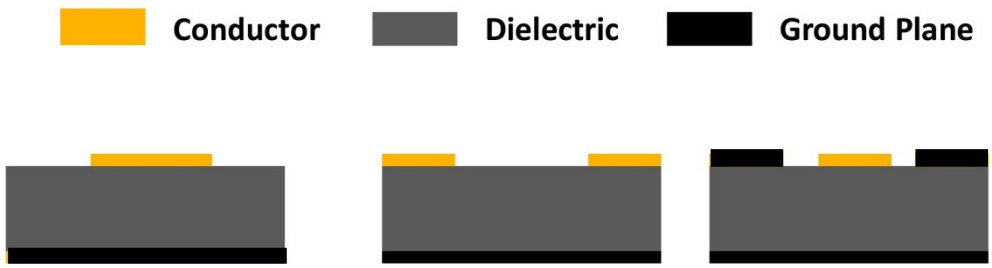

Figure.7.1. Planar transmission lines (a) Microstrip (b) Slotline (c) coplanar waveguide

Figure.7.1. shows three different common types of planar transmission lines used in monolithic microwave integrated circuits (MMICs) [6]. Microstrip and coplanar waveguide (CPW) are most popular of these structures because the mode propagation can be approximated to the transverse elec-

tromagnetic mode (TEM). The TEM mode of propagation on a microstrip and CPW has low dispersion and RF loss and hence offers the potential in the construction of wide band circuits and components. In CPW circuits by eliminating via holes and the associated parasitic source inductance of integrated transistors, the gain of MMIC circuits using CPW can be enhanced[7]. The other advantage of the CPW over the microstrip line is the use of surface mount components and interconnection [8]. CPW also allows the use of computer controlled on-wafer measurement techniques for device and circuit characterisation up to many tens of GHz [9]. These advantages make CPW based MICs and MMICs cost effective in large volume. These days with complex electromagnetic simulators, microstrip line and CPW can be simulated using commercial software (HFSS, CST, ADS, Sonnet and so on) to calculate circuit S-parameter, radiation patterns, gain and RF losses. In this work, Advanced Design System (ADS-2009) was used to design and simulate high frequency coplanar waveguide resonators. The resonators were designed on two different materials with a dielectric constant of 12.9 for GaAs substrate and 12.4 for InP substrate. The results showed that the choice of using GaAs or InP substrate made little difference to the performance of the radial or diamond resonator respectively.

7.3. COPLANAR WAVEGUIDE RESONATORS

The CPW waveguide was first proposed by Wen in 1969 [10] and had a number of advantages over the microstrip line (MIC). The advantages of the CPW include being able to mount lumped element components in shunt and series configuration on the top surface of the substrate thereby eliminating drilling of holes (known as via holes) through the substrate to reach the metalized ground plane as would be required for MIC format. The performance of CPW is superior to microstrip (MIC) in terms of higher frequency, lower cross talk and lower propagation losses primarily as the ground plane is on either side of the center metalized line [3]. Also CPW transmission format enables reduction in the circuit size by about 30% when compared to similar

circuits in microstrip line format [11]. Active devices for example MES-FETs can be more easily connected to the CPW transmission line as it is totally planar. A schematic view of the CPW is shown in **Figure.7.2.** It consists of a dielectric substrate and three metalized conductors on the top surface. The transmission conductor forms a center strip separated by a narrow gap from two ground plane conductors. The conductor width (W), separation (S) from the ground plane, conductor thickness (h) and permittivity(ε_t) of the dielectric substrate determine the effective dielectric constant (ε_{er}), characteristics impedance (Z_0) and the attenuation of the line. The effective dielectric constant for the CPW can be derived by using quasi static (low frequency) expression which is given by [12], [13]

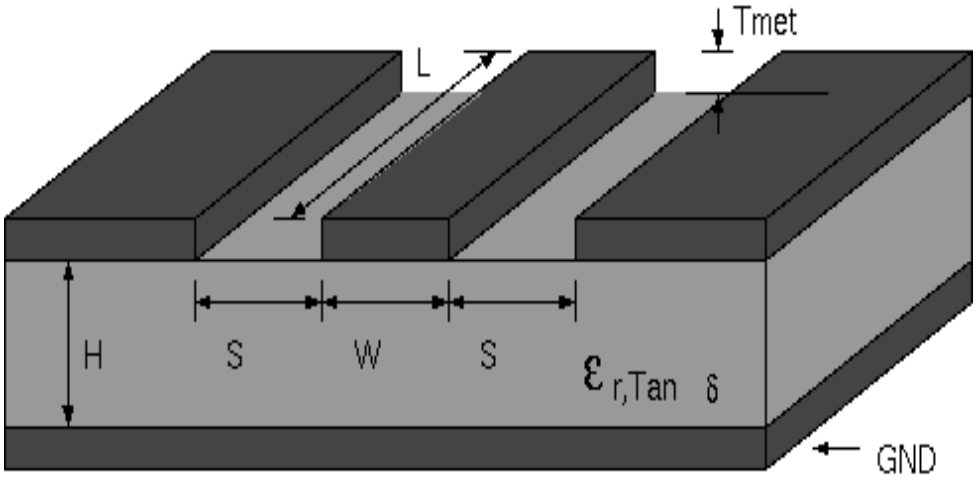

Figure.7.2. Coplanar Waveguide

$$\varepsilon_{re}(0) = \begin{cases} \frac{\varepsilon_r+1}{2} + \frac{\varepsilon_r-1}{2} * \left(1 + 12 * \left(\frac{h}{W}\right)^{-\frac{1}{2}}\right) for \frac{W}{h} > 1 \\ \frac{\varepsilon_r+1}{2} + \frac{\varepsilon_r-1}{2} * \left(1 + 12 * \left(\frac{h}{W}\right)^{-\frac{1}{2}} + 0.004\left(1 - \left(\frac{W}{h}\right)^2\right)\right) for \frac{W}{h} < 1 \end{cases}$$

(7.1)

where h = thickness of the dielectric material

W = Width of the conductor

ε_r = dielectric constant of the material

ε_{re} = effective dielectric constant of the material

Alternatively the expression for the quasi static approximation can be found by Hammerstad & Jensen [14] and Sheng Hong [13].The quasi static expression needs a dispersion correction for frequencies higher than 8 GHz. One possible solution is based on an empirical formula for the dispersive phase velocity (v_p) of a coplanar waveguide [3].

$$f_n = \frac{f}{f_c^1} = \frac{4h\sqrt{\epsilon_r - 1}}{\lambda_0} \tag{7.2}$$

where λ_o = wavelength; h = thickness of the dielectric material; ε_r = dielectric constant of the material and f_n=resonant frequency. Then the dispersive phase velocity (v_p) can be calculated as

$$v_p = \frac{1}{\sqrt{\epsilon_0 \epsilon_{re}(0)}} \frac{f_n^2 \sqrt{\epsilon_{re}(0)} + \sqrt{\epsilon_r}}{f_n^2 + 1} \tag{7.3}$$

Finally [12]

$$\varepsilon_{eff}(f) = \left(\frac{c}{v_p}\right)^2 \tag{7.4}$$

c is the velocity of the light which is $2.98 \times 10^8 \approx 3 \times 10^8$

The characteristics impedance (Z_o) of the CPW resonators was calculated by fixing the space (s) and it is given by 7.5.

$$Z = \frac{120\pi h}{W_{eff}\sqrt{\varepsilon_{re}}} \tag{7.5}$$

where h = height of the dielectric substrate, W_{eff} is the effective width of the conductor ($W_{eff} = W + \frac{t}{\pi}[\ln\left(\frac{2h}{t}\right) + 1]$), t is the thickness of the substrate and ε_{re} effective dielectric constant. The RF losses of CPW resonators can be calculated and described in the next section.

7.3.1. CONDUCTOR LOSS

Conductor loss (α_c) for the coplanar waveguide was derived by Owyang and Wu [15] and Tuncer et al [16] in 1958. Laterin 1993 Ghione [17] proposed an expression for the conductor loss by using the Wheelers incremental inductance method which is given by:

$$\alpha_c = \frac{R_s\sqrt{\varepsilon_{re}}}{480\pi.K(k_1).K'(k')(1-k_1^2)} \times \left(\frac{1}{a}\left[\pi + \ln\frac{8\pi a\,(1-k_1)}{t\,(1+k_1)}\right] + \frac{1}{b}\left[\pi + \ln\frac{8\pi b\,(1-k_1)}{t\,(1+k_1)}\right]\right) \quad (7.6)$$

$K(k_1)$ and k_1' can be derived by using the complete elliptical integral of first order and it is given by $a = \frac{W}{2}, b = s + \frac{W}{2}$ and $k_1 = \frac{W}{W+2S}$; $K'(k_1) = K\,(k_1')$ and $k_1' = \sqrt{1-(k_1)^2}$

where W= width of the conductor;

R_s = sheet resistance of the conductor and briefly discussed in Chapter-3

7.3.2. DIELECTRIC LOSS

Dielectric loss (α_{du}) is independent of the geometry for a uniformly filled CPW transmission line and can be written as [3].

$$\alpha_{du} = \frac{w}{2}\sqrt{\frac{\mu}{\epsilon'}\epsilon''} = \frac{w}{2}\sqrt{\mu\epsilon'}\tan\delta \quad (7.7)$$

where ϵ' is the real part and $\epsilon''$is the imaginary part of the complex permittivity of the dielectric, w is the angular frequency and tan δ is the loss tangent (which is 0.004 for both GaAs and InP materials) . For a lossless transmission line the imaginary part is zero but in practice there will be some losses in the material. When the upper dielectric constant (air) is assumed to be a lossless, the dielectric loss (α_{du}) can be [3]

$$\alpha_d = 27.3\,\frac{\varepsilon_r}{\sqrt{\varepsilon_{eff}(f)}}\,\frac{[\varepsilon_{eff}(f)-1]}{(\varepsilon_r-1)}\,\frac{\tan\delta}{\lambda_o} \quad \mathrm{dB/(unit\ length)} \quad (7.8)$$

where $\epsilon_{re}(f)$ is the effective dielectric constant and is generally dispersive

7.3.3. RADIATION LOSS

In addition to the conductor and dielectric losses, coupling of power to the surface waves and radiation from unwanted (parasitic) modes all contribute to the total loss of the CPW transmission line. The parasitic mode in the CPW is the odd mode with anti-phase voltage between the two gaps (S).

This mode can be excited at discontinuities, and radiation may occur. Radiation from this mode can be minimized by maintaining symmetry of the circuit and thus avoiding the excitation or by using the air bridges at regular intervals to equalise the potential of the two ground conductors. Air bridging is shown on a radial resonator in **Figure 7.3.**

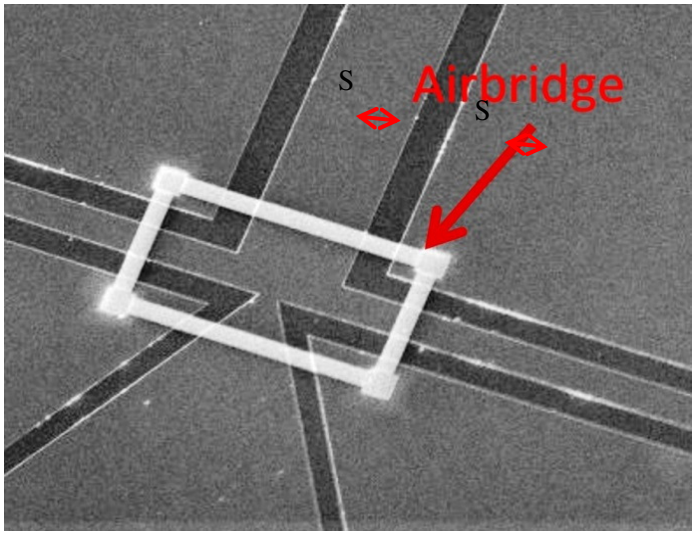

Figure.7.3. SEM image of the Air-bridge on top of the CPW line

7.3.4. QUALITY FACTOR

The quality factor Q of a CPW can be written as [18], [19]

$$Q_T = \frac{\beta}{2\alpha_t} = \frac{\beta}{2\,(\alpha_c + \alpha_d)} \tag{7.9}$$

where Q_T is the total unloaded Q factor of the resonator, α_t is the total loss in the resonator, and $\beta = 2\pi/\lambda$ phase constant.The loaded and unloaded Q_T factor of the CPW depends on the conductor (Q_c), dielectric (Q_d), radiation loss (Q_r) and external loss (Q_e) it can be expressed us

$$\frac{1}{Q_T}(\text{Unloaded}) = \frac{1}{\text{Q}_\text{c}} + \frac{1}{Q_d} + \frac{1}{Q_r} \tag{7.10-a}$$

$$\frac{1}{Q_L}(\text{Loaded}) = \frac{1}{Q_T}(\text{Unloaded}) + \frac{1}{Q_e} \tag{7.10-b}$$

where Q_e is the external loss and it can be calculated or evaluated for any given coupling structure.

7.4. DESIGN OF COPLANAR WAVEGUIDE RESONATORS

Microwave resonators have many applications in microwave and millimetric wave circuits. For example, it is an important component in the design of microwave filters [20], [21], microwave oscillators [22] and microstrip antennas [23], [24] . The requirements for these integrated resonators include small physical size to increase packing density in microwave monolithic integrated circuits (MMIC), high frequency of resonance and low loss i.e. a high Q_T quality factor. To realize high frequency oscillator performance from the planar Gunn diode, planar circuit elements (which can be connected to the active device) and a low loss planar circuit medium is required: for this reason CPW was chosen. To maximize the Q_T of the oscillator the resonator is required to be as close as possible to the diode to minimize the conductor losses and therefore increase the $Q_T$factor of the resonator. The challenge with planar circuits is obtaining a high Q_T resonator in a small area on the integrated circuit. The radial resonator was first reported in 1993 by Simons [25] and later he proposed a double stub radial resonator [26] to increase the Q_T factor of the resonator but when compared to the single stub radial resonator the Q_T factor of device was increased by approximately 8%,and occupied a lot of chip area.

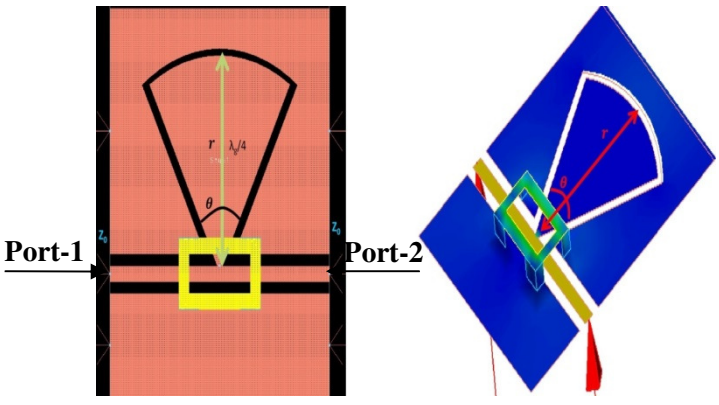

Figure.7.4. (a) 2D radial stub resonator(b) 3D view of the radial line resonator

The resonator design in this work was carried out using the Advanced Design System-2009 (ADS) software and the internal package - method of momentum. Method of momentum is an electromagnetic simulator that

computes S-parameters for general planar circuits including microstrip, slot-line, stripline, coplanar waveguide and other technologies. Vias and airbridge connect topologies between layers; multilayer structures, RF and microwave circuits can also be simulated using ADS-2009. Using the method of momentum it was found that the mesh size was of particular importance to obtain realistic return-losses of the resonator particularly at high frequency. Initial simulation and measurement results on radial stub resonator showed that it had superior performance over the quarter wavelength stub; it was shorter in physical length, had a wider bandwidth and a higher loaded Q_L. **Figure 7.4.** shows a typical structure of a radial stub resonator with an air-bridge to equalise the potential between the two ground electrodes. The simulated result for a 400 μm radius radial resonator is shown in **Figure 7.5.** The resonant frequency of the radial stub resonator was defined when S_{21} approached a low loss and the s_{11} a high return loss.

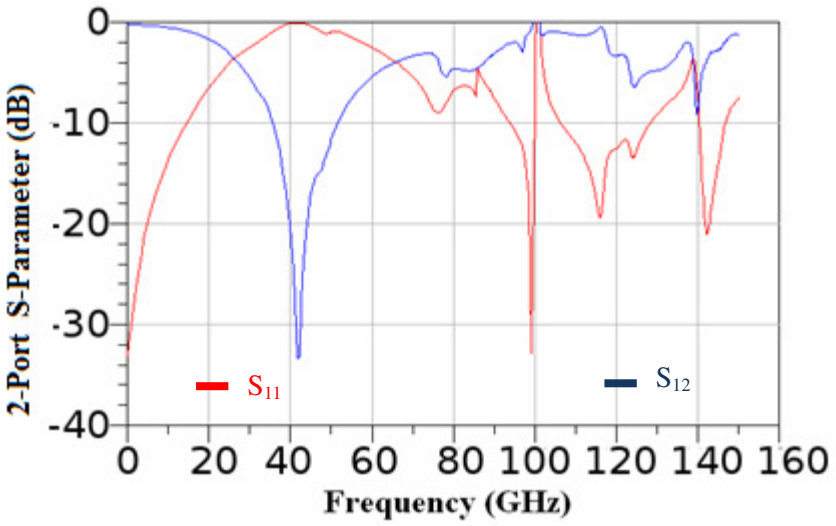

Figure.7.5. Return loss of the radial stub resonator

In practical terms it is difficult to calculate the radius of a radial resonator for a particular resonant frequency. In 2012 Li Chong reported a polynomial equation (resonant frequency (f_0) as a function of radius (r) and radial stub inner angle (θ)) to enable the design of high frequency radial stub resonators [27]. Similar work has been carried out and similar polynomial equations relating resonator radius and internal angle to resonant frequency have been obtained and are in good agreement with the published work by Simon and

Li Chong[2], [26]. **Figures 7.6 and 7.7** show the computed resonant frequency of the radial stub as a function of radius and angle respectively. The resonant frequency was defined when S_{21} approached a low loss and the s_{11} a high return loss.

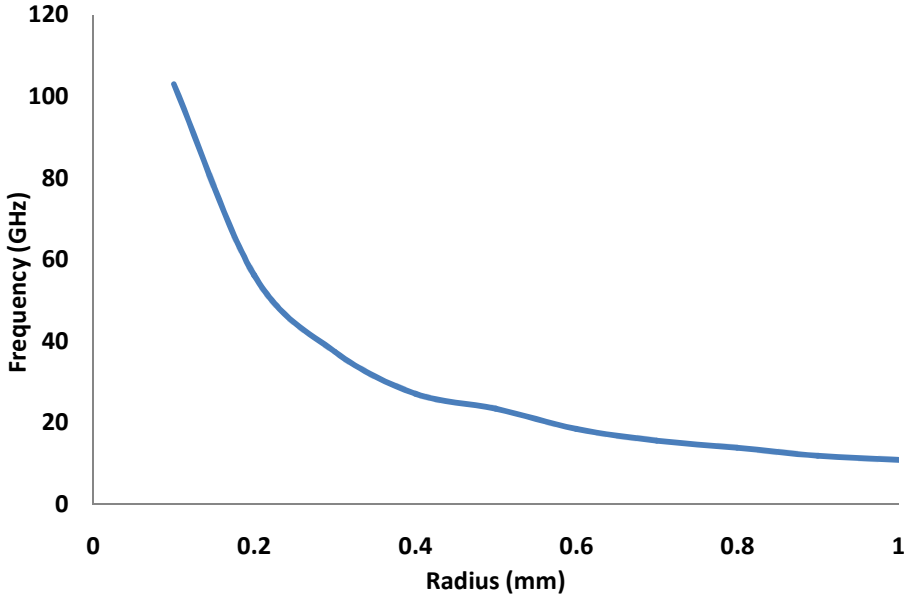

Figure.7.6. Resonant frequency as a function of the radius of a radial resonator

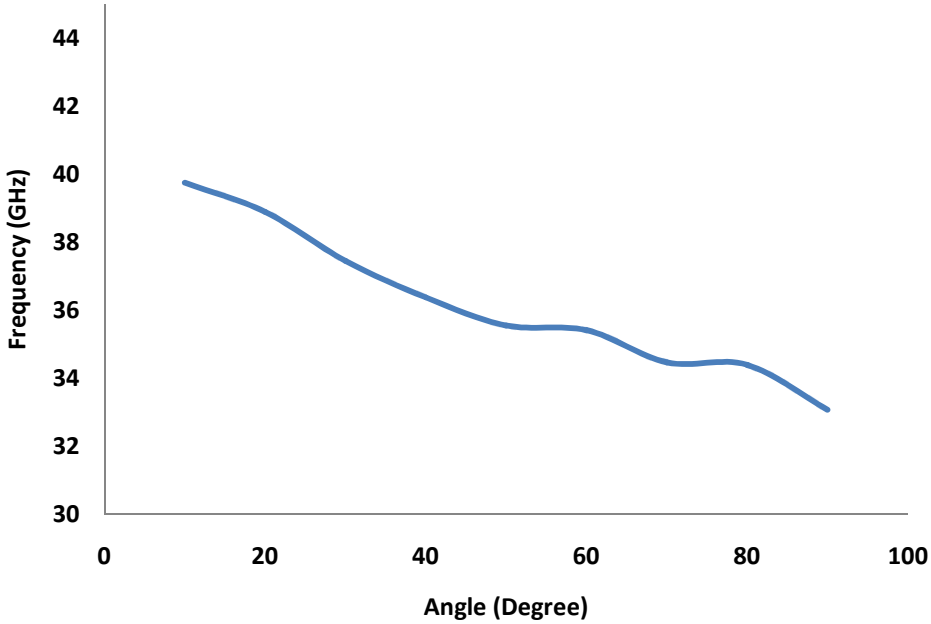

Figure.7.7. Resonant frequency as a function of the angle of a radial stub resonator

7.4.1. FABRICATION AND RF CHARACTERISATION OF RADIAL STUB RESONATORS

The fabrication of radial stub resonators was carried out using EBL lithography techniques, which was briefly discussed in Chapter-4, to control the dimensions of the device (**Figure 7.8**) shows an SEM image of a fabricated radial stub resonator on a semi-insulating GaAs substrate. The gold metallisation thickness of the radial stub resonator was approximately 0.4 microns (T≈ 0.4 μm). The fabricated resonators were measured using the high frequency network analyser (10 MHz to 110 GHz).Two port S-parameter measurements were made to determine the reflection (S_{11}) and transmission (S_{21}) coefficient of loaded radial stub resonators from 10 Hz to 110 GHz using the Agilent vector network analyser (VNA). The 40-60-40μm pitch 50 Ohm CPW RF probes from GGB industries were connected to the VNA and the system was calibrated from 10 Hz to 110 GHz using a calibration substrate (109-102B) from Cascade Microtech (described in chapter-3, section 3.5).

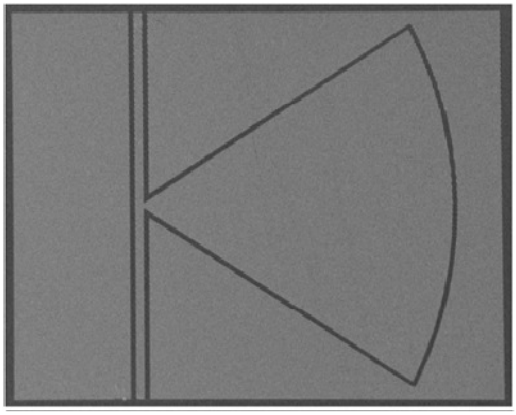

Figure.7.8. SEM image of radial stub resonator without airbridge

7.4.2. MEASUREMENT RESULTS OF RADIAL STUB RESONATOR WITHOUT AIR-BRIDGE

Figure.7.9. shows a comparison of simulated and measured results (S_{11}) of a loaded radial stub resonator without an air-bridge. In the design the inner angle of the radial stub was kept constant (60^0) and the magnitude of the radius of the radial stub was varied. From **Figure.7.9**, it can be seen that the resonant frequency of the simulated radial stub resonator was in good

agreement with the measured results. **Figure.7.10.** compares the resonant frequency of measured and simulated results for a radial stub resonator as a function of the inner angle which was varied from 10 to 90 degrees, maintaining a constant radius of 600 μm. From **Figure.7.10)** it can be seen that the resonant frequency of the simulated radial stub resonators were in good agreement with the measured results.

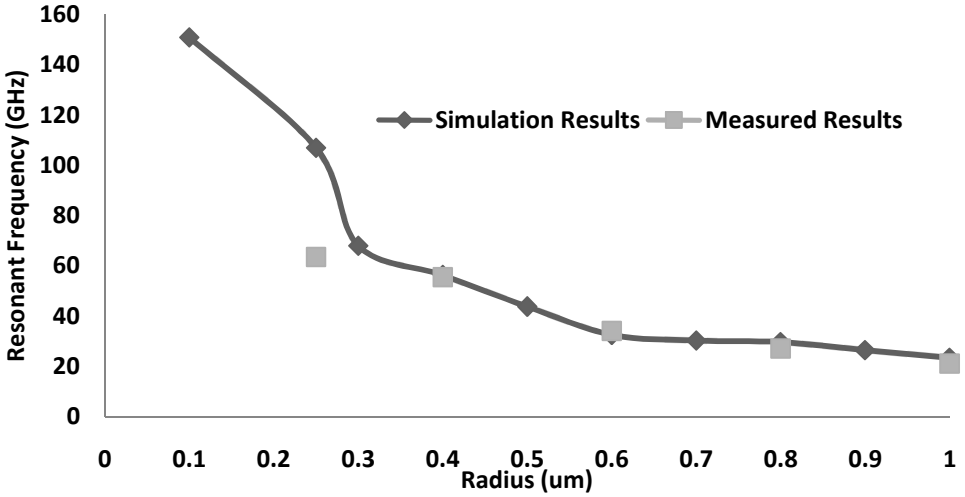

Figure.7.9. Comparison of simulated and measured results for the resonant frequency as a function of the radius of a radial resonator

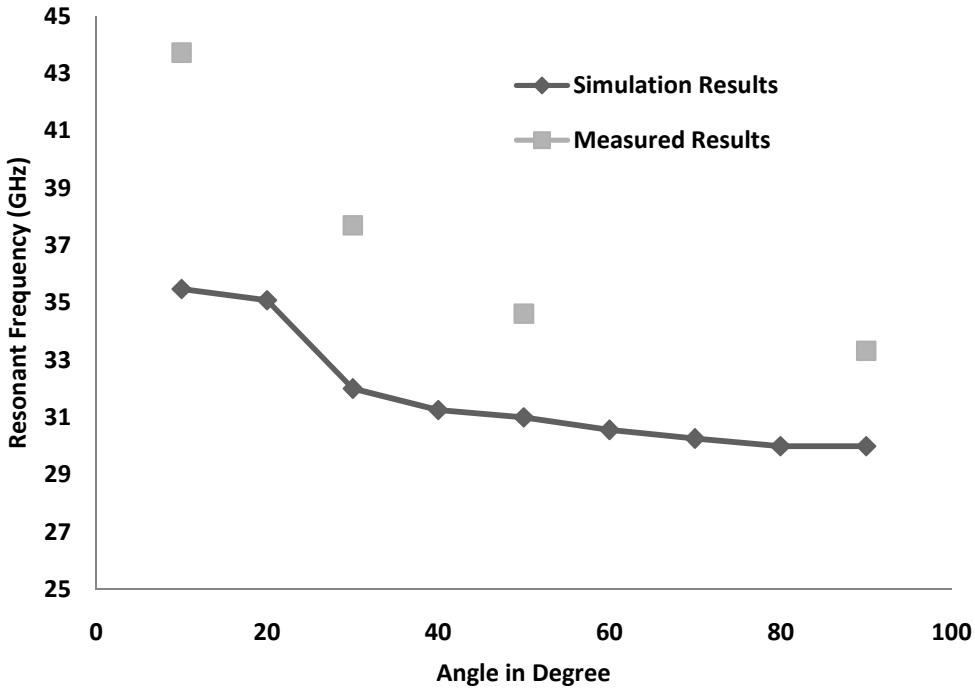

Figure.7.10. Comparison of simulated and measured results for the resonant frequency as a function of the internal angle of a radial stub resonator

The loaded Q_L of the radial stub resonator was estimated using the expression (7.10 and 7.11) and is given by Foss in 1966 [28] . The loaded Q_L-factor of the radial stub resonator was measured when s_{21} approached a low loss and the s_{11} a high return loss. The Q_L factor of a radial stub resonator with a sectorial angle of 60^0 was plotted as a function of the resonator radius in **Figure.7.11.Figure.7.11** indicates that there is an optimum radius for a particular sectorial angle for a maximum loaded Q_L.

$$Q_L = \frac{(Energy\ stored)}{Energy\ dissipated} = \frac{1}{\tan\delta} = \frac{f_o}{\Delta f} \qquad (7.11)$$

where Δf is the -3dB bandwidth

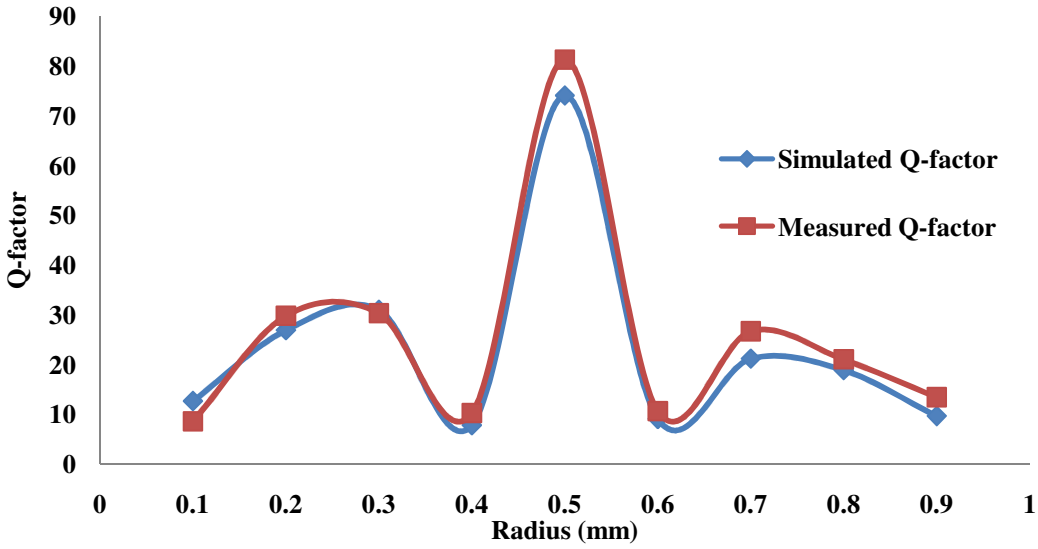

Figure.7.11 Comparison of simulated and measured results for the quality factor of a radial stub resonator as a function of radius

7.5. DESIGN OF DIAMOND RESONATORS

A novel diamond resonator was designed and developed using the software package Advanced Design Systems (ADS-2009). The author believes this is the first time this shaped coplanar waveguide resonator has been realised and offers a number of advantages over the radial stub resonator in a coplanar waveguide format [29]. **Figure.7.12.** shows a schematic view of the coplanar waveguide diamond stub resonator. The resonator has a metallised thickness of T and a length L with an inner angle θ, the apex corner of the resonator is directly fed from a CPW 50 Ohm line. The diamond stub resonator was fab-

ricated by using gold metallisation on a semi-insulating gallium arsenide substrate and RF characterised from 10 Hz to 110GHz using a high frequency network analyser. The loaded diamond stub resonator was fully analysed using the momentum model in the electromagnetic package within ADS. Again like the radial stub resonator it was necessary to choose the correct mesh size ($0.028*\lambda_g/4$) to obtain realistic simulation results (S_{11}) particularly for small length(L), high frequency, diamond stub resonators. The fabricated diamond resonator contained no air bridging to equalise the potential between the two earth electrodes. It was found by reducing the inner length L of the resonator the resonant frequency was increased. The experimental measurements made on the loaded diamond stub resonators were directly compared with the simulation results and these will be discussed in the next section. The novel diamond resonator structure was found to have a higher loaded Q_L when compared to published results on CPW quarter wavelength [30] and radial stub resonators[31] operating at the same resonant frequency (with 50 ohm matching impedance). An important feature of the diamond resonator was that it took up less circuit area when compared to the radial resonator operating at the same frequency.

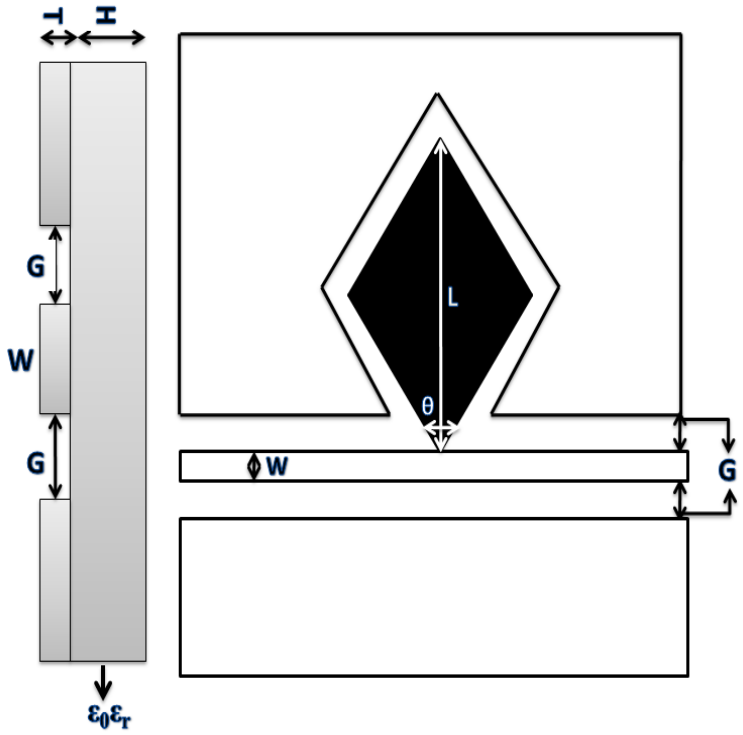

Figure.7.12. CPW Diamond resonator

7.5.1. FABRICATION AND RF CHARACTERISATION OF DIAMOND STUB RESONATORS

Similar technology was used to fabricate the diamond stub resonator as was used to fabricate the radial stub resonator, for example using EBL discussed in Chapter-4, to control the dimensions of the device.**Figure7.13**. shows a SEM image of a fabricated diamond stub resonators on a semi-insulating GaAs substrate. The gold metallisation thickness (T) of the diamond stub resonator was approximately 0.4 microns (T≈ 0.4 μm). The RF measurements were made on the diamond stub resonator by using the high frequency network analyser. Two port S-parameter measurements were made to determine the reflection (S_{11}) and transmission (S_{21}) coefficient of the loaded diamond stub resonators from 10 Hz to 110 GHz using the Agilent vector network analyser (VNA). Two 40-60-40μm pitch 50 Ohm CPW RF probes from GGB industries were connected to the VNA and the system was calibrated from 10 Hz to 110 GHz using a calibration substrate (109-102B) from Cascade Microtech (described in chapter-3, section 3.5).

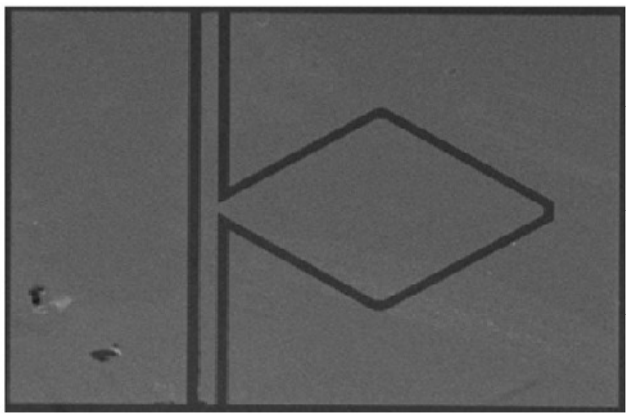

Figure.7.13. SEM image of diamond stub resonator without airbridge

7.5.2. SIMULATION RESULTS

As discussed the resonant frequency of a CPW radial line resonator was dif-

ficult to calculate because of the closed form equations reported in [25], and this was overcome by using a polynomial equation to fit the experimental results [2]. A similar method for designing the diamond resonator was adopted; the simulated resonant frequency (f_0) was plotted as a function of L at a constant sectorial (inner) angle of 60 degrees and then fitted to a 4th order polynomial equation 7.12.

$$f_0 = 3221L^4 - 8368L^3 + 7827L^2 - 3180L + 530.9 \quad (7.12)$$

The coefficients of the polynomial equation will be modified for different sectorial angles and was very sensitive to the sectorial angle of the diamond. **Figure.7.14.** shows a comparison between the simulated CPW diamond and radial stub resonator. The results clearly show that the diamond geometry will resonate at a higher frequency than the radial stub resonator with a comparable length (L) and the same sectorial angle. The plot shows that for a radial stub resonator with a radius of 0.6mm the resonant frequency was 32.56 GHz, whereas for the diamond resonator with an inner length of 0.6mm the resonant frequency was 44.87 GHz. The diamond resonator also had an overall smaller physical outline when compared to radial stub resonator which is shown in the **Figure.7.15.** From the plot the diamond resonator of inner length 0.6 mm required approximately 55 % less chip area when compared to the radial stub resonator of radius 0.6mm.

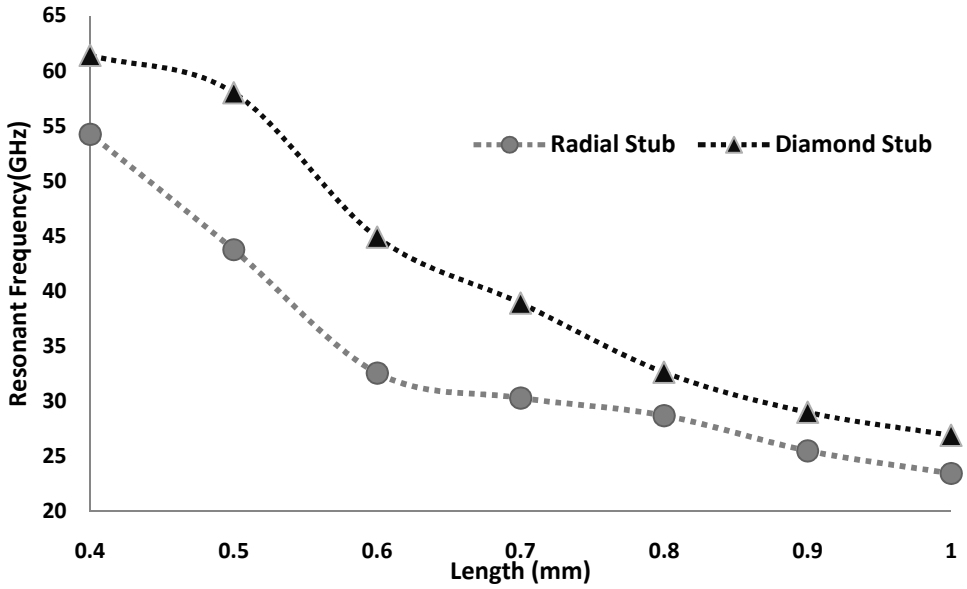

Figure.7.14. Comparison of the resonant frequency of CPW Diamond and Radial stub resonators as a function of resonator length on a semi-insulating GaAs substrate

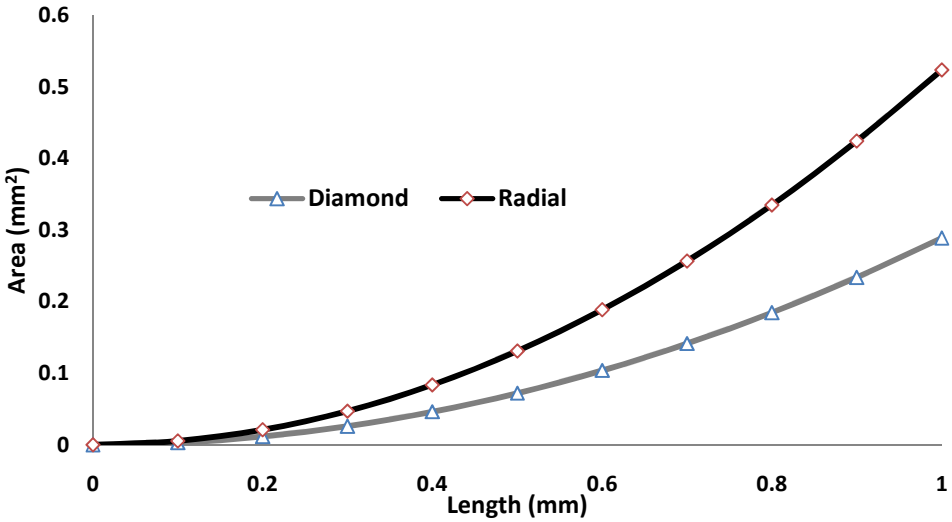

Figure.7.15. Area of diamond and radial stub resonators on GaAs semi-insulating substrate

Figure.7.16. show the comparison between the simulated CPW loaded diamond resonator on a semi-insulating GaAs and InP substrate of commercially available thicknesses 620 and 600 microns respectively. The simulation results show that there was not much variation (0.78 %) in the resonating frequency this is due to the similar dielectric properties of both materials.

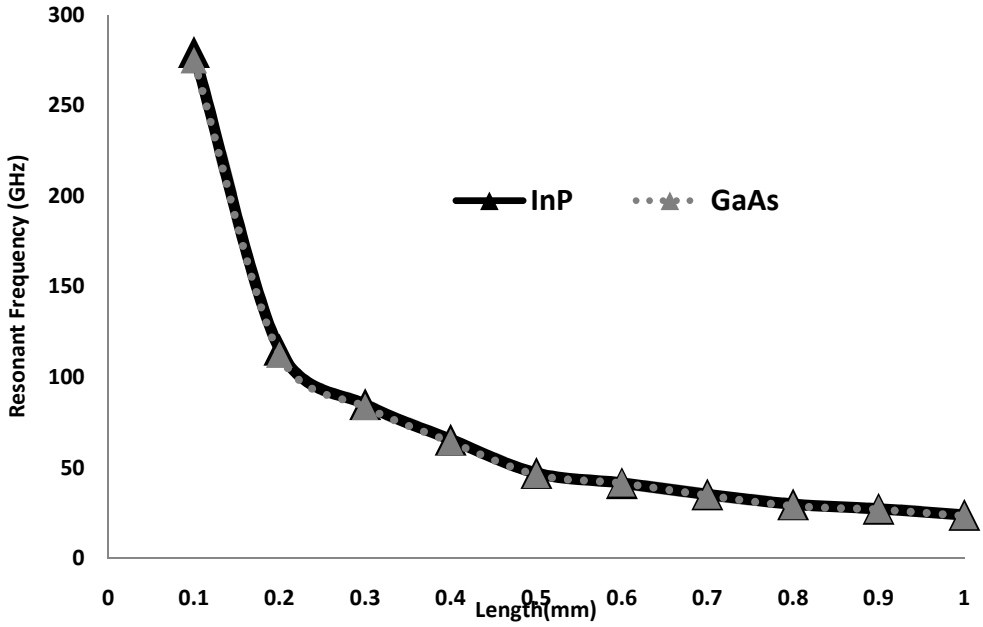

Figure.7.16. Comparison of the resonant frequency of CPWdiamond on GaAs and InP substrates

7.5.3. EXPERIMENTAL RESULTS

A number of CPW diamond resonators with a sectorial angle of 60^0 with an inner length of 0.1 to 1.0 mm were fabricated on a 620 μm thick semi-insulating GaAs wafer. The metallization thickness of the resonator structure was 0.4 μm to minimise conductor losses and the structure was fed using 50 Ohm CPW line which is shown in **Figure.7.13.** The resonator structures were fabricated in James Watt Nanofabrication Centre at University of Glasgow

The resonators were characterised using two port S-parameter measurements from 100 MHz to 110 GHz by connecting to calibrated RF probes (Cascade MicroTech ACP11-100) coupled to an Agilent E8364B network analyser. The experimental and simulated resonant frequency of the loaded diamond resonator with increasing L, are directly compared in **Figure.7.17**. The plot shows very good agreement between experiment and simulation for inner resonator line length varying from 1 to approximately 0.3 mm. The experimental results departed from the simulation when L < 0.3mm and this was thought to be due to restriction in mesh size and geometrical parasitic effects not taken into account in the simulation. The 0.6 mm and 60^0 sectorial angle diamond resonators had a simulated loaded Q_L-factor of 46; the measured loaded Q_L-factor was 38.

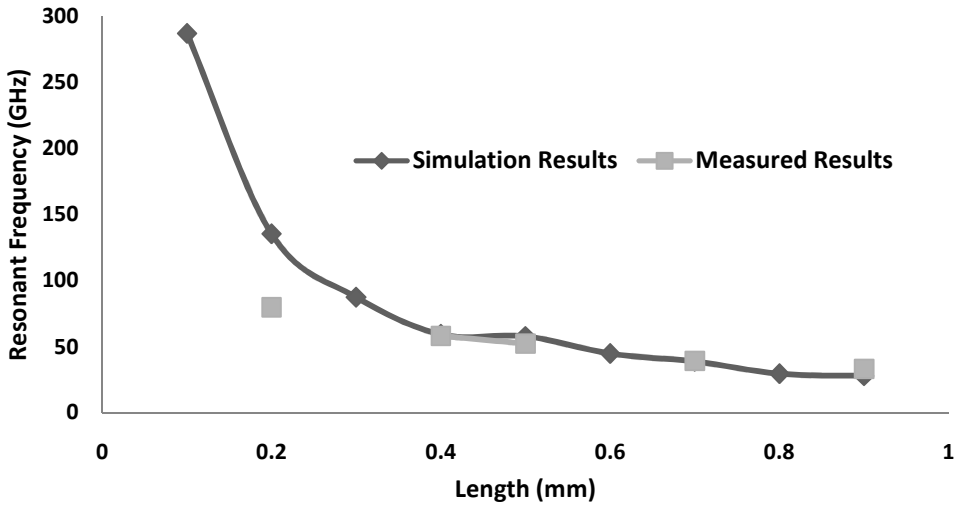

Figure 7.17. Measured resonance frequency of a diamond resonator as a function of resonator length, and constant sectorial angle of 60^0

7.6. REFERENCES

[1] E. J. Denlinger, "Losses of Microstrip Lines," *IEEE Trans. Microw. Theory Tech.*, vol. 28, no. 6, pp. 513–522, Jun. 1980.

[2] C. Li, "Design and Characterisation of millimeter-wave planar Gunn diode and integrated circuits," University of Glasgow, 2011.

[3] K.C.Gupta, R. Garg, I. Bahl, and P. Bhartia, *Microstrip Lines and Slotlines*. Boston and London: Artech House Publishers, 1996.

[4] B. J. T. Edwards and Climer, "Book review: "Foundations for microstrip circuit design," *J. Electron. Manuf.*, vol. 02, no. 02, pp. 89–90, Jun. 1992.

[5] R. A. Pucel, "Design Considerations for Monolithic Microwave Circuits," *IEEE Trans. Microw. Theory Tech.*, vol. 29, no. 6, pp. 513–534, Jun. 1981.

[6] K.U.Yen, D.Chuss, and J.Wollack, "Planar Transmission Line Technologies," in *Antenna and Proporgation*, 2002, pp. 1–8.

[7] R. Majidi-Ahy, M. Riaziat, C. Nishimoto, M. Glenn, S. Silverman, S. Weng, Y. C. Pao, G. Zdasiuk, S. Bandy, and Z. Tan, "5-100 GHz InP CPW MMIC 7-section distributed amplifier," in *IEEE Symposium on Microwave and Millimeter-Wave Monolithic Circuits*, 1990, pp. 31–34.

[8] J. Brown, "Broadband amps sport coplanar waveguide," *Microw. RF journals*, vol. 26, pp. 131–134, 1987.

[9] T. M. Weller, L. P. B. Katehi, and G. M. Rebeiz, "High performance microshield line components," *IEEE Trans. Microw. Theory Tech.*, vol. 43, no. 3, pp. 534–543, Mar. 1995.

[10] C. P. Wen, "Coplanar Waveguide: A Surface Strip Transmission Line Suitable for Nonreciprocal Gyromagnetic Device Applications," *IEEE Trans. Microw. Theory Tech.*, vol. 17, no. 12, pp. 1087–1090, Dec. 1969.

[11] S. Hussain, M. Kumar, P. A. K. Jaiswal, and E. Rohini, "Dispersion and Characterization of Coplanar Waveguide Based On Conformal Mapping Technique," *Int. J. Eng. Res. Appl.*, vol. 3, no. 4, pp. 1121–1125, 2013.

[12] Nikolova, "Microstrip antennas," McMaster University, 2010.

[13] Jia-Sheng Hong, *Microstrip Filters for RF/Microwave Application*, 2nd Editio. Wiley, 2001, pp. 0–656.

[14] E. Hammerstad and O. Jensen, "Accurate Models for Microstrip Computer-Aided Design," in *MTT-S International Microwave Symposium Digest*, 1980, vol. 80, no. 12, pp. 407–409.

[15] G. Owyang and T. Wu, "The approximate parameters of slot lines and their complement," *IRE Trans. Antennas Propag.*, vol. 6, no. 1, pp. 49–55, Jan. 1958.

[16] E. Tuncer, M. S. Islam, and D. P. Neikirk, "Quasi-static conductor loss calculations in transmission lines using a new conformal mapping technique," *IEEE Trans. Microw. Theory Tech.*, vol. 42, no. 9, pp. 1807–1815, 1994.

[17] G. Ghione, "A CAD-oriented analytical model for the losses of general asymmetric coplanar lines in hybrid and monolithic MICs," *IEEE Trans. Microw. Theory Tech.*, vol. 41, no. 9, pp. 1499–1510, 1993.

[18] M. J. Lancaster, "Wide-band superconducting coplanar delay lines," *IEEE Trans. Microw. Theory Tech.*, vol. 53, no. 7, pp. 2348–2354, Jul. 2005.

[19] G. Hasnain, A. Dienes, and J. R. Whinnery, "Dispersion of Picosecond Pulses in Coplanar Transmission Lines," *IEEE Trans. Microw. Theory Tech.*, vol. 34, no. 6, pp. 738–741, Jun. 1986.

[20] M. Ismaeel, T. Jayanthy, and S. Sathyamurthy, "Comparison of rectangular and T-shaped microstrip antenna," in *Proceedings of the 8th WSEAS international conference on Electronics, hardware, wireless and optical communication*, 2009, pp. 185–189.

[21] M. Ismaeel and A. Kumar, "Aanlysis of electromagnetic interface filters for power systems and telephone," in *10th International conference on electromagnetic interference and compatibility (INCEMIC 2008)*, 2009, p. 433.

[22] M. I. Maricar, J. Glover, G. A. Evans, A. Khalid, V. Papageorgiou, L. Chong, G. Dunn, and C. H. Oxley, "Planar Gunn diode characterisation and resonator elements to realise oscillator circuits," in *International Conference on Advanced Nanomaterials & Emerging Engineering Technologies ICANMEET-2013*, 2013, pp. 674–678.

[23] V. R. Anitha, S. N. Reddy, and M. Ismaeel, "Design of a 4X4 square microstrip planar array," *Int. J. Intell. Electron. Systsmes*, vol. 3, no. 1, pp. 70–74, 2009.

[24] T. Jayanthy, M. Sugadev, J. M. Ismaeel, and G. Jegan, "Design and simulation of Microstrip M-patch antenna with double layer," in *2008 International Conference on Recent Advances in Microwave Theory and Applications*, 2008, pp. 230–232.

[25] R. N Simons and S. R. Taub, "Coplanar waveguide radial line stub," *Electron. Lett.*, vol. 29, no. February, pp. 7–9, 1993.

[26] R. N. Simons and S. R. Taub, "Coplanar waveguide radial line double stub and application for filter circuits," *Electron. Lett.*, vol. 29, no. 17, pp. 1584–1586, 1993.

[27] C. Li, A. Khalid, L. B. Lok, N. J. Pilgrim, M. H. Holland, G. M. Dunn, and D. R. S. Cumming, "Millimeter-Wave Planar Gunn Diodes," in *(Unknown Conference in Sheffield)*, 2010.

[28] R. C. Foss and B. J. Green, "Q factor, Q stability and gain in active filters," *Electron. Lett.*, vol. 2, no. 3, p. 99, 1966.

[29] M. I. Maricar, J. Glover, G. Evans, D. Cumming, and C. Oxley, "Design and characterization of a novel diamond resonator," *Microw. Opt. Technol. Lett.*, vol. 56, no. 7, pp. 1691–1693, Jul. 2014.

[30] D.M. Pozar, *Microwave Engineering*. John Wiley & Sons, Inc., 1998.

[31] R. N. Simons, *Coplanar Waveguide Circuits, Components, and Systems*. New York, USA: John Wiley & Sons, Inc., 2001.

Chapter: 8

Extraction of harmonic frequencies from the planar Gunn diode

8.1. INTRODUCTION

The last two chapters have discussed the design, fabrication and power performance of the GaAs and InP based planar Gunn diodes respectively. To meet future practical applications, it will be necessary to increase the output RF power and also increase the oscillation frequency of the planar Gunn diode. Firstly, to increase the RF output power performance external matching elements will be required. Secondly to increase the oscillation frequency of the planar Gunn diode, a smaller anode to cathode separation (L_{ac}) will be required, and/or extraction of the second or third harmonic oscillation frequency. This chapter will describe the design, fabrication and test of a simple novel planar Gunn integrated oscillator in which the second harmonic was extracted and the fundamental oscillation frequency was suppressed.

8.2. IMPORTANCE OF THE PASSIVE COMPONENTS IN PLANAR GUNN DIODE DESIGN

It is well known that the Gunn diode is a negative resistance device that can generate a self-sustaining oscillation and was first demonstrated by J. B. Gunn in 1963 [1]. The early Gunn diodes were 'vertical' technology (which was discussed in chapter 2) which precluded easy on chip integration. In 2007 Ata Khalid et all [2] demonstrated the first planar Gunn diode operating at frequencies above 100 GHz in CPW format, which for the first time

enabled the potential of integrating the Gunn diode into milli-metric or even terahertz integrated circuit technologies.

A vertical Gunn diode is usually embedded in a waveguide or coaxial circuit in order to resonate [3], [4] and match the diode to obtain high RF output power at a stable frequency of oscillation [5]. **Figure 8.1**) shows a schematic diagram of a vertical Gunn diode in a waveguide circuit. A metallic disc resonator was used to obtain a high quality (Q) factor approaching 1000 to ensure the Gunn oscillator circuit operates with a stable frequency and low phase noise. A low pass inductive filter was used to DC bias the Gunn diode preventing RF entering the DC bias line which would result in bias circuit oscillations. The waveguide provided the DC block to RF load. The DC block in a planar circuit can be realized by using a series capacitor or a coupler, which will decouple the DC but will allow the RF signal to flow to the RF load. Li Chong [6] used a similar approach as was used for the vertical Gunn diode but in CPW format to enable the design and realization of a planar Gunn diode oscillator which is shown as a schematic in **Figure.8.2.**

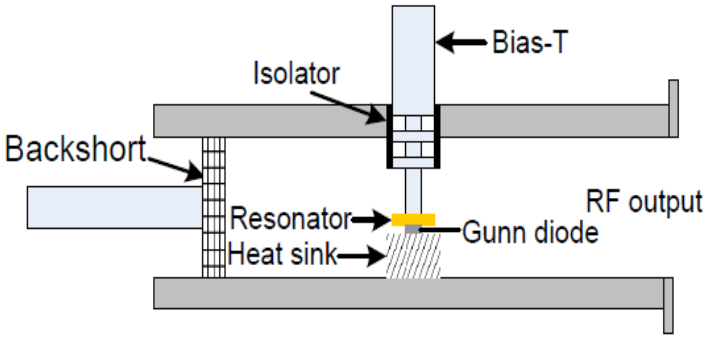

Figure.8.1.Circuits elements for Vertical Gunn diode

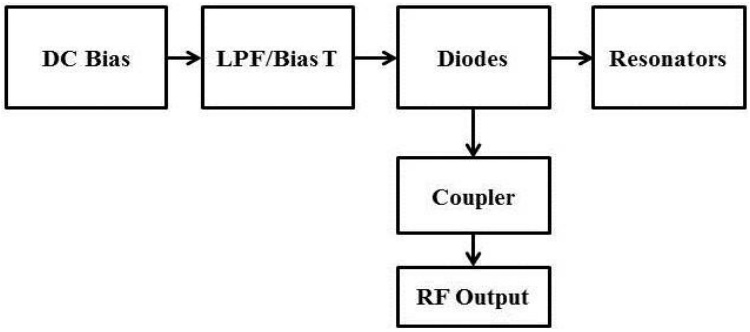

Figure.8.2. Developed integrated planar Gunn oscillator by Li Chong [6]

The vertical Gunn diode can be described using a simple electrical equivalent circuit model consisting of a capacitor in parallel with a negative resistor (or negative conductance). A similar approach as the vertical Gunn diode was used to describe the planar Gunn diode, shown in **Figure 8.3**. The value of the capacitor and negative conductance was estimated from small-signal S-parameter measurements which will be discussed later in the chapter. As discussed in the Chapter-5, the planar Gunn diode capacitance can be resonated (f_0) by a series inductor. The planar Gunn diode can also be resonated by a parallel inductor which can be realized as a shunt/open circuit stub.**Figure.8.4**. shows the shunt/open circuit matching stub to resonate the planar Gunn diode, the length of the stub was derived using the equation (8.1) [7]

$$Z_{op} = -jZ_o \cot \beta L \tag{8.1}$$

where Lis the line length

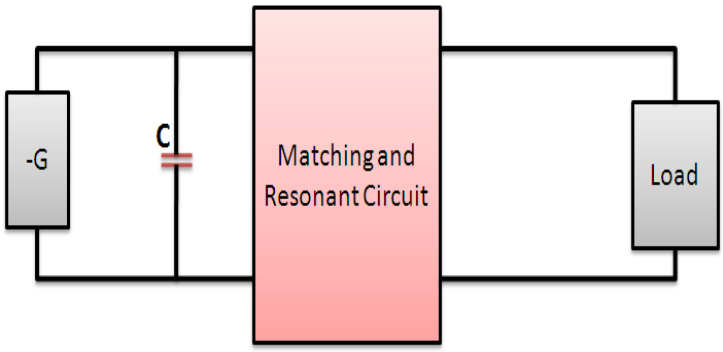

Figure.8.3. Generalequivalent circuit model for the planar Gunn diode

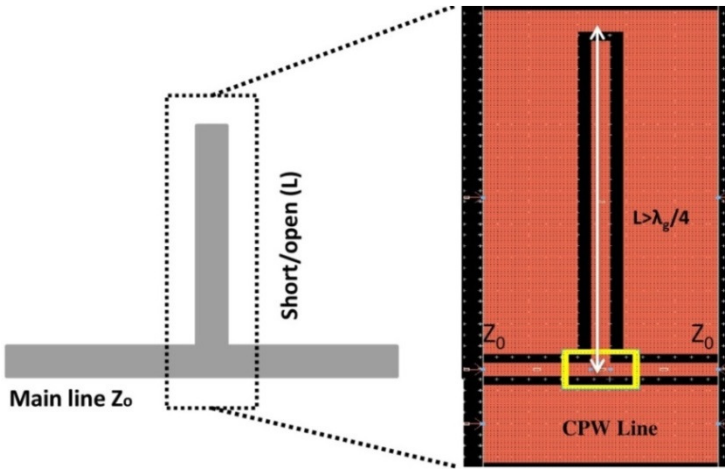

Figure.8.4. Simple open/ shut matching element in CPW format

8.3. EXTRACTION OF SECOND HARMONIC FROM InP BASED PLANAR GUNN DIODES

The CPW format planar Gunn diode can be easily fabricated as part of a microwave monolithic integrated circuit (MMIC) making the feasibility of including simple two terminal devices as frequency sources. As discussed, the transit oscillation frequency of the planar Gunn diode is determined by the spacing between anode and cathode electrodes. The frequency of operation of these devices can be further extended into the millimeter band and to the lower terahertz frequencies by reducing the active length below 1µm and efficiently extracting the second or third harmonic frequency. A novel method to extract the second harmonic frequency from the planar Gunn diode was developed using coplanar waveguide (CPW) matching elements, and a radial stubor the novel diamond stub resonator [8]. A schematic of the oscillator is shown in **Figure.8.5.** The CPW open circuit stub was used to resonate (f_0) the diode capacitance of the planar Gunn diode and the radial stub or the diamond stub resonator was designed at f_0 to suppress the fundamental oscillation frequency so the second harmonic frequency from the planar Gunn diode could be extracted

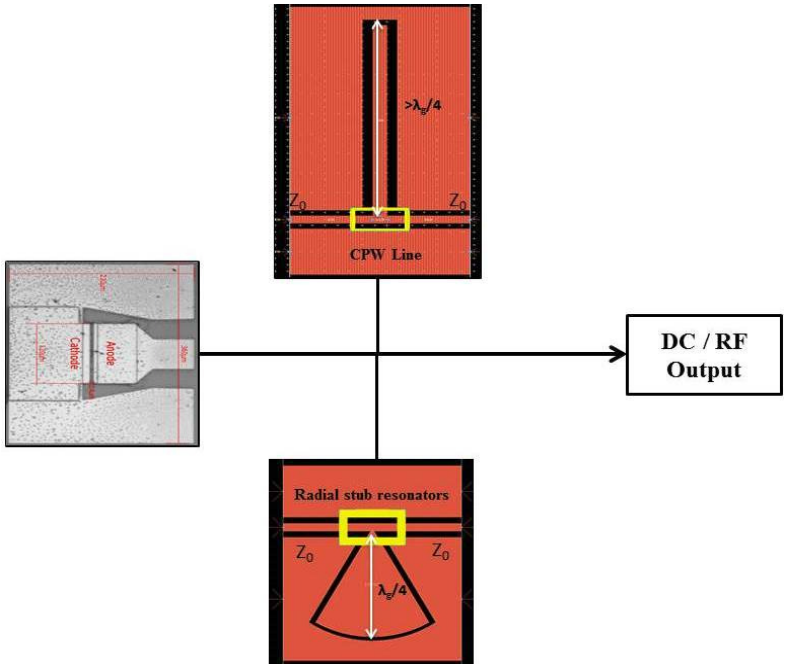

Figure.8.5. Proposed integrated model for the planar Gunn diode to extract the second harmonic

The work was carried out using by using both AlGaAs and $In_{0.53}Ga_{0.47}As$ hetero-structure Gunn diodes fabricated on GaAs and InP substrates respectively. The Gunn diode was fabricated with an active channel length of 4 µm and the width of 120 µm providing a fundamental frequency of oscillation around 25 GHz for GaAs based planar Gunn diode and 60GHz for InP based planar Gunn diode. This geometry was chosen as the lower frequency made it easier to microwave characterise the oscillator circuits and particularly at the harmonic frequencies. The matching circuit and resonator structures were designed using Advanced Design System (ADS2009) simulation package, which was briefly discussed in chapter-7. The diodes and on chip integrated circuits were fabricated in Nanotechnology Center and then tested in the milli-metric wave laboratory at University of Glasgow. The fabrication and measurement techniques were fully discussed in chapters 3 and 4.

Initially a simple electrical circuit model was developed to describe InP planar Gunn diode (L_{ac} = 4 microns) matching circuit elements and resonator structure to investigate extraction of the second harmonic oscillation frequency using ADS 2009. **Figure.8.6**. shows the ADS electrical circuit model used to investigate the extraction of the second harmonic from the InP planar Gunn diode. The circuit model consisted of a CPW open circuit transmission line with a characteristic impedance $Z_0 \approx 32$ Ohm to match out the diode capacitance, and a radial stub resonator with a resonate frequency of 60.5 GHz. The experimentally measured S-parameter measurements of an InP based Type-C planar Gunn diode were loaded into ADS-2009 using S1P tool (which is the inbuilt tool to load the measured S-parameter in ADS 2009). The S-parameter measurements of the Type-C device were used to obtain the input impedance of the diode at the fundamental oscillation frequency (because the magnitude of the S11 > 1 at 60.27 GHz). **Figure.8.7**. shows measured S-parameter results of a 4 microns planar Gunn diode. It can be seen that when the applied bias voltage is greater than the threshold voltage, the magnitude S_{11} is greater than one (S_{11}>1) which indicates that the device is operating in its negative resistance region. The S-parameters of the Type-C

device were de-embedded by using the equation 8.2. According to the following equation the resistance and reactance (Z_0 = R+ jX_C) of the de-embedded results of the planar Gunn diode can be calculated and are plotted as shown in **Figure 8.8. Figure 8.8 (a)** shows the negative resistance of the planar Gunn diode and **Figure 8.8. (b)** the reactance of the planar Gunn diode which is negative and so represents a capacitance. From 0 to 32 GHz the plot can to a first order be represented by a single capacitive reactance.

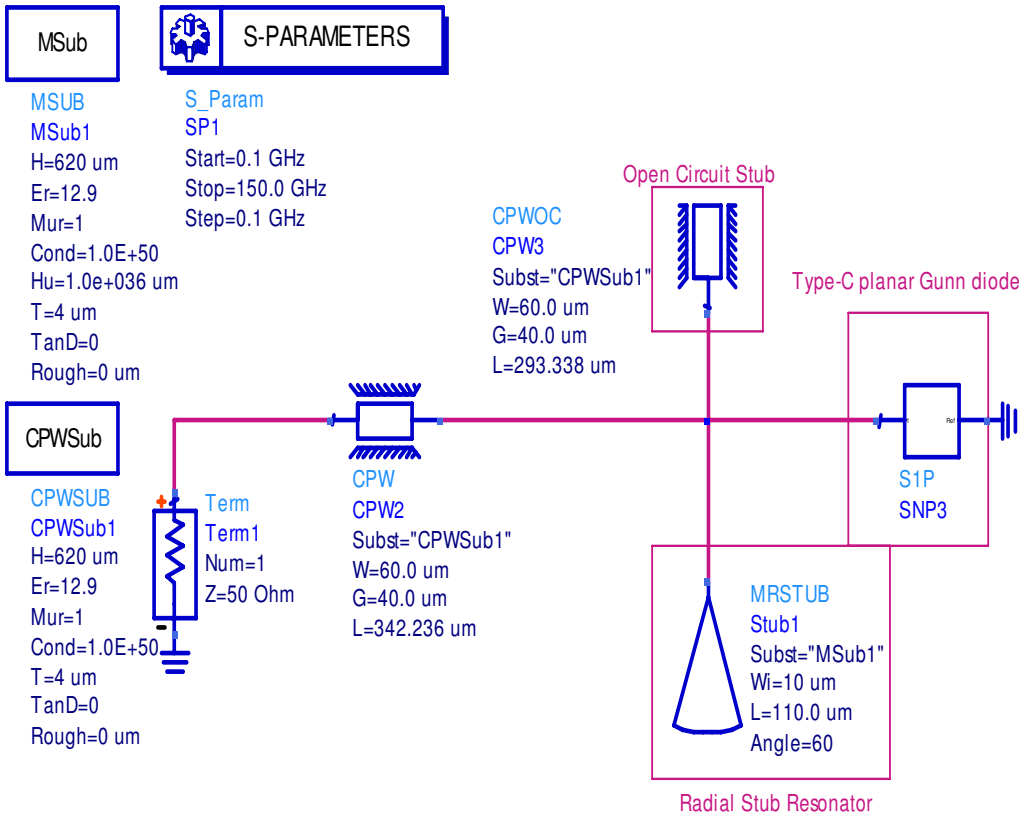

Figure.8.6. Simple equivalent Circuits model to extract second harmonic from the planar Gunn diode

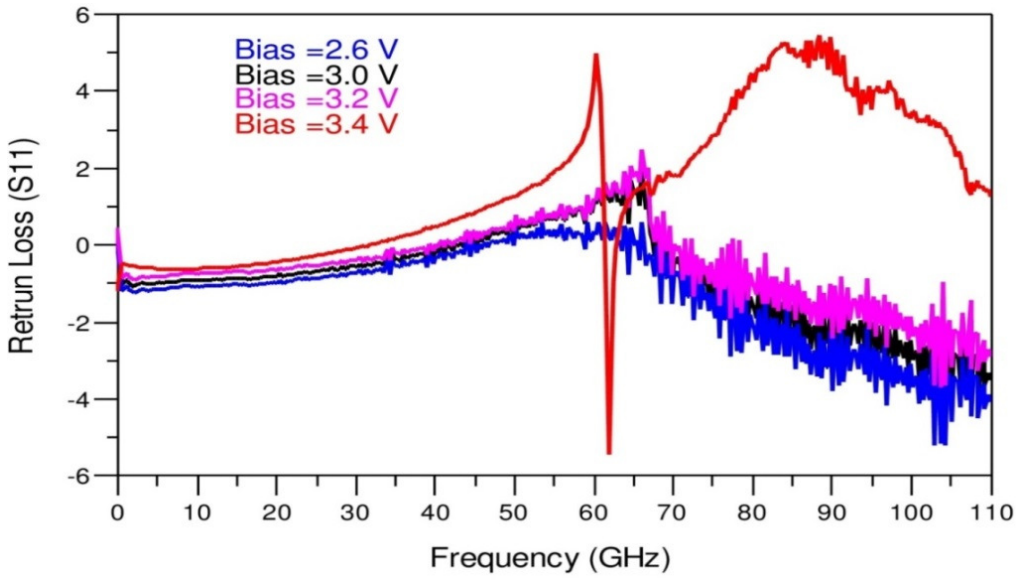

Figure.8.7. Measured S-parameters of the Type-C planar Gunn diode Response

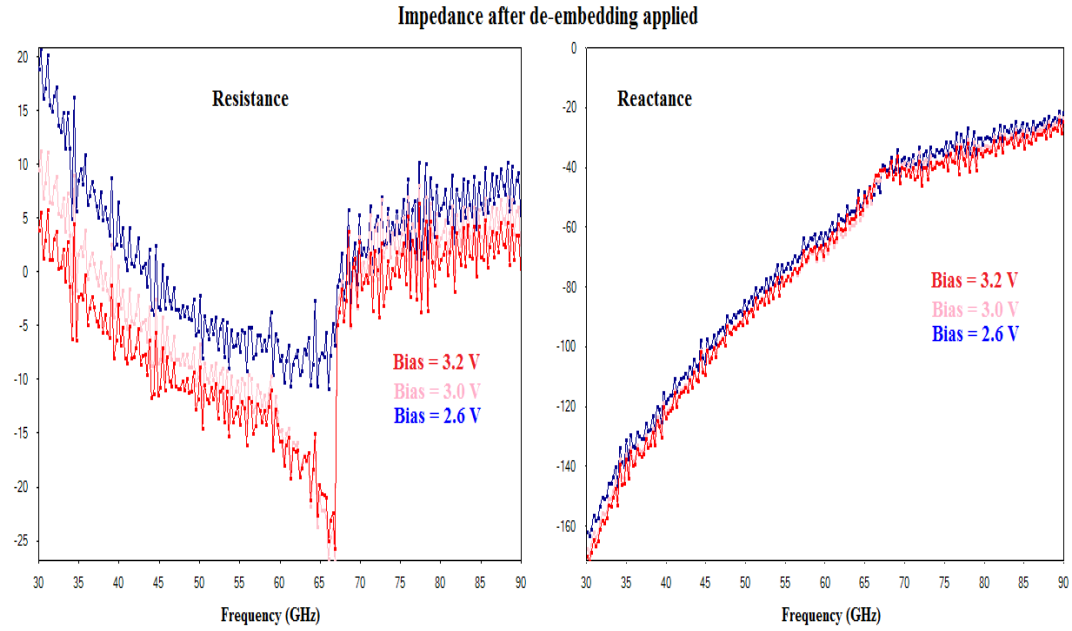

(a) **(b)**

Figure.8.8. Measured (a) one-port reflection coefficient $|S_{11}|$ and Impedance (resistance and reactance) of a 4 micron Type-C planar Gunn diode

$$Z = Z_0 \left[\frac{Z_o sin\beta l + Z_L \cos \beta l}{Z_o cos\beta l - Z_L \sin \beta l}\right] \quad (8.2)$$

Note for equation 8.2, l is the length of CPW 50 Ohm line de-embedded in order that the S-parameters are close to the active region of the diode and it is done by using ADS-2009.

It is also noticeable that the maximum frequency of the planar Gunn diode for a 0 dB reflection coefficient decreases as the bias voltage increases. For the frequencies between 10 MHz to 40 GHz, the reflection coefficients was always less than 0 dB for all applied bias voltages. The impedance (Z = -22-j 31.72) of the Type-C planar Gunn diode was extracted from the de-embedded s-parameters at the oscillation frequency (60.27 GHz).The measured diode impedance was used to derive the shunt/open circuit transmission line which resonated out the capacitive element at 60.27GHz of the diode using the Smith Chart and linecalc tools in ADS-2009 (which is within the inbuilt software in ADS-2009). The open circuited transmission line length was 478 μm which was loaded into the developed circuit model. A radial stub resonator (R=110 μm was used to suppress the fundamental frequency (f_0 = 60.3GHz) of the planar Gunn diode and enable the second harmonic to be dissipated in the 50 Ohm load. At the second harmonic frequency the radial stub resonator will present an open circuit to the diode, whereas the fundamental frequency it will present a short circuit. The required radial stub resonant frequency was calculated using the derived polynomial equation discussed in chapter-7. The simulated output reflection match of the planar Gunn diode oscillator circuit is shown in **Figure 8.9.** indicating a good match (S_{11} = 20.65 dB) at the extracted second harmonic at 123.2 GHz and the fundamental oscillation frequency of 61.56 GHz suppressed as the match was poor (S_{11}=1.26 dB). Similar procedure has been followed to extract the second harmonic from the planar Gunn diode using the diamond stub resonator.

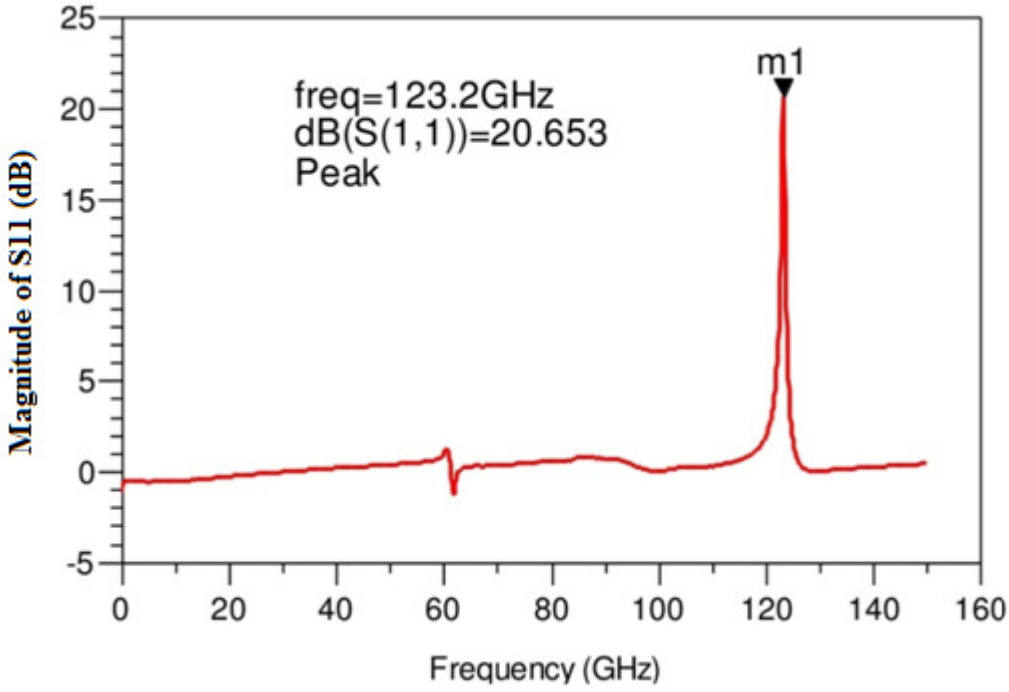

Figure.8.9. Extraction of second harmonic from the Type-C planar Gunn diode

The above simulated circuit was fabricated on an InP substrate using a In-GaAs planar Gunn diode**. Figure.8.10 (a)** shows a SEM image of a 4 µm active channel length hetero-structure InP planar Gunn diode with an integrated CPW open circuit matching stub with a characteristic impedance of 32 Ohm, and line length of 478 µm; the radial stub resonator had a radius of 400µm[9]. The complete structure was fabricated on a 620 micron thick semi-insulating InP substrate. **Figure.8.10 (b)**shows the SEM image of a 4 µm active length hetero-structure InP planar Gunn diode with integrated CPW open circuit matching stub with a characteristic impedance of 33 Ohm and electrical length of 478 µm, but this time the novel diamond resonator of length 400 µm was used. The CPW open circuit stub inductive line matches the transistor reactive component at the fundamental frequency of 60 GHz and the radial stub resonator suppresses the fundamental component allowing the harmonics to pass to the load via the 50 Ohm CPW line with a pitch of 40-60-40 µm. The device and integrated circuit were passivated by depositing silicon nitride to suppress trapping and minimize surface oxidation [10].

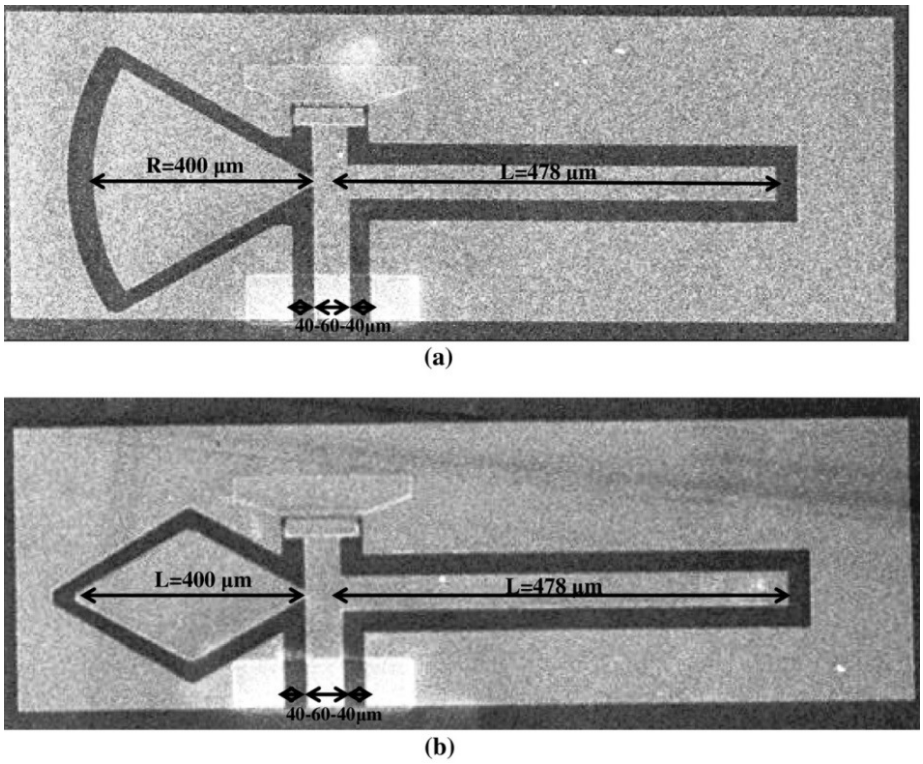

Figure.8.10. SEM image of planar Gunn diode to extract the second harmonics by using the (a) radial stub resonator and CPW line (b) novel diamond resonator and CPW line

8.3.1. EXPERIMENTAL RESULTS OF PLANAR GUNN DIODES

A numbers of experiments were carried out to investigate the oscillation frequency of the planar Gunn diode and these are discussed.

8.3.1.1. *DC MEASUREMENT RESULTS*

The DC characteristics of both types of circuit were measured using a semiconductor device analyser (Agilent Technologies B1500A), which was connected to an automated probe station (Cascade Microtech). Figure.8.11) shows the pulsed IV characteristics of the hetero-structure InP planar Gunn diode integrated with matching circuit and radial stub and a diamond stub resonator respectively. The pulsed measurement was used to identify the negative differential resistance (NDR) region which occurred at a bias voltage of approximately 3.36 V with a peak current of 88 mA for the device with radial resonator. Whereas, for the device with diamond stub resonator the maximum NDR occurred at 3.12 V with a

peak current of 87 mA, so both devices were very similar as would be expected.

The InP Gunn diode integrated oscillator circuits were RF characterised by measuring the second harmonic frequency, output power and the effectiveness of suppressing the fundamental frequency. The experimental set-up for measuring the second harmonic was discussed in chapter-3. It consisted of a W band RF probe with a G-S-G pitch of 40-60-40 microns, the probe had an integrated bias tee to enable biasing the Gunn diode while coupling the RF signal to a Farran mixer and local oscillator, the base-band frequency was fed directly to an Agilent E4448 spectrum analyser.

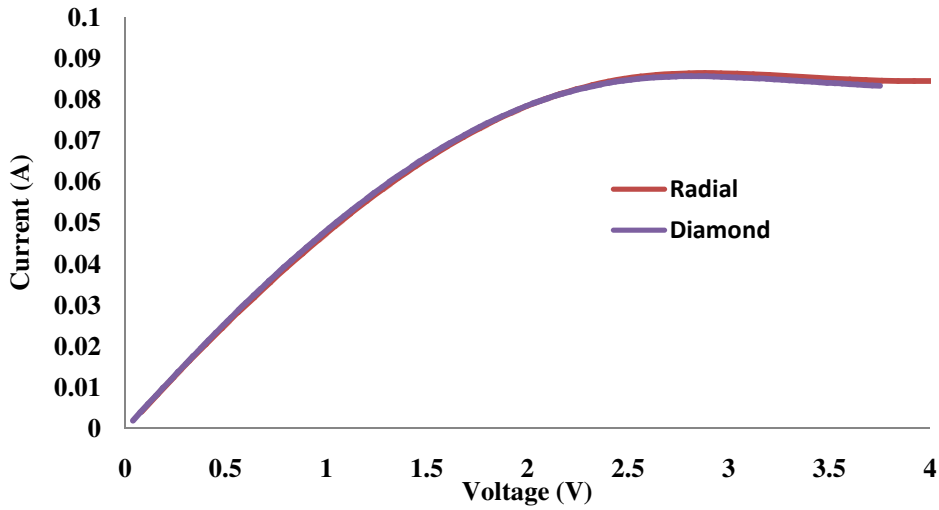

Figure.8.11. Measured current-voltage characteristics of a typical 4 x 120 µm $In_{0.53}Ga_{0.47}As$ planar Gunn diode

8.3.1.2. *SPECTRUM ANALYSER MEASUREMENT RESULTS ON InP PLANAR GUNN DIODE WITH RADIAL STUB RESONATORS*

The integrated heterostructure InP planar Gunn diode oscillator circuits were experimentally measured initially at the second harmonic and then fundamental frequency. The extended W band experimental set-up for measuring the second harmonic was discused in chapter 3. It consisted of a RF probe with a G-S-G pitch of 40-60-40 µm, the probe had an integrated bias-tee to enable biasing (2.91 V) the Gunn diode while coupling the RF signal to a Farran mixer with an internal local oscillator, the base-band frequency coupled directly to an Agilent E4448 spectrum analyser. The

measured RF loss of the mixer was ≈ -50 dB over an extended W band to 125 GHz. Preliminary RF measurements identified a second harmonic signal at 118 GHz with an output power of -20 dBm which is shown in **Figure 8.12.** The fundamental response from the same circuit and bias conditions (2.91 V) was measured using a similar set-up working over V-band (50 to 75 GHz). The set-up briefly consisted of a V-band RF probe (GGB Technologies) with GSG pitch of 40-60-40 µm, bias tee, feeding a V-band mixer (Farran Technologies) and the down converted frequency was fed to the spectrum analyser (Agilent E4448). In all the spectrum analyser measurments the bandwidth was set to 3 MHz. The measured RF loss of the mixer at 60 GHz was measured to be ≈ –50 dB. The measurement indicated the fundamental signal was in the noise floor of the measurement set-up. To verify the harmonic response of the above circuit, an identical planar Gunn diode with matching circuit and no radial resonator was tested with the same applied bias voltage of 2.91 V. A fundamental frequency of 59 GHz with an RF output power of approximatley -19 dBm was detected; the harmonic was simialr to the noise level in the circuit.

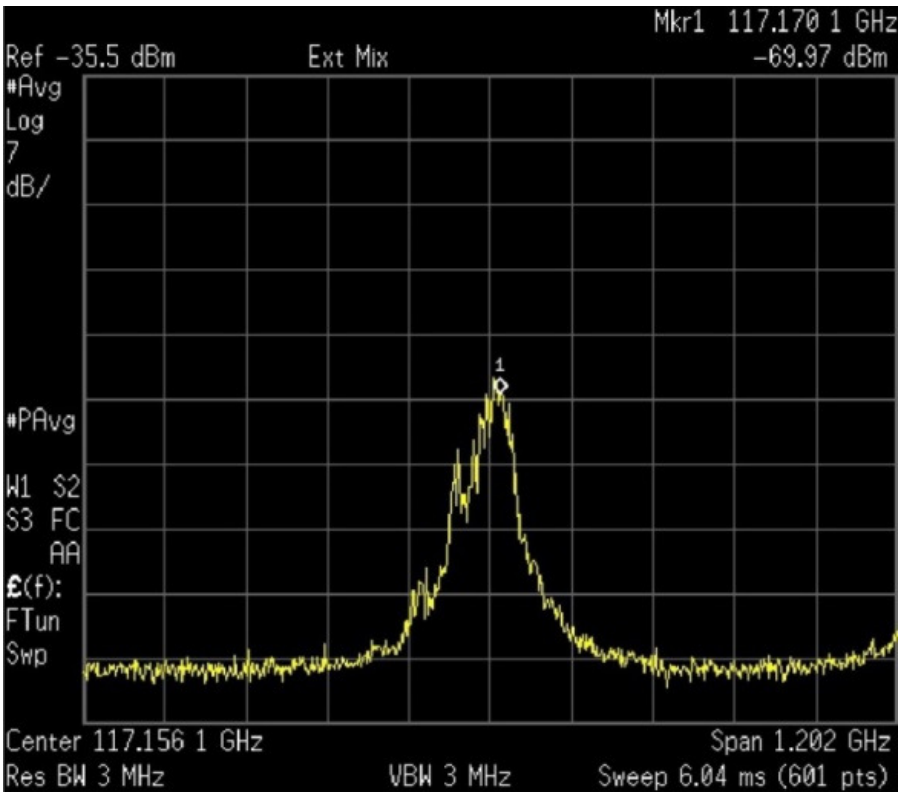

Figure.8.12.Extraction of second harmonic from the integrated planar Gunn diode with radial stub resonator

8.3.1.3. *SPECTRUM ANALYSER MEASUREMENT RESULTS ON InP PLANAR GUNN DIODE WITH DIAMOND STUB RESONATORS*

Similar designs were fabricated with a novel diamond resonator on a 620 micron thick InP semi-insulating substrate and it was again RF characterised by measuring its second harmonic output power and the effectiveness of suppressing the fundamental frequency. Preliminary RF measurements identified a second harmonic signal at 121 GHz with an output power of -14 dBm, and the bias voltage was 2.8V. The fundamental response from the same circuit under identical bias conditions (2.8V) was measured using a similar set-up but working over V-band (50 to 75 GHz) which was discussed in chapter-3. The measurement indicated that the fundamental frequency was in the noise floor of the spectrum analyser. The same CPW open circuit matching stub with planar Gunn diode but without the diamond resonator was also fabricated on the same process wafer as the second harmonic extraction circuit. The circuit was tested at the fundamental frequency and gave an RF output power of -9 dBm at 66 GHz, showing the effectiveness of the diamond resonator suppressing the fundamental frequency. The small difference in the fundamental frequency between the two integrated circuits (integrated circuit with radial stub and diamond stub resonators) was thought to be due to slight differences in the optimum bias voltages.**Figure.8.13** shows the measured output spectrum centred at 121.688 GHz with the output power of -14.1 dBm[11].

A comparison of simulated and measured results of an integrated heterostructure InP planar Gunn diode is shown in ***Table.8.1.*** The measurement results show that the fundamental oscillation frequency of the planar Gunn diode was suppressed and the second harmonic was extracted around 120 GHz with the highest RF output power of -14.11 dBm.

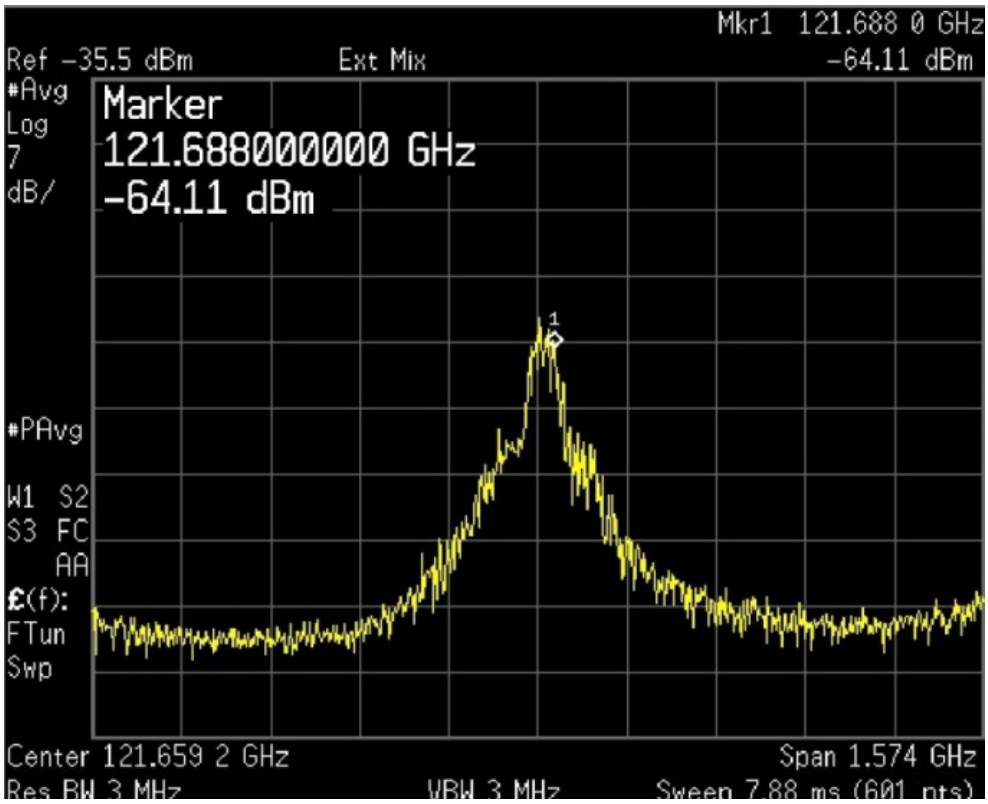

Figure.8.13Extraction of second harmonic from the integrated planar Gunn diode with a diamond stub resonator

Device and wafer number	Fundamental Frequency (GHz)			Second harmonics Frequency (GHz)		
	Simulated results in ADS-2009 (GHz)	Measured oscillation frequency by using Spectrum Analyser (GHz)	Measured power by using Spectrum Analyser (dBm)	Simulated results in ADS-2009(GHz)	Measured oscillation frequency by using Spectrum Analyser (GHz)	Measured power by using Spectrum Analyser (dBm)
Diode with radial stub resonator (S18158)	61.6	59.15	SIN	123.2	118.31	-28.67
		58.58	SIN		117.17	-19.97
		59.81	SIN		119.63	-31.78
Diode with diamond stub resonator (S18158)	62.3	60.84	SIN	124.6	121.68	-14.11
		58.99	SIN		117.98	-21.33
		59.38	SIN		118.76	-21.90
		60.46	SIN		120.93	-25.14
		58.56	SIN		117.73	-21.79

SIN represents Signal in Noise

Table.8.1. Comparison of simulated and measured results of an integrated InP planar Gunn diode

Measurements results published by Ata Khalid [12] show the planar Gunn diode oscillating at fundamental frequency of 298 GHz. By applying the second harmonic technology as described here, it should be possible to fabricate the InGaAs Gunn diode working at 596 GHz. More work will be required to improve the RF output power performance.

8.4. REFERENCES

[1] J. B. Gunn, "Microwave oscillations of current in III–V semiconductors," *Solid State Commun.*, vol. 1, no. 4, pp. 88–91, Sep. 1963.

[2] A. Khalid, N. J. Pilgrim, G. M. Dunn, M. C. Holland, C. R. Stanley, I. G. Thayne, and D. R. S. Cumming, "A Planar Gunn Diode Operating Above 100 GHz," *IEEE Electron Device Lett.*, vol. 28, no. 10, pp. 849–851, Oct. 2007.

[3] F. L. Warner and P. Herman, "Miniature X band Gunn oscillator with a dielectric-tuning system," *Electron. Lett.*, vol. 2, no. 12, p. 467, 1966.

[4] H. Barth, "A Wideband, Backshort-Tunable Second Harmonic W-Band Gunn-Oscillator," in *MTT-S International Microwave Symposium Digest*, 1981, vol. 81, pp. 334–337.

[5] S. Yngvesson, *Microwave Semiconductor Devices*. Boston, MA: Springer US, 1991.

[6] C. Li, "Design and Characterisation of millimeter-wave planar Gunn diode and integrated circuits," University of Glasgow, 2011.

[7] G. E. Ponchak and L. P. B. Katehi, "Open- and short-circuit terminated series stubs in finite-width coplanar waveguide on silicon," *IEEE Trans. Microw. Theory Tech.*, vol. 45, no. 6, pp. 970–976, Jun. 1997.

[8] M. I. Maricar, J. Glover, G. Evans, D. Cumming, and C. Oxley, "Design and characterization of a novel diamond resonator," *Microw. Opt. Technol. Lett.*, vol. 56, no. 7, pp. 1691–1693, Jul. 2014.

[9] M. I. Maricar, A. Khalid, J. Glover, G. A. Evans, P. Vasileious, C. Li, D. Cumming, and C. H. Oxley, "Extraction of second harmonic from the In0.53Ga0.47As planar Gunn diode using radial stub resonators," *Solid. State. Electron.*, vol. 99, pp. 38–40, Sep. 2014.

[10] S. Helland, "Electrical Characterization of Amorphous Silicon Nitride Passivation Layers for Crystalline Silicon Solar Cells," Norwegian University of Science and Technology, 2011.

[11] Mohamed Ismaeel Maricar, James Glover, Ata Khalid, Chong Li, G Evans, D. S. R. C. and C. H. O. "Extraction of second harmonic from an InP based planar Gunn diode using diamond resonator for milli-metric wave frequencies," *Solid State Commun.*, 2014.(Submitted)

[12] A. Khalid, G. M. Dunn, R. F. Macpherson, S. Thoms, D. Macintyre, C. Li, M. J. Steer, V. Papageorgiou, I. G. Thayne, M. Kuball, C. H. Oxley, M. Montes Bajo, A. Stephen, J. Glover, and D. R. S. Cumming, "Terahertz

oscillations in an In0.53Ga0.47As submicron planar Gunn diode," *J. Appl. Phys.*, vol. 115, no. 11, p. 114502, Mar. 2014.

Chapter: 9

Conclusion and Future work

9.1. CONCLUSION

In the last several years, the fast growing millimetre-wave terahertz application markets, for example communication, radar imaging, spectroscopy and security screening has driven the development of reliable and flexible signal sources. Gunn devices or transferred electron devices are excellent device to be considered to meet the demand due to their small size, excellent phase noise performance and simple structures. However, the conventional vertical Gunn devices have a limitation of fundamental operational frequency of around 90 GHz for GaAs and 164 GHz for InP based materials respectively[1], [2]. Higher operational frequency can be achieved by extracting the second or third harmonic frequencies from these devices.

With the very recent research and development on planar Gunn diodes the attractiveness of this technology is even greater due to the ease of integration of the Gunn diode in MMIC technologies, and the fundamental transit frequency being controlled by the separation between the anode and cathode electrodes. As seen in this work there are two areas of requirement (i) extending the frequency of operation of the planar Gunn diode and (ii) increasing the RF output power. The former has been the main aim of this work by extracting the second harmonic from the planar Gunn device.

As reported in the thesis, there were a number of planar Gunn diodes with a range of electrode configurations fabricated on both GaAs and InP based materials. The electrode configurations for example enable improved de-embedding of the active region of the diode (Type C) and a series matching inductor fabricated close to the

active region of the diode (Type D). A GaAs planar Gunn diode (Type D) with a 1 micron cathode to anode separation and with the on chip series inductor matching wasRF characterized and gave the highest experimentally measured fundamental frequency of 121 GHz obtained to date from a GaAs based (vertical or planar) Gunn diode [3].

An $In_{0.47}Ga_{0.53}As$ fabricated on lattice matched InP planar Gunn diode was also investigated. The InP based Gunn diode provided a higher transit mode oscillation frequency due to the high saturation velocity which was shown in this work. [4]. The work also described and experimentally determined the dead space of the$In_{0.53}Ga_{0.47}As$ planar Gunn diode fabricated on an InP substrate. To the author's knowledge for the first time the dead space for this material set was found to be 0.21 microns, and was slightly less than for the GaAs based materials. There was also some experimental evidence which suggests the dead space is smaller when the sub-micron active regions of 1 micron are approached which agree with recent published work by Ata et al [5].

Another important part of the work reported in this thesis was the development of several device/circuits which included CPW resonators -radial stub and a novel diamond resonator. The diamond resonator was developed using ADS-2009 software and to the authors knowledge the shape has never been report in the literature. It gave a number of advantages over the radial resonator which included a reduction in chip area by as much as 55% and a higher loaded Q factor. Design equation for the novel diamond resonator was developed to enable resonator design at any frequency. Both CPW radial and diamond resonators were fabricated and experimentally characterized and compared with the respective simulation results.

The main aim of the thesis was met as novel integrated circuit was developed to extract the second harmonic frequency from an $In_{0.53}Ga_{0.47}As$ planar Gunn diodewith an anode to cathode separation of 4 microns. The fundamental frequency was measured as 60GHz and therefore the second harmonic frequency could be measured with the existing equipment which went to 125GHz. Both radial and diamond cpw resonators were used to short circuit the fundamental frequency of oscillation, enabling the second harmonic frequency to pass to the load. The integrated Gunn

circuits were fabricated in James watt nanofabrication centre at Glasgow University and RF measurements were made at Glasgow University. The experimental measurement results were directly compared with simulation results of the integrated planar Gunn diode oscillator circuit using ADS non-linear modelling techniques. The results showed that the fundamental frequency of oscillation was successfully suppressed and the second harmonic was extracted at 121 GHz with an RF output power of -14.1 dBm [6], [7]. Experimental results published by Ata Khalid [5] show an $In_{0.53}Ga_{0.47}As$ planar Gunn diode oscillating at fundamental frequency of 298 GHz. By applying the second harmonic technology it will be feasible to fabricate an $In_{0.53}Ga_{0.47}As$ Gunn diode working at a second harmonic frequency of 596 GHz.

9.2. FUTURE WORK

This work has shown that it is feasible to extract the second harmonic frequency of 120 GHz [6], [7] from an integrated planar Gunn diode with an anode to cathode separation of 4 microns. Ata et al [5] has shown that experimentally it was possible to obtain a fundamental frequency of 298GHz from sub 1 micron $In_{0.53}Ga_{0.47}As$ planar Gunn. Work will be required to experimentally show that it is possible to extract the second harmonic at these much higher frequencies where parasitics will become start to dominate all the circuit elements.

On problem with technology is low output power. This may be a result of inadequate circuit matching to the Gunn diode. To obtain improved matching circuit design a good equivalent circuit model for the planar Gunn diode needs to be developed. This is a very important area and may be one of the many reasons Gunn diodes are unable to compete with FET is due to lack of electrical equivalent circuit. It may be possible to combine lots of planar Gunn diodes to get higher output power using combiner technology as adopted by Li Chong [4]. For a higher power GaN material can be used.

9.3. REFERENCES

[1] A. Khalid, C. Li, V. Papageogiou, G. M. Dunn, M. J. Steer, I. G. Thayne, M. Kuball, C. H. Oxley, M. Montes Bajo, A. Stephen, J. Glover, and D. R. S. Cumming, "In0.53Ga0.47As Planar Gunn Diodes Operating at a Fundamental Frequency of 164 GHz," *Electron Device Lett. IEEE*, vol. 34, no. 1, pp. 39–41, Jan. 2013.

[2] A. Baca and C. Ashby, *Fabrication of GaAs Devices*. The Institution of Engineering and Technology, Michael Faraday House, Six Hills Way, Stevenage SG1 2AY, UK: IET, 2005.

[3] Mohamed Ismaeel Maricar, James Glover, Ata Khalid, Chong Li, G Evans,D. S. R. C. and C. H. Oxley. "An AlGaAs/GaAs based planar Gunn diode oscillator with a fundamental frequency operation of 120GHz," *Microw. Opt. Technol. Lett.*, 2014. (Accepted)

[4] C. Li, "Design and Characterisation of millimeter-wave planar Gunn diode and integrated circuits," University of Glasgow, 2011.

[5] A. Khalid, G. M. Dunn, R. F. Macpherson, S. Thoms, D. Macintyre, C. Li, M. J. Steer, V. Papageorgiou, I. G. Thayne, M. Kuball, C. H. Oxley, M. Montes Bajo, A. Stephen, J. Glover, and D. R. S. Cumming, "Terahertz oscillations in an In0.53Ga0.47As submicron planar Gunn diode," *J. Appl. Phys.*, vol. 115, no. 11, p. 114502, Mar. 2014.

[6] M. I. Maricar, A. Khalid, J. Glover, G. A. Evans, P. Vasileious, C. Li, D. Cumming, and C. H. Oxley, "Extraction of second harmonic from the In0.53Ga0.47As planar Gunn diode using radial stub resonators," *Solid. State. Electron.*, vol. 99, pp. 38–40, Sep. 2014.

[7] Mohamed Ismaeel Maricar, James Glover, Ata Khalid, Chong Li, G Evans, D. S. R. C. and C. H. Oxley. "Extraction of second harmonic from an InP based planar Gunn diode using diamond resonator for milli-metric wave frequencies," *Solid State Commun.*, 2014. (Submitted)